INVESTIGATION OF THE EFFECTS OF RAILWAY TRACK QUALITY ON PASSENGER COMFORT USING ONBOARD INERTIAL SYSTEMS

by

Alfredo Peinado Gonzalo

A thesis submitted to the University of Birmingham for the degree of

DOCTOR OF PHILOSOPHY

Birmingham Centre for Railway Research and Education

School of Engineering

College of Engineering and Physical Sciences

University of Birmingham

March 2023

UNIVERSITY OF
BIRMINGHAM

University of Birmingham Research Archive

e-theses repository

This unpublished thesis/dissertation is copyright of the author and/or third parties. The intellectual property rights of the author or third parties in respect of this work are as defined by The Copyright Designs and Patents Act 1988 or as modified by any successor legislation.

Any use made of information contained in this thesis/dissertation must be in accordance with that legislation and must be properly acknowledged. Further distribution or reproduction in any format is prohibited without the permission of the copyright holder.

ABSTRACT

Condition monitoring activities in railways are crucial for detecting track and vehicle faults early and minimising their disruptive effects. Nowadays, in-service vehicles are increasingly used due to their availability and low disruption. Installing sensors either on the axlebox, bogie or cab of these vehicles provides information that can be used for a wide range of applications.

This thesis describes the use of a set of inertial sensors installed onboard passenger vehicles for track quality and ride quality monitoring. A novel method for speed estimation is presented and complemented with a method to estimate distance using track geometry.

This work investigates the use of passenger comfort as an indicator of track quality, using current standards, and comparing the comfort results to track quality and driver reports.

Finally, the relevance of the location of sensors in the vehicle is discussed. Two case studies are presented to illustrate the impact of the orientation of the vehicle and direction of travel on the signal received.

DEDICATION

First of all, I want to thank Dr Mani Entezami and Dr Clive Roberts, whose support made it possible to keep on this project despite the many difficulties I had during this time. I owe you many packs of doughnuts. Then I want to thank Paul Weston, for showing me how little I know about English and how much I still have to learn about railways, research, and anything in general. Also, the rest of the staff in BCRRE and UKRRIN for their help whenever I needed it.

Network Rail and Eurostar for providing me with the data and allowing me to install the sensors on the train, especially Mick Hayward, who sadly passed away during the period of this thesis.

My fellow PhD colleagues and soon-to-be doctors: Sina, Rabee, Jovan, Jie, Achila, and many others, for their company, support, lunchtimes, and nights out. The Spanish flatmates and friends I was lucky to have during the time I lived in Birmingham: Miguel, Claudia, and Bea, for taking me out of my room to get the fresh air I much needed.

My parents Pedro and Pilar and my sister Melania, for their understanding when I decided to do this, and the countless support calls when I hesitated to keep this path. The rest of my family, for their support and transport between airports, stations, and houses. And my two nephews Leo and Eloy, my two shining stars.

My colleagues in Ingenium: Fausto, Isaac, Sergio, Pedro, Alba, and Ana, for hosting me in the last stages of my thesis and the coffee breaks. My girlfriend Rosa, for the places we travelled to, and the places we will travel to. My friends back home: Asier, José Miguel, and Lidia, for the drinks together. Certain pirate crew, for the countless hours chatting. And my ex.

And all the rest of the people I forgot to mention and somehow helped me during this whole journey.

ACKNOWLEDGEMENTS

This research was funded by EPSRC Track to the Future (EP/M025276), Shift2Rail Innovation Program Project IN2TRACK2 (work package 3), the Innovate UK Smart Grant on Track and Ride Condition Correlation for Optimized Rail Maintenance under Grant 103294, and the On the Move research grant.

Data used in this project was provided by MoniRail and Network Rail.

TABLE OF CONTENTS

Chapter 1 . Introduction 1

1.1. Motivation 1

1.2. Railway track definition, structure and faults 3

1.3. Railway vehicle components and faults 9

1.4. Comfort 11

1.5. Positioning in railways 15

1.6. Hypothesis and Objectives 16

1.7. Thesis structure 17

Chapter 2 . Literature Review on In-service Railway Monitoring 21

2.1. Introduction 21

2.2. Trackside monitoring and inspection 22

2.3. Onboard monitoring and inspection 24

2.3.1. Track monitoring and inspection 25

2.3.2. Onboard vehicle component monitoring 27

2.4. Vehicle location and positioning 28

2.5. Signal processing 30

2.6. Conclusions 32

Chapter 3 . Speed and distance estimation using onboard inertial sensors 35

3.1. Introduction 35

3.2. Track and test conditions 35

3.3. Speed estimation method 38

3.3.1. Section 1. Ashford International to Ebbsfleet International 47

3.3.2. Section 2. Ebbsfleet International to Stratford Station 48

3.3.3. Section 3. Stratford Station to St. Pancras International 49

3.4. Distance alignment using crosslevel 51

3.4.1. Section 1. Ashford International to Ebbsfleet International 55

3.4.2. Section 2. Ebbsfleet International to Stratford Station 55

3.4.3. Section 3. Stratford Station to St. Pancras International 57

3.5. Alignment comparison to other methods 59

3.5.1. Cross-correlation 59

3.5.2. Dynamic time warping 61

3.6. Conclusions 64

Chapter 4 . Assessment of comfort for ballasted and slab track 67

4.1. Introduction 67

4.2. Comfort assessment 68

4.2.1. Ballasted track 68

4.2.2. Slab track 74

4.3. Slab and ballasted track comparison 78

4.4. Evolution of vertical comfort 79

4.5. Conclusions 83

Chapter 5 . Effects of vehicle orientation and direction 85

5.1. Introduction 85

5.2. Test conditions 86

5.3. Comparison between components 88

5.4. Comparison between configurations 95

5.5. Conclusions 108

Chapter 6 . Switch and crossing case study 111

6.1. Introduction 111

6.2. Test conditions and equipment 111

6.3. Analysis of data 113

6.3.1. Component comparison 113

6.3.2. Differences between configurations 118

6.3.3. Track evolution 130

6.4. Conclusions 143

Chapter 7 . Relationships between track quality and ride comfort 145

7.1. Introduction 145

7.2. Case 1: Stanley Icn. to Inverness Stn. 146

7.3. Case 2: Carmont 151

7.4. Correlation between DRRR and comfort 155

7.4.1. Rough rides and Class 158 156

7.4.2. Rough rides and Class 170 157

7.5. Conclusions 158

Chapter 8 . Conclusions 161

8.1. Introduction 161

8.2. Key achievements 161

8.3. Hypothesis and objectives discussion 162

8.4. Publications and collaborations 163

References I

Appendix A. Comfort indices XIII

Appendix B. Kalman filter XIX

Appendix C. Results obtained for long-wavelength track feature XXIII

C.1. Data displayed per sensor XXIII

C.2. Data displayed per configuration XXIX

Appendix D. Results obtained for switch and cross XXXV

D.1. Data displayed per sensor XXXV

D.2. Data displayed per configuration XLI

D.3. Evolution of data XLV

Appendix E. Research Poster Conference 2019 LI

Appendix F. WCRR 2019 LIII

Appendix G. Research Poster Conference 2021 LV

Appendix H. Journal article 1 LVII

Appendix I. CONTROL 2022 LIX

Appendix J. Rail Live 2022 LXI

Appendix K. Journal article 2 LXIII

LIST OF FIGURES

Figure 1.1. Schematic structure of a ballasted (left) and slab (right) track. 3

Figure 1.2. Track geometry parameters. 4

Figure 1.3. Example of rail corrugation in a ballasted track. 5

Figure 1.4. Example of a missing screw in a fastening system. 6

Figure 1.5. Examples of damaged wheels showing rolling contact fatigue. 9

Figure 1.6. Comparison between comfort indices. 14

Figure 2.1. Self-propelled vehicle (left), towed coach (centre), and hi-rail vehicle (right) [4]. 25

Figure 2.2. Typical frequency ranges of excitation, adapted from [12]. 31

Figure 3.1. Track route and stations 36

Figure 3.2. IMU axis system with respect to the vehicle. 37

Figure 3.3. Comparison between GNSS speed estimation and axlebox frequency spectrum. 39

Figure 3.4. Spectrograms of bogie accelerometers. 40

Figure 3.5. Spectrograms of bogie gyroscopes. 40

Figure 3.6. Spectrograms of cab accelerometers. 41

Figure 3.7. Spectrograms of cab gyroscopes. 41

Figure 3.8. Curve fitting for selected signals. 42

Figure 3.9. Speed estimation comparison. 46

Figure 3.10. Speed estimation error comparison. 46

Figure 3.11. Axlebox accelerometer spectrograms and speed estimates for Section 1. 48

Figure 3.12. Axlebox accelerometer spectrograms and speed estimates for Section 2. 49

Figure 3.13. Axlebox accelerometer spectrograms and speed estimates for Section 3. 50

Figure 3.14. Crosslevel comparison between bogie, cab, and reference. 51
Figure 3.15. Differences between distance estimation and reference. 52
Figure 3.16. Detail of identified transitions in crosslevel for bogie, cab, and reference. 53
Figure 3.17. Crosslevel comparison before and after correction for Section 1. 54
Figure 3.18. Absolute error in distance estimation for Section 1 before and after correction. 54
Figure 3.19. Crosslevel comparison before and after correction for Section 2. 56
Figure 3.20. Absolute error in distance estimation for Section 2 before and after correction. 56
Figure 3.21. Crosslevel comparison before and after correction for Section 3. 57
Figure 3.22. Absolute error in distance estimation for Section 3 before and after correction. 58
Figure 3.23. Application of cross-correlation to a track segment. 60
Figure 3.24. Application of cross-correlation to a segment of a run. 61
Figure 3.25. Application of dynamic time warping to crosslevel. 62
Figure 3.26. Speed estimation and distance correction flowchart. 63
Figure 4.1. Ballasted track geometry. 69
Figure 4.2. Speed, lateral and vertical comfort on a ballasted track on a high-speed line. 70
Figure 4.3. Comfort (dark blue) and cab acceleration (light blue) for a ballasted track. 71
Figure 4.4. Vertical comfort on the track. 71
Figure 4.5. Lateral comfort on the ballasted track. 72
Figure 4.6. Event-based comfort for a ballasted track. 73
Figure 4.7. Slab track geometry 74
Figure 4.8. Vehicle location for slab track. 75
Figure 4.9. Speed and continuous comfort for a slab track. 76
Figure 4.10. Continuous comfort and acceleration for a slab track. 76
Figure 4.11. Event-based comfort for a slab track. 77

Figure 4.12. Vehicle speed for the different dates. 79

Figure 4.13. Evolution of cab vertical displacement. 80

Figure 4.14. Evolution of vertical comfort. 81

Figure 4.15. Evolution of lateral comfort. 82

Figure 5.1. Vertical alignment (top), crosslevel (center) and curvature (bottom) of the track segment. 86

Figure 5.2. Sensor configurations for the test. 87

Figure 5.3. Axlebox, bogie and cab vertical acceleration. 89

Figure 5.4. Axlebox, bogie and cab vertical acceleration spectrograms. 90

Figure 5.5. Axlebox, bogie and cab wavelength filters of vertical displacement. 91

Figure 5.6. Passenger comfort according to EN 12299. 94

Figure 5.7. Speed data for all the configurations. 96

Figure 5.8. Spectrogram comparison for the axlebox left sensor. 98

Figure 5.9. Spectrogram comparison for the axlebox right sensor. 98

Figure 5.10. Spectrogram comparison for the bogie sensor. 99

Figure 5.11. Spectrogram comparison for the cab sensor. 99

Figure 5.12. Axlebox left displacement comparison between configurations. 100

Figure 5.13. Axlebox right vertical displacement comparison between configurations. 101

Figure 5.14. Bogie vertical displacement comparison between configurations. 103

Figure 5.15. Cab vertical displacement comparison between configurations. 104

Figure 5.16. Vertical comfort comparison between configurations. 106

Figure 5.17. Lateral comfort comparison between configurations. 106

Figure 6.1. Schematic representation of Nashenden crossovers. 112

Figure 6.2. Vertical acceleration comparison between components. 114

Figure 6.3. Vertical acceleration spectrograms comparison between components. 115
Figure 6.4 Vertical displacement comparison between components. 116
Figure 6.5. Vehicle passenger comfort. 117
Figure 6.6. Vehicle speed comparison between configurations. 119
Figure 6.7. Acceleration spectrogram for the axlebox left sensors. 120
Figure 6.8. Acceleration spectrogram for the axlebox right sensors. 121
Figure 6.9. Acceleration spectrogram for the bogie sensors. 121
Figure 6.10. Acceleration spectrogram for the cab sensors. 122
Figure 6.11. Axlebox left vertical displacement comparison between components. 123
Figure 6.12. Axlebox right vertical displacement comparison between configurations. 124
Figure 6.13. Bogie vertical displacement comparison between configurations. 125
Figure 6.14. Cab vertical displacement comparison between configurations. 127
Figure 6.15. Vertical comfort comparison between configurations. 128
Figure 6.16. Lateral comfort comparison between configurations. 129
Figure 6.17. Vehicle speed comparison over time. 130
Figure 6.18. Left axlebox vertical acceleration spectrogram evolution. 131
Figure 6.19. Right axlebox vertical acceleration spectrogram evolution. 132
Figure 6.20. Evolution of left axlebox vertical displacement. 134
Figure 6.21. Evolution of right axlebox vertical displacement. 134
Figure 6.22. Bogie vertical acceleration spectrogram evolution. 136
Figure 6.23. Evolution of bogie vertical displacement 137
Figure 6.24. Cab vertical acceleration spectrogram. 139
Figure 6.25. Evolution of cab vertical displacement. 140
Figure 6.26. Evolution of vertical comfort. 141

Figure 6.27. Evolution of lateral comfort. 142

Figure 7.1. Class 170 and Class 158 suspensions. 146

Figure 7.2. Ride quality results for the track on a Class 170 vehicle. 147

Figure 7.3. Vertical comfort on the map and location of rough ride report. 148

Figure 7.4. Vertical displacement and comfort for a Class 170 vehicle. 149

Figure 7.5. Vertical ride comfort for a Class 158 vehicle. 150

Figure 7.6. Ride quality comparison between Class 170 and Class 158 vehicles. 151

Figure 7.7. Ride comfort map for Class 170 on the up line. 152

Figure 7.8. Ride comfort map for Class 158 on the up line. 152

Figure 7.9. Ride comfort map for Class 170 on the down line. 154

Figure 7.10. Ride comfort map for Class 158 on the down line. 154

Figure A.1. Frequency weighting curves for vehicle vibrations [11]. XIV

Figure A.2. Health guidance caution zones [70]. XVIII

Figure C.1. Bogie and cab lateral acceleration. XXIII

Figure C.2. Bogie and cab lateral acceleration spectrogram. XXIV

Figure C.3. Bogie and cab lateral displacement. XXIV

Figure C.4. Bogie and cab longitudinal acceleration. XXV

Figure C.5. Bogie and cab longitudinal acceleration spectrogram. XXV

Figure C.6. Bogie and cab longitudinal displacement. XXVI

Figure C.7. Bogie and cab yaw rate. XXVI

Figure C.8. Bogie and cab yaw rate spectrograms. XXVII

Figure C.9. Bogie and cab pitch rate. XXVII

Figure C.10. bogie and cab pitch rate spectrograms. XXVIII

Figure C.11. Bogie and cab roll rate. XXVIII

Figure C.12. Bogie and cab roll rate spectrograms. XXIX
Figure C.13. Axlebox left vertical displacement (35-m wavelength filter). XXIX
Figure C.14. Axlebox left vertical displacement (70-m wavelength filter). XXX
Figure C.15. Axlebox right vertical displacement (35-m wavelength filter). XXX
Figure C.16. Axlebox right vertical displacement (70-m wavelength filter). XXXI
Figure C.17. Bogie vertical displacement (35-m wavelength filter). XXXI
Figure C.18. Bogie vertical displacement (70-m wavelength filter). XXXII
Figure C.19. Cab vertical displacement (35-m wavelength filter). XXXII
Figure C.20. Cab vertical displacement (70-m wavelength filter). XXXIII
Figure D.1. Bogie and cab lateral displacement. XXXV
Figure D.2. Bogie and cab lateral displacement spectrograms. XXXVI
Figure D.3. Bogie and cab Lateral displacement. XXXVI
Figure D.4. Bogie and cab longitudinal acceleration. XXXVII
Figure D.5. Bogie and cab longitudinal acceleration spectrograms. XXXVII
Figure D.6. Bogie and cab longitudinal displacement XXXVIII
Figure D.7. Bogie and cab yaw rate. XXXVIII
Figure D.8. Bogie and cab yaw rate spectrograms. XXXIX
Figure D.9. Bogie and cab pitch rate. XXXIX
Figure D.10. Bogie and cab pitch rate spectrograms. XL
Figure D.11. Bogie and cab roll rate. XL
Figure D.12. Bogie and cab roll rate spectrograms. XLI
Figure D.13. Axlebox Left vertical displacement (35-m wavelength filter). XLI
Figure D.14. Axlebox left vertical acceleration (70-m wavelength filter). XLII
Figure D.15. Axlebox right vertical displacement (35-m wavelength filter). XLII

Figure D.16. Axlebox right vertical displacement (70-m wavelength filter)..... XLIII
Figure D.17. Bogie vertical displacement (35-m wavelength filter). XLIII
Figure D.18. Bogie vertical displacement (70-m wavelength filter). XLIV
Figure D.19. Cab vertical displacement (35-m wavelength filter). XLIV
Figure D.20. Cab vertical displacement (70-m wavelength filter). XLV
Figure D.21. Evolution of left axlebox vertical displacement (35-m wavelength filter)..... XLV
Figure D.22. Evolution of left axlebox vertical displacement (70-m wavelength filter).... XLVI
Figure D.23. Evolution of right axlebox vertical displacement (35-m wavelength filter).. XLVI
Figure D.24. Evolution of right axlebox vertical displacement (70-m wavelength filter). XLVII
Figure D.25. Evolution of bogie vertical displacement (35-m wavelength filter)..... XLVII
Figure D.26. Evolution of bogie vertical displacement (70-m wavelength filter)..... XLVIII
Figure D.27. Evolution of cab vertical displacement (35-m wavelength filter). XLVIII
Figure D.28. Evolution of cab vertical displacement (70-m wavelength filter). XLIX

LIST OF TABLES

Table 1.1. Comfort perception reference for ISO 2631-1 [70]. 12

Table 1.2. Comfort perception reference for EN 12299 [11]. 13

Table 1.3. Reference for the mean comfort indices [11]. 13

Table 2.1. In-service railways condition monitoring scenarios. 22

Table 3.1. Track sections characteristics. 36

Table 4.1. Comfort perception reference for EN 12299 [11]. 69

Table 4.2. Comparison of comfort indices for ballasted and slab track. 78

Table 5.1. Available runs for each orientation and configuration. 96

Table 6.1. Reported events over time. 112

Table 6.2. Available runs for each orientation and configuration. 118

Table 7.1. Identification of Class 158 DRRR statistics. 156

Table 7.2. Identification of Class 170 DRRR statistics. 157

Table A.1. Comfort perception reference for ISO 2631-1 [70]. XV

Table A.2. Comfort perception reference for EN 12299 [11]. XVI

Table A.3. Reference for the mean comfort indices [11]. XVII

LIST OF ACRONYMS

- DRRR: Driver Rough Ride Report
- GNSS: Global Navigation Satellite System.
- IMU: Inertial Measurement Unit.
- NDT: Non-Destructive Testing.
- RMS: Root Mean Square.
- S&C: Switch and Crossing.
- C_{Cz}: Continuous comfort in the vertical direction according to the standard EN 12299.
- C_{Cy}: Continuous comfort in the lateral direction according to the standard EN 12299.
- C_{Cx}: Continuous comfort in the longitudinal direction according to the standard EN 12299.
- N_{MV}: Mean comfort using the standard method according to the standard EN 12299.
- N_{VD}: Mean comfort using the complete method according to the standard EN 12299.
- P_{CT}: Comfort in curve transitions according to the standard EN 12299.
- P_{DE}: Comfort in discrete events according to the standard EN 12299.

Chapter 1. Introduction

1.1. MOTIVATION

Currently, the use of railways as a means of transport is increasing in the United Kingdom, from less than 360 million passenger journeys in 2012 to more than 460 million in 2019 [1]. The COVID-19 pandemic in 2020 caused a massive drop, and currently there is a tendency to return to the pre-pandemic number of journeys. Such a large use of the railways ultimately causes infrastructure degradation and wear, and low availability for maintenance and inspection. It is necessary to establish methods to monitor vehicles and tracks to detect and mitigate faults, as most of the issues in the railway industry appear in these systems [2].

In railways, monitoring tasks can be divided into four categories:

- Onboard track monitoring.
- Onboard vehicle monitoring.
- Trackside vehicle monitoring.
- Trackside track monitoring.

Onboard monitoring for track quality is often carried out using dedicated vehicles. These vehicles have advanced equipment and specialist teams working on inspecting the track, carrying out tasks such as evaluating track quality and detecting faults on the railheads [3, 4]. However, the use of these vehicles is limited by their expensive operation and maintenance and dedicated teams, as well as being subject to track availability, so their inspection frequency is

generally less than desired. These measurement vehicles can cost up to £8m to purchase and about £5m to run per annum [5, 6].

Trackside track monitoring aims to detect changes in the track condition and evaluate track degradation over time. This method is expensive if sensors are to be fitted on long sections of the track as it requires large amounts of sensors, with large associated costs and complex installation.

To overcome the difficulties arising from dedicated vehicles and trackside monitoring, this thesis presents the use of a relatively inexpensive measurement system installed on in-service vehicles to quickly monitor both track and train, thus allowing frequent and cheap monitoring. This measurement system comprises a set of inertial sensors, named inertial measurement unit (IMU), and a Global Navigation Satellite System (GNSS) receiver. Furthermore, processing of the inertial data aims to develop new means of assessing track geometry and train ride quality. The system can geographically locate track geometry and ride quality issues detected using the inertial sensors to determine track degradation over time and identify areas where track and vehicle interaction cause uncomfortable rides for the passengers, based on the standards presented in this chapter.

This chapter introduces track structure and geometry parameters and vehicle components, as well as the need for accurate positioning and the use of ride quality monitoring on railways. The main hypotheses and structure of the thesis are presented afterward.

1.2. RAILWAY TRACK DEFINITION, STRUCTURE AND FAULTS

Railway tracks are often ballasted, composed of rails, sleepers, ballast, sub-ballast, and subgrade, although there are tracks where ballast is substituted by a concrete base, known as slab track, mostly used for high-speed lines [7]. The schematics of the ballasted and slab track structure are presented in Figure 1.1.

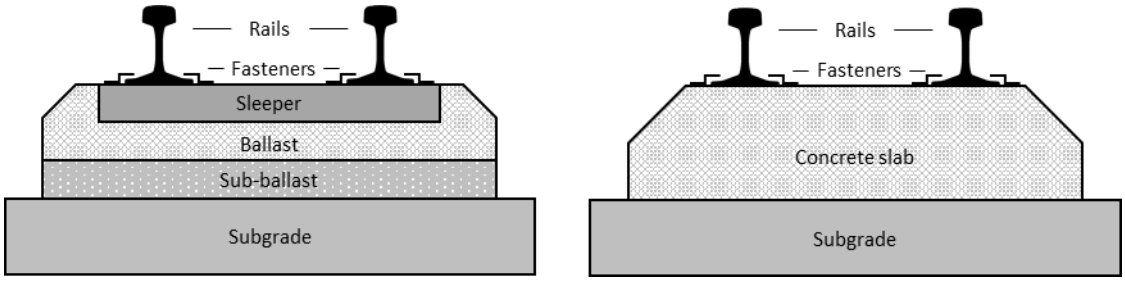


FIGURE 1.1. SCHEMATIC STRUCTURE OF A BALLASTED (LEFT) AND SLAB (RIGHT) TRACK.

Railway tracks have a specific geometry, defined by a set of measurable parameters of a railway track. Definitions of the most important track geometry parameters are presented in standards such as GC/RT 5017 [8], EN 13848-1 [9], and EN 13803 [10], as well as limitations for geometry variations for safety and passenger comfort reasons [11]. These geometry parameters are defined below and presented in Figure 1.2.

- Gauge: Distance between the internal surface of two rails, expressed in mm.
- Crosslevel: Difference in height between two rails computed from the sine of the angle between the top surface and the horizontal plane, expressed in mm. It is also referred to as cant in curved track sections.
- Curvature: Rate of change of the track centre line with respect to distance along the track, expressed as m^{-1}. It is the reciprocal of the instantaneous radius of the curve. Its sign depends on the orientation of the curve (left or right).

- Profile: Profile of the track in the vertical or horizontal plane. It is generally expressed as a function of distance along the track in mm.
- Vertical alignment (Longitudinal level): Deviation in the vertical direction of rails, defined in wavelength ranges and expressed in mm.
- Lateral alignment: Deviation of the alignment with respect to the design in the lateral direction of the rails or track, defined in wavelength ranges and expressed in mm.
- Twist: Crosslevel variation along the track length, expressed as mm/m.

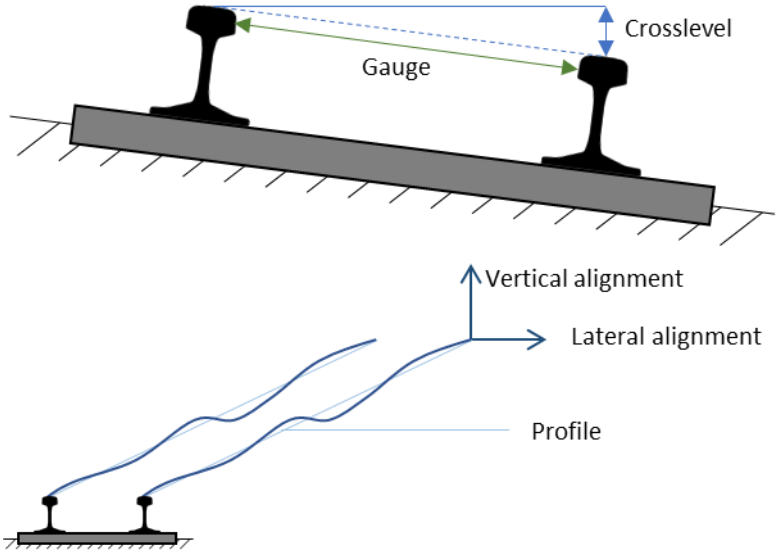


FIGURE 1.2. TRACK GEOMETRY PARAMETERS.

These parameters are defined in the spatial domain, and low-pass filters in the spatial domain are applied for detecting issues in different wavelength ranges. The wavelength filters applied in this work are 35, 70 and 140-m for vertical alignment, based on the wavelength applied for filtering. The 35 and 70-m wavelength filters are applied considering the resonances of the vehicle body, in the order of 1 Hz [12] considering a maximum vehicle speed in the order of 50 m/s, thus obtaining wavelengths in the order of 50 m. The 140-m wavelength filter is applied for high-speed lines in which the 70-m filter is not enough to include the body resonance

frequency. Twist is calculated either over 3 or over 5 m, which is based on the spacing of two wheelsets on a typical bogie.

Tracks need to support the weight of the vehicles and guide them. Track faults increase wear and tear and may become dangerous for vehicle operation. The following paragraphs explain track components and layers, and summarize the most relevant track faults, classified by track component, and their causes and effects. Faults in switches and crossings (S&Cs) and transitions between track segments are explained as well.

Rails guide the wheels along the track and serve as the interface between the vehicle and the track. Faults in rails are generally caused by manufacturing issues [13]. Cracks can appear anywhere in the rail and can cause rails to weaken and ultimately break, compromising track safety. Running surface defects such as corrugation, squats or fatigue lead to quicker wear and rail failures, affecting ride quality [14]. Figure 1.3 shows an example of corrugation in a rail, a periodic fault caused generally by poor wheel-track interaction conditions [14].



FIGURE 1.3. EXAMPLE OF RAIL CORRUGATION IN A BALLASTED TRACK.

Fastening systems are the components that attach the rails to the sleepers or slabs and prevent the rails from moving too much [7]. Faults associated with fasteners are mainly breakage and loss [15], which cause the rails to lose stability and thus generate rail vibration and degradation when vehicles pass. An example of a missing screw in a fastening system is presented in Figure 1.4



FIGURE 1.4. EXAMPLE OF A MISSING SCREW IN A FASTENING SYSTEM.

Most sleepers are made of timber, concrete, or, occasionally, steel [16-18]. Ferdous and Manalo [19] made an exhaustive review in which they explain the faults these three types of sleepers typically exhibit. The main failure types affecting timber sleepers are fungal decay, causing 50% of the sleepers to fail, followed by end splitting and bug attacks. Concrete sleepers mostly suffer from rail-seat deterioration, caused by friction and wear between rail and sleeper; many sorts of cracks due to high impacts or tensile forces; and corrosion caused by chemical reactions of concrete materials with environmental agents, such as minerals dissolved in the ground and moisture or ice on or within the sleepers [20]. Finally, research on steel sleepers reports that their most important failure mode is corrosion caused by environmental conditions. Sleeper inspection is commonly carried out using sensors such as fibre Bragg grating, accelerometers, strain gauges, or cameras [21].

Ballast is a crushed granular material, generally stone, in which sleepers are embedded, aimed at retaining their position and distributing pressure over the soil. Common faults are cracks and particle breakage, settlement and voiding, and fouling, leading to the ingress of aggregates that reduce its efficacy [22, 23], ultimately causing component failure. These faults can affect track quality, therefore inspection and maintenance must be carried out to prevent these faults [24, 25]. Ballast is inspected directly using Non-Destructive Testing (NDT) such as visual inspection, laser [26], or radar [27], or implicitly by measuring track geometry and studying ballast degradation [28]. Ballast maintenance routines include tamping, cleaning, stone-blowing, and re-ballasting [24]. However, these routines can also damage the ballast, causing degradation over time [29] and restricting the maintenance activities that can be carried out [25, 28]. Different maintenance strategies are commonly applied to minimize intervention on the track, aiming to minimize costs and ballast damage, thus maximizing the availability and life of the track [29, 30].

Slab tracks are used for high-speed railways and in passenger stations in many countries, since they tend not to be as noisy as ballasted tracks, although they are more expensive to produce, install, and repair [31]. As they are made of concrete and mortar, their failure modes are similar to concrete sleepers: cracks, abrasion, and chemical corrosion [32]. Inspection is carried out using the same NDTs as for the ballasted track.

The subgrade is the track layer dedicated to supporting the rest of the layers and draining water [33]. Faults associated with the subgrade are shear failure, plastic deformation or settlement, and mud pumping, and their most notable effects are track deterioration, as well as the formation of wet spots. Subgrade inspection is mainly performed via ground penetrating radar [34, 35], as it allows the subgrade condition to be studied without damaging the infrastructure and can be performed from inspection vehicles [36].

Turnouts, or switches and crossings (S&Cs), are track substructures that allow two tracks to merge or to split, hence allowing vehicles to switch from one track to another depending on the direction of travel [7]. Common failure modes in S&Cs are cracks, wear, settlement, voiding, deformation and ultimately breakage, causing the same effects as stated in the paragraphs on rails and ballast [22, 37]. Up to 17% of the track maintenance and renewal budget is dedicated to S&Cs [37], without considering the costs derived from disruption and delays due to their complex monitoring and maintenance [29, 38]. Turnout inspection is carried out via visual sensors (laser scanners), geophones, and inertial sensors, among others [39, 40].

Transitions connect regular track segments with different infrastructures, such as level crossings [41], tunnels, or bridges [42]. Due to the change in track types, transitions often suffer from larger displacements and quicker degradation than regular tracks [43, 44], and thus require more frequent inspection and maintenance than regular track sections [45, 46]. These inspection and maintenance tasks are carried out to detect the faulty component or layer.

In summary, track components are designed to support vehicles passing by for long periods, thus subject to large static and dynamic forces that may cause them to fail, causing safety issues. It is then necessary to inspect all of them regularly to prevent failures and monitoring the degradation and health of track components is essential for track maintenance. The next section considers vehicle components and their related fault modes.

1.3. RAILWAY VEHICLE COMPONENTS AND FAULTS

Railway vehicles run on tracks, transporting passengers and goods, and are roughly divided into passenger, freight, empty coaching stock and inspection vehicles. The basic structure of any railway vehicle is divided into wheelsets, primary suspension, bogie, secondary suspension and cab; with variations on component design depending on model, application and vehicle type.

Wheelsets, composed of wheels and axle, are in direct contact with the rail surface and withstand the forces and vibrations in the wheel-rail interface. Wheel faults are mostly wheel flats, fatigue-related faults, geometry changes [47, 48], metal build-up, and corrugation; generally caused by differential wear or thermal expansion and poor driving [49, 50]. Axle faults are generally related to pitting corrosion and, less commonly, to fatigue [49]. Monitoring techniques applied to wheelsets are wheel flat detectors, wheel impact monitors and profile measurement systems [51, 52]. Figure 1.5 shows an example of damaged wheels.



FIGURE 1.5. EXAMPLES OF DAMAGED WHEELS SHOWING ROLLING CONTACT FATIGUE.

Bearings are complex pieces vital for the functioning of rotary machinery – are made of race and balls, and come in a wide variety of types, in which the most important faults are related to lubrication issues [53]. Common NDTs for bearing monitoring are hot box detectors, accelerometers, acoustic sensors, strain gauges, optical or visual sensors, and eddy current sensors [54].

Bogies are the structures in charge of supporting the vehicle mass, dampening vibrations produced by wheel-track interactions, and providing traction or braking to the system [55]. Most research on the bogie system focuses on fault monitoring of suspension, brakes or wheelsets, as they are more prone to failure [56]. Bogie frames mostly suffer from mechanical fatigue [57], hence most research is oriented towards fatigue detection and prevention. Bogie frames are commonly inspected via vibration sensors [58, 59] and ACFM [60].

Railway vehicle suspensions are divided into primary (between axlebox and bogie) and secondary (between bogie and car body). The primary suspension is designed to maintain the contact between wheel and rail, whilst the secondary suspension is dedicated to keeping the bogie and cab stable and isolated from vibrations caused by irregularities on the track [61]. Vehicle suspensions are traditionally modelled as a system of springs and dampers with varying complexity and degrees of freedom depending on the application [62, 63]. Suspension systems are mostly monitored with inertial sensors [64], in which faults related to the damping system are the most common ones [65], with resonances ranging from 0.1 to 10 Hz [66]. Vehicle-track interactions are influenced by the vehicle suspension and track condition. Hence, dynamic vehicle-track interaction models are developed to study the effects of these interactions, generally modelling the system as a set of interconnected springs and dampers [62, 63]. Dynamic models study the suspension, as it connects the wheels to the bogie (primary) and the

bogie to the cab (secondary), partially dampening the vibrations and forces transmitted from the track-train interaction [67, 68].

The vehicle car body is the structure in charge of transporting passengers and goods, thus cab types are separated by the cargo transported in them. Current practices focus on modelling the cab structure and finding its vibration modes usually via Finite Element Modelling (FEM) and simulations [62, 69].

To sum up, railway vehicles are complex structures that must transport passengers and goods securely. Wheelsets and suspension suffer the highest loads as they directly interact with tracks that are not always in optimal condition. Material wear and tear make necessary frequent and deep inspection of all components to avoid negative and even catastrophic consequences. Similar to the previous section, here the most common faults and inspection methods associated with each major vehicle component have been introduced to provide a context for this thesis.

1.4. COMFORT

According to ISO 2631 [70, 71], "In railways, comfort is understood as a compound of sensations (noise, vibrations, temperature, humidity, seating quality) perceived by passengers that affect the experience of travel". Since the focus of this thesis is on condition monitoring using inertial sensors, only vibration is considered for comfort. Research explaining the influence of comfort based on noise, pressure, or temperature amongst, others can be found in [72-74]. The ISO 2631 standard is the basis for EN 12299 [11], and both are applied to evaluate the effects of comfort based on vibrations on railway passengers. Another method to evaluate comfort is the Sperling index [75-77], although not as common as the standards as its use is not extended in European railways. All methods propose thresholding levels to evaluate ride

comfort but, as this is heavily influenced by the passenger perception and expectations, these values are only indicative and serve more as a qualitative than a quantitative indication of comfort. The main comfort indices and their use are presented in this section. A deeper explanation of these comfort indices and their applications is presented in Appendix A. Comfort indices.

Both ISO 2631 and EN 12299 use different frequency weighting functions depending on the location of the passenger and the application (comfort, health or motion sickness). ISO 2631 uses directly the weighted acceleration ($a_W(t)$) as a guide for comfort, providing Table 1.1 as a reference.

TABLE 1.1. COMFORT PERCEPTION REFERENCE FOR ISO 2631-1 [70].

$a_W(t) \leq 0.315\ m/s^2$	Not uncomfortable
$0.315\ m/s^2 \leq a_W(t) \leq 0.63\ m/s^2$	A little uncomfortable
$0.5\ m/s^2 \leq a_W(t) \leq 1\ m/s^2$	Fairly uncomfortable
$0.8\ m/s^2 \leq a_W(t) \leq 1.6\ m/s^2$	Uncomfortable
$1.25\ m/s^2 \leq a_W(t) \leq 2.5\ m/s^2$	Very uncomfortable
$2\ m/s^2 \leq a_W(t)$	Extremely uncomfortable

BS 12299 calculates the Root Mean Square (RMS) acceleration labelling the resulting indices as continuous comfort indices. Comfort evaluation is separated into three types: continuous, mean and event-based; the latter is subdivided into comfort in discrete events and comfort in curve transitions. The reference for continuous comfort according to EN 12299 is presented in Table 1.2, defined only for lateral comfort (C_{Cy}) and vertical comfort (C_{Cz}). Longitudinal comfort (C_{Cx}) can also be calculated, but it is not used for continuous comfort evaluation in the standard.

TABLE 1.2. COMFORT PERCEPTION REFERENCE FOR EN 12299 [11].

$C_{Cy}(t)\ ,\ C_{Cz}(t) < 0.20\ m/s^2$	Very comfortable
$0.20\ m/s^2 \leq C_{Cy}(t)\ ,\ C_{Cz}(t) < 0.30\ m/s^2$	Comfortable
$0.30\ m/s^2 \leq C_{Cy}(t)\ ,\ C_{Cz}(t) < 0.40\ m/s^2$	Medium
$0.40\ m/s^2 \leq C_{Cy}(t)\ ,\ C_{Cz}(t)$	Less comfortable

EN 12299 also provides two methods to evaluate comfort over longer periods, named standard method (N_{MV}) and complete method (N_{VD}). The standard method considers only acceleration measured on the vehicle floor, whilst the complete method considers both measurements on the floor and the vehicle seat. The reference scale for mean comfort is presented in Table 1.3.

TABLE 1.3. REFERENCE FOR THE MEAN COMFORT INDICES [11].

$N_{MV} < 1.5$	Very comfortable
$1.5 \leq N_{MV} < 2.5$	Comfortable
$2.5 \leq N_{MV} < 3.5$	Medium
$3.5 \leq N_{MV} < 4.5$	Uncomfortable
$4.5 \leq N_{MV}$	Very uncomfortable

There is a third type of indices considered in the standard EN 12299, denominated event-based comfort, and divided into discrete events and curve transitions. The standard understands comfort on discrete events (P_{DE}) as the sudden change of the feeling of ride comfort due to local track irregularities, and comfort on curve transitions (P_{CT}) as the sudden change of the feeling of ride comfort due to vehicle behaviour on interactions with compound curves. In this case, the indices are defined as the percentage of passengers dissatisfied with comfort on the discrete event or curve transition.

The standard ISO 2631 also covers passenger perception, health and motion sickness derived from vibration. Passenger vibration perception is considered as a threshold value of 0.015 m/s^2,

whilst both health and vibration indices are determined through a dose value. Passenger health is determined by the weighted acceleration over time as explained in detail in Appendix A.

Motion sickness is also defined based on the dose value over the whole journey, with the index representing the total amount of people who may vomit. The standard explains that this index is primarily applied for ships and that the prevalence of symptoms is likely to vary between individuals and due to adaptation.

To provide an approximate comparison between indices, Figure 1.6 presents the normalised values of the comfort indices against each other, where C_C^{max} and N_{MV}^{max} correspond to the continuous and mean comfort indices according to the standard EN 12299, and a_W^{max} corresponds to the comfort perception reference for ISO 2631.

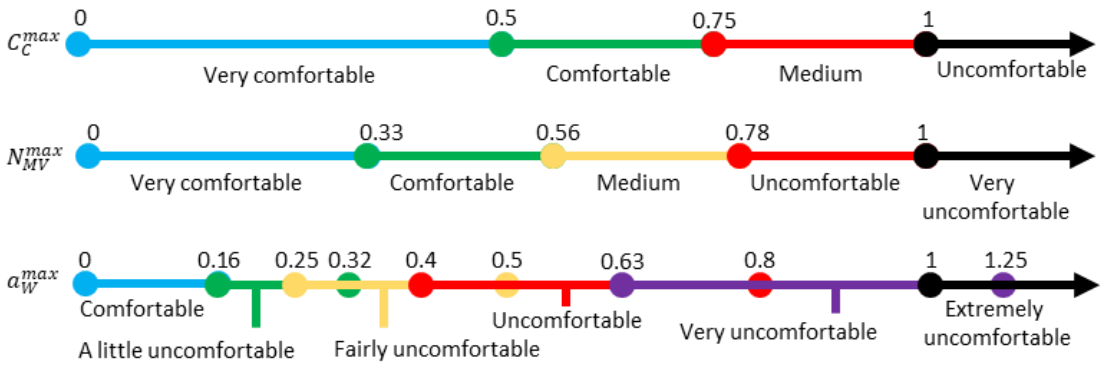


FIGURE 1.6. COMPARISON BETWEEN COMFORT INDICES.

These indices are obtained via different methods, mostly between the standards and the Sperling index, so an exact comparison is not presented here, but in a further chapter of this thesis. Studies found compare the standards and the Sperling index under different circumstances [75, 78, 79]. Amongst the findings, the Sperling index is always larger than the EN 12299 indices [75, 80]. Dumitriu and Leu [78], and Kim et al [79] attempted to establish a correlation between comfort indices and found that comfort indices values increase based on speed, although not

linearly, and that their values also depend on sensor position, showing that passengers located above the bogie have the worst experience. Comfort is used to evaluate passenger experience, but it can also be used to identify vehicle or track faults [80]. Comfort indices can be applied to monitor track and vehicle conditions and degradation over time. It is also worth mentioning the influence of other variables on comfort, such as vehicle speed [81], the sensor location and orientation on the seats [82, 83], and exposure time [84].

The use of comfort in this work is to detect track quality changes and faults, and to analyse their influence on the car body and passenger experience.

1.5. POSITIONING IN RAILWAYS

Railway positioning systems, divided into trackside and onboard, are applied for different purposes. Positioning may be based on absolute coordinates provided by a GNSS system or relative to the track the vehicle is using.

Trackside vehicle localisation is generally aimed at locating vehicles on known track points or segments to coordinate them and avoid collisions, and vehicle identification by comparing signals measured to a reference [85, 86]. Common equipment for this purpose are balises, wheelset detection systems, and axle counting systems [87]. These systems are connected to the network operator to approximate vehicle location and coordinate vehicle operations through the different lines [86]. This trackside equipment may also be used to characterize vehicles and quickly inspect wheelset components [88, 89]. However, these systems are often capable only of locating the vehicle in a track segment instead of the actual position within that segment.

Common onboard positioning systems in railways are Global Navigation Satellite Systems (GNSS) and tachometers [86]. GNSS use a network of satellites to pinpoint the position and

speed of a vehicle in an absolute frame with precision in the order of metres, although these systems are heavily dependent on signal availability and cannot provide position in some locations, such as tunnels [86, 90]. Amongst the most well-known are the United States GPS, the European Galileo, and the Chinese Beidou networks [90, 91]. Tachometers installed on railway vehicles measure speed using wheel rotation [92], although these systems often suffer slippage and wear [93, 94], making correction factors necessary for speed and distance estimation.

In summary, vehicle positioning systems are required for vehicle coordination, as well as to locate elements in the track. Current technologies have disadvantages such as inaccuracies or signal availability. Thus, there is a need for more accurate and robust positioning techniques. A novel method to estimate distance is presented in Chapter 3 of this thesis.

1.6. HYPOTHESIS AND OBJECTIVES

The ride quality of passenger trains is significantly influenced by various factors such as track geometry, specific track-related components, vehicle speed, driver style, and the performance of the train suspension system. Train drivers have a perception of travel influenced by these factors and their expectations, and produce inaccurate reports on both the state of the track (e.g.: drivers passing over bridges often do not report rough ride as they expect poorer track condition), and the location of the issue due to the delay between the event occurring, the reaction time, and the event reporting. The main hypothesis is that sensors onboard in-service vehicles can provide useful information about the state of the track through its effect on ride quality, that could be used to substitute driver rough ride reports, thus providing more consistent monitoring of track condition (at least from the point of view of rough ride).

To test this hypothesis, the work has been divided into the following objectives:

1. **Localisation of Track Irregularities using in-service vehicles:** To identify accurate positions of track irregularities in tunnels and areas with poor Global Navigation Satellite System (GNSS) signals, as driver reports are at inaccurate locations and accurate positioning allows to detect issues more consistently.
2. **Assessment of Ride Quality and Passenger Comfort using in-service data:** To employ inertial sensors to evaluate ride quality and passenger comfort, and to investigate the impact of different track types and track features on inertial measurements considering working conditions.
3. **Evaluation of Sensor Placement:** To examine variations in signals received based on the position of sensors within the train, and to analyse how the placement of sensors influences the quality and reliability of data collected.
4. **Effects of Track Quality on Vehicle Movement and Perception:** To assess the influence of track quality on vehicle movement, and to compare results obtained through comfort standards with reported issues such as Driver Rough Ride Reports (DRRRs) to gauge the impact of track condition on ride quality perception.

1.7. THESIS STRUCTURE

The structure of this thesis is as follows:

The literature review is presented in Chapter 2, explaining the state of the art of current railway inspection and monitoring techniques, which focuses on onboard inspection and monitoring. It also covers trackside monitoring and vehicle location.

A novel method to estimate vehicle speed and distance is developed and explained in Chapter 3. This chapter describes the equipment and test conditions used for the tests. The method to estimate speed is based on frequency analysis, extracting information from the inertial signal harmonics, and additional distance correction is carried out using crosslevel from the signal and a reference provided. This method is compared to cross-correlation and dynamic time warping, and the use of cross-correlation is added to increase its accuracy. This method is applied to align signals and compare data in the following chapters.

Chapter 4 presents a comparison between comfort indices for different case studies. The standards ISO 2631 and EN 12299 are compared to evaluate the most adequate for each situation. Two types of tracks (ballasted and slab track) are analysed, and a comparison between them is provided.

Chapter 5 and Chapter 6 present two case studies using inertial sensors on the axlebox, bogie and cab of a high-speed train. The case study in Chapter 5 shows the differences between the measurements depending on the position on the train, i.e., axlebox, bogie and cab, the direction of travel, and the location of sensors inside the vehicle, after secondary suspension. Chapter 6 Chapter 6shows the effects of an S&C on the vehicle components, as well as the effects of tamping operations and a wheel flat on ride quality.

Chapter 7 addresses the issue of correlating track quality issues with poor ride quality. Several case studies are discussed, comparing reports provided on poor ride quality with data acquired from in-service vehicles. The relationship between these reports and ride quality indices is discussed further in another section of this chapter.

Chapter 8 presents a summary of the main achievements of the thesis, and a discussion on the hypothesis validity and the achievement of the objectives. Additionally, publications derived from the thesis are listed.

Chapter 2. Literature Review on In-service Railway Monitoring

2.1. INTRODUCTION

Condition monitoring is a major component of predictive maintenance, aimed at developing and scheduling actions to be taken to prevent, identify or mitigate faults and failures. These activities save money, prevent delays and, ultimately, increase the life cycle of the monitored assets. Monitoring and maintenance operations are split in the introduction depending on monitored systems (track or trains) and by the inspection equipment location (onboard or trackside). There are then four scenarios considered for railway monitoring, summarised in Table 2.1. Knowing the location of the vehicle along the track is also needed for comparison and degradation monitoring, hence different vehicle location techniques are discussed in this chapter.

TABLE 2.1. IN-SERVICE RAILWAYS CONDITION MONITORING SCENARIOS.

System / Location	Track			Vehicle		
	Requirements	Advantages	Limitations	Requirements	Advantages	Limitations
Track	Sensors on track sections (S&Cs, transitions, bridges…) or long lengths of track	Detailed inspection of specific parts of track	Numerous sensors required, can be costly when applied to large sections	Sensors on concrete sections of track, short lengths of track and relatively few sensors	Frequent inspection of vehicle	Only possible to inspect wheel-track interaction and basic vehicle monitoring
Vehicle	Sensors on components of the vehicle (cab, bogie, axlebox)	Frequent inspection of track	Inspection of track condition subject to vehicle frequency and affected by vehicle behaviour	Sensors on components of vehicle	Deep inspection of the vehicle, separated by components	Harsh monitoring conditions, difficult placement of sensors

A distinction between monitoring and inspection is necessary before the review depending on the test conditions and purpose of research. In this regard, monitoring is considered as the set of actions aimed at observing railway assets for a period to observe their evolution and possible degradation, whilst inspection is a deep examination of the assets to evaluate their condition at a moment in time. The following sections present the state of the art on railways monitoring and inspection, either from the vehicle or from the track, and vehicle location.

2.2. TRACKSIDE MONITORING AND INSPECTION

There is a wide variety of sensors applied for trackside monitoring and inspection, and amongst them, the most common are accelerometers and geophones for measuring track deformation and vibration; strain gauges; visual for wheel inspection, electromagnetic; and acoustic for

wheel and bearing inspection [13, 85]. Ultrasound sensors are the most common for inspecting rails both from the track and from the vehicle [95] , concretely the rail head [13, 96].

Track monitoring includes observing track layers and their associated geometry, and their evolution over a certain period, or evaluating their dynamic response to vehicles passing over determined track sections. Sensors applied for track monitoring and inspection depend on the component: rails are commonly inspected using acoustic, magnetic and visual sensors [96]; sleepers are monitored using visual sensors, inertial sensors and geophones [39, 85]; ballast is inspected using particle analysis and studying its dynamic behaviour [25, 26]; and the subgrade is inspected via ground penetrating radar [35, 97]. Changes in lower layers affect the behaviour of the rest of the track and its stiffness; issues in these layers can be detected using inertial and vibration sensors [98-100]. Other track components such as S&Cs are monitored using inertial sensors [41] to analyse their dynamic behaviour. In summary, many sensors are applied for trackside monitoring and inspection; each sensor provides different advantages and disadvantages and thus is applied for different track layers or components. Amongst them, inertial sensors are the most versatile, as they can be used for assessing the condition of different layers.

The study of track dynamic behaviour focuses on analysing track response to vehicles passing by, and determining track parameters. The most important parameters used for track dynamic behaviour assessment are lateral and vertical movements [68, 101], and deflection [43, 45, 102] using inertial, visual sensors or geophones. Dynamic modelling is performed considering the track and the train as a set of interconnected masses, dampers and springs reacting to the effect produced by vehicles passing over them [42, 103, 104].

Trackside vehicle monitoring and inspection equipment is mostly applied to the wheelset, usually wheels and bearings [105, 106]. Wheels are inspected using acoustic, inertial and visual sensors [54, 107, 108]. Regarding bearings, thermography, acoustic and inertial sensors are most commonly used [106, 109]. Frequency and signal analysis are frequently applied for signal analysis on both components [110, 111], as the most extended sensing techniques are inertial and acoustic.

In conclusion, trackside monitoring focuses on long-term track state measurement and track dynamic behaviour, as well as vehicle wheelset inspection. Accelerometers, magnetic, and acoustic sensors are the most used ones as their technologies are well developed and provide a wide range of uses. Amongst them, inertial sensors are the more versatile. These sensors can be applied for track and vehicle inspection, as well as for analysing track dynamic behaviour. The following section presents sensors applied for onboard inspection and monitoring.

2.3. ONBOARD MONITORING AND INSPECTION

Vehicles, both dedicated and in-service (passenger or freight), with sensors installed on them, are used for inspection and monitoring. Dedicated measurement vehicles require skilled workers and traffic scheduling and allocation. Due to the restricted schedules for inspection and monitoring, dedicated vehicles are mostly used for track inspection. Research on the use of in-service vehicles is focused on monitoring, as they already use the track frequently and data acquired can be used for assessing track degradation. The following sections discuss the applications of sensors on in-service railway monitoring and inspection, divided into track and vehicle component monitoring and inspection.

2.3.1. Track monitoring and inspection

Track inspection and monitoring are usually carried out by in-service vehicles or dedicated measurement fleets. Dedicated vehicles are equipped with a wider variety of sensors than in-service vehicles, which allows for more in-depth inspections. However, these vehicles require dedicated scheduling and workers, which limit their use [112]. Early examples of dedicated vehicles are the design by Elmer Sperry in the 1920s [113] capable of detecting internal rail defects using an induction system; or Hronik *et al*. in the 1970s [114], estimating track geometry using capacitive probes. Current inspection vehicles are divided into self-propelled vehicles, towed coaches and hi-rail vehicles [3, 4, 115], shown in Figure 2.1. These measurement units use technologies such as laser, image processing [116-118], ground penetrating radar, ultrasounds and electromagnetic sensors [3].



FIGURE 2.1. SELF-PROPELLED VEHICLE (LEFT), TOWED COACH (CENTRE), AND HI-RAIL VEHICLE (RIGHT) [4].

Because of technological advances, sensors can be small enough to be easily installed on in-service vehicles, so the measurements will be more frequent than compared to dedicated vehicles. However, depending on where the equipment is installed, the sensors may have to cope with harsh environmental conditions, such as those in the axlebox or the bogie, where sensors can be exposed to high vibration levels up to 144 m/s^2 RMS at the axlebox level or 31 m/s^2 for bogie-mounted equipment [119] for long periods.

Research on the use of in-service vehicles focuses on both short- and long-term maintenance. Short-term maintenance focuses on track inspection and fault detection, as well as maintenance and repair planning, whilst long-term monitoring focuses on detecting track degradation and faults developing over longer periods. The most used sensors for track monitoring are inertial (accelerometers and gyroscopes), optical (cameras and laser), acoustic (generally ultrasonic) and magnetic (eddy current sensors) [96, 98, 120, 121].

Inertial sensors, namely accelerometers and gyroscopes, measure acceleration or rotation rate, respectively. Their use in railway track inspection is relatively recent [96, 120]. Depending on the location of the sensors, different information can be extracted: sensors installed on the axlebox and bogie are applied for assessing track condition [122-124], extracting track geometry parameters such as alignment [81, 125, 126] or crosslevel [127-129], and detecting issues such as voiding [130-133], and assessing the condition of track components such as crossings [134, 135] or structures such as bridges [136-138]. Sensors installed on the cab can also be used for track quality monitoring [125, 139-141] or for evaluating passenger comfort [75, 81]. Inertial sensors are broadly used and merged with other sensors such as Global Navigation Satellite Systems (GNSS). Depending on the component the sensors are installed on (axlebox, bogie, suspension, cab), different information can be extracted, such as wheel-track interaction, dynamic effects of suspension, or comfort.

In summary, onboard track monitoring and inspection are generally carried out using in-service vehicles, as their higher frequency allows to evaluate the evolution of the track. Issues such as sensor installation in the vehicle must be considered, as they may affect the measurements. Amongst the most commonly used sensors, inertial sensors are the most advantageous, due to their robustness and versatility. Signals acquired from the installed sensors are commonly

combined to overcome the limitations that a single type of sensor may have, thus providing more complete information on the track condition.

2.3.2. Onboard vehicle component monitoring

Railway vehicles are complex systems with a wide variety of components with different characteristics and requirements depending on the harshness of the environment. The different sensors and techniques applied for condition monitoring are discussed in this subsection.

Vibration sensors can help to identify any harmonics or resonances that indicate faults or changes in the behaviour of components such as the wheels, bearings or suspension. Sensors applied for wheelset monitoring are commonly installed on the axlebox [142-144], and dedicated to bearing and wheel fault detection and monitoring. Their behaviour is generally analysed using frequency and statistical analysis tools, such as harmonic detection, cepstrum analysis and kurtosis analysis [142].

In short, the most commonly used sensors and techniques for vehicle component monitoring are magnetic, acoustic, thermal, visual and inertial [54, 145] for brakes, pressure sensors [146, 147] for the power system, voltage measurements [148, 149] for the suspension, inertial and dynamic models [62, 150, 151]; and for the cab, modelling [69, 152].

Onboard component monitoring is applied by instrumenting vehicles and evaluating their condition over time. Inertial sensors are the most versatile, as they can be used for many components. Other sensors, such as visual, acoustic or thermal, can only be applied to certain components and conditions, thus limiting their usefulness. Due to the dynamic behaviour of the system, considering resonance frequencies may be useful to associate faults with certain components. Identifying the position of vehicles and elements in tracks is also necessary for

monitoring and inspection, and as such, the following section summarizes the techniques applied for vehicle and element localisation in railways.

2.4. VEHICLE LOCATION AND POSITIONING

Railway positioning systems, as discussed in the introduction, are applied for the localisation of vehicles along the track, elements that require inspection, and vehicle coordination amongst the lines. The focus of this section is on current techniques applied for onboard vehicle positioning, the use of sensor fusion for improving the estimation, and signal alignment.

Railway vehicles are commonly equipped with tachometers, that estimate speed using wheel rotation rate multiplied by the wheel circumference, and odometers, that estimate distance travelled using the pulses per revolution and circumference [92]. Wheel slippage and wear affect the estimated distance and speed, hence a correction factor is applied for improving the estimation. Combinations of their estimations with estimations from other devices, such as inertial sensors or GNSS receivers, are also used to improve their estimation [93, 94].

Signals from inertial sensors for position and speed estimation are often combined with other sensors using Kalman filters [153-155], as the combined estimations are improved and the errors reduced. The basis of the Kalman filter is explained in Appendix B. Kalman filter, and the use of the Kalman filter in this work is detailed in Chapter 3. Combinations of inertial sensors with odometers and tachometers reduce the odometer and tachometer error in varying adhesion conditions whilst the use of odometers and tachometers compensates for signal noise from the inertial sensors [156-159]. Combinations with GNSS receivers (such as GPS [160-163], BeiDou [164] or Galileo [165]) associate the vehicle speed and position with the geographical location of the vehicle on the track [90].

Probabilistic methods for GNSS and IMU integration are proposed by the German Institute of Communications and Navigation, in publications by García Crespillo *et al.* [161] and Heirich *et al*. [128, 166], using a Bayesian approach and particle filters. They tested the accuracy of their model under different conditions, and observed a heavy dependency on the available number of GPS satellites, as well as distance estimation errors in the IMU data that increase quadratically with time and distance when there is no GPS signal available. Signal correlation is also applied, using sensors located at different positions of the vehicle to calculate the vehicle velocity from the time difference between signals received for the same track element [167].

Map matching approaches combine GNSS data and odometers [168] or GNSS and inertial sensors [154, 155] to estimate both the distance along the track and the geographical position of the vehicle. The use of track irregularities [169] or track features [170], such as S&Cs or curves to associate the position of the vehicle to the track is also found in literature.

Regarding visual sensors, Li and Siu [171] developed a location system based on a single camera, focusing on varying speeds and scenarios. Their method is divided into two parts: key frame identification, in which the filter is trained and identifies the referencing frames of a determined route; and scene recognition and tracking, in which the system identifies the scene, considering if the speed is varying or not. Möckel *et al*. [172] developed an obstacle detector based on active (video cameras, LIDAR and RADAR) and passive (fixed camera) visual sensors. To evaluate their system, they compare their results to a modelled human driver, obtaining better detection probabilities in low light conditions as well as small and medium distances. Other sensors based on visual data are LIDAR, RADAR and Doppler [173, 174], which are used to detect obstacles and estimate vehicle speed based on their relative change in position of such obstacles.

To summarise, vehicle location is necessary to ensure functional comparison from run-to-run measurements which can help to identify the degradation and lead to optimised maintenance of railway vehicles and tracks. However, inaccuracies in the positioning of the fault may arise when reporting data, due to the criteria employed for the fault localisation or the reaction time of the driver. It is necessary to develop positioning systems that allow for precise fault localisation. Vehicle coordination is done via trackside equipment, considering track sections as blocks without providing precise vehicle location. The latter is done with onboard sensors such as tachometers, GNSS and inertial sensors. These sensors may suffer from signal availability, noise or delay, so sensor fusion is a powerful tool applied to overcome their issues. Data alignment is necessary to evaluate track evolution and degradation over time, with powerful algorithms developed for this purpose, although limited in the lengths available to align. This, and other methods for signal processing, is discussed in the following section.

2.5. SIGNAL PROCESSING

This section summarizes the methods applied for signal processing in the railway industry and research, with the focus on inertial sensors. These methods are categorised, according to Li *et al.* [175], into signal-based methods (time or frequency domain and correlation analysis) and model-based methods (such as Kalman and particle filters).

Signal-based processing using inertial sensors is commonly carried out by analysing the frequency domain of the signals. Resonances or frequency harmonics can be used to define which component is affected depending on the signal. Research by Connolly *et al*. [12] defined the range of frequencies in which each component is most affected, where vehicle resonances range from 0.1 to 30 Hz, and track resonances 40 to 30000 Hz depending on the layer, component or fault. Figure 2.2 summarizes the range for each component.

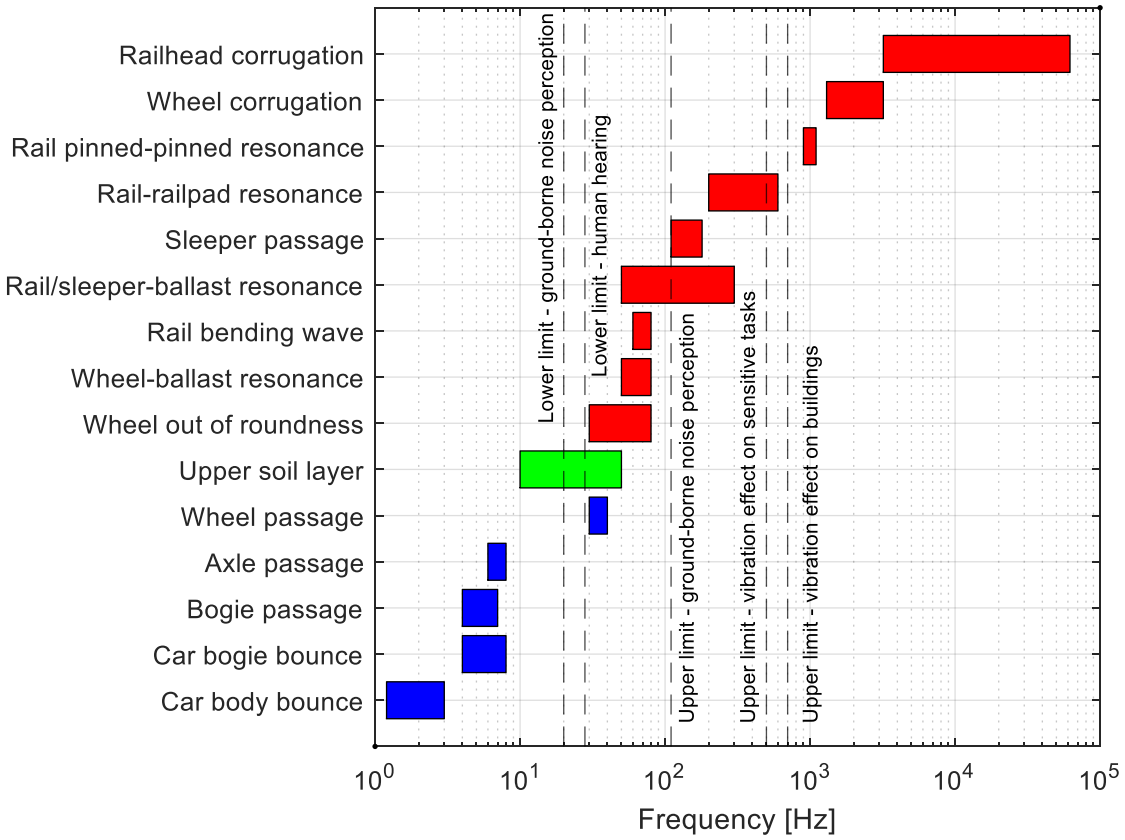


FIGURE 2.2. TYPICAL FREQUENCY RANGES OF EXCITATION, ADAPTED FROM [12].

Model-based monitoring consists of comparing the data to previously known models to identify the condition of either vehicles or tracks, or to model systems based on information extracted from the sensors. Suspension modelling is carried out by extracting information from inertial sensors, as the suspension state can be analysed through its dynamic behaviour [150, 151]. Common model-based methods using inertial sensors are suspension parameter estimation using software such as Matlab [67] and fault detection, mostly related to the dampers [64, 176].

Related to signal processing for railways monitoring is data alignment, most relevant when using onboard sensors, due to the differences in distance estimations provided by each vehicle and sensors. There are different approaches to overcome this, as explained by Palese *et al*. [177]. In that work, the authors explain the use of cross-correlation and dynamic time warping

as common methods, and explain their method, considering datasets as functions that are resampled according to a reference. The limitation found for this method is that it is lengths of track in the order of hundreds of metres, not usable for longer track sections. Khosravi *et al*. [178, 179] compared cross-correlation, dynamic time warping, alignment by Fourier transform and correlation-optimized warping, and proposed a method combining the last two, showing better results than the individual methods. Eklöf *et al.* [180] segmented track geometry parameters (such as vertical alignment and twist) and a tachometer to align runs, applying cross-correlation to segments of several hundreds of metres.

In short, signal processing methods are applied to extract information from sensors. Applied to inertial sensors, the most common methods are frequency analysis and modelling. The use of onboard sensors makes data alignment necessary for evaluating track evolution and degradation. So far, no methods have been found to align long sections of track, as the focus of research is on aligning short segments for maintenance and inspection.

2.6. CONCLUSIONS

In this chapter, a review of the most common applications of sensors for railway condition monitoring and vehicle positioning has been presented. The focus of the review is the use of inertial sensors onboard in-service passenger vehicles, although a context for trackside monitoring and other sensors has been provided.

Trackside monitoring techniques are usually applied for vehicle component inspection, mainly wheelsets. Component inspection is generally quick but shallow, and capable of detecting faults, although only when they are in an advanced state. Thus, earlier fault detection is needed for more efficient maintenance. Regarding track inspection, most activities focus on track

parameter characterisation. Trackside monitoring is inefficient and expensive for large sections of track, due to the number of sensors and the complexity of the installation procedures. Onboard inspection is preferred for longer sections, as information for the whole track is obtained, although not as complete as for data acquired from the track.

Onboard sensors allow to monitor large sections of track, although the depth of the inspection depends on the sensor, the vehicle speed, and the monitored asset. Generally, only the upper track layers and components are inspected, as lower layers require dedicated measurement vehicles or trackside equipment for site inspection. Thus, common faults and problems found using onboard sensors are associated with the rails, sleepers or ballast and can miss faults in lower layers, unless the faults have already affected the track alignment and can be detected by onboard sensors. It is necessary to consider the use of these types of sensors to obtain information from lower track layers indirectly, e.g., observing the evolution of track geometry and detecting issues that arise from its changes.

Inspection of vehicle components using onboard sensors allows for extensive inspection and monitoring, as the sensors can be installed on the selected component. Amongst the sensors used, vibration and acoustic sensors are the most common, as moving parts generate vibrations that can be analysed to identify their condition. Monitoring the resonance frequencies can be applied to certain components or faults, such as the vehicle suspension or wheelsets.

Vehicle location combined with onboard inspection allows to evaluate the state of the track on different points, to locate track faults reliably and to monitor the degradation of specific areas correctly. Alignment algorithms are necessary for evaluating degradation over time, although these are limited to certain track lengths. New methods to align longer track sections are needed for a more complete track monitoring and inspection. Apart from this, the use of reports from

the operators is beneficial as they provide information on the location and characteristics of the possible fault. However, these reports may be inaccurate, due to the response time and criteria of the driver to raise an issue, amongst other aspects.

Regarding sensors used, inertial sensors are the most versatile. These sensors are used due to their robustness, and versatility, as compared to sensors such as visual, acoustic or thermal. Thus, these sensors have been chosen to be used for acquiring data during this research. The following chapters demonstrate the use of inertial sensors on the axlebox, bogie and carbody of in-service vehicles for different purposes.

Chapter 3. Speed and distance estimation using onboard inertial sensors

3.1. INTRODUCTION

This chapter describes the use of inertial sensors on a passenger train to estimate vehicle speed and distance along the track. Track geometry parameters from a measurement train were used to assess the accuracy of the estimation. This chapter is based on previous research already published in Vehicle System Dynamics [181], of which the author is the main contributor as well as the lead author. The published research has been expanded with further improvements in the code and methodology. Other commonly used methods to align data are cross-correlation and dynamic time warping. Their use for this case is discussed in Section 3.5. of this chapter.

3.2. TRACK AND TEST CONDITIONS

The route on which tests have been carried out is a stretch of 90 km between Ashford International and London St. Pancras International stations. This route is divided into three sections of variable length and GNSS availability, as presented in Table 3.1.

TABLE 3.1. TRACK SECTIONS CHARACTERISTICS.

Section	Route	Distance [km]	Line speed range [km/h][182]	Maximum vehicle speed [k/mh]	GNSS availability [%]
1	Ashford-Ebbsfleet	54.2	230-300	264	94
2	Ebbsfleet-Stratford	27.1	216-230	226	47
3	Stratford-St. Pancras	9.2	0-230	216	20

The map of the route is presented in Figure 3.1, where the segments without GNSS signal, caused by tunnels, are marked with a white line. Sections 1, 2 and 3 of the track are indicated with a black, blue and red line, respectively. The segments without available GNSS signal correspond to tunnels, where the vehicle runs on a slab track.

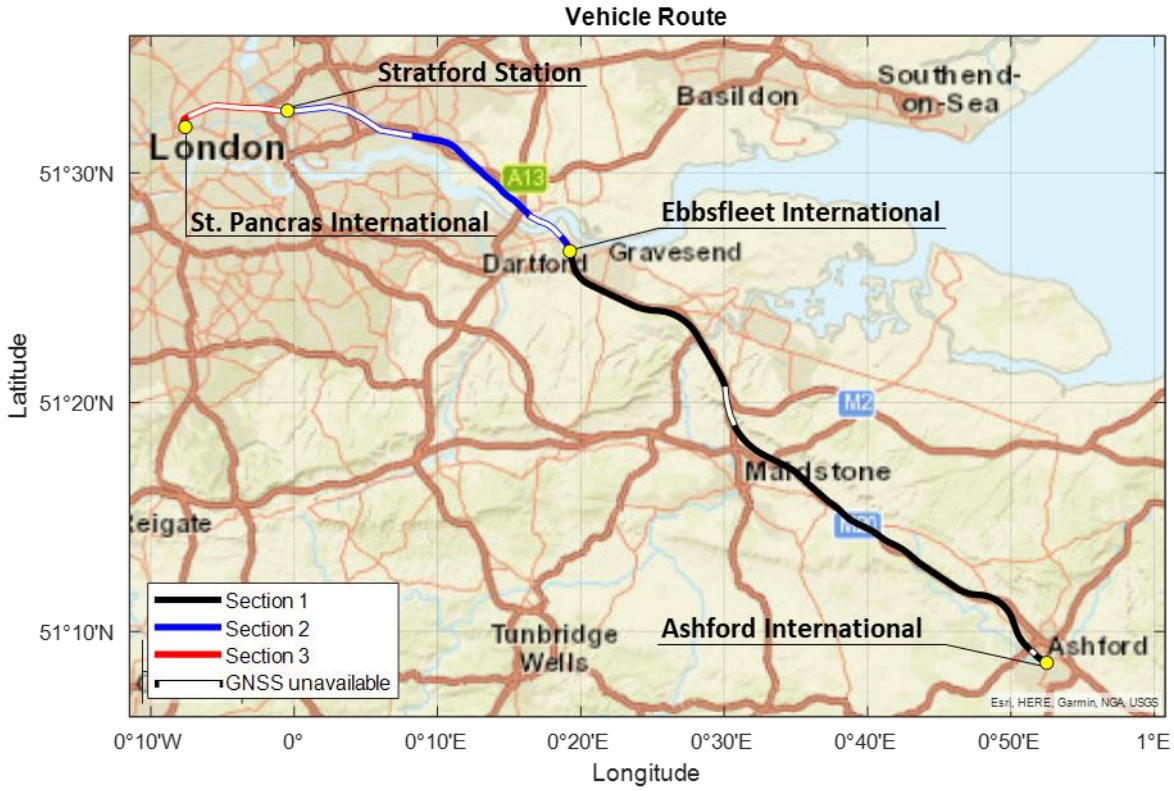


FIGURE 3.1. TRACK ROUTE AND STATIONS

The tests were carried out on a British Class 374 (Eurostar), equipped with sensors on the axlebox (A), the centre of the bogie (B) and the cab (C), on top of the bogie. The test device is based on a previous development by BCRRE [89, 126]. The leading axleboxes are equipped with vertically sensing accelerometers, acquiring data at a sample rate of 2500 samples per second. The bogie and the cab are each equipped with a GNSS receiver measuring latitude and longitude, speed and heading at 4 Hz, and an IMU with accelerometers and gyroscopes acquiring data in each direction at 250 Hz. The standards EN 14363 [183] and EN 12299 [11] require a minimum sampling rate of 200 Hz, so using a higher sampling rate provides a margin for measurements. Figure 3.2 shows the IMU reference system with respect to the vehicle. The X axis is the direction of travel, also referred to as the longitudinal axis in the text, the Y axis corresponds to the lateral direction, and the Z axis corresponds to the vertical direction of the plane.

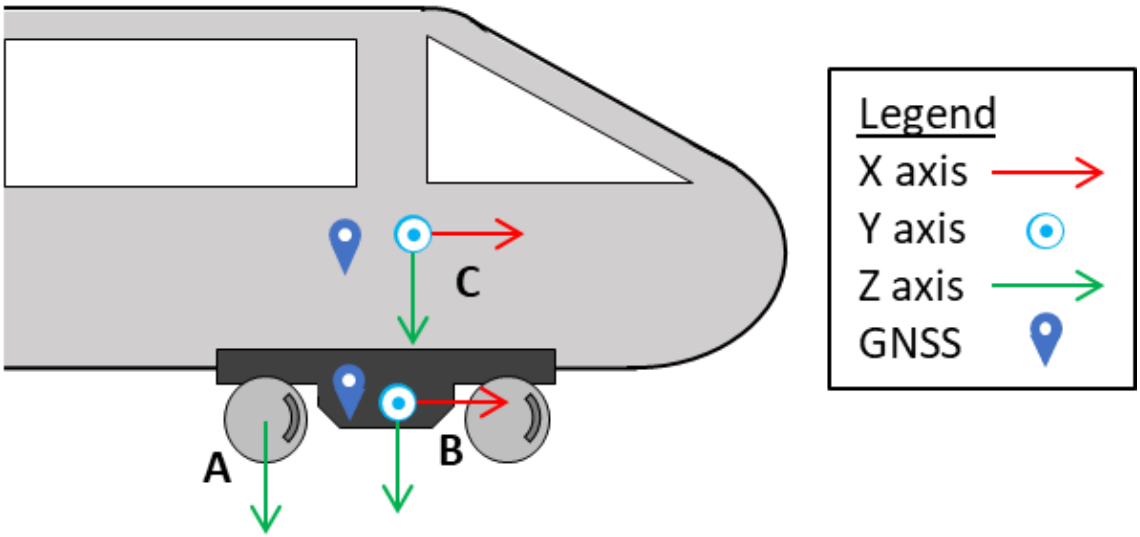


FIGURE 3.2. IMU AXIS SYSTEM WITH RESPECT TO THE VEHICLE.

No other sources of information from the train were provided for the measurements, in particular, the speed data was not available from the train tachometer.

3.3. SPEED ESTIMATION METHOD

This section describes the method developed to estimate vehicle speed using resonance frequencies, or harmonic content, observed in the inertial sensor signals. These harmonics are caused by vibrations transmitted from the wheels and track interactions, and from the wheels to the cab through the suspension [184]. Previous research has demonstrated the relationship between vehicle speed and vibration magnitude and frequency [143, 185], although its use to estimate speed in railway vehicles has not been discussed.

Figure 3.3 shows a comparison between the GNSS estimated speed and the spectrograms of the axlebox sensors. There are several harmonics showing a correlation to speed, and slight differences in the spectrum in tunnels (areas shaded in grey). The harmonic used for the study is believed to be generated by the track upper layers, and whose frequency and magnitude, as perceived by the vehicle, varies depending on speed [12]. Determining the causes of the phenomena is out of the scope of this thesis and this chapter, whose objective is to use the harmonic to estimate the vehicle speed and integrate it into the parameters applied to obtain distance. The figures presented to demonstrate the method are within Section 1, between Ashford International and Ebbsfleet International.

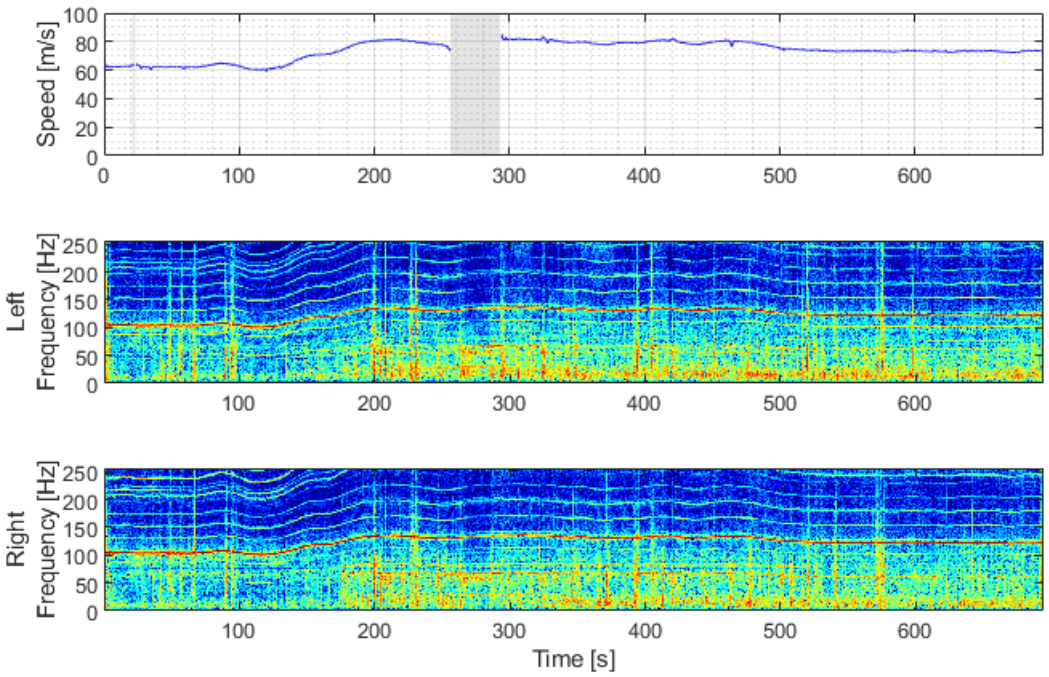


FIGURE 3.3. COMPARISON BETWEEN GNSS SPEED ESTIMATION AND AXLEBOX FREQUENCY SPECTRUM.

Prior to the speed estimation, the data from each sensor are aligned using the timestamps in the signals and selected to start and end in determined stations. Once the data are aligned, the spectrograms are obtained to identify the harmonics and their relationship to speed. Their time window is 1 s, and their overlap is 1/100 s. The lower frequency range of the axlebox spectrograms is presented in Figure 3.3, whilst Figures 3.4 to 3.7 show the spectrograms of the inertial sensors installed in the bogie and cab for their whole frequency range. Apart from the harmonic at 100 Hz, there is a general increase in the magnitude of the signal beyond 180 s, associated with the increasing vibrations due to vehicle speed [143, 185].

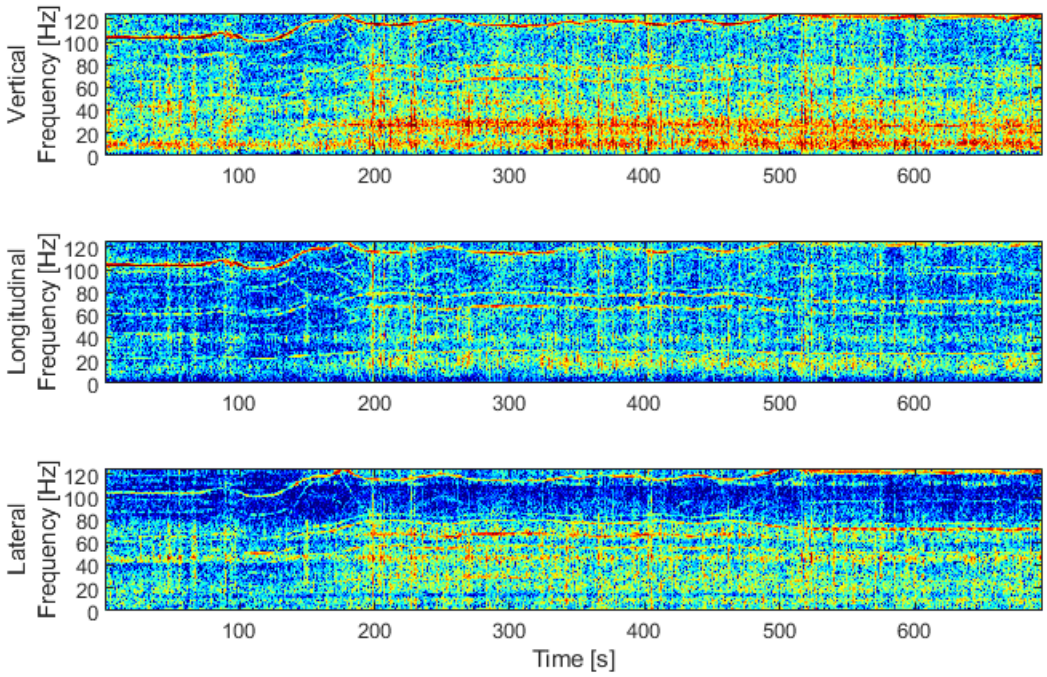


FIGURE 3.4. SPECTROGRAMS OF BOGIE ACCELEROMETERS.

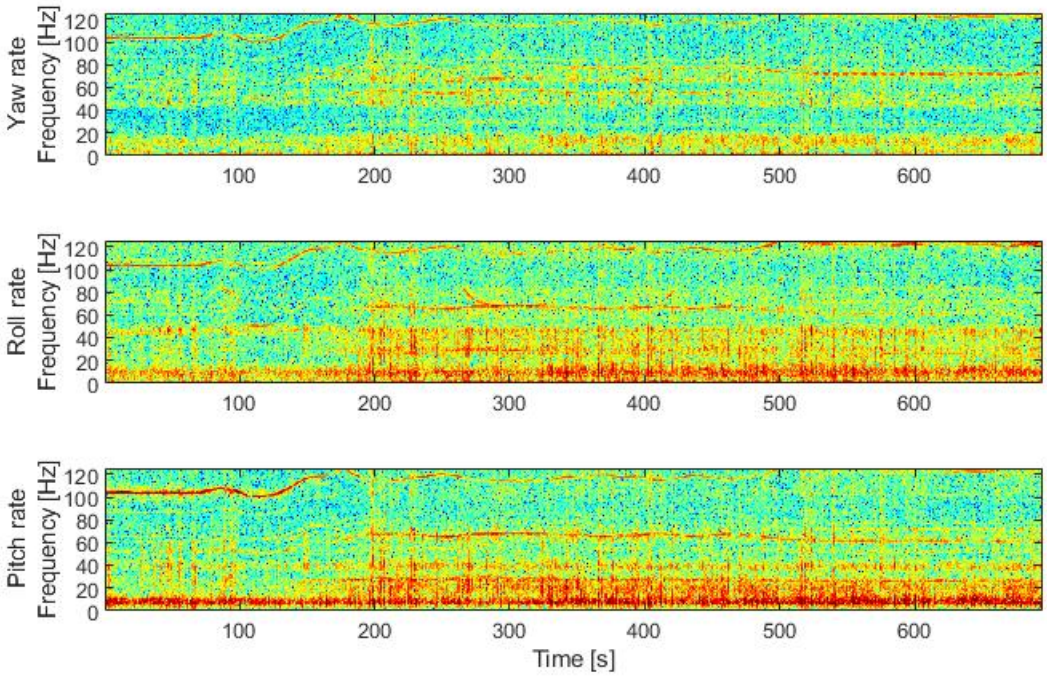


FIGURE 3.5. SPECTROGRAMS OF BOGIE GYROSCOPES.

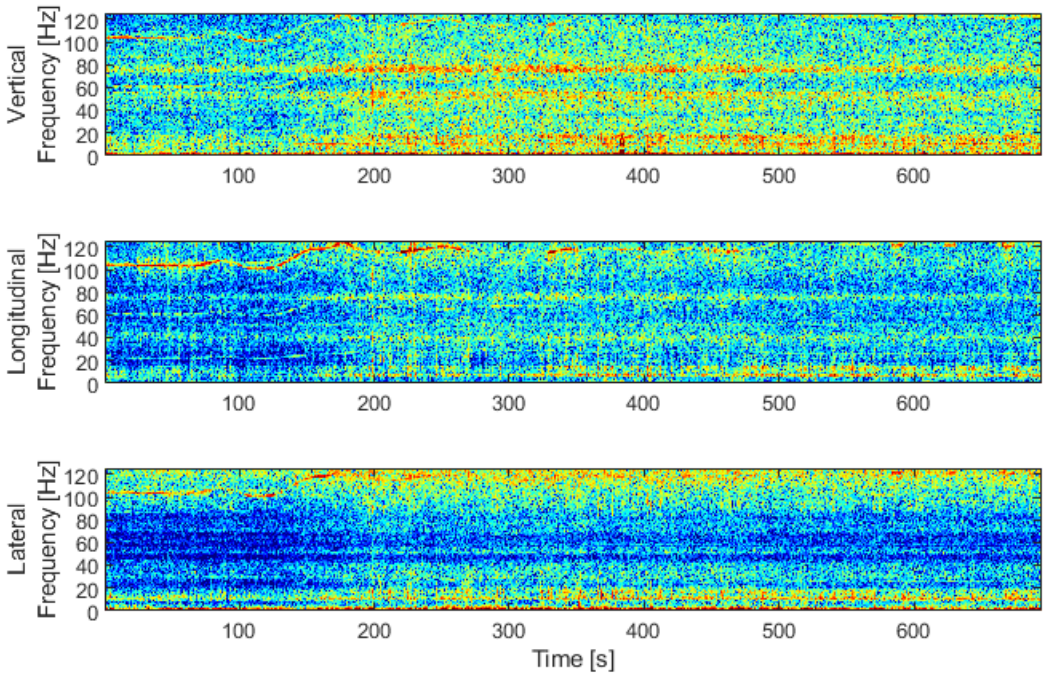


FIGURE 3.6. SPECTROGRAMS OF CAB ACCELEROMETERS.

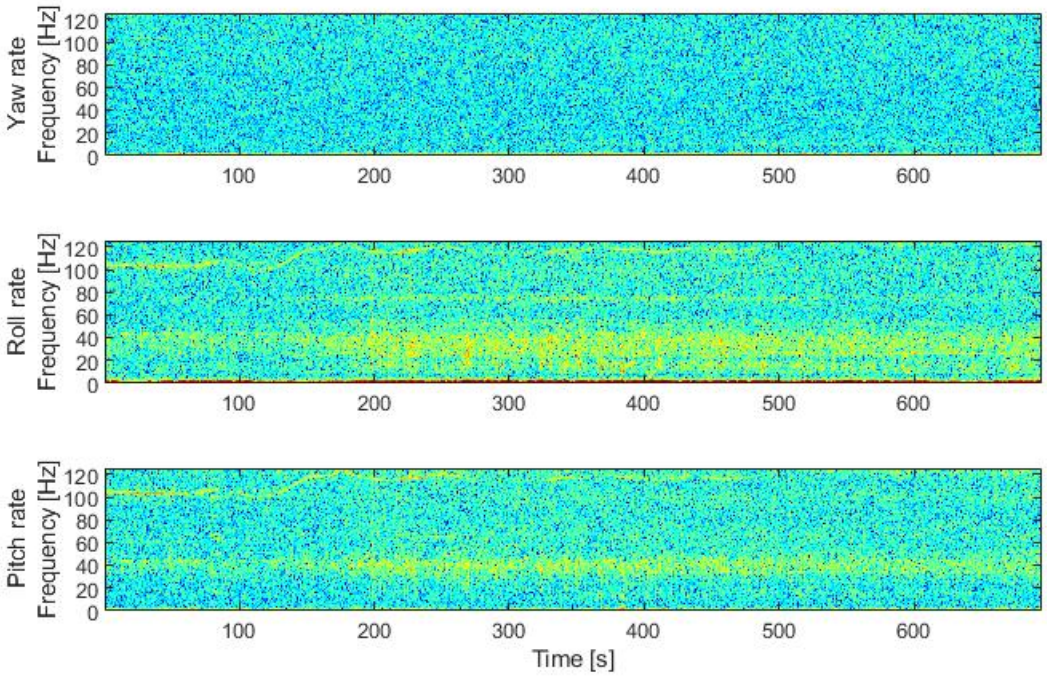


FIGURE 3.7. SPECTROGRAMS OF CAB GYROSCOPES.

The harmonic is observed in most of the figures, proportional to speed, with an approximate value of 100 Hz in this case. This harmonic is especially visible for the vertical acceleration in both the axlebox and bogie. The rest of the sensors show the harmonic, but its magnitude compared to the rest of the signal is too low to be considered for further processing. Thus, the harmonics on the vertical accelerometers are selected to estimate speed. The speed estimation is extracted by obtaining the highest frequency with a peak in the magnitude of the spectrogram and applying a low-pass filter to the signal to smooth the result.

Figure 3.8 shows the estimation for each of the vertical accelerometers. The estimations from the axlebox and the bogie are the most accurate compared to the GNSS speed, as the magnitude of the harmonic respect to the rest of the signal is proportionally higher for these components than for the cab. This is most likely due to the dampening effect of the vehicle secondary suspension, which filters out most of the frequency components of the vibrations above 120 Hz.

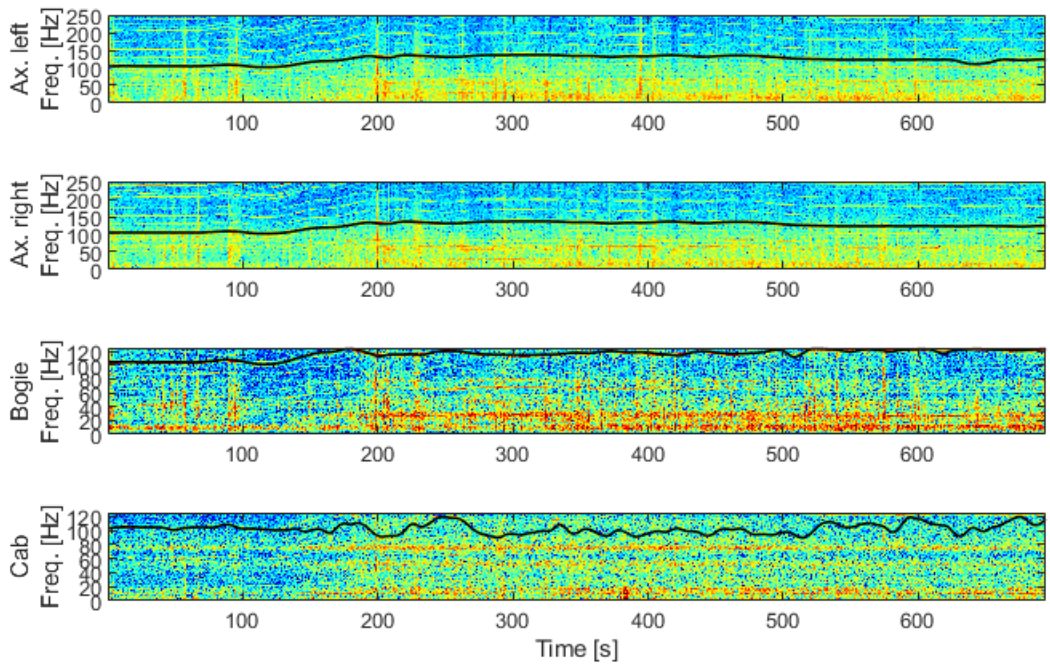


FIGURE 3.8. CURVE FITTING FOR SELECTED SIGNALS.

Due to the low magnitude of the harmonic in the cab beyond 200s compared to the rest of the signal, it is not possible to extract a reliable estimation of its value. The magnitude of the rest of the signal interferes with the estimation producing inaccuracies in the estimation. Hence, it is not applied for the estimation process.

Once the estimates for each signal have been obtained, the ratio between harmonic and speed is calculated by dividing the values of the harmonics by the speed curve at each sampling point (e.g. at a speed of 62 m/s, the value of the harmonic is 104 Hz), and averaging the values, obtaining a value of 0.596 m. This value is associated with the distance between sleepers on a ballasted track [186].

The estimates are then combined via a Kalman filter [153], whose mathematical basis is explained in Appendix B. Kalman filterAppendix B, using the bogie GNSS speed (v_{GPS}^{B}) and cab GNSS speed (v_{GPS}^{C}), and the estimation from the harmonics ($v_{H}^{AxLeft}, v_{H}^{AxRight}, v_{H}^{B}$) as measurements. All the units applied for the estimation are in the international system (metres, seconds…). The GNSS speed is not used where signal is unavailable, such as in tunnels. All the speed estimations are considered at this point because the combination of estimates reduces the error of the system [153, 187]. The longitudinal acceleration measured in the bogie (a_X^B) and cab (a_X^C) are considered as correction factors using the acceleration to obtain the change of speed over time, as presented in Equation (3.1).

$$\Delta V = \begin{bmatrix} a_X^B \\ a_X^C \end{bmatrix} \cdot \Delta t \ \ (ms^{-1}) \tag{3.1}$$

where the speed (V) is the differential of acceleration, applied to correct the previous estimation from the filter, and Δt is the time between the samples $\Delta t = 1/Fs$ where Fs is the GNSS sampling frequency of 4 samples per second, as well as the update rate of the Kalman filter. The signals from the inertial sensors have been downsampled to match the update rate of the

Kalman filter. This formula is then applied for the a priori prediction presented in Equation (3.2).

$$\begin{cases} x_{t+1}^{*} = A \cdot x_t + B_t \cdot u_t \\ P_{t+1}^{*} = P_t + Q \end{cases} \tag{3.2}$$

where x_{t+1}^{*} and x_t are the a priori and a posteriori predictions, respectively, which are the estimated vehicle speed in this case; Fs_B and Fs_C are the bogie and cab sampling frequencies, respectively; P_{t+1}^{*} and P_t are the a priori and a posteriori covariance matrices, respectively; and Q is the process noise covariance matrix. For this particular case, the dimensions of the matrices are 1x1, i.e., these are scalars. The prediction for this case is presented in Equation (3.3).

$$\begin{cases} x_{t+1}^{*} = [1] \cdot x_t + \left[0.5 \cdot \frac{1}{Fs_B} \quad 0.5 \cdot \frac{1}{Fs_C}\right] \cdot \begin{bmatrix} a_X^B \\ a_X^C \end{bmatrix} \cdot \Delta t \\ P_{t+1}^{*} = P_t + Q = P_t + [10] \end{cases} \tag{3.3}$$

The estimation is updated with the innovation factor η_{t+1}, adding the speed estimation from the GNSS and the spectrograms, considering signal availability by modifying the covariance measurements matrix R in the system presented in Equations(3.4) and (3.5).

$$\begin{cases} \eta_{t+1} = z_t - H \cdot x_{t+1}^{*} \\ S_{t+1} = H \cdot P_{t+1}^{*} \cdot H' + R \\ K_{t+1} = P_{t+1}^{*} \cdot H' \cdot S_{t+1}^{-1} \end{cases} \tag{3.4}$$

where H is the measurements matrix, S_{t+1} is the innovation covariance matrix, R is the measurements noise covariance matrix and K_{t+1} is the Kalman gain. The result is presented in Equation (3.5).

$$\begin{cases} \eta_{t+1} = \begin{bmatrix} v_{GNSS}^{B} \\ v_{GNSS}^{C} \\ v_{H}^{AxLeft} \\ v_{H}^{AxRight} \\ v_{H}^{B} \end{bmatrix} - \begin{bmatrix} 1 \\ 1 \\ 1 \\ 1 \\ 1 \end{bmatrix} \cdot x_{t+1}^{*} \\ S_{t+1} = \begin{bmatrix} 1 \\ 1 \\ 1 \\ 1 \\ 1 \end{bmatrix} \cdot P_{t+1}^{*} \cdot [1 \quad 1 \quad 1 \quad 1 \quad 1] + \begin{bmatrix} \alpha(V) & 0 & 0 & 0 & 0 \\ 0 & \alpha(V) & 0 & 0 & 0 \\ 0 & 0 & \beta(V) & 0 & 0 \\ 0 & 0 & 0 & \beta(V) & 0 \\ 0 & 0 & 0 & 0 & \beta(V) \end{bmatrix} \\ K_{t+1} = P_{t+1}^{*} \cdot H' \cdot S_{t+1}^{-1} \end{cases} \tag{3.5}$$

where $\alpha(V)$ and $\beta(V)$ are functions that depend on whether the GNSS signal is valid (1) or not (0). The value of $\alpha(V)$ is increased from 0.01 to 10^6 when the GNSS signal is not valid, whilst the value of $\beta(V)$ is decreased from 1 to 0.1 when the GNSS signal is not valid, to account for the signal uncertainty. This correction is applied to the a priori predictions as presented in Equation (3.6).

$$\begin{cases} x_{t+1} = x_{t+1}^{*} + K_{t+1} \cdot \eta_{t+1} \\ P_{t+1} = P_{t+1}^{*} - K_{t+1} \cdot H \cdot P_{t+1}^{*} \end{cases} \tag{3.6}$$

where x_{t+1} is the a posteriori prediction used for the estimation. Figure 3.9 shows the speed estimate from each source, and Figure 3.10 shows the error with respect to the bogie GNSS. As the segments without GNSS signal do not have a speed estimate, the error cannot be calculated there. The GNSS speed is used as a reference as there is no other source of information obtain the vehicle speed, neither tachometers nor odometers. GNSS signal is unavailable in tunnels, it has low sampling rate, and its accuracy is limited to the order of meters for moving objects [90, 162]. However, GNSS receivers are relatively inexpensive, non-invasive, and provide vehicle speed as an output, Therefore, their estimation can be considered useful for a first estimation. In the following section, a more accurate reference distance provided by the infrastructure manager is used.

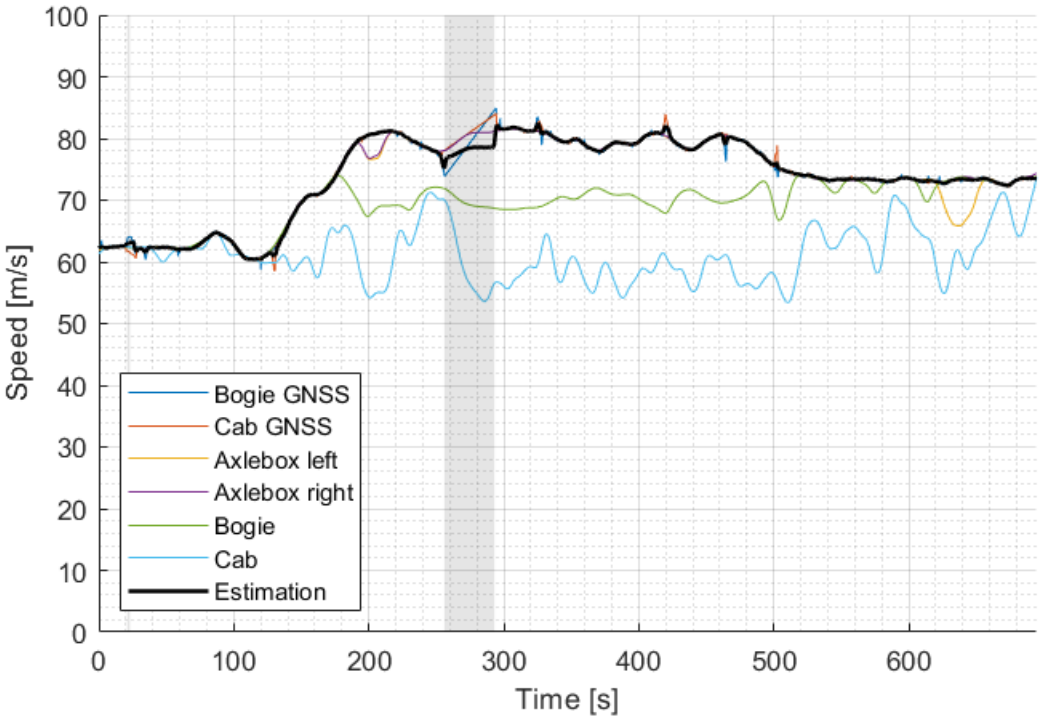


FIGURE 3.9. SPEED ESTIMATION COMPARISON.

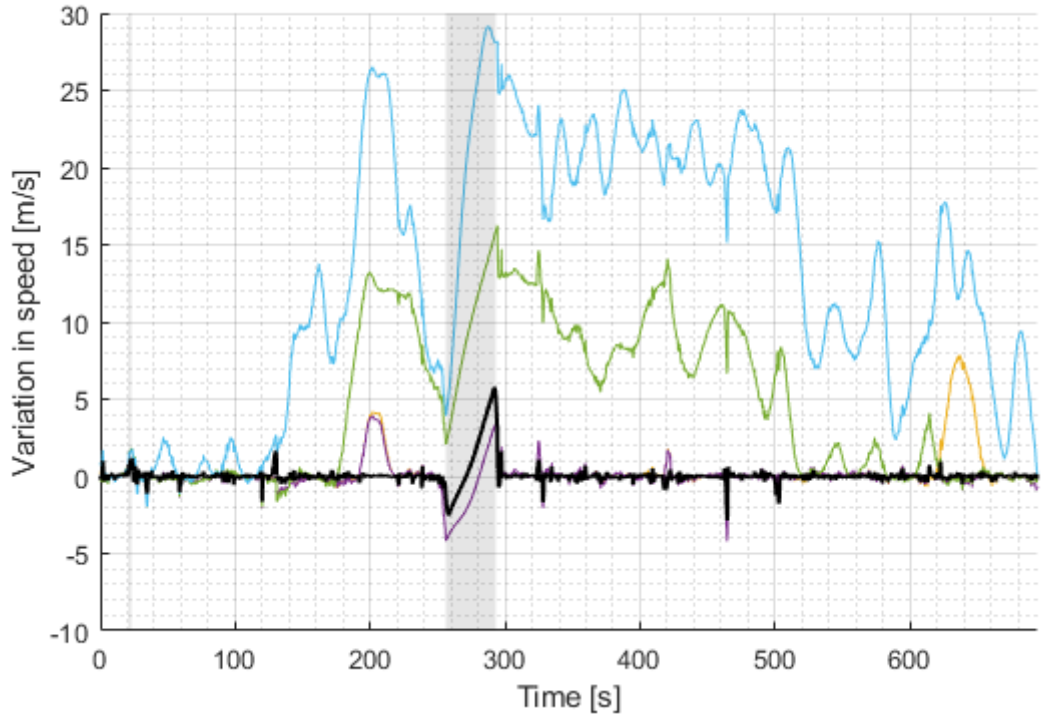


FIGURE 3.10. SPEED ESTIMATION ERROR COMPARISON.

It is observed that the error in the estimation is generally below 2 m/s, and lower with the Kalman filter, considering the bogie GNSS estimation as ground truth. Both axlebox sensors are the most accurate, whilst the bogie estimation has errors up to 15 m/s, and almost 30 m/s for the cab estimation. This is most likely due to the damping effect of the primary and secondary suspensions. In the tunnels, the error cannot be determined without GNSS, although the estimation is good enough for its practical use, as the magnitude of speed is similar to outside it.

The estimation method is applied for the three sections of the track, showing its use in different conditions of speed and GNSS signal availability. The results of its application are discussed in the following sections.

3.3.1. Section 1. Ashford International to Ebbsfleet International

Approximately 94% of the track has a valid GNSS signal and the maximum line speed is about 300 km/h (83 m/s), being the one with the highest GNSS availability and speed. Figure 3.11 shows a detail of the axlebox spectrograms and the speed estimates in the time domain. The missing GNSS signal segment highlighted in grey corresponds to the vehicle running through the North Downs Tunnel.

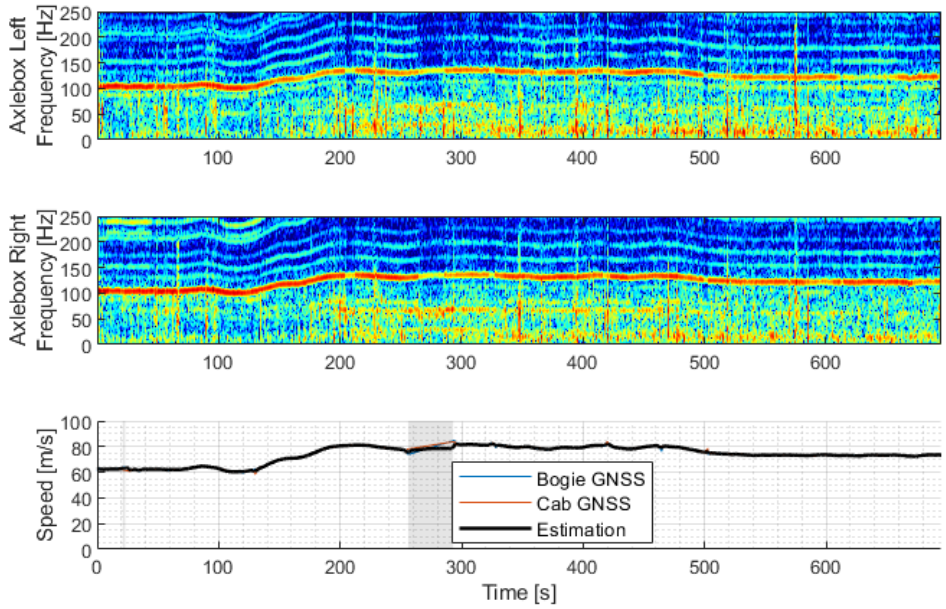


FIGURE 3.11. AXLEBOX ACCELEROMETER SPECTROGRAMS AND SPEED ESTIMATES FOR SECTION 1.

The GNSS availability allows the comparison between the estimated speed and the GNSS estimate for most of the track, showing minor differences between the GNSS and the estimation. This has shown the practicality of the method on ballasted tracks at high speeds. Its application on slab tracks corresponding to tunnels, lower signal availability and lower speeds is discussed in sections 3.3.2. and 3.3.3. of this chapter.

3.3.2. Section 2. Ebbsfleet International to Stratford Station

This section is underground as the vehicle passes through London tunnel 1 and under the River Thames, having a maximum speed of 226 km/h (63 m/s) and GNSS coverage for only 47% of the route. The track in the tunnels is slab track, whilst it is ballasted outside the tunnels. Comparing the signal inside and outside the tunnel, different behaviour is observed, such as the larger power in the harmonics range between 200 and 500 Hz for the tunnel, and the lower power of the harmonic used for speed estimation. This is expected as different types of track

are likely to have different dynamic behaviours, as the dynamic behaviours of ballasted and slab track differ [188]. Figure 3.12 shows the axlebox spectrograms and the speed estimates for this track section.

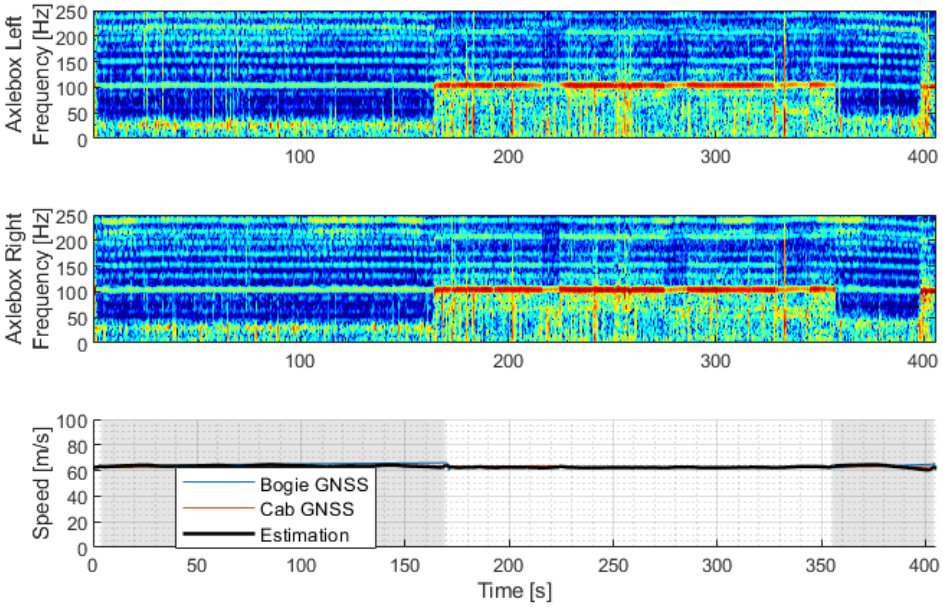


FIGURE 3.12. AXLEBOX ACCELEROMETER SPECTROGRAMS AND SPEED ESTIMATES FOR SECTION 2.

Despite the lower GNSS availability, the estimates are still accurate, with differences lower than 0.5 m/s for the axlebox and Kalman Filter estimates. The bogie and cab show maximum differences with the Kalman Filter estimates of 8 m/s, mostly in tunnels. This is due to the harmonic having less power and a low signal-to-noise ratio, and thus reducing the accuracy of the estimation, as a noisier signal produces more errors and hinders the speed estimation.

3.3.3. Section 3. Stratford Station to St. Pancras International

This section is underground for most of the time with only 20% GNSS signal availability and a speed varying from 0 to 60 m/s. Figure 3.13 shows the axlebox spectrograms and the speed estimates for this track section. GNSS signal is unavailable for most of the journey, so no

comparison to the estimation can be done in this case. The GNSS speed estimation is a linear interpolation to provide data for the Kalman filter, although it is considered highly inaccurate. In this figure, the direction of travel is indicated with a black arrow.

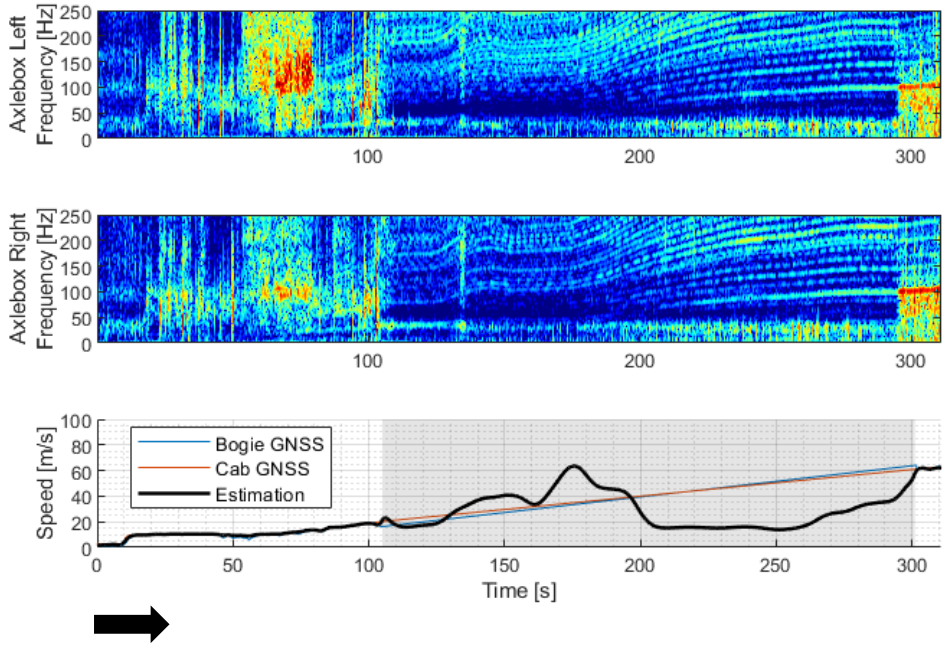


FIGURE 3.13. AXLEBOX ACCELEROMETER SPECTROGRAMS AND SPEED ESTIMATES FOR SECTION 3.

The harmonic appears at 50 Hz, only in the axlebox accelerometer spectrograms, as observed from 200 s. This sets the minimum train speed for the method in tunnels, as it is not possible to extract the harmonic at lower speeds. It is not possible to extract information from the first 100 s due to the combination between low speed and complexity of the track, as the train is leaving the station and entering a tunnel in this case.

From these observations, it is concluded that an accurate speed estimation using vehicle resonances is possible. To estimate distance, speed is integrated with respect to time. The distance estimate is less accurate at low speeds and its accuracy cannot be determined in tunnels, so an improvement of this estimation is provided in the following section, by aligning the results to reference data, i.e., the crosslevel, provided by the infrastructure manager (Network Rail).

3.4. DISTANCE ALIGNMENT USING CROSSLEVEL

As stated above, the distance estimation obtained using harmonics is unreliable below a certain speed. This section presents a process to improve the estimated distance using crosslevel estimated from the vehicle IMU and reference geometry data provided from track recording vehicles. To calculate crosslevel, the integral of the roll rate provides the angle and the sine of the angle multiplied by the gauge provides the difference in height between the two rails [9], see Equation (3.7).

$$CL = \text{gauge} \cdot \sin\left(\int g_x(t)dt\right) \tag{3.7}$$

where CL is crosslevel and $g_x(t)$ is the vehicle roll rate. Figure 3.14 shows the comparison between crosslevel estimates from the bogie, the cab and the reference data.

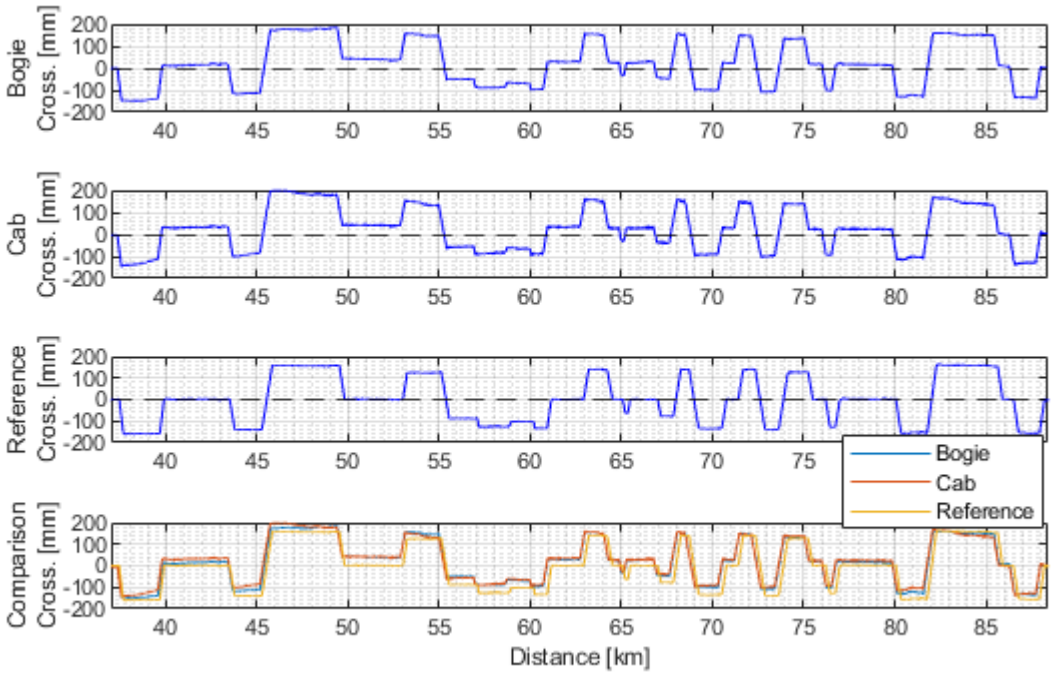


FIGURE 3.14. CROSSLEVEL COMPARISON BETWEEN BOGIE, CAB, AND REFERENCE.

There are differences between the estimated distance and the reference, as shown in detail in Figure 3.15. Thus, a correction is necessary to improve the distance estimates. There are also differences in the value of crosslevel, although these need not be corrected for the distance estimation and correction, since the correction is only considering the variation along distance and not the value of crosslevel.

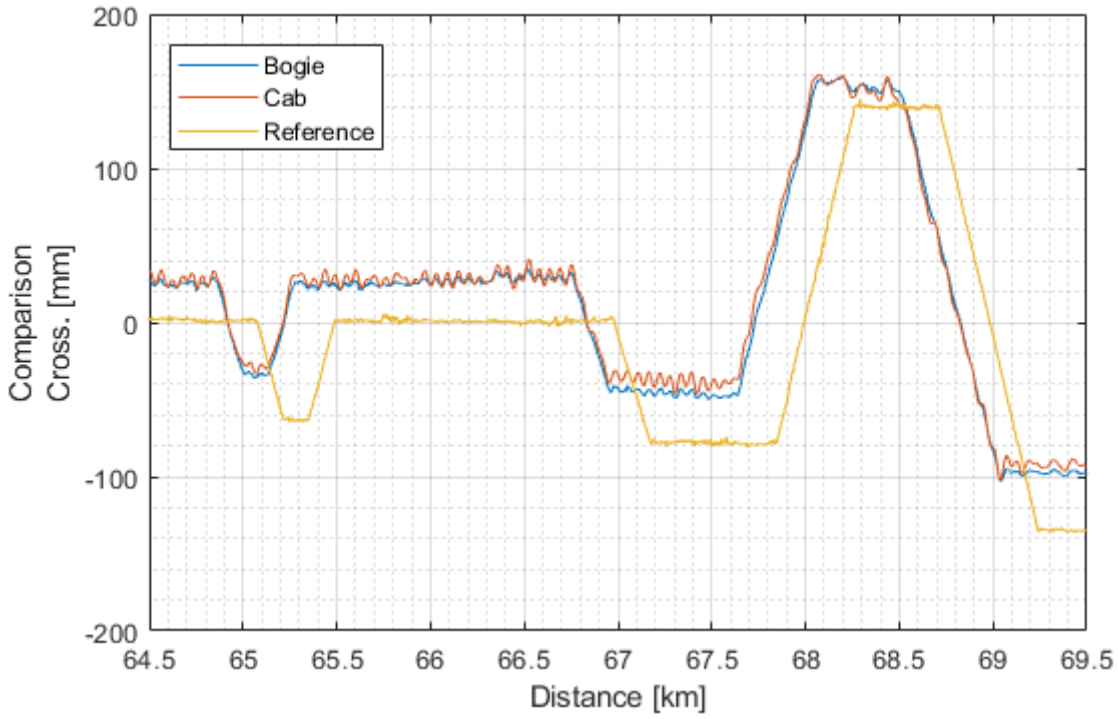


FIGURE 3.15. DIFFERENCES BETWEEN DISTANCE ESTIMATION AND REFERENCE.

The correction technique uses the transitions between constant levels, identified using the vehicle roll rate, as constant values different from 0 (neglecting signal noise) correspond to a transition. Figure 3.16 shows a detail of the transitions detected in the crosslevel signal extract from the bogie, the cab, and from the reference data. These transitions are numbered for identification and further processing, removing false positives, such as Transition #18 in the middle graph.

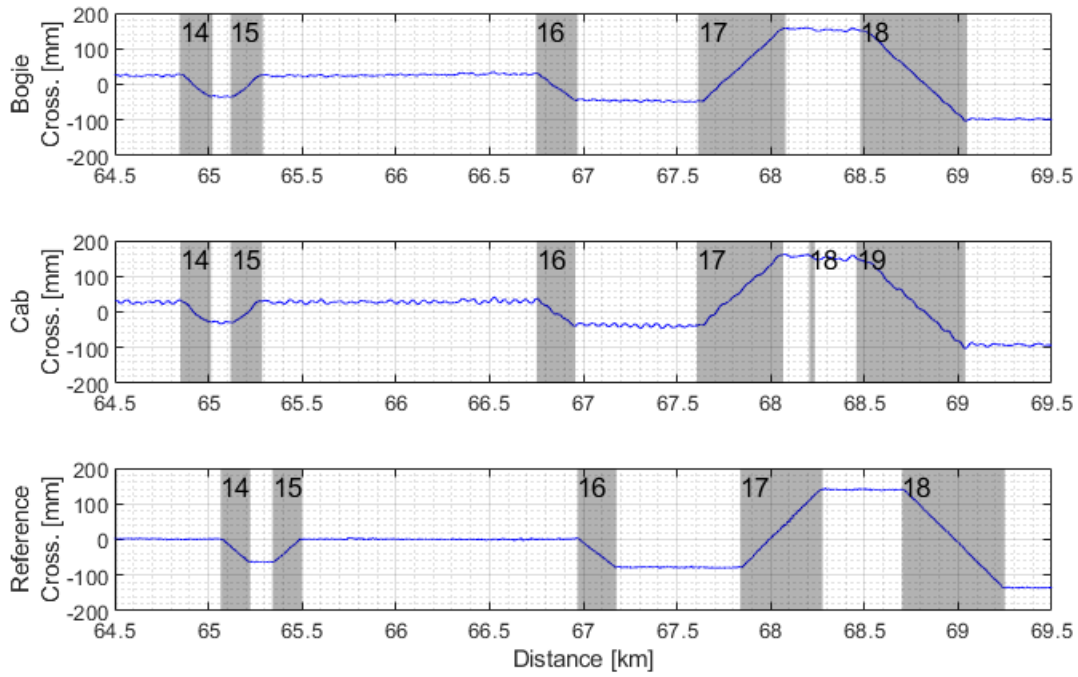


FIGURE 3.16. DETAIL OF IDENTIFIED TRANSITIONS IN CROSSLEVEL FOR BOGIE, CAB, AND REFERENCE.

Once transitions are correctly identified, crosslevel is corrected horizontally by linearly interpolating the original distance estimation to the reference. Figure 3.17 shows the crosslevel against distance before and after the estimation, and Figure 3.18 shows the absolute errors of the original estimation and corrected crosslevel compared to the reference. The tunnels are shaded in grey.

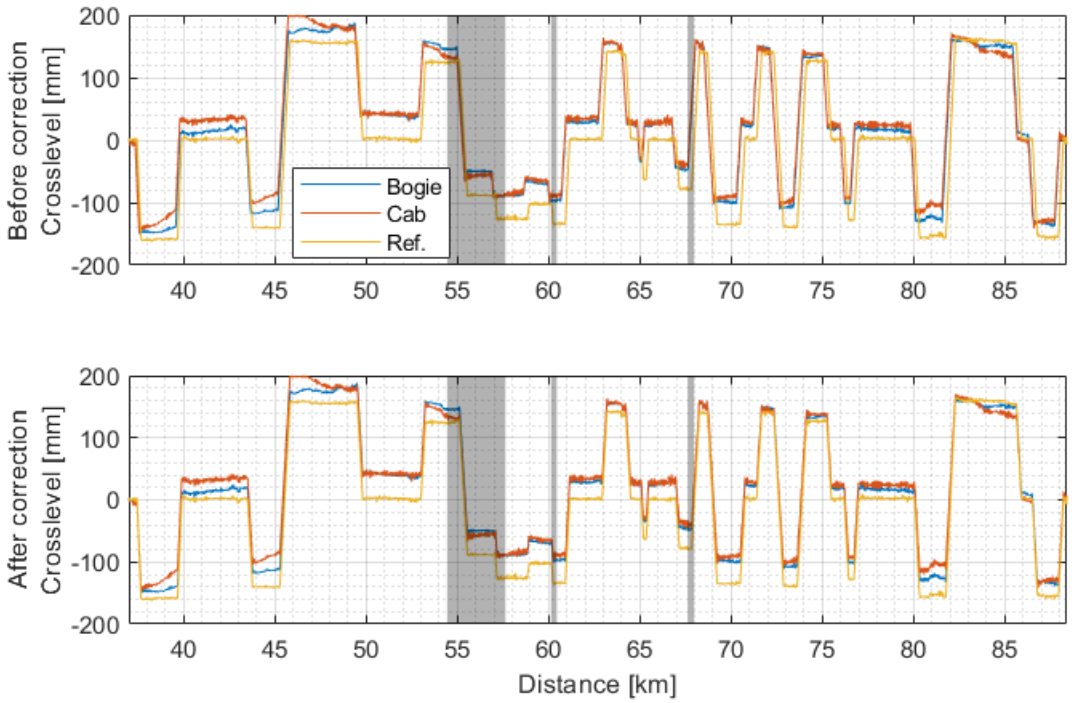


FIGURE 3.17. CROSSLEVEL COMPARISON BEFORE AND AFTER CORRECTION FOR SECTION 1.

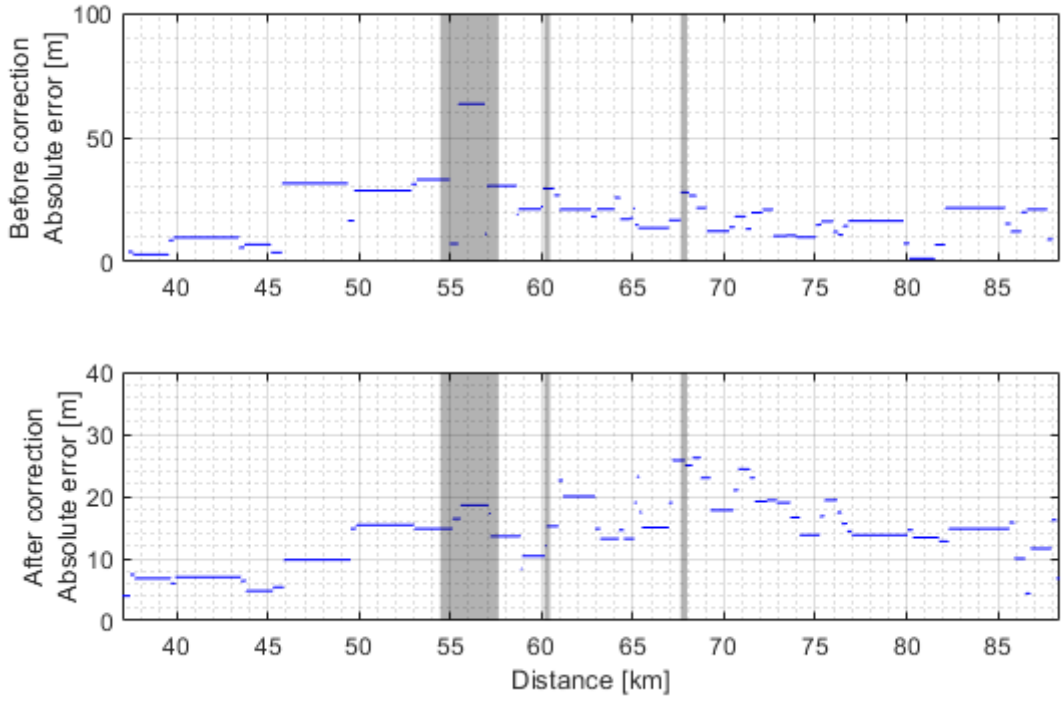


FIGURE 3.18. ABSOLUTE ERROR IN DISTANCE ESTIMATION FOR SECTION 1 BEFORE AND AFTER CORRECTION.

It is observed that the absolute error is generally below 40 m, in lengths spanning kilometres, and generally lower in longer segments, in the order of 15 m, showing how this method is preferable for positioning and aligning long sections of track, using methods discussed further for a more precise element positioning, such as cross-correlation and dynamic time warping. A discussion of the application of the crosslevel alignment method for each track section is presented in the paragraphs below.

3.4.1. Section 1. Ashford International to Ebbsfleet International

The distance estimation prior to the correction is expected to be highly accurate for this section as it has the highest GNSS signal availability and speed and thus, the best conditions for the speed estimation method presented in Section 3.3. The correction is presented in Figure 3.17, and the estimation error in Figure 3.18. It is observed that the estimation error is generally low, in the order of 20 metres. This shows that the estimation is, as expected, highly accurate for high speeds.

3.4.2. Section 2. Ebbsfleet International to Stratford Station

The GNSS availability in this section is only 47%, so the distance estimation is expected to be less accurate compared to the reference. Figure 3.19 shows the crosslevel before and after the correction, and Figure 3.20 shows the absolute errors before and after the corrections. Opposite as expected, both the absolute errors are generally lower than for Section 1 of the track, showing the accuracy of the estimation even without GNSS when the speed is relatively high and constant.

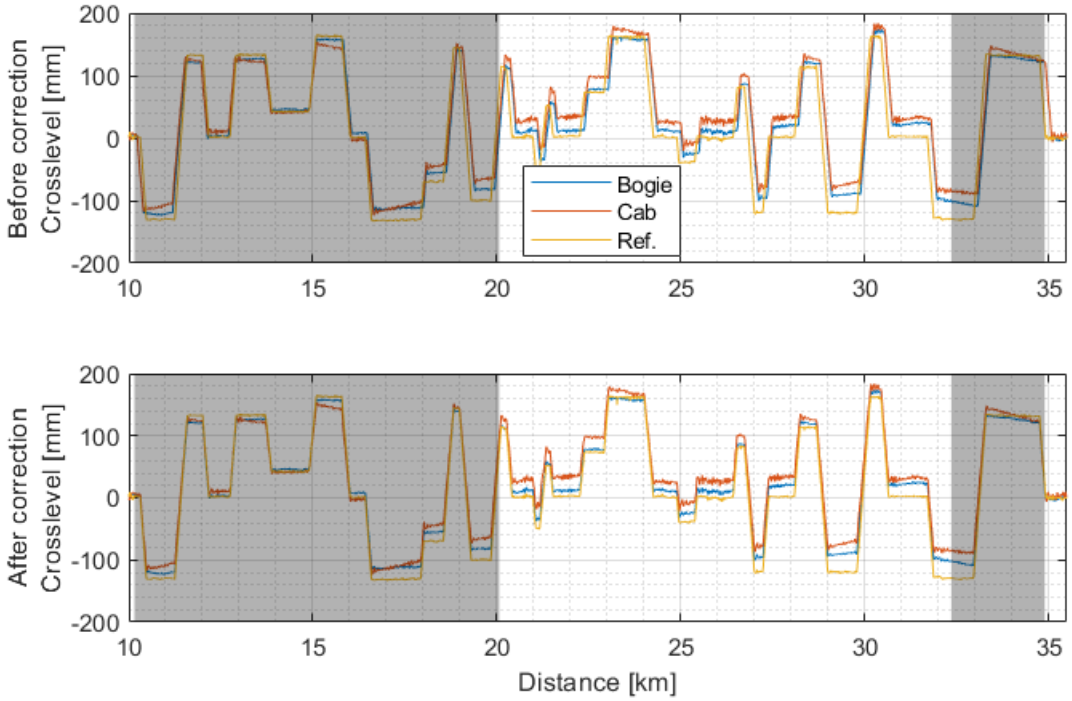


FIGURE 3.19. CROSSLEVEL COMPARISON BEFORE AND AFTER CORRECTION FOR SECTION 2.

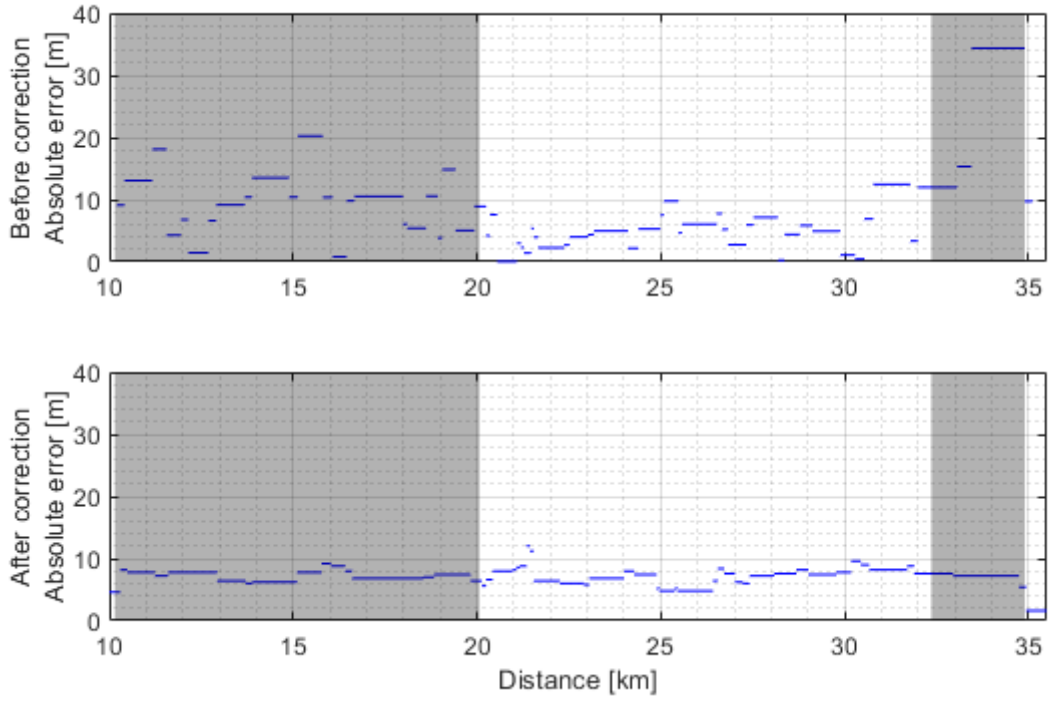


FIGURE 3.20. ABSOLUTE ERROR IN DISTANCE ESTIMATION FOR SECTION 2 BEFORE AND AFTER CORRECTION.

3.4.3. Section 3. Stratford Station to St. Pancras International

About 80% of this section is underground in London, with no GNSS availability and the vehicle accelerates from the start of the journey. The distance estimates are expected to be inaccurate. Figure 3.21 shows the crosslevel, and Figure 3.22 the absolute errors before and after the correction, respectively.

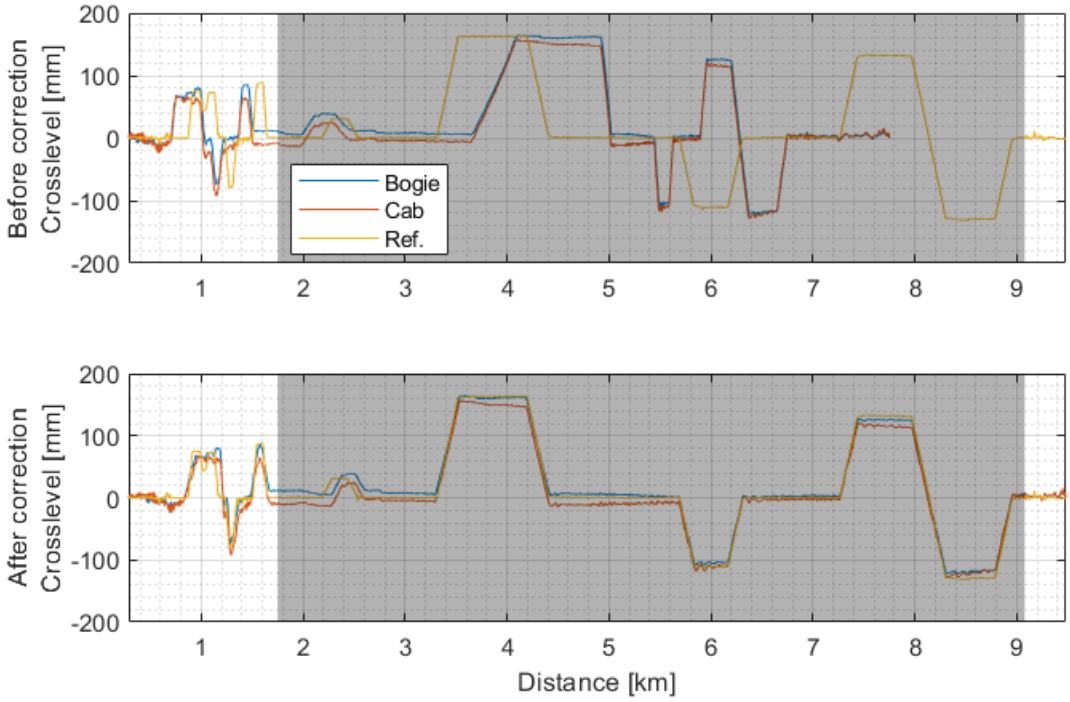


FIGURE 3.21. CROSSLEVEL COMPARISON BEFORE AND AFTER CORRECTION FOR SECTION 3.

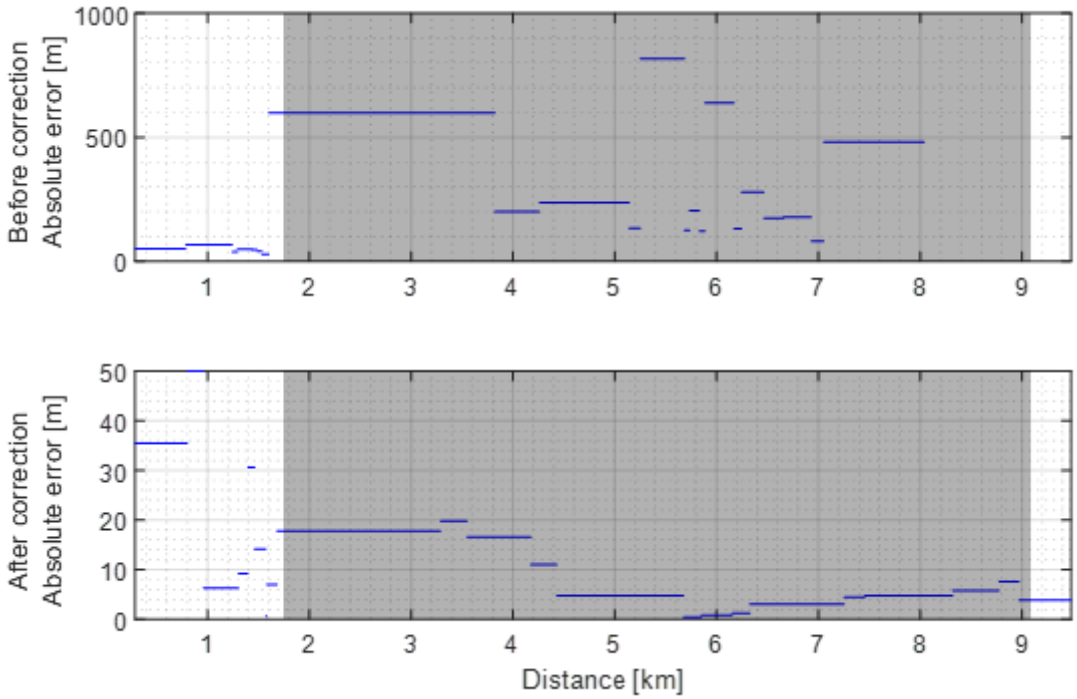


FIGURE 3.22. ABSOLUTE ERROR IN DISTANCE ESTIMATION FOR SECTION 3 BEFORE AND AFTER CORRECTION.

There are several false positives and negatives in the identification of transitions for bogie, cab and reference, so in some cases, the correction could be difficult to automate. The unreliable speed estimation causes the distance estimation to be unreliable, with high absolute error values. However, the correction using crosslevel compensates for this and aligns the signals accurately, with errors generally below 20 m compared to the reference provided.

From the results presented above, it can be concluded that the method to correct distance estimation using crosslevel and a reference is accurate enough for further application, mostly in large segments of track, in the orders of kilometres. One of its main applications would be the alignment of runs on the same track for comparison. If the reference is missing, a possible solution would be to use one of the runs as a reference and then align the rest of them to it.

Other commonly used methods to align data are cross-correlation and dynamic time warping, due to their relative simplicity and ease of interpretation. These methods are compared to the

crosslevel alignment method, and their advantages and disadvantages are presented in this chapter in the following section.

3.5. ALIGNMENT COMPARISON TO OTHER METHODS

This section presents the use of two common methods to align signals to compare them to the method presented in the chapter: cross-correlation and dynamic time warping.

3.5.1. Cross-correlation

Cross-correlation is a measure of the similarity between two series of data with a relative displacement between them. It is commonly applied for finding relationships between sets of data in the same domain, as discussed in the research by Eklöf *et al.* [180].

Before comparing signals, a conversion to the same domain must be done, as cross-correlation only works with data in the same domain. Since the reference is in the spatial domain, both the bogie and cab estimations have been converted to the spatial domain using linear interpolation similarly to the previous section, but without applying any alignment to the data. Cross-correlation is then applied to the spatial-domain estimations, as presented in Figure 3.23.

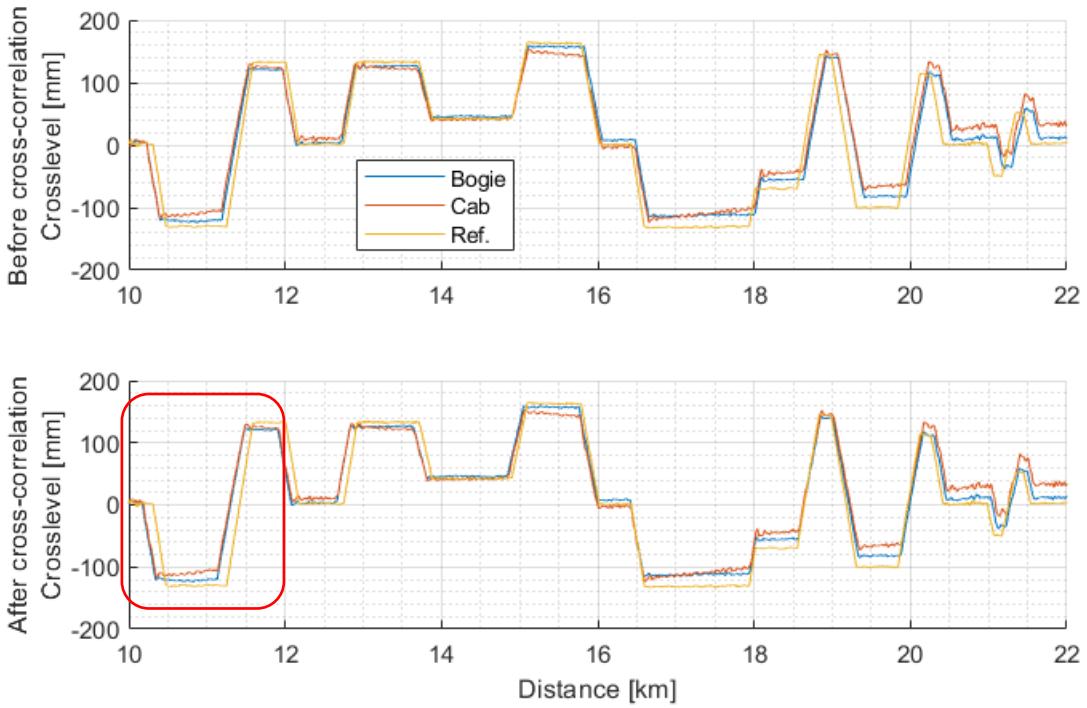


FIGURE 3.23. APPLICATION OF CROSS-CORRELATION TO A TRACK SEGMENT.

The results show that this is not effective, as the differences in distance vary along the distance axis, due to the changes in estimated speed and thus in estimated distance for each point, as observed in kms 10 to 12. In this case, the correction using crosslevel alignment is superior to cross-correlation for large distances. However, crosslevel alignment requires a reference for comparison, and cannot be used in sections of constant crosslevel. Cross-correlation can be applied in these cases for aligning data in track lengths lower than several kilometres and relatively constant speeds without the need for a reference. Figure 3.24 shows the application of cross-correlation to a segment of the track for aligning data.

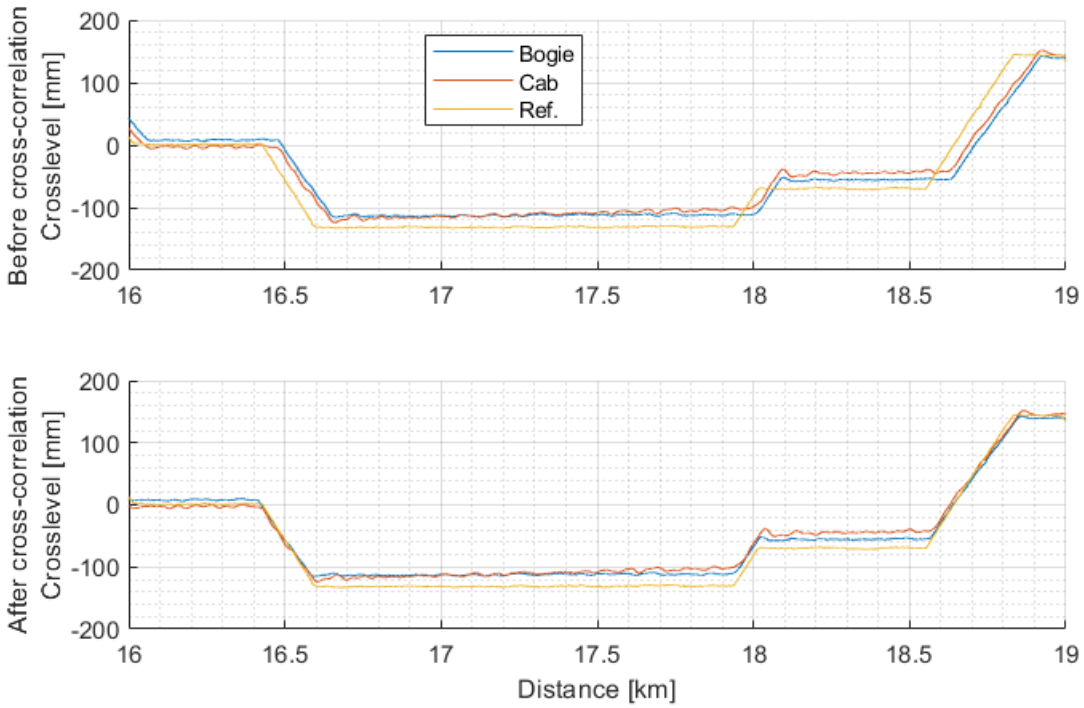


FIGURE 3.24. APPLICATION OF CROSS-CORRELATION TO A SEGMENT OF A RUN.

It is observed that data is aligned with accuracy, and thus comparisons between the reference, the bogie and the cab can be performed. The most notable differences are the average value of crosslevel for bogie and cab being not zero due to drift and inaccuracies of the signal, and the dominance of low-frequency components in the cab signal. The differences between signals are discussed in Chapter 5 and Chapter 6 of this thesis.

3.5.2. Dynamic time warping

Dynamic time warping (DTW) is a measure of similarity between two signals with different lengths. In this case, vehicles with varying speeds and thus, varying distances between sampling points. Signals also must be in the same domain; bogie and cab signals are in the time domain, so they must be converted to the spatial domain, that is the domain for the reference. A

comparison between crosslevel from the bogie, cab and reference with and without dynamic time warping is presented in Figure 3.25.

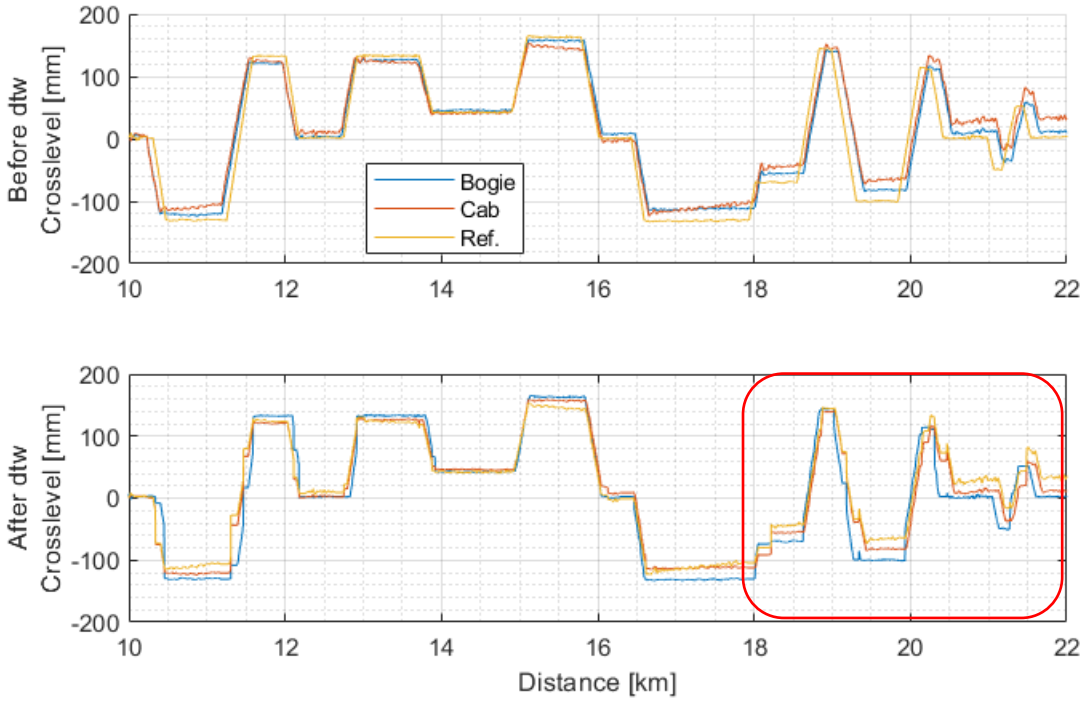


FIGURE 3.25. APPLICATION OF DYNAMIC TIME WARPING TO CROSSLEVEL.

The alignment shows a high level of accuracy in segments such as between km 16 and 18. However, the segments with larger differences in alignment show distortions in the signal, such as between km 18 and 22. Compared to cross-correlation, this alignment is more accurate for short segments but ineffective for longer distances. Crosslevel alignment is similar to DTW but uses a reduced number of sampling points to align data. Compared to DTW, this method is simpler to apply and can be used for longer sections of track.

In summary, this section showed how crosslevel alignment can be used for long-distance sections of the track, but is limited by the geometry of the track to minimum lengths in the order of kilometres, whilst cross-correlation and dynamic time warping are best used below this range. The complementary use of the different methods (cross-correlation in this case) is then

necessary for aligning the data to extract information from the tracks for an analysis of their state. The steps for estimating speed and distance, and correcting the estimation are shown in Figure 3.26, where the speed estimation is on the left, the distance correction using crosslevel is on the top right, and the use of cross-correlation is on bottom right.

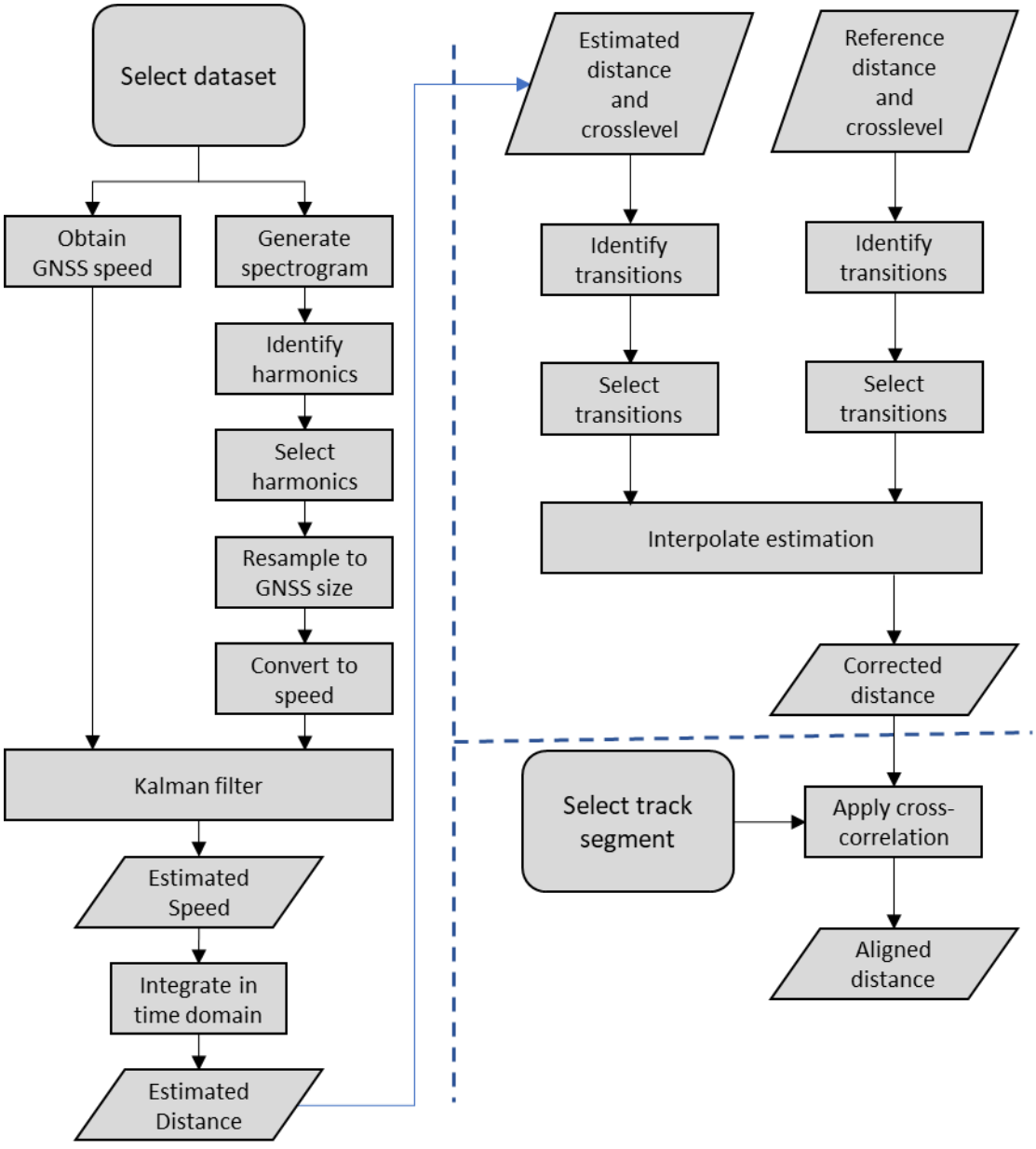


FIGURE 3.26. SPEED ESTIMATION AND DISTANCE CORRECTION FLOWCHART.

3.6. CONCLUSIONS

This chapter of the thesis has presented a novel method to estimate vehicle speed and distance using harmonics detected on inertial sensors on a high-speed railway vehicle, and to correct the derived distance estimation using crosslevel alignment. The distance estimation is performed using a Kalman filter that combines the GNSS speed estimates with the harmonics detected, providing errors below 5 m/s at high vehicle speeds, although this estimation is proven unreliable at speeds lower than 50 m/s. Then, a correction to the estimated distance is made by aligning the crosslevel estimation to a reference.

Frequency analysis has shown the appearance of harmonics in the sensors of different components of the vehicle. The highest signal-to-noise ratio appears in the vertical acceleration sensors, so these have been selected for the estimation. The harmonic also appears in the other accelerometers, although with a lower magnitude. This harmonic is proportional to the vehicle speed, with a ratio of 1.68 between frequency and vehicle speed, appearing when the vehicle speed exceeds 50 m/s (180 km/h). The effects of the track are also observed, as the dynamic response of the vehicle changes whether the vehicle is on a slab or a ballasted track.

A method to correct the distance estimation has also been developed. This method uses significant changes in crosslevel to detect transitions between constant levels, associated with straight or curved segments, and corrects the estimated distance by using a reference provided by the infrastructure owner. The errors in the estimation are generally below 20 m on track segments spanning kilometres, demonstrating its accuracy. Additionally, using a tachometer would improve the estimation, as its signal can be used in tunnels and at lower speeds.

A comparison with cross-correlation and dynamic time warping showed how the combination of both methods can be used for aligning runs in distances ranging from hundreds of metres to

tens of kilometres. Crosslevel alignment is preferable for distances above kilometres, whilst cross-correlation and dynamic time warping are used for distances below kilometres, showing how their combination can be used for the whole range of track length. These methods are applied in Chapter 5 and Chapter 6 for aligning runs and components for signal analysis.

Further work to be developed from this chapter is the improvement of the speed extraction from the harmonics, especially at lower speeds, and the further automation of the crosslevel alignment method, mostly in the part relative to selecting transitions. Discovering the causes of the apparition of the harmonics would also be useful to investigate if these harmonics appear in other train models and conditions. Finally, further challenges to be addressed are the need to increase the method's accuracy at low speeds and to study its accuracy where no GNSS signal is available as there is no speed reference.

Chapter 4. Assessment of comfort for ballasted and slab track

4.1. INTRODUCTION

This chapter presents a comparison between the comfort indices explained in the introduction of the thesis. The objective of this chapter is the assessment of comfort for track quality on both ballasted and slab tracks, as raw acceleration needs to be processed to provide more meaningful information than just its magnitude, and thus to correlate comfort, acceleration, and track quality. The indices and methods discussed in this chapter belong to the standards ISO 2631 [70, 71] and EN 12299:2009 [11], and are deeply explained in Appendix A. Comfort indices. Their main application is the assessment of comfort based on vibrations and, in specific cases, these indices can be used for assessment of health, motion sickness or ride quality. Since the human body has a different response depending on the frequency range, the vibrations and their frequencies are specifically weighted, as defined in Chapter 1 and Appendix A.

The following section compares the assessment of comfort using each of the methods on a ballasted track. The arrangement of sensors in this chapter is the same as the one described in Chapter 3, although only the sensors installed in the cab (secondary suspension) are considered in this chapter. In summary, a set of accelerometers and gyroscopes acquiring signals in the

vertical, lateral, and longitudinal directions of travel are installed in the vehicle cab, with a sampling rate of 256 samples per second. Additionally, a GNSS receiver provides the vehicle geographical location and speed, where signal is available.

4.2. COMFORT ASSESSMENT

In the standard ISO 2631, comfort is defined as "a compound of sensations (noise, vibrations, temperature, humidity, seating quality) perceived by passengers that affect the experience of travel" [70]. Depending on the standard or method applied, different aspects of comfort and passenger experience are obtained: ISO 2631 [70] provides a general assessment of passenger comfort, and the effects of vibrations on health and motion sickness; EN 12299 [11] provides an in-depth analysis of comfort, its use providing continuous comfort, mean or averaged comfort, and comfort based on aspects such as curve transitions or discrete events.

This section presents a comparison of the comfort indices obtained by each method under different scenarios such as a regular ballasted track, a tunnel/slab track, passing over an S&C, and passing over a bridge.

4.2.1. Ballasted track

Ballasted tracks are the most extensively used type of track. Their geometry is affected by aspects such as track stiffness [101, 189] or issues such as degradation or ballast settlement [22, 23]. Both track condition and train suspension affect vibrations produced in the vehicle, mostly in the lateral and vertical directions. The longitudinal direction is mostly affected by the driving style, which is not covered here. These vibrations are transmitted to the vehicle cab, thus affecting the passenger experience during travel. This section shows the comfort indices

obtained for a segment of ballasted track based on different standards. The geometry of the track is presented in Figure 4.1, which shows the vertical alignment on the top subfigure and the curvature on the bottom subfigure. There are two crossing points marked as vertical dashed lines, and three viaducts, shaded in magenta.

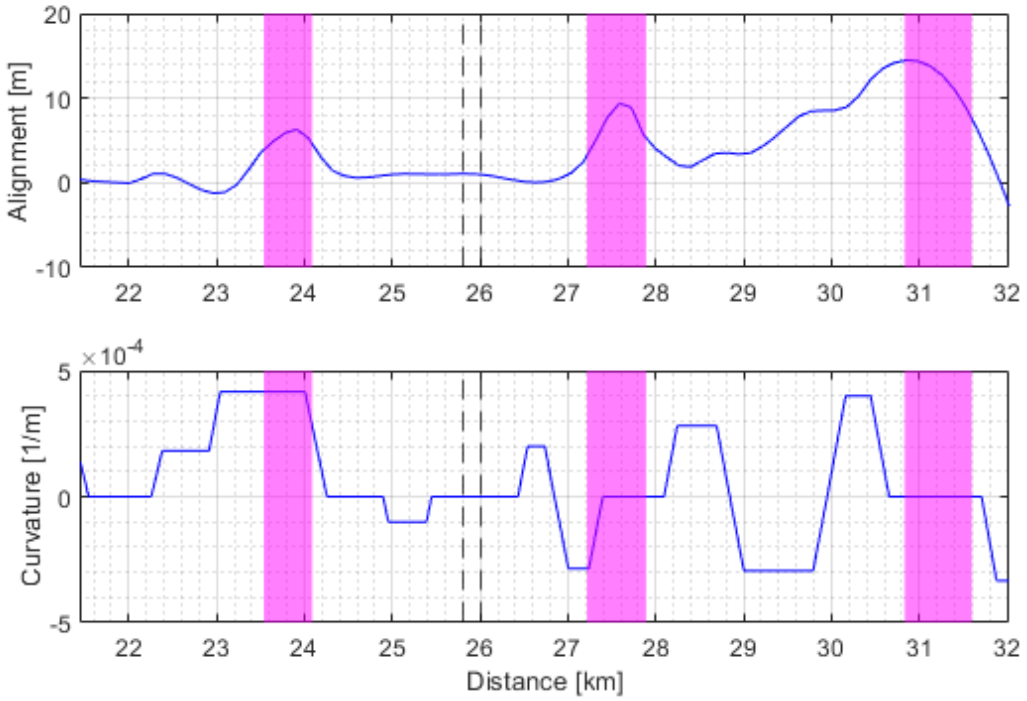


FIGURE 4.1. BALLASTED TRACK GEOMETRY.

The threshold levels in the comfort subfigures are based on the standard EN 12299 and summarised in Table 4.1. The process to obtain the comfort indices consists in filtering the acceleration using frequency weighing functions, and then averaging the result using the root-mean-square on the result with a moving window of 5 s (see Appendix A).

TABLE 4.1. COMFORT PERCEPTION REFERENCE FOR EN 12299 [11].

Index value	Comfort perception	Colour
$C_{Cy}(t)$, $C_{Cz}(t) < 0.20\ m/s^2$	Very comfortable	Blue
$0.20\ m/s^2 \leq C_{Cy}(t)$, $C_{Cz}(t) < 0.30\ m/s^2$	Comfortable	Green
$0.30\ m/s^2 \leq C_{Cy}(t)$, $C_{Cz}(t) < 0.40\ m/s^2$	Medium	Yellow
$0.40\ m/s^2 \leq C_{Cy}(t)$, $C_{Cz}(t)$	Less comfortable	Red

Figure 4.2 shows the vehicle speed and continuous comfort indices for a ballasted track against distance. The data were acquired from the cab floor of a British Class 374 (Eurostar), at 250 Hz, following the same arrangements as Chapter 3. Comfort indices were obtained according to the standard EN 12299 [11], as described in Chapter 1 and Appendix A. There are two crossing points marked as vertical dashed lines, and three viaducts, shaded in magenta.

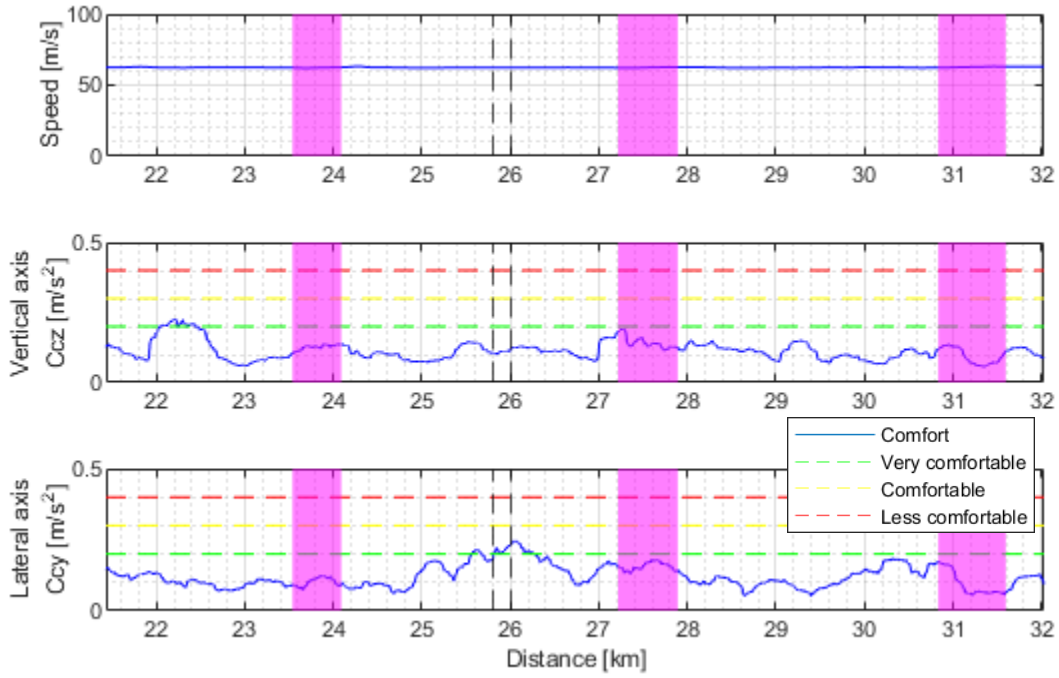


FIGURE 4.2. SPEED, LATERAL AND VERTICAL COMFORT ON A BALLASTED TRACK ON A HIGH-SPEED LINE.

Figure 4.3 shows the vertical and lateral comfort indices, and cab vertical and lateral acceleration against distance, to show the relationship between these signals. The acceleration is in light blue, whilst comfort is in dark blue. Figure 4.4 shows vertical comfort on the map. Figure 4.5 shows lateral comfort on the map. The colour code for these figures is the same as for Figure 4.2 and is presented in Table 4.1. There are two S&Cs in km 25.8 and 26, marked as a dashed line, and tunnels marked as magenta patches. The tunnels are marked as red rectangles on the maps, and the S&Cs are marked with a brown circle on the map.

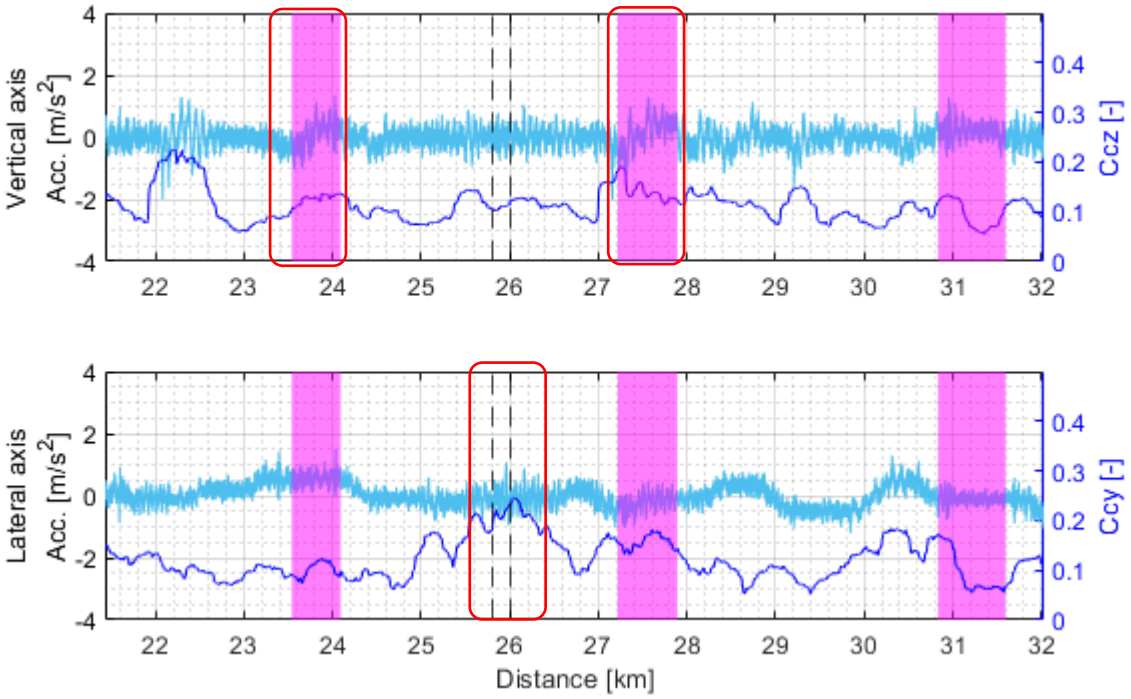


FIGURE 4.3. COMFORT (DARK BLUE) AND CAB ACCELERATION (LIGHT BLUE) FOR A BALLASTED TRACK.

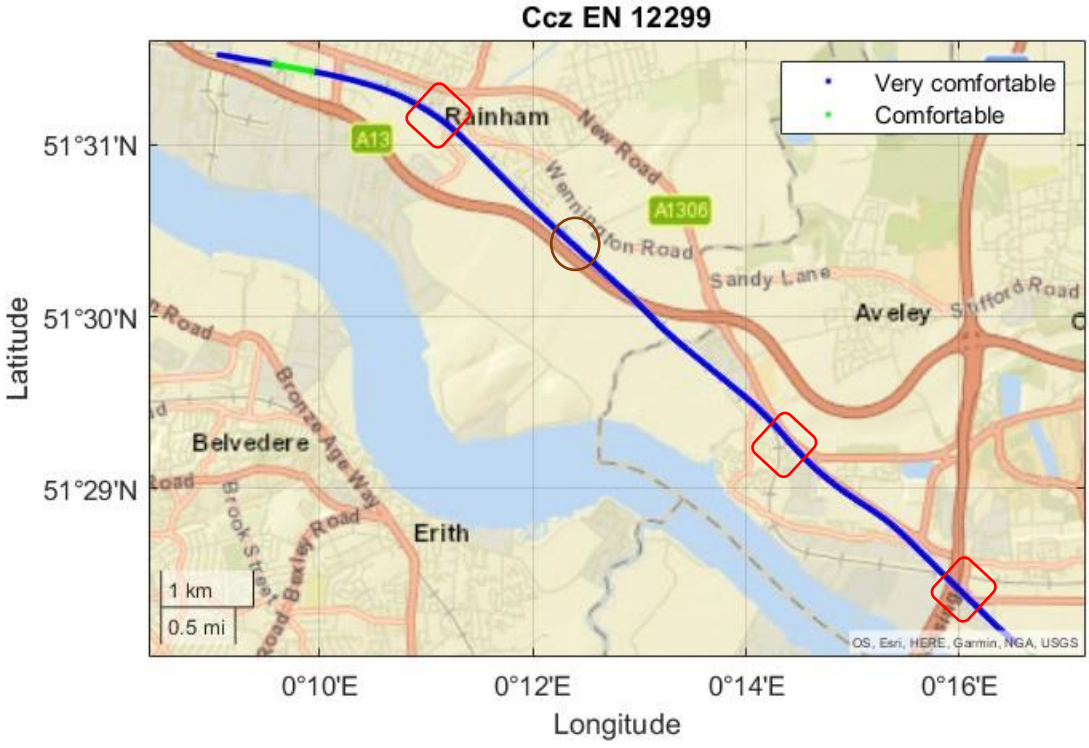


FIGURE 4.4. VERTICAL COMFORT ON THE TRACK.

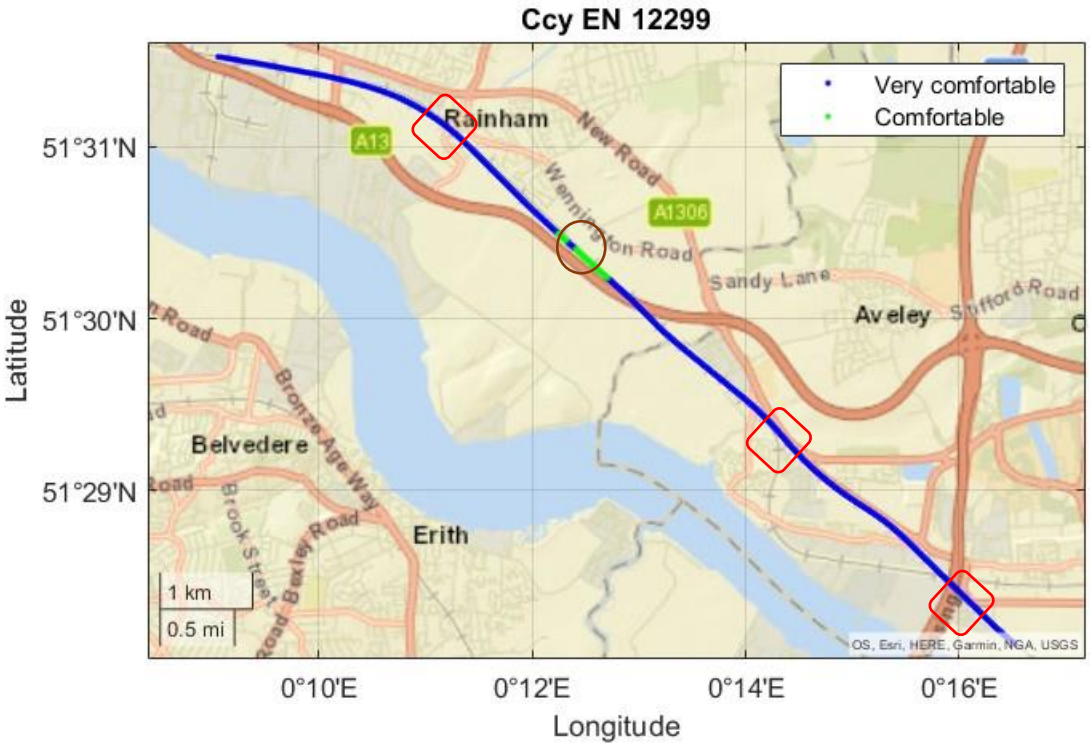


FIGURE 4.5. LATERAL COMFORT ON THE BALLASTED TRACK.

As expected, there is a clear correlation between acceleration magnitude and comfort indices, as observed in Figure 4.3. The changes in vertical comfort in km 23.5 to 24 are associated with the Rainham viaduct in the C_{Cz}, in km 25.8 to 26 with the Wennington crossover in the C_{Cy}, an S&C, and the Aveley viaduct in km 27.2 to 27.9 in the C_{Cz}, as highlighted with red rectangles in the figures.. Although the S&C is in a short length of track, the increased magnitude of acceleration and the signal averaging cause the lateral comfort index to increase in a longer section of track. However, details of the effect of each S&C component on comfort are not possible to be evaluated due to the processing.

According to EN 12299, the section in green, transition zones of the viaduct and S&C are considered as "comfortable" parts of the journey, while the rest is "very comfortable", a better value in comparison. The analysis using ISO 2631, which uses the same filtering as EN 12299 as explained in Appendix A, shows only a decrease to "a little uncomfortable" on the S&C. The

mean comfort based on EN 12299 is 1.68, meaning that the passenger experience over that section is “comfortable”.

EN 12299 also provides an assessment for event-based comfort, such as curves and discrete events. Figure 4.6 presents event-based comfort for a ballasted track, concretely comfort in curve transitions. Comfort in curve transitions (P_{CT}) provides the percentage of travellers dissatisfied with the journey in curves and transitions, whilst comfort in discrete events (P_{DE}) provides the percentage of travellers dissatisfied with events such as passing through an S&C or a sudden change in acceleration.

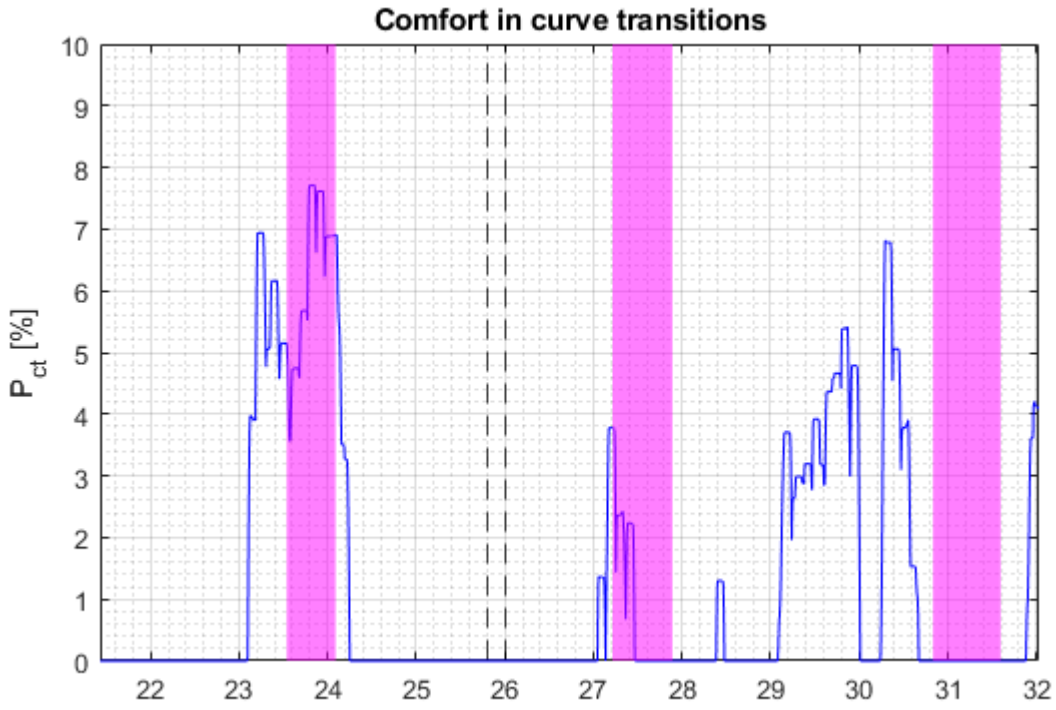


FIGURE 4.6. EVENT-BASED COMFORT FOR A BALLASTED TRACK.

The increased values of P_{CT} correspond to the aforementioned viaducts and curved track. The peak at km 23 to 24.2 corresponds to a short passage under a bridge. The values of P_{DE} are 0 for the whole segment, which is why there is no figure showing it, showing that the S&C causes no apparent effect on the passenger experience according to that index. It is necessary to

mention that, whilst, both C_{Cy} and P_{DE} are calculated using the cab lateral acceleration, the filter and processing applied are different. This is why the results obtained from each index differ, and the reason why C_{Cy} is preferable to P_{DE} in this case, as its magnitude changes can be associated with track elements.

4.2.2. Slab track

The segment presented in this section is inside a tunnel built with slab track. Slab track is commonly installed in tunnels and stations, as it produces less noise and vibrations. The geometry of the track is presented in Figure 4.7, with the alignment on top and the curvature on bottom. The viaduct is highlighted as a grey shading in this and subsequent figures.

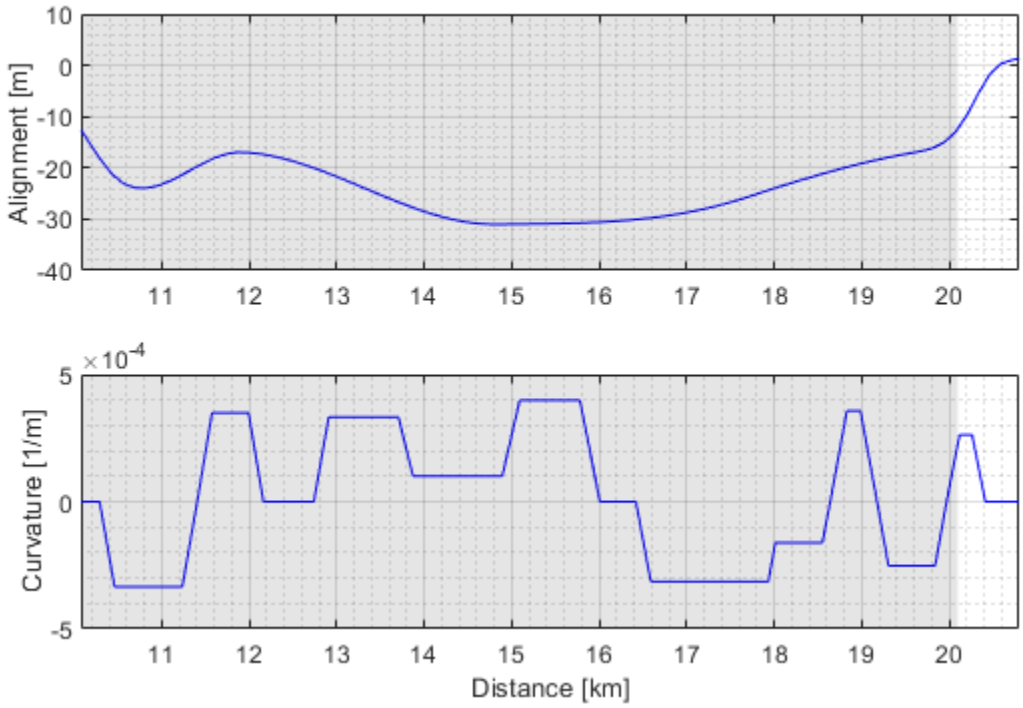


FIGURE 4.7. SLAB TRACK GEOMETRY.

The map presented in Figure 4.8 shows only the location of the vehicle at the entrance and exit of the tunnel since there is no GNSS signal inside it. There are no S&Cs in this segment. Hence, no indication of their position appears in the figures. The entrance and exit of the tunnel have been highlighted with red rectangles.



FIGURE 4.8. VEHICLE LOCATION FOR SLAB TRACK.

Figure 4.9 shows vehicle speed and comfort as in the previous section, using the colour code provided in Table 4.1. Figure 4.10 shows comfort superimposed on cab acceleration, Figure 4.11 shows the event-based comfort indices on the slab track. The tunnel is highlighted with a grey shading in the figures.

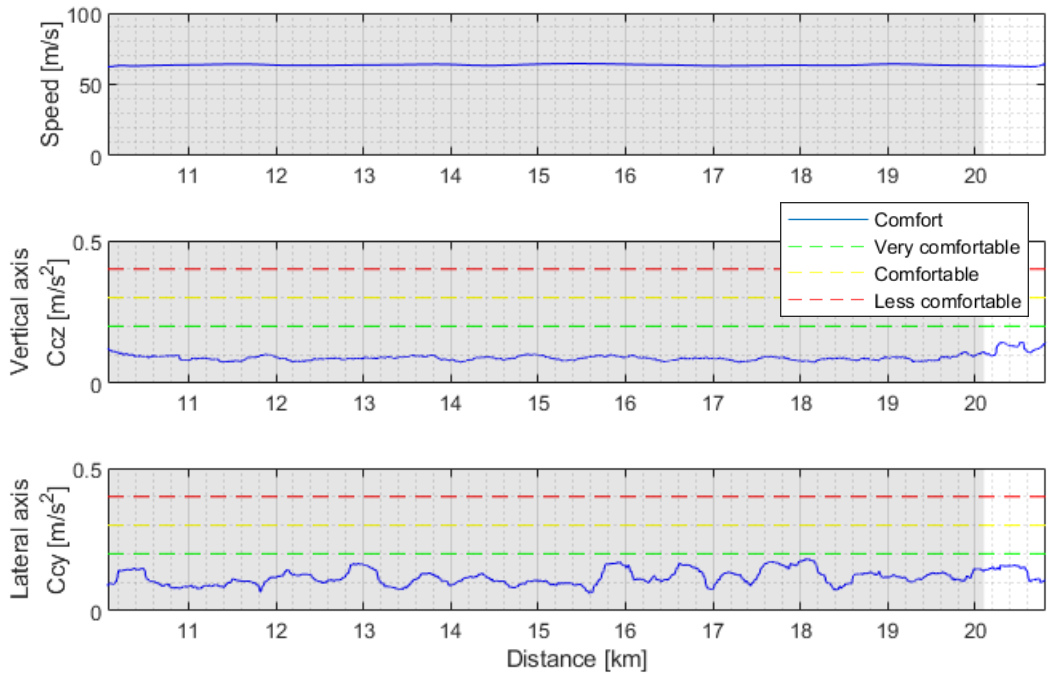


FIGURE 4.9. SPEED AND CONTINUOUS COMFORT FOR A SLAB TRACK.

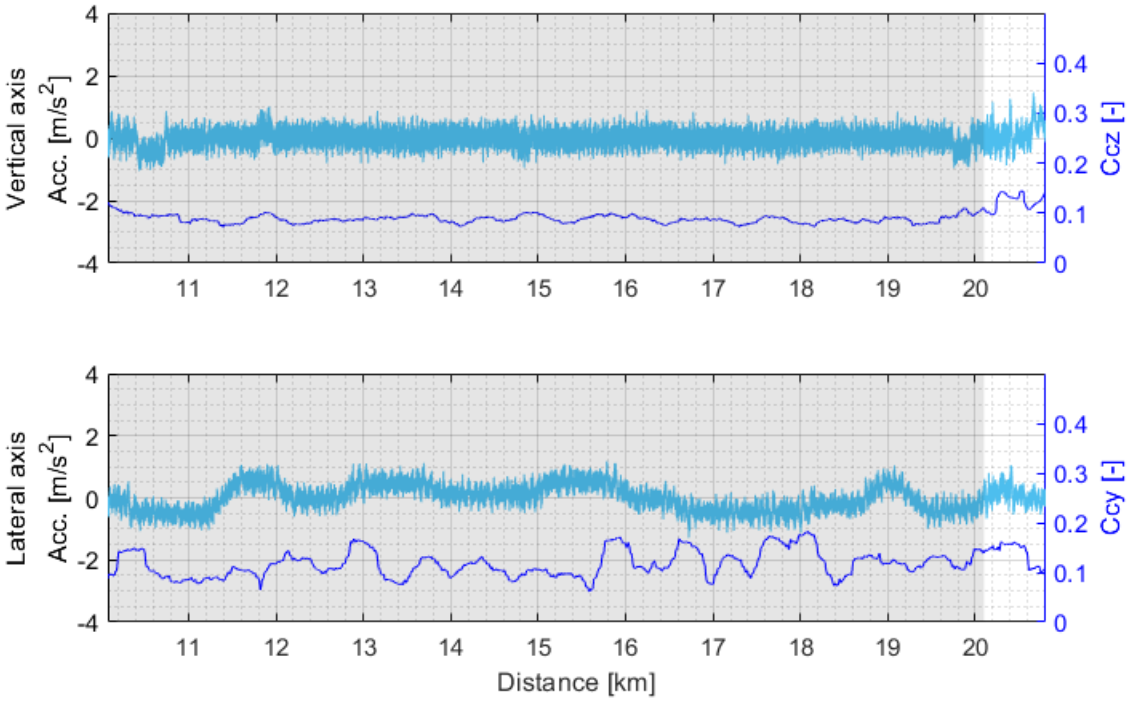


FIGURE 4.10. CONTINUOUS COMFORT AND ACCELERATION FOR A SLAB TRACK.

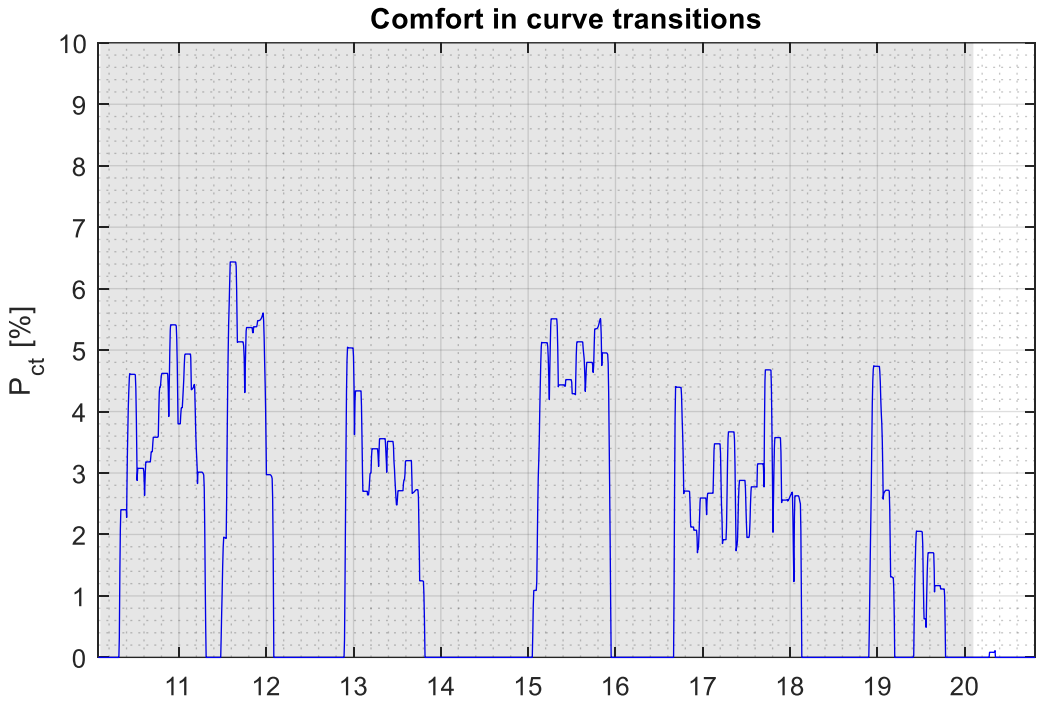


FIGURE 4.11. EVENT-BASED COMFORT FOR A SLAB TRACK.

The comfort indices show a generally lower value, on average Ccz is 20% lower than for the ballasted track, and Ccy is 5% lower, indicating a more comfortable track compared to ballasted track. No value of continuous comfort is above the threshold between "very comfortable" and "comfortable" (0.2 m/s^2), and there are no appreciable changes in vertical comfort associated with the tunnel. The reduction of vertical comfort in km 20 onwards is related to the exit of the tunnel, whilst the changes in lateral comfort are again associated with curved segments in the track, as lateral forces in the vehicle cause vibrations in that direction. The mean values for comfort cannot be calculated for this segment, as the time spent travelling is too low for their estimation (170 s).

In addition to ride comfort (or discomfort), the standard ISO 2631 describes the use of indices designed for assessing passenger health and motion sickness. These indices are designed for

longer periods, in the order of several hours, so these are out of the scope of this thesis. Nevertheless, these indices are explained in Appendix A. Comfort indices.

4.3. SLAB AND BALLASTED TRACK COMPARISON

The sections presented above are using the same vehicle running at the same speed (63 m/s) and have a similar track geometry for most of the selected distance, as observed in Figure 4.1 and Figure 4.7. It is possible to compare comfort between them to evaluate their similarities and differences. Table 4.2 presents all the discussed indices between ballasted and slab track, showing the maxima and mean values for comparison.

TABLE 4.2. COMPARISON OF COMFORT INDICES FOR BALLASTED AND SLAB TRACK.

Type of track	Ballasted track	Slab track	
Index			Units
$\max(C_{Cz})$	0.225	0.144	m/s^2
$mean\ C_{Cz}$	0.114	0.091	m/s^2
C_{Cy}	0.246	0.182	m/s^2
$mean\ C_{Cy}$	0.122	0.118	m/s^2
$\max(P_{CT})$	7.71	6.43	%
$mean\ P_{CT}$	1.23	1.8	%
$\max(P_{DE})$	0	0	%
$mean\ P_{DE}$	0	0	%

All comfort indices from EN 12299 and ISO 2631 show higher values for the ballasted track, showing that ride quality and health are generally worse for ballasted than for slab track. Still, both tracks are mostly “very comfortable” and show the good quality of the track. There are elements in the ballasted track, such as the viaducts and the S&C, that affect comfort, although this effect cannot be compared to the slab track, as these elements do not appear in this segment.

Thus, according to the data presented in the previous sections, it is concluded that slab track is more comfortable than ballasted track and that there are elements of the track that influence

vehicle comfort, such as S&Cs and viaducts. This fact can be used for evaluating track elements or detecting possible faults using sensors located on the vehicle body (secondary suspension).

4.4. EVOLUTION OF VERTICAL COMFORT

As discussed in the previous sections, comfort can be used to assess the state of a track. Data collected over time would provide information on the evolution of the track. In this subsection, vertical and lateral comfort indices based on EN 12299 are obtained for runs spanning several months and compared to evaluate the changes in track condition, and observe the effects of varying speed on comfort. Same as for the previous sections, the tunnel segments are shaded in grey and the S&Cs are marked with a dashed line. Figure 4.12 shows the vehicle speed estimates for ten journeys spanning four months. Speed and distance have been estimated using the method presented in Chapter 3.

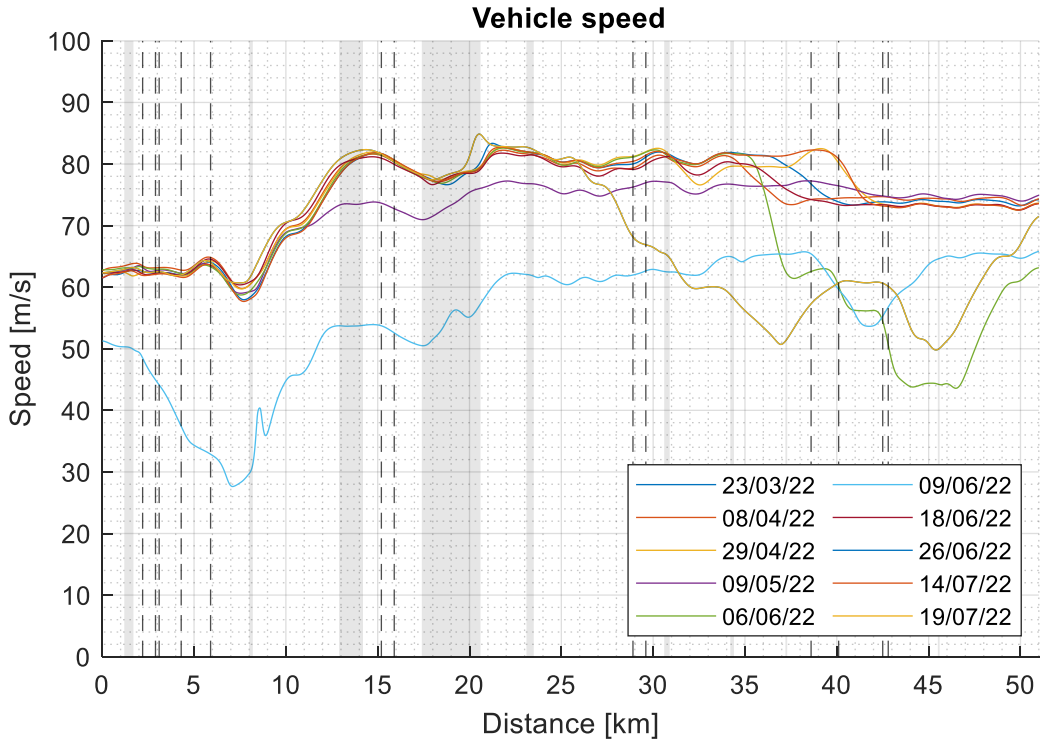


FIGURE 4.12. VEHICLE SPEED FOR THE DIFFERENT DATES.

Some journeys, such as the ones on 9 of June and 19 of July (blue and orange lines respectively), have lower speeds. The journey on 9 of June is generally at 80% of the speed of the other runs, whilst the journey on 19 of July is at a similar speed up to km 25, in which speed decreases to 75% of regular speed. This is expected to affect comfort, as previous research proved the influence of speed on vertical vibrations and comfort [81]. The evolution of cab vertical displacement is presented in Figure 4.13, in order of date from top to bottom and roughly 2 weeks apart each. Vertical displacement is filtered using a low-pass 70-m wavelength filter, allowing only shorter wavelengths to pass.

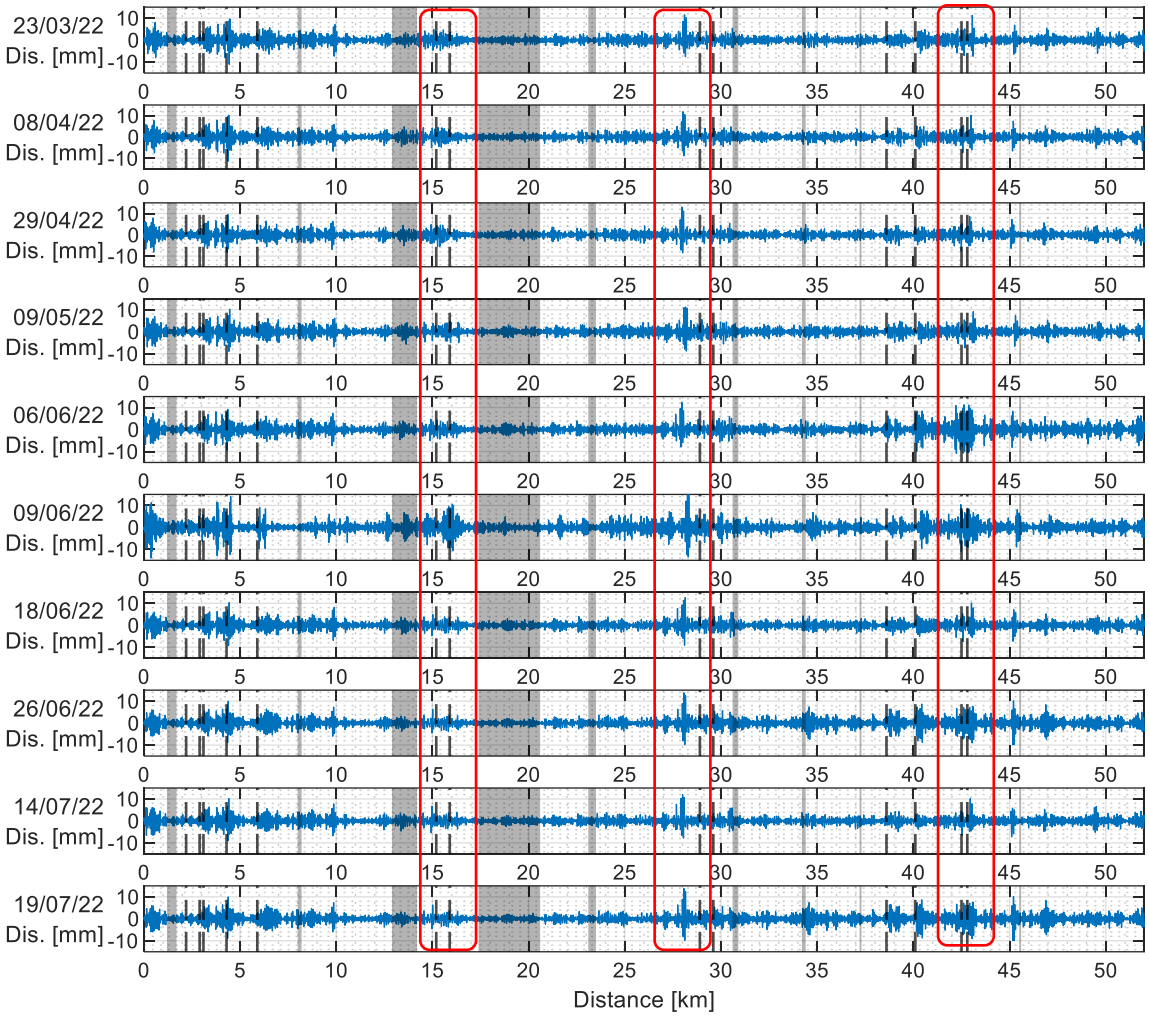


FIGURE 4.13. EVOLUTION OF CAB VERTICAL DISPLACEMENT.

There are changes in vertical displacement, most notably in the runs on the 6 and 9 of June, most observable close to S&Cs such as in km 16, 28 and 42, highlighted with a red border. This is due to the changes in their condition and further replacement of these components, such as the switch nose in km 42 being repaired in early June, and shows how the state of the track affects the vehicle measurements, and how this can be observed from the vehicle cab, as a worse track quality increases the vertical displacement of the cab. The evolution of vertical comfort according to EN 12299 (Ccz) over time is presented in Figure 4.14, whilst the evolution of lateral comfort (Ccy) is presented in Figure 4.15. The thresholds are based on the standard EN 12299: below 0.2 the journey is very comfortable, between 0.2 and 0.3 is comfortable, between 0.3 and 0.4 is medium, and over 0.4 is less comfortable. The journeys with lower speeds (9 June and 19 July) are highlighted with a red rectangle in the date axis.

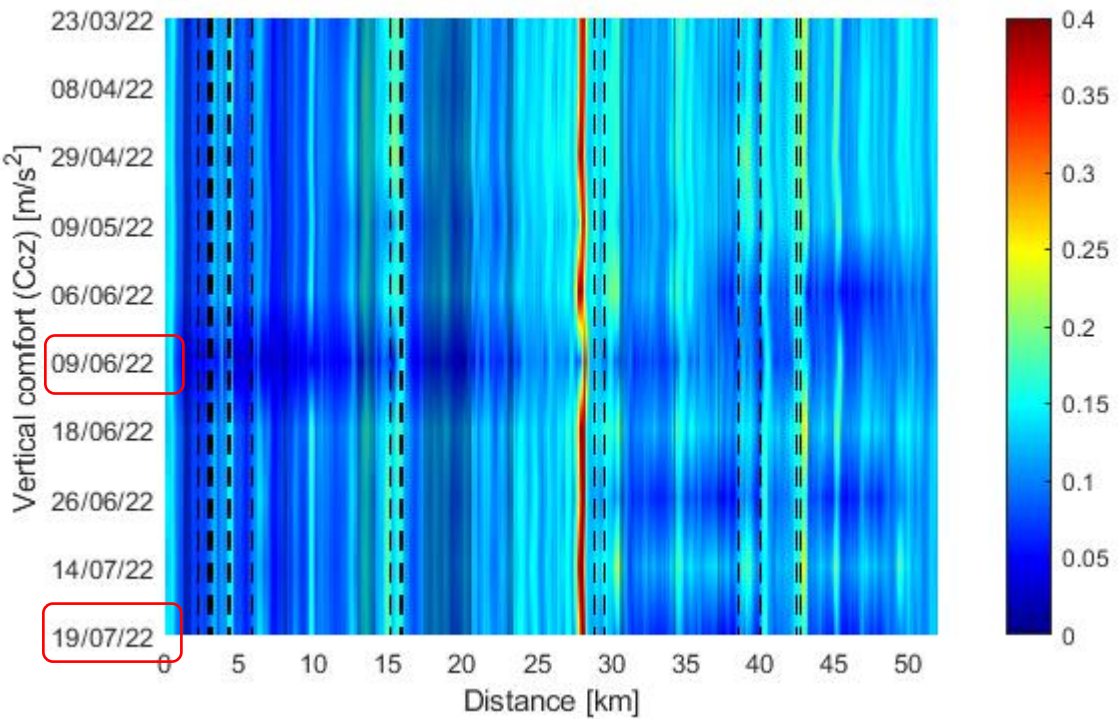


FIGURE 4.14. EVOLUTION OF VERTICAL COMFORT.

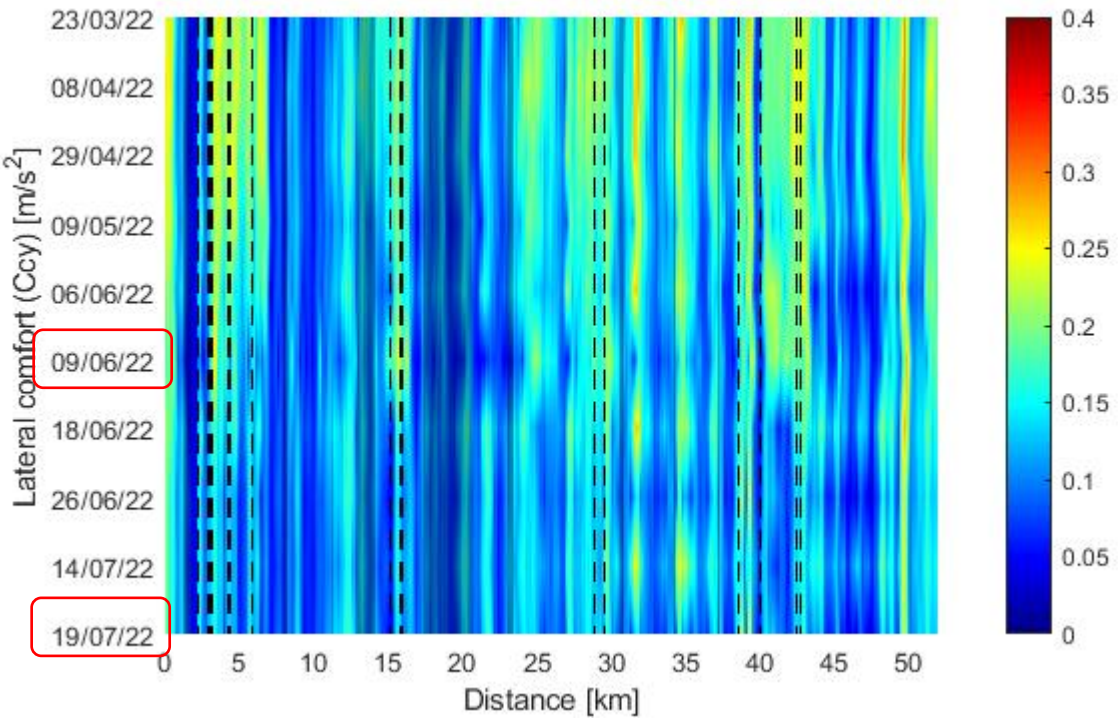


FIGURE 4.15. EVOLUTION OF LATERAL COMFORT.

There are differences in comfort due to speed observed, in the journeys on the 6, 9 and 26 of June, mostly visible in the vertical comfort. This agrees with the results from [81], which show a worsening comfort perception as speed increases. The effects of viaducts in km 28 are observed in all the journeys, with changes in comfort magnitude over time due to its condition and the comfort index approximating the highest threshold. The effects of the S&Cs are observed, with a notable increase in vertical comfort magnitude in most of the S&Cs, showing the effects of these components on vehicle comfort. Data through the tunnel in km 17 to 21 show little difference, mostly due to the small variations of vehicle speed in the tunnel.

4.5. CONCLUSIONS

In this chapter, the comparison of comfort according to the standards EN 12299 and ISO 2631 was presented. The results from ISO 2631 do not differ much from the ones presented by the standard EN 12299, as the interpretation of data provided is similar. The guidelines for the interpretation and reporting of results are much clearer for EN 12299, as this standard is explicitly designed for railway applications, whilst ISO 2631 is designed for a more general purpose. Thus, this standard is preferred for the evaluation of comfort in railways. The other procedures can be useful for longer runs, although the mean comfort values provided could be extrapolated to motion sickness and health assessment.

Regarding the track, the effects of different track elements, such as a viaduct and an S&C are observed in the vehicle, showing how the condition of these elements can be evaluated using sensors in the vehicle body. The differences between ballasted and slab track have been evaluated, showing how slab track is generally more comfortable than ballasted track for a running passenger vehicle. However, some short-wavelength features of the track may not be observable using comfort, so it would be necessary to use other processing methods to complement these indices.

Differences between journeys have been observed. The most notable differences are caused by speed variations between runs on the same location, showing the dependency of passenger comfort to speed, and due to the condition of the track and its different elements, such as viaducts, S&Cs and tunnels. Thus, the effects of vehicle speed must be considered when estimating passenger comfort.

In summary, this chapter presented the differences between commonly established comfort indices, as well as the differences between ballasted and slab tracks and their evolution over

time. Comfort according to the EN 12299 has been proven the most useful to show these differences and the general state of the track more accurately, while the results from the standard ISO 2631 show a less detailed overview of the journey. Hence, the EN 12299 standard is chosen for comfort evaluation and is used in the subsequent chapters to assess the state of the track by comparing the comfort indices to vertical acceleration and displacement. It is to be noted that using comfort estimation alone is not enough to assess track quality, as short-wavelength features are likely to be overlooked. Comfort indices must be used complementary to other information extracted from the data, such as the frequency response or the vehicle displacement. These indices should not be disregarded in passenger trains, as they provide valuable information on the condition of the vehicle and the expected passenger experience throughout the journey.

Chapter 5. Effects of vehicle orientation and direction

5.1. INTRODUCTION

The previous chapters presented a method to estimate vehicle speed and position, and the attempts to use passenger comfort for track quality assessment, explaining both their capabilities and limitations. This chapter shows the similarities and differences between signals measured in the different components of a railway passenger vehicle (axlebox, bogie and cab in this chapter). The effects of the sensor location and the direction of travel are evaluated as well. To do so, a section of track characterised by a long-wavelength change in vertical alignment and the track gradient is selected, as its effects are present in all the components. The arrangement of sensors in this chapter is the same as the one described in Chapter 3: the axlebox sensors are installed on both wheels of the wheelset, the bogie and cab have installed accelerometers and gyroscopes measuring in all directions, and a GNSS receiver measuring vehicle speed and location.

5.2. TEST CONDITIONS

The segment of track selected for this chapter is a 1.4 km stretch of ballasted track with a change in vertical alignment, in the centre of the segment between 21.9 and 22.25 km in the figures.

The vertical alignment, crosslevel and curvature of this segment (provided by the reference) are presented at the top, centre and bottom of Figure 5.1, respectively. Dashed lines in the vertical alignment, or vertical level subplot show the distance where it changes. The vertical alignment is indicative of the changes in track geometry in the vertical direction, whilst the crosslevel and curvature are indicative of the changes in the lateral direction, showing the position and orientation (left or right) of track curves, as tracks curves generally have an inclination of the lateral plane to avoid vehicle derailment at high speeds.

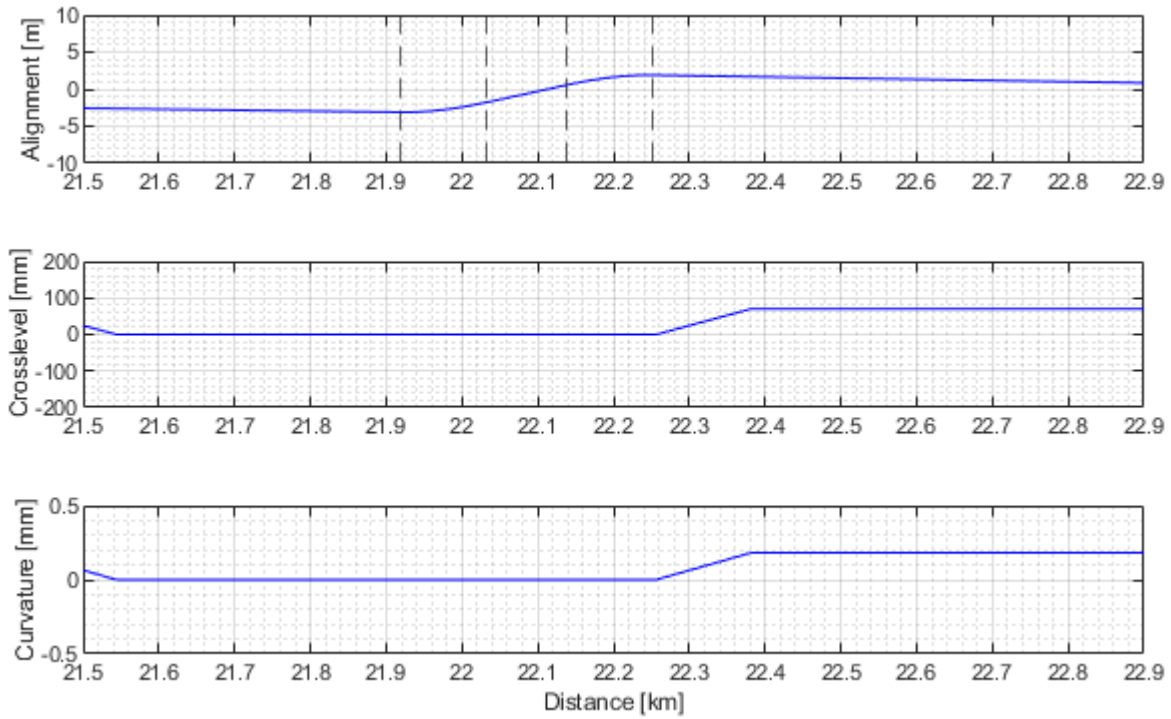


FIGURE 5.1. VERTICAL ALIGNMENT (TOP), CROSSLEVEL (CENTER) AND CURVATURE (BOTTOM) OF THE TRACK SEGMENT.

The vehicle travels on either the up or down (to and from London) lines, where the down line (from London to Eurotunnel) is the direction for which the track mileage increases. Depending on the vehicle orientation, sensors acquire signals either on the leading or trailing coach (vehicle). There are then four different configurations to be considered, presented in Figure 5.2, and described as:

A. Vehicle on the up line with sensors in the leading coach.

B. Vehicle on the up line with sensors in the trailing coach.

C. Vehicle on the down line with sensors in the leading coach.

D. Vehicle on the down line with sensors in the trailing coach.

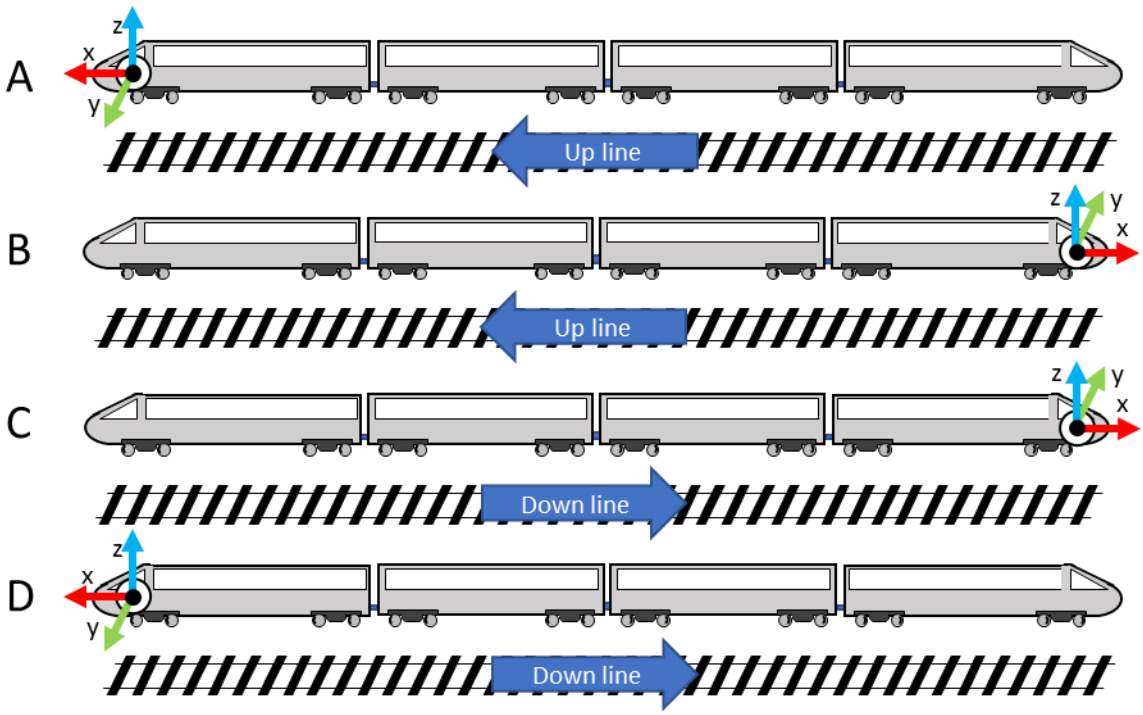


FIGURE 5.2. SENSOR CONFIGURATIONS FOR THE TEST.

The configuration used to align all the other configurations is the down line with sensors in the leading coach, as the orientation of the sensors and the direction of travel are the same as the reference. After a reference configuration is chosen, signals are aligned to the track, between sources (axlebox, bogie and cab), and between journeys, as described in the following paragraphs. In this chapter and the following one, an arrow pointing at the direction of travel is added to the figures, as this also influences the results obtained.

Alignment to the track is carried out as described in Chapter 3, using crosslevel as a reference. Alignment between sources is carried out using cross-correlation on the vertical displacement because the signals of each component are not synchronised. Finally, alignment between journeys is also performed using cross-correlation, as the variations between speed and distance are small enough to consider this method over dynamic time warping, as discussed in Chapter 3

Once all datasets have been mutually aligned, and converted to the spatial domain, it is possible to analyse their similarities and differences. Signal processing methods applied in this chapter are frequency analysis and wavelength filtering, which are similar to methods provided in EN 13848-1 [9], and comfort estimation is based on EN 12299 [11]. Observations extracted from these signal processing methods on the data are discussed in this chapter.

5.3. COMPARISON BETWEEN COMPONENTS

This section presents the comparisons between the signals from the axlebox, bogie and cab for a single journey. Vertical acceleration is the only signal available for all components, hence the comparison between them is carried out using this signal. The rest of the signals (longitudinal and lateral acceleration, and yaw, roll and pitch rate) are compared using only bogie and cab

data. Figure 5.3 shows the vehicle vertical acceleration against distance. The direction of travel is represented with a black arrow.

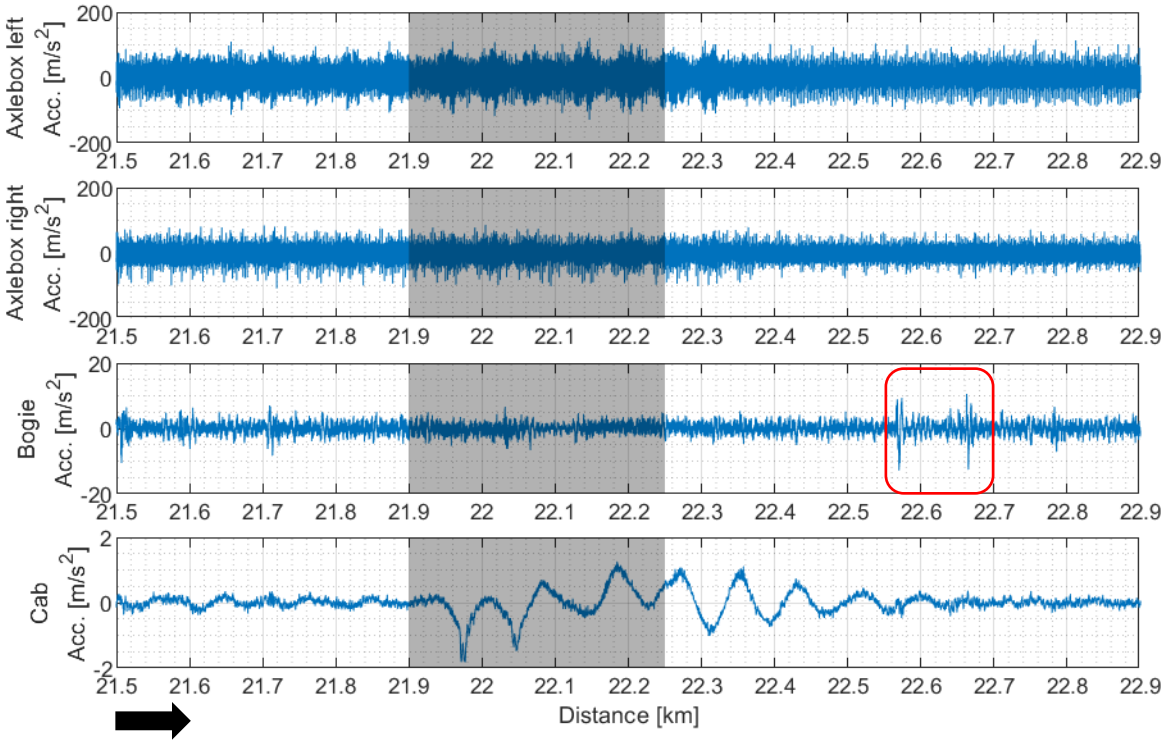


FIGURE 5.3. AXLEBOX, BOGIE AND CAB VERTICAL ACCELERATION.

Both axlebox sensors show similar behaviour, with high-frequency components dominating the signal and a peak-to-peak amplitude in the order of 75 m/s^2. The bogie sensor shows peaks in the order of 10 m/s^2 at km 22.58 and 22.68 and the peak-to-peak amplitude of the signal in the rest of the segment is in the order of 4 m/s^2 whilst the cab shows a prevalence of low-frequency components, as observed between km 21.9 and 22.6. The acceleration amplitude on the left axlebox is higher than on the right, due to differences in the state of each wheel. The bogie signal shows a decrease in magnitude due to the primary suspension. Regarding the cab, the magnitude of the signal is much lower than both the bogie and the axlebox, due to the primary and secondary suspension springs and damping. The frequency domain version of the signals

is presented in the spectrograms in Figure 5.4. The direction of travel is represented with a black arrow.

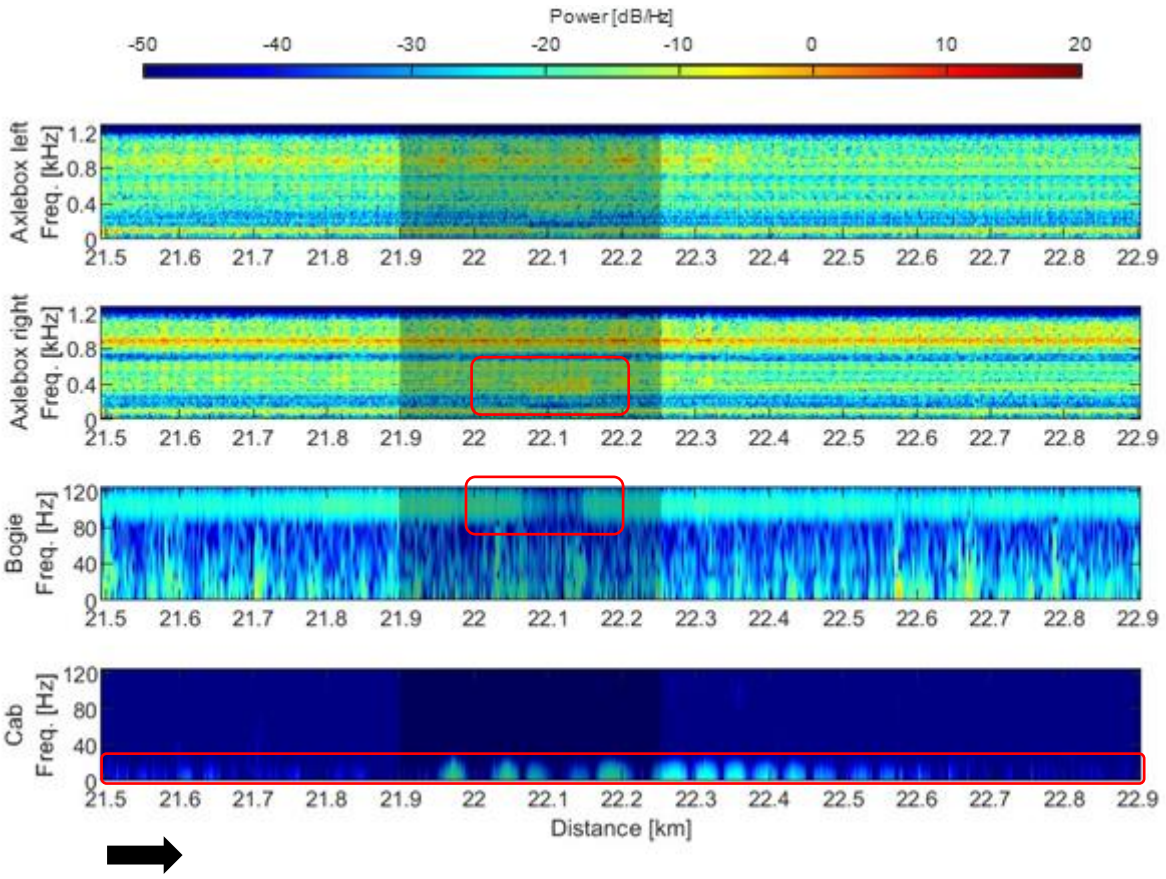


FIGURE 5.4. AXLEBOX, BOGIE AND CAB VERTICAL ACCELERATION SPECTROGRAMS.

The main differences observed between spectrograms are the decreasing magnitude of signals and the shift to lower frequencies from axlebox to bogie to cab. This can be attributed to both the damping effects of the primary and secondary suspensions, filtering out higher frequencies, and the increasing size of the components. However, there is a harmonic at 105 Hz whose magnitude is significantly reduced, observed in the frequency domain between km 22 and 22.2 in the axlebox and bogie signals. As discussed in Chapter 3, this harmonic is believed to be generated by the interaction of the vehicle with the upper track layers. Determining the causes of the harmonic is out of the scope of this thesis and this chapter, which is focused on analysing

the effects of the change in vertical alignment in the track. The variations in frequency perceived by the vehicle are due to speed variations [12], as well as a magnitude increase of these vibrations directly related to speed [143, 185]. The cab shows a prevalence of signal energy in the frequency range below 20 Hz due to its resonances, so most of the information that can be extracted from the signal is concentrated in this range.

The effects of the change in vertical alignment are also noticeable in the displacement of the vehicle components, that is filtered using different wavelength filters as presented in Figure 5.5. The direction of travel is represented with a black arrow.

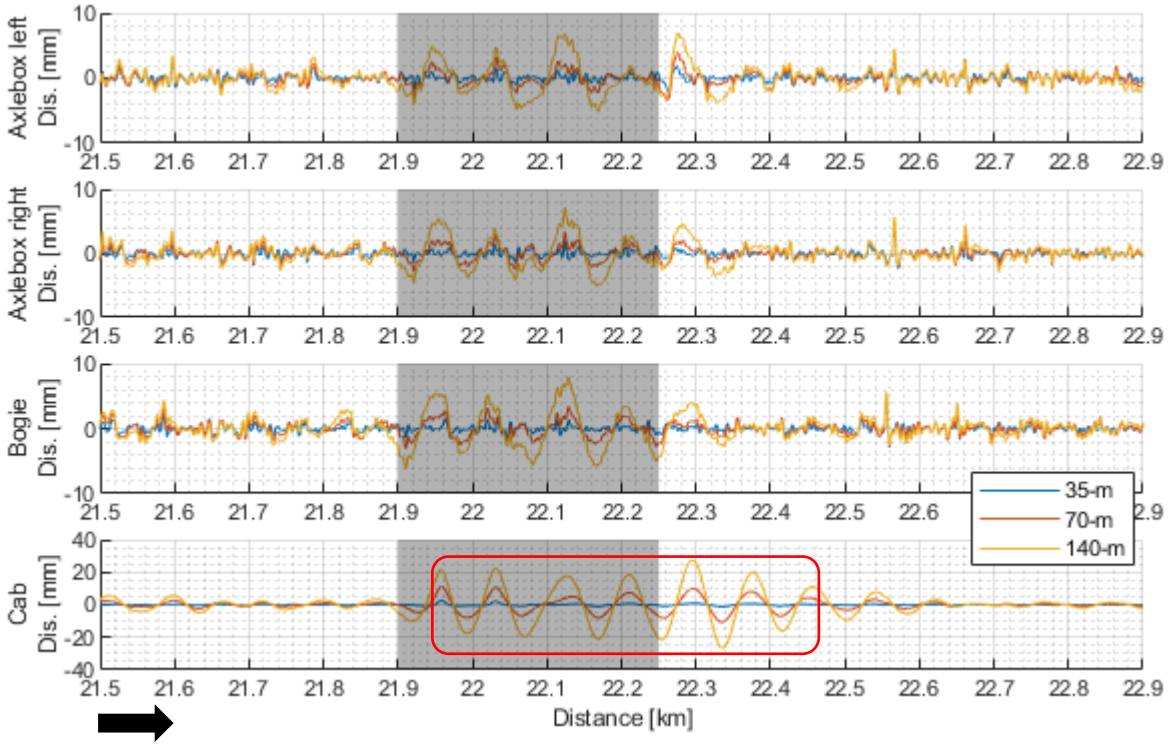


FIGURE 5.5. AXLEBOX, BOGIE AND CAB WAVELENGTH FILTERS OF VERTICAL DISPLACEMENT.

The axlebox and bogie show a displacement with a peak-to-peak amplitude of up to 15 mm, and the cab shows up to 40 mm measured for the highest peak-to-peak range in the 140-m wavelength filtered displacement, with a wavelength of approximately 80 m in km 22 to 22.4. It is observed that the cab movement persists, although the bogie and axlebox have already

stopped their displacement. If the relative movement between the bogie and the cab is too large, depending on the train design, the secondary suspension stops can suffer damage.

The effects of the change in vertical alignment may also be apparent on other sensors, as the changes in the journey conditions may be reflected in the rest of the directions. The sensors acquiring signal in these directions are only installed on the bogie and cab. Thus, comparisons can only be made between these two components. Their respective figures are presented in Appendix C.

The magnitude of lateral acceleration in the bogie and cab is notably lower than for vertical acceleration. This shows that more energy due to vehicle-track interactions is transmitted in the vertical direction than in the others. The effects of the change in vertical alignment are appreciable in both components, although the variation in the signal magnitude is lower. The variation in high-frequency signal in longitudinal acceleration at km 22.1 can be attributed to the decrease in speed due to the change in gradient, whilst the increases in lateral acceleration magnitude in the low-frequency range, observed in km 21.9 to 22.4 can be attributed to the curves in the track, although the relationship is not as clear as for the vertical direction.

The harmonic at 105 Hz can be observed in all of the signals, mostly in the bogie; the lower magnitude of the cab signal (20 dB approximately) shows how the secondary suspension dampens the higher frequencies. Similar to the acceleration figures, the effects of the gradient change are mostly noticeable in the longitudinal axis, mostly in the cab, whilst the lateral axis shows the presence of curves in the low-frequency domain of the cab. The effects of the gradient change and curves are also observed in the displacement, in the different wavelength filters.

Similar to the vertical axis, the signals with the largest magnitude appear in the longest wavelength range, although their magnitude is half the magnitude of displacement for the

vertical axis. This is concordant with the acceleration results. The higher magnitude of lateral displacement of the bogie (up to 12 mm) and cab (25 mm) observed can be attributed to changes in the track curvature in that segment (see Figure 5.1), although the relationship is not as clear as for the vertical direction.

The vehicle yaw, roll and pitch rate also provide information on the track condition, either on their own or in combination with other sensors, therefore they are also analysed. These data are presented in Appendix C. The effects of the change in vertical alignment can be observed mostly in the cab pitch rate sensor, whilst the curved segments are noticeable in both yaw and roll rate sensors. The yaw rate sensor is excited with curves whilst the roll rate sensor is excited in transitions between curved and straight track segments. Most of the information is in the low-frequency range, below 30 Hz, and complements the information extracted from the accelerometers. As explained in Chapter 2, these variations are used to extract track geometry information, such as its crosslevel and curvature.

Within gyroscope signals, a behaviour similar to the accelerometers is observed, with a decrease in the magnitude of the signal from bogie to cab, and a prevalence of the low frequencies in the cab. All the sensors show a dominance of signal in the low frequencies and the presence of the harmonic at 105 Hz. The effects of the change in vertical alignment are observed in the decreased magnitude of the harmonic at 105 Hz, whilst the curved segments are mostly visible in the yaw rate spectrograms.

Ride comfort has also been calculated for this segment of the track to evaluate the effects of the change in vertical alignment on passenger comfort, and to assess the possibility of detecting track faults using sensors installed on the secondary suspension (cab in this case), comparing the value of comfort to a reference. Figure 5.6 shows continuous ride comfort indices according

to the standard EN 12299 in the track segment. The direction of travel is represented with a black arrow. The green, yellow, and red lines correspond to the thresholds between levels of comfort, as explained in Chapter 1 and Appendix A.

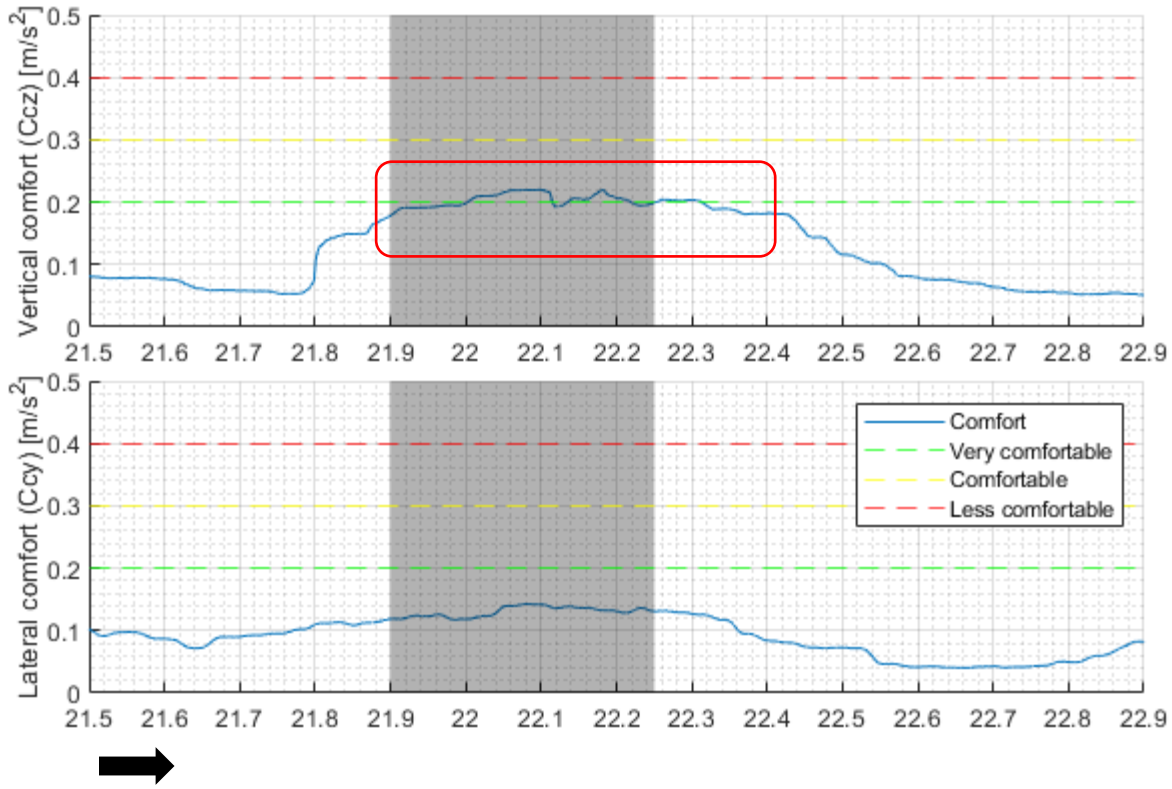


FIGURE 5.6. PASSENGER COMFORT ACCORDING TO EN 12299.

The effects of the change in vertical alignment can be observed in the vertical direction between km 21.9 and 22.4, which crosses the "very comfortable" threshold and moves to the "comfortable" range. The lateral comfort index also increases its value, although less significantly.

In summary, vertical alignment affects the signals on all sensors and components, but mainly the vertical acceleration and, slightly the lateral acceleration. This is also visible in the spectrogram results and estimated displacements. The filtering effects of the primary and secondary suspension are noticeable in the differences between components. The long wavelength and low frequency of this geometry feature affects mostly the cab, due to its larger

size and inertia, compared to the axlebox and bogie. This feature is observed in the 70-m wavelength-filtered displacement, but mostly in the 140-m filter, showing the usefulness of this filter applied for high-speed vehicles.

Regarding the information available, raw acceleration or roll rate do not provide much detail on the effects of track geometry on the vehicle, hence the necessity to process them to obtain values that are easier to analyse and to associate with track condition. The spectrograms show the magnitude of vibrations and their frequency more clearly, so it is possible to extract resonances and harmonics from them, such as the harmonic at 105 Hz observed in most of the sensors. Displacement and alignment, in any direction, show the physical effects of the track on the different components of the vehicle, and the track geometry and state, thus their value for analysis. Finally, comfort shows the effects of changes in track geometry on the passengers and can be used to complement displacement to show the state of the track.

Differences in measurements due to the location of the sensors relative to the vehicle travel direction also arise, hence additional analysis is presented in the following section. Since most of the information can be extracted from the vertical accelerometers, the analysis of the signal in the following section is carried out focusing on vertical acceleration and its derived measurements. For a clear and accessible text, only the displacement using a 140-m wavelength filter and comfort figures are presented in the section. The rest of figures are presented in Appendix C of this work.

5.4. COMPARISON BETWEEN CONFIGURATIONS

As explained in Section 5.2 of this chapter, there are four different configurations for the vehicle travelling through the track (up or down line) and the positions of the sensors (leading or

trailing). The effects of the track quality on the vehicle, vertical alignment in this example, vary depending on the configuration and are discussed in this section. For a correct comparison, the speed of the vehicle for all tests must be similar, and signals must be aligned. For this chapter, there are 52 runs available, distributed as presented in Table 5.1.

TABLE 5.1. AVAILABLE RUNS FOR EACH ORIENTATION AND CONFIGURATION.

Direction	Orientation	Available runs
Up	Leading	9
Up	Trailing	12
Down	Leading	10
Down	Trailing	21

Figure 5.7 shows the vehicle speed of all the configurations. The black arrow in each subfigure indicates the direction of travel.

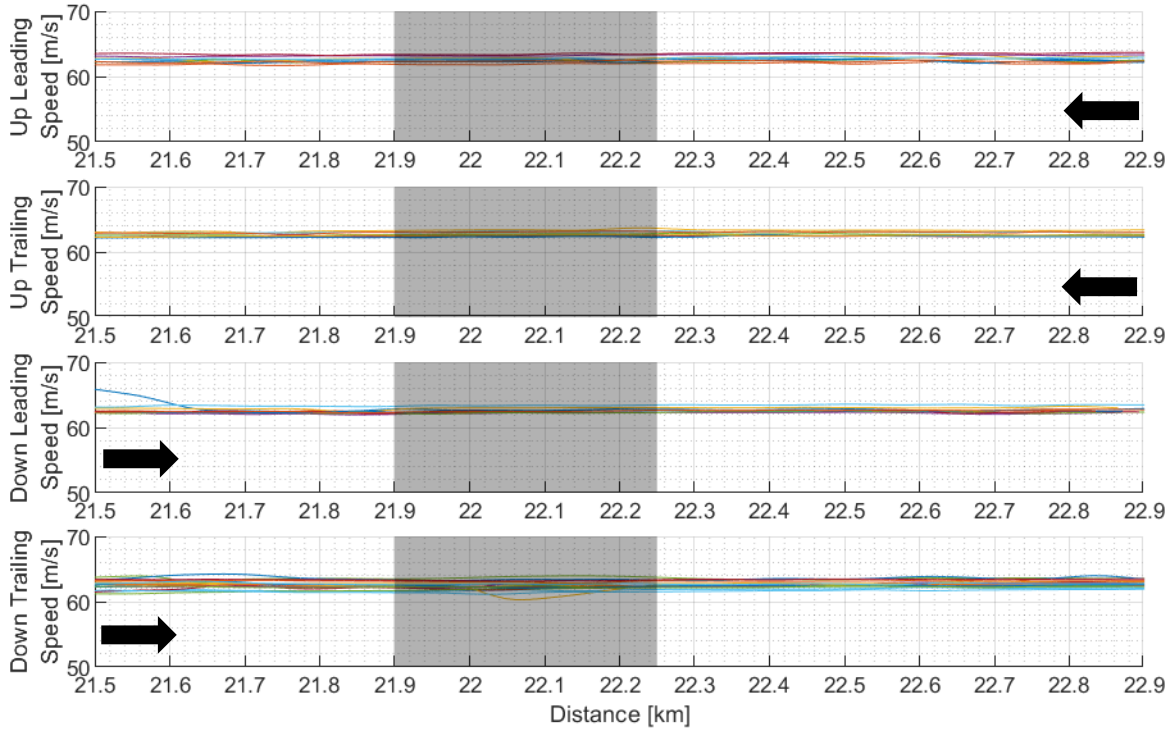


FIGURE 5.7. SPEED DATA FOR ALL THE CONFIGURATIONS.

The vehicle speeds are similar for all the configurations; therefore, a comparison especially on the ride quality is fair. Prior to the comparison, signals are aligned using the same method as explained in Chapter 3 combining crosslevel alignment and cross-correlation. The runs in the up line have been reversed and aligned using the reference provided for that line and aligned to the runs in the down line using cross-correlation in the selected segment.

The first comparison is made through vertical acceleration. There are slight differences in some of the signals that can be attributed to differences in the lines, most notably in km 21.7 and 22.3 in the axlebox and bogie signals, and between km 21.9 and 22.5 in the cab signal, as the up and down lines are likely to have slight differences in vertical alignment but generally not in the long-wavelength range. A similar behaviour is observed on the bogie signal, which is more affected by changes in the track, as explained in the previous section. The most notable differences are in the cab sensors, showing a higher acceleration for the trailing coaches and a longer-lasting signal magnitude increase. The behaviour of the cab may be caused by the connection to the rest of the vehicle, in which the movement of the leading coaches is restrained by the rest of the vehicle, whilst the trailing coaches move more freely.

The frequency behaviour of each component can be observed in the spectrograms in the following figures. The datasets used in these figures are from similar dates and serve as examples for the whole set of runs. The data represented is in Figure 5.8 for the left axlebox, Figure 5.9 for the right axlebox, Figure 5.10 for the bogie, and Figure 5.11 for the cab. The black arrow in each subfigure indicates the direction of travel.

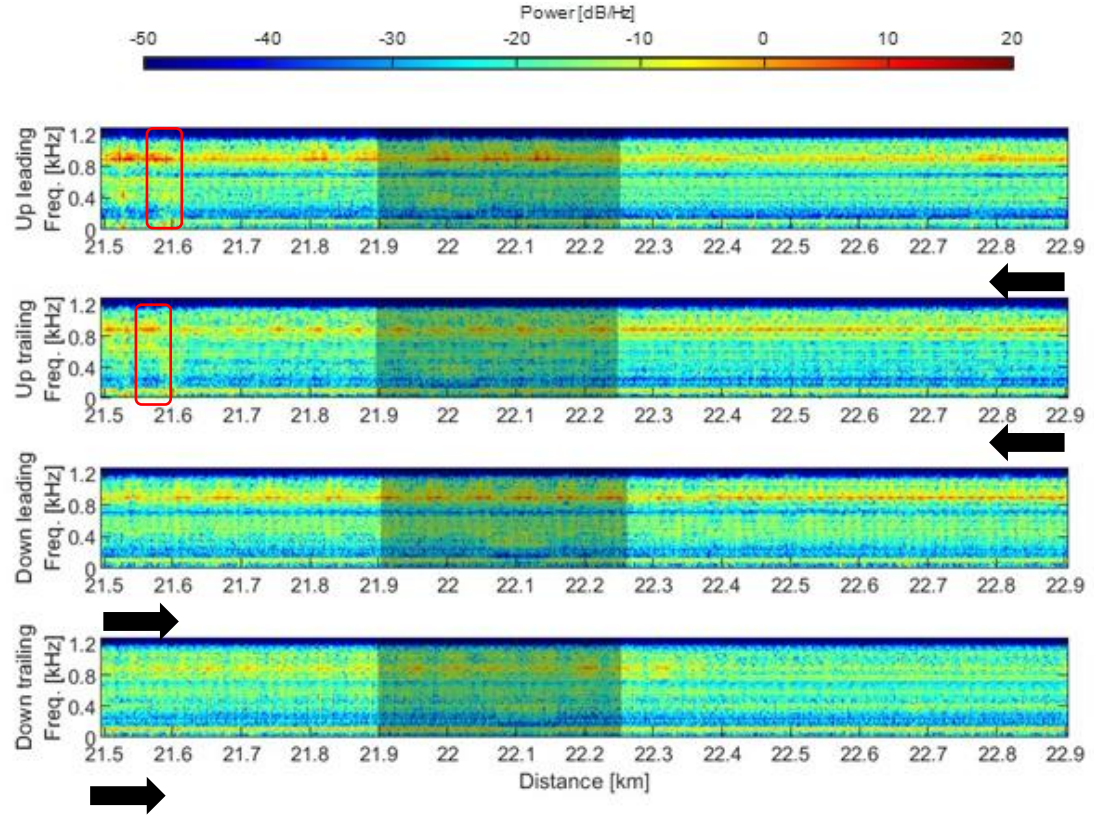


FIGURE 5.8. SPECTROGRAM COMPARISON FOR THE AXLEBOX LEFT SENSOR.

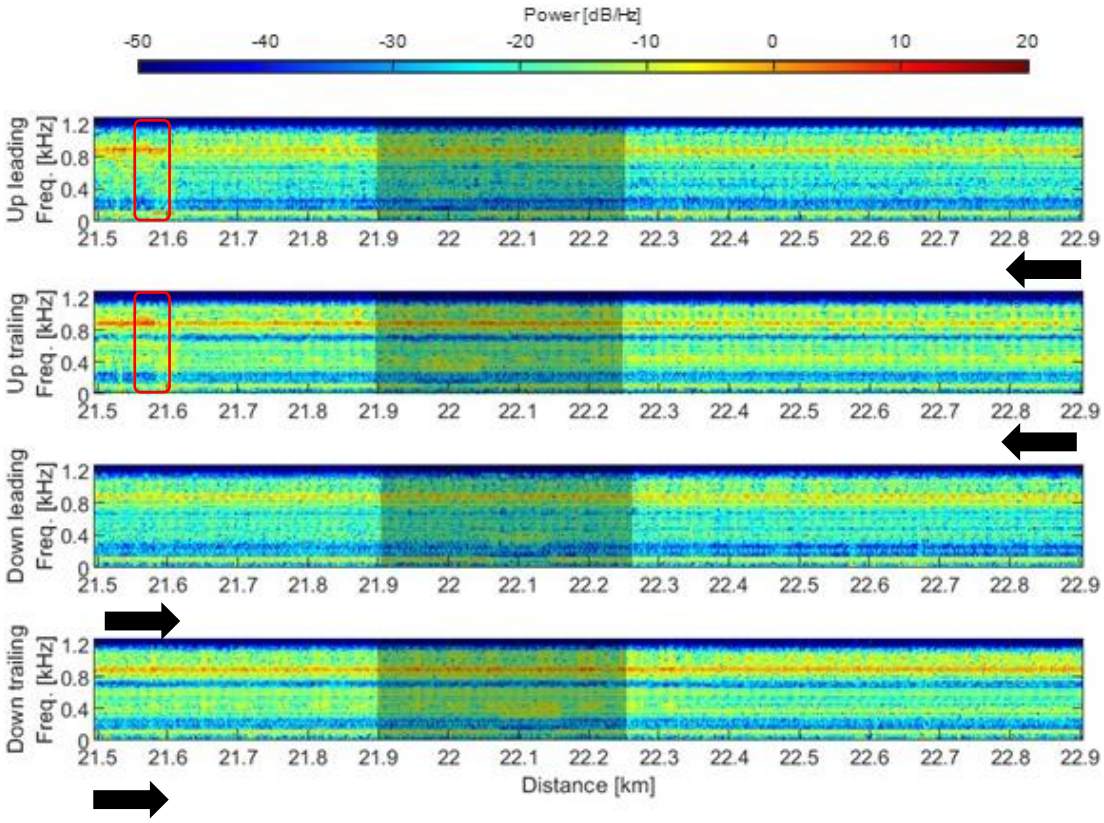


FIGURE 5.9. SPECTROGRAM COMPARISON FOR THE AXLEBOX RIGHT SENSOR.

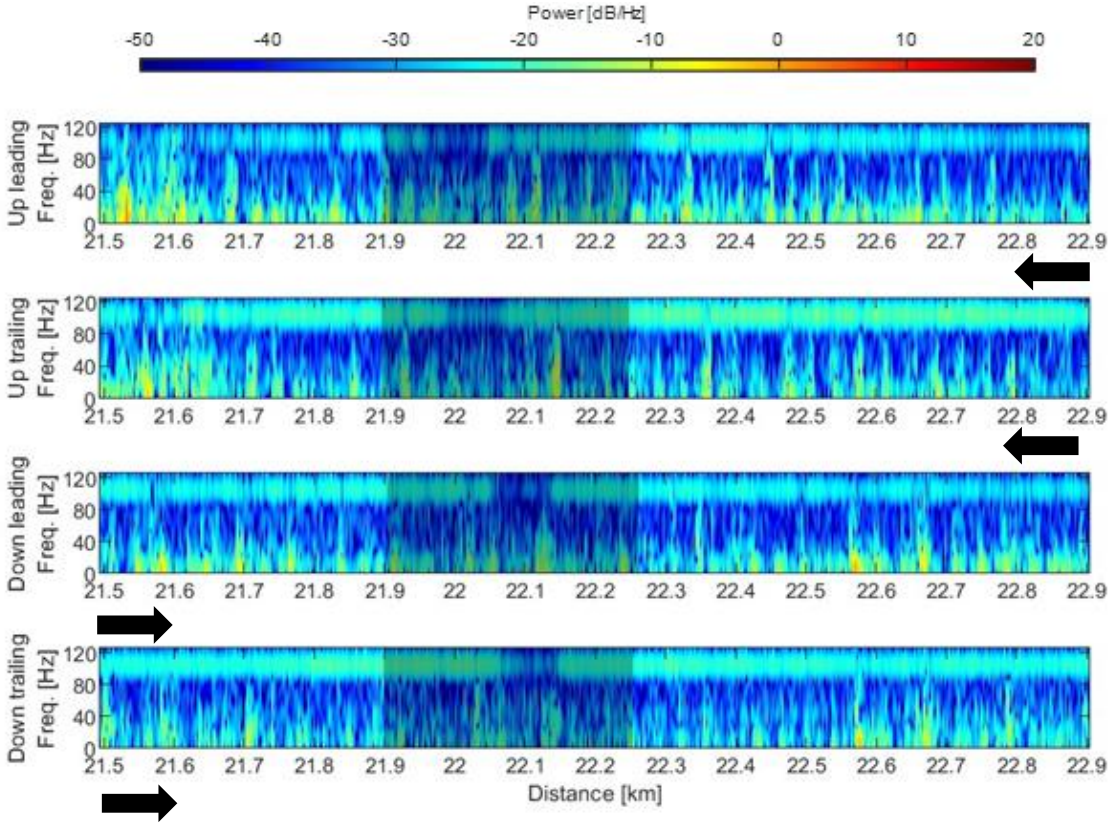


FIGURE 5.10. SPECTROGRAM COMPARISON FOR THE BOGIE SENSOR.

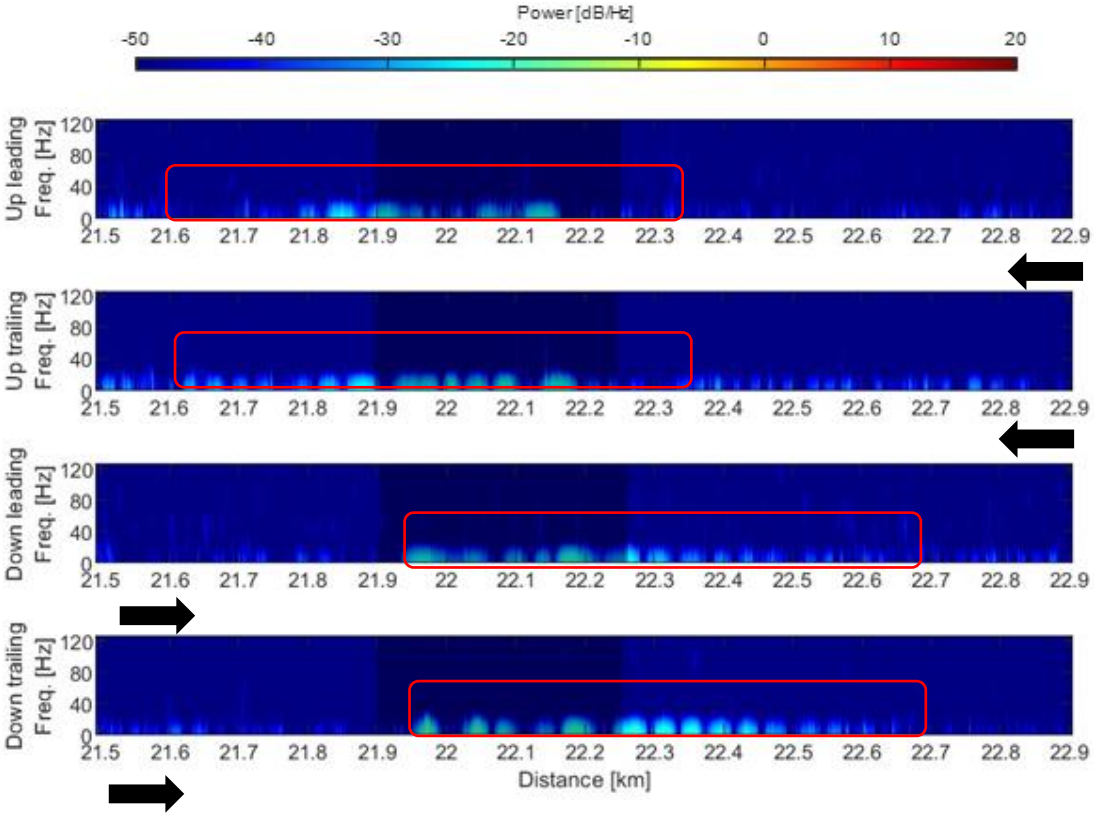


FIGURE 5.11. SPECTROGRAM COMPARISON FOR THE CAB SENSOR.

None of the axlebox spectrograms shows significative differences in the magnitude of the signal, other than the appearance of high-power points in the km 21.6 in the up-line sensors, most likely due to an unidentified track feature in that location. There are slight differences in magnitude between leading and trailing coaches, and the leading coaches have a 5% higher magnitude of acceleration in the axlebox signals. The most notable differences are in the cab sensors, as the trailing sensors have a generally higher magnitude of signal (up to 20% of the magnitude, as highlighted as red rectangles in Figure 5.11) and a longer lasting effect of the longer wavelength track features, up to 200 m longer for the trailing coaches.

The differences in displacement are commented on the following paragraphs. For a clearer text, only the 140-m wavelength-filtered displacement is presented in this chapter. Displacement estimated using the remaining filters is presented in Appendix C. Figure 5.12 shows the 140-m wavelength-filtered displacement of the axlebox left sensors, whilst Figure 5.13 shows the 140-m wavelength-filtered displacement of the axlebox right sensors. The change in vertical alignment is highlighted as a grey shading.

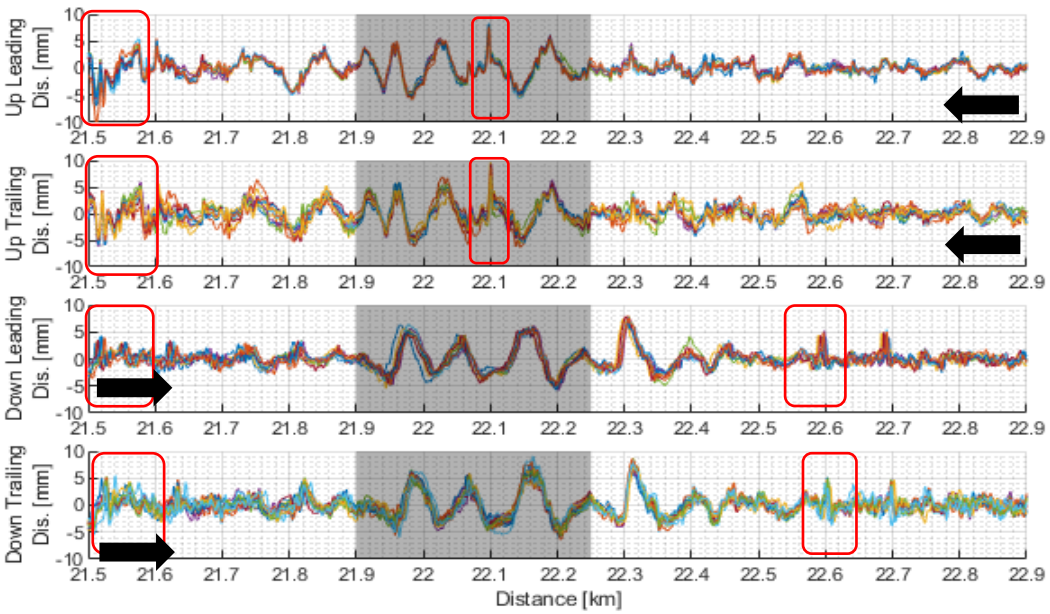


FIGURE 5.12. AXLEBOX LEFT DISPLACEMENT COMPARISON BETWEEN CONFIGURATIONS.

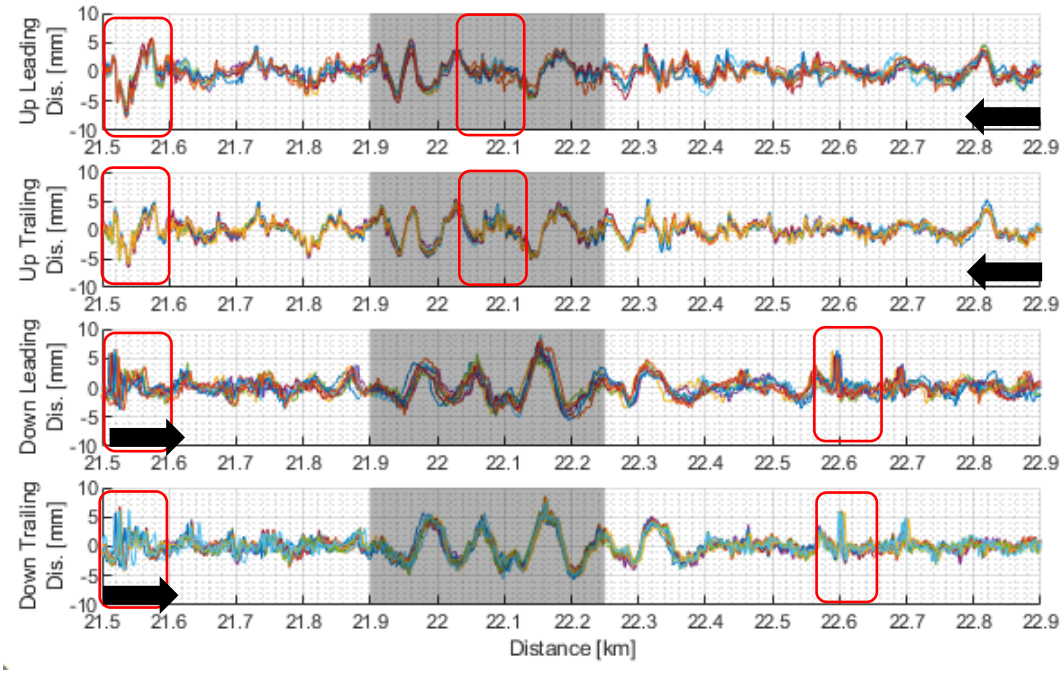


FIGURE 5.13. AXLEBOX RIGHT VERTICAL DISPLACEMENT COMPARISON BETWEEN CONFIGURATIONS.

Regarding the axlebox, the 35-m wavelength-filtered displacement shows little variation, as expected since this is a long-wavelength track geometry feature. In general, the peak-to-peak amplitude of displacement is lower than 3 mm, in both lines and coaches. Both lines show differences due to slight changes in track geometry. There are however several points in which displacement is higher, with an amplitude over 8 mm (in km 21.5 and 22.1 in the up line, and 21.5 and 22.6 in the down line). In these points, the displacement of the trailing coaches is approximately 1 mm larger than for leading coaches. If the amplitude of displacement is 8 mm, this supposes an approximate 12.5% increase, which is not negligible. There are also notable differences in the amplitude of displacement between left and right sensors (such as km 22.1 in the up line, and km 21.5 and 22.6 in the down line), although these can be attributed to differences in the state of the rails, which is out of the scope of this work.

The 70-m wavelength-filtered displacement shows a generally higher magnitude, as expected since more wavelengths are allowed through the filter. The peaks discussed with the 35-m

wavelength-filtered displacement also appear, with a higher magnitude and show consistently that the vertical displacement of the axlebox is larger for the trailing coaches. The change in vertical alignment is observed in the figures, mostly in the ones corresponding to the down line, and highlights the relevance of the direction of travel regarding data acquisition. The differences in magnitude are similar to the 35-m wavelength-filtered displacement, between 10 and 15% throughout the change in vertical alignment.

Finally, regarding the 140-m wavelength-filtered displacement, the effects of the change in vertical alignment are fully noticeable, with a magnitude of displacement larger than for the features discussed above. A larger displacement magnitude and variability is observed in the trailing coaches, due to the movement of the vehicle over the change in vertical alignment. The differences between this filter and the 70 and 35-m filters prove the usefulness of considering several wavelength filters over the same track section to evaluate different track features.

The vertical displacement of the bogie is discussed in the following paragraphs. The 140-m wavelength-filtered vertical displacement is presented in Figure 5.14, where the change in vertical alignment is highlighted with a grey shading, and a black arrow in each subfigure shows the direction of travel. The 35 and 70-m wavelength-filtered displacements are presented in Appendix C.

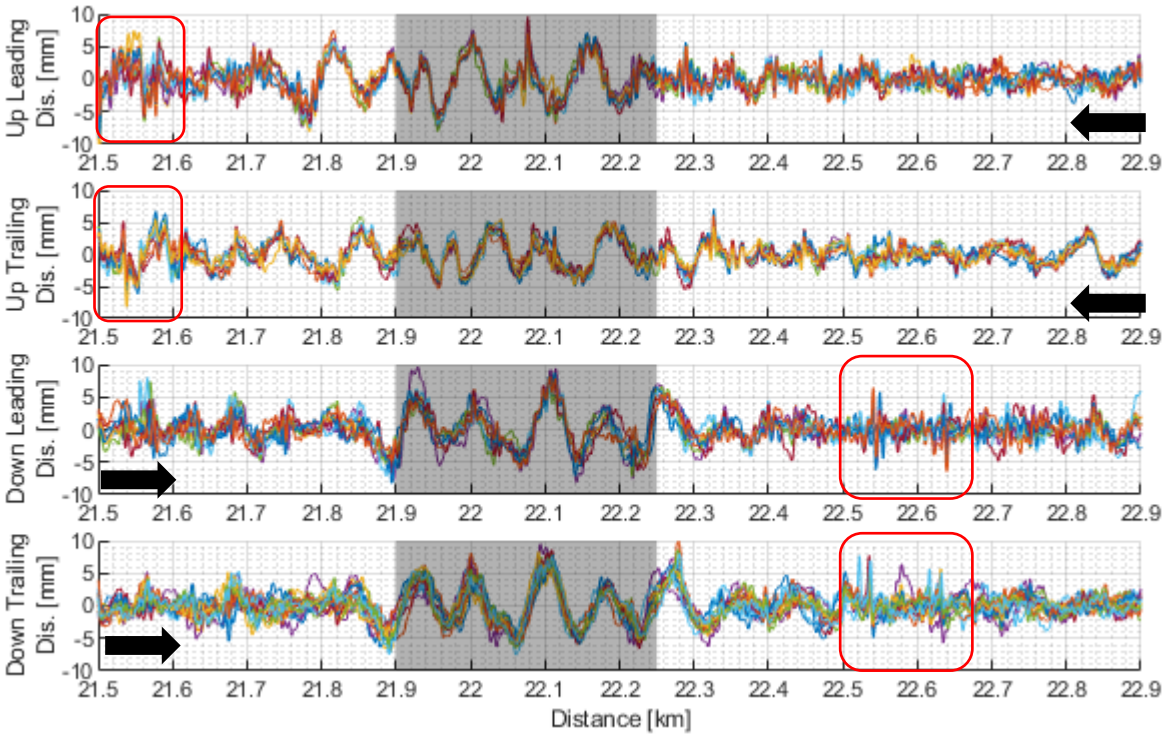


FIGURE 5.14. BOGIE VERTICAL DISPLACEMENT COMPARISON BETWEEN CONFIGURATIONS.

The movement of the bogie is similar to the axlebox in all cases, with slight differences in magnitude due to the relative location of the sensors to the journey. This is expected as the purpose of the primary suspension is to keep the wheels in contact with the track, other than damping the vibrations between the axlebox and bogie. The 35-m wavelength-filtered displacement shows peaks in the same position as the axlebox (in km 21.5 for the up line, and km 22.5 and 22.7 for the down line). However, there are some peaks damped or removed, such as the ones at km 21.5 and 22.1, most likely caused by the primary suspension. The general peak-to-peak amplitude of displacement is slightly larger than for the axlebox, over 4 mm for the whole segment.

The 70-m wavelength-filtered displacement of the bogie shows results consistent with the axlebox displacement: a larger magnitude of displacement, and the appearance of the change in vertical alignment. The high similarity between axlebox and bogie signals is due to the primary

suspension, which is designed for keeping contact between wheels and track, and whose dampening effects are not appreciable in the displacement.

The 140-m wavelength-filtered displacement shows a magnitude larger than the previous filters. Same as for the previous filters, the magnitude of the displacement for leading coaches is slightly larger in the change in vertical alignment, more noticeably in the up line. This shows that the position of sensors, as well as the wavelength filter applied, influence differently the signals acquired.

The vertical displacement of the cab is discussed in the following paragraphs. The 140-m wavelength-filtered vertical displacement is presented in Figure 5.15, where the change in vertical alignment is highlighted with a grey shading, and a black arrow in each subfigure shows the direction of travel. The 35 and 70-m wavelength-filtered displacements are presented in Appendix C.

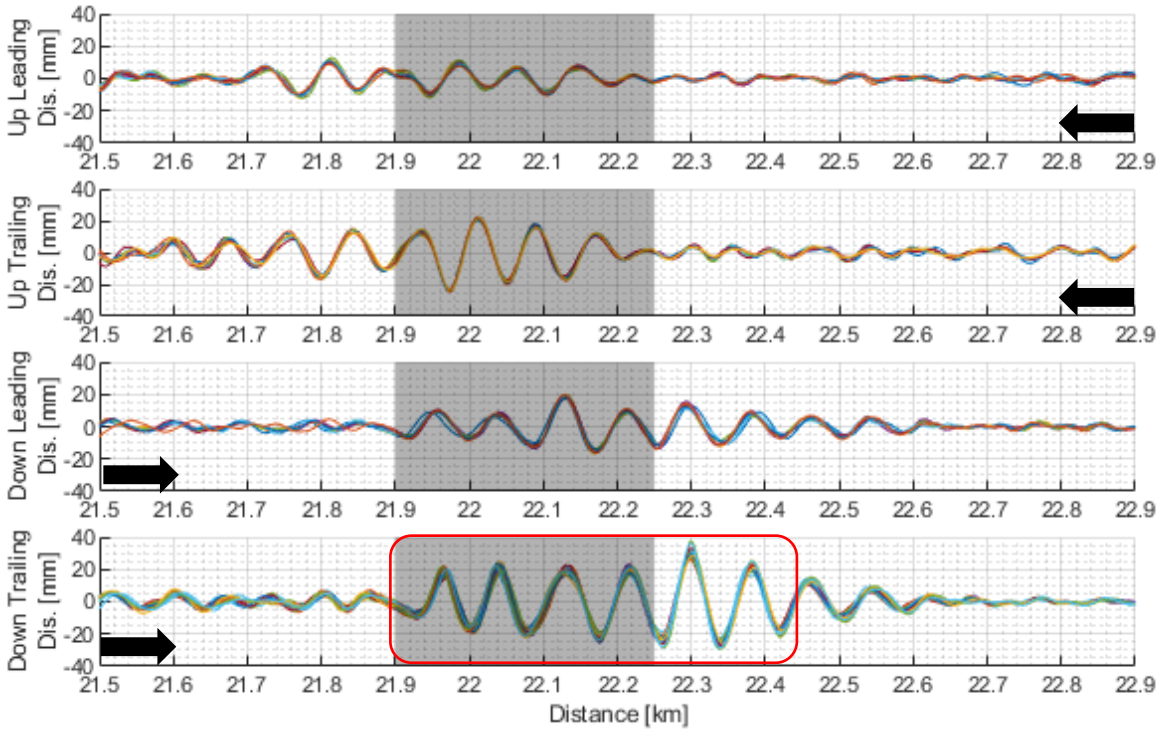


FIGURE 5.15. CAB VERTICAL DISPLACEMENT COMPARISON BETWEEN CONFIGURATIONS.

The cab shows the largest variations between filters, directions, and orientations, as observed in Figure 5.15. The low magnitude of the movement in the 35-m wavelength-filtered displacement is consistent with the results from the axlebox and the bogie, due to the low frequency of the movement. The general magnitude of displacement is below 2 mm, due to the secondary suspension damping most of the high-frequency components of movement. In this filter, there are already appreciable differences between leading and trailing coaches, as observed between km 21.9 and 22.4 in the down line, in which the magnitude of displacement is twice as large in the trailing coaches than in the leading coaches.

The 70-m wavelength-filtered displacement shows the differences between configurations much more clearly, mainly through the change in vertical alignment. The wavelength of the movement is approximately 80 m, hence the difficulty to be detected via the 35-m wavelength filter. In the up line, the maximum magnitude of displacement for the trailing coaches is 20 mm, more than double the magnitude of displacement for the leading coaches. This is also observed in the down line, where the trailing coaches have a maximum displacement of up to 25 mm compared to the 12 mm of the leading coaches. The bouncing of the vehicle is observed to appear for a longer distance in the trailing coaches, which show displacement up to 400 m after the change in vertical alignment.

The 140-m wavelength-filtered displacement shows a much larger magnitude, mainly in the trailing coaches. The similarities and differences between configurations and lines are consistent with the ones evaluated through the 70-m wavelength filter, although the magnitude of displacement is generally twice the magnitude of the previous filter. The differences and similarities in the vehicle behaviour between configurations can also be observed in the vertical comfort estimation in Figure 5.16 and lateral comfort estimation in Figure 5.17.

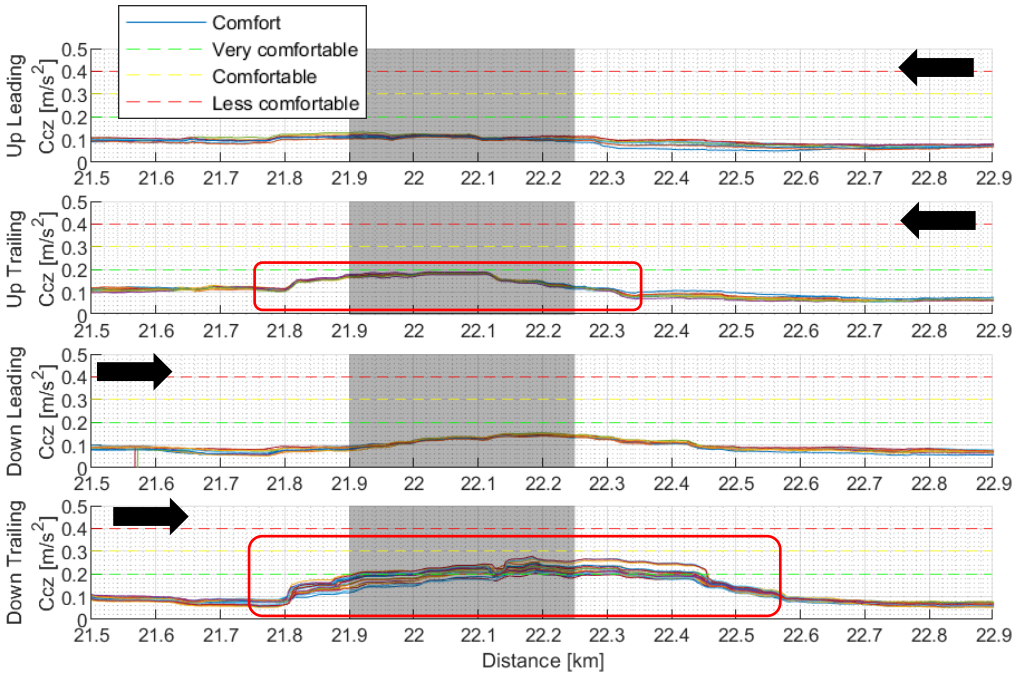


FIGURE 5.16. VERTICAL COMFORT COMPARISON BETWEEN CONFIGURATIONS.

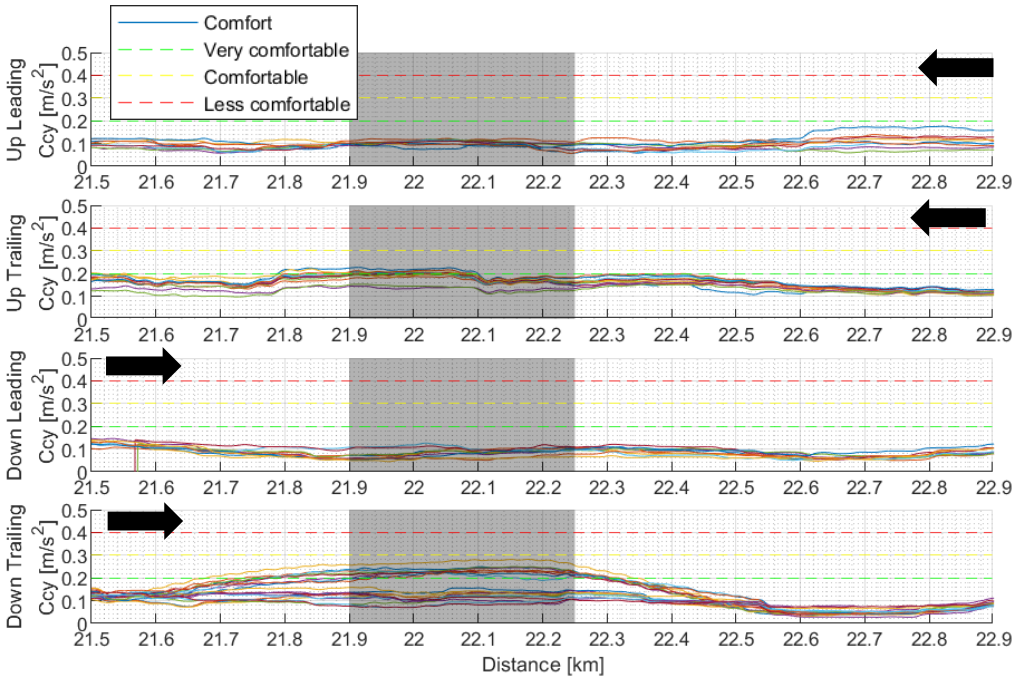


FIGURE 5.17. LATERAL COMFORT COMPARISON BETWEEN CONFIGURATIONS.

In both lines, the vertical comfort index clearly shows a higher value, and thus worse passenger experience, in the trailing coaches. The change in vertical alignment is appreciable in the up line between km 21.8 and 22.3, with the comfort index approaching the first threshold of

“comfortable”. On the down track, comfort is generally worse, and most of the runs in the trailing coach pass the first threshold along the change in vertical alignment, some even approaching the second threshold. The length of the magnitude increase is longer for the down line, observed between 21.8 and 22.6 reinforcing the statement that the signals perceived and the passenger experience differ depending on the direction of travel and the position within the vehicle.

The lateral comfort index shows low variation in both leading coaches, which are apparently unaffected by the change in vertical alignment. Opposed to this, the trailing coaches show notable increases in magnitude. Concretely, in the down line, on the trailing coach, there is a clear difference between runs due to an unreported change in the track conditions that negatively affects the passenger experience.

In conclusion, this section has demonstrated how the direction of travel of a train and the position of sensors inside it cause differences in the information received and the perception of travel. The differences between components observed in the previous section are consistent for all the configurations, although the trailing car has generally a larger car body reaction to long-wavelength track changes. This is because the leading coach is connected to the rest of the vehicle on its back end and the additional mass from the car behind hinders its movement; this does not happen in the trailing car as it does not have any connection to the vehicle on its back end and can move freely. Finally, comparing the different sensors it is concluded that the vertical acceleration signal measured from the vehicle provides information about the track, although it must be complemented by the rest of the signals for a complete assessment of track quality and vehicle comfort. Analysing the vehicle displacement and comfort has proven the usefulness of these processing methods to assess track quality.

5.5. CONCLUSIONS

This chapter presented inertial data from onboard sensors to evaluate the effects of a change in vertical alignment on the different components of the vehicle, as well as the differences derived from the travel direction and position of the sensors within the vehicle.

Regarding differences between components, results show the effects of the primary and secondary suspensions on filtering out the high-frequency contents of the data, mostly visible in the spectrograms of each component and the differences between vertical displacement considering the different wavelength filters.

The effects of train direction and sensor location have been discussed in detail in this chapter. The differences between configurations are observed in the signals acquired, most notably due to the position of sensors relative to the vehicle direction. In general, the displacement of the vehicle is larger in the trailing coaches, as observed for all the components and especially the cab. The long wavelength nature of the change in vertical alignment made it only present in the 70 and 140-m wavelength filters, whilst the 35-m wavelength filter allowed to show shorter-wavelength features, such as peaks in the track. Comfort is also affected by the relative position of the sensors, as it is poorer in the trailing coaches.

The phenomena observed in this chapter show the necessity to consider the position of the sensors in the whole vehicle for data acquisition. Standards such as the EN 13848 for track geometry [9], or the EN 12299 for passenger comfort [11], consider the position of the sensors within the coach to assess track geometry or passenger comfort, respectively. The results presented in this chapter proved that it is also necessary to consider the position of the sensors relative to the vehicle and the direction of travel to properly assess such parameters.

The following chapter presents a case study of the differences in signals acquired depending on the component, and the relative location and direction of travel. Furthermore, an analysis of the evolution of the track geometry is also presented.

Chapter 6. Switch and crossing case study

6.1. INTRODUCTION

In the previous chapter, the differences in the signals based on the position of sensors installed on it were discussed. This chapter describes the use of vertical acceleration, displacement and comfort to monitor the change in the data of a UK high-speed train passing through a switch and cross (S&C). The test conditions and operations carried out in the track and vehicle are explained in the following section.

6.2. TEST CONDITIONS AND EQUIPMENT

Several maintenance operations have been carried out on the track. Such maintenance affects the vehicle behaviour and, hence, the data returned by the sensors. A representation of the S&C is presented in Figure 6.1. The switch toes in the up line are at km. 52.23 and 52.904, whilst the switch toes in the down line are at km. 52.517 and 52.617. The toes correspond to the rail ends at the crossings, whilst the switch noses, or frogs, correspond to the crossing point between rails.

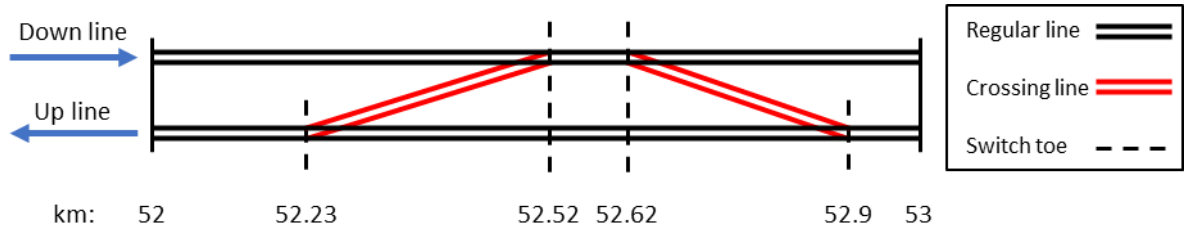


FIGURE 6.1. SCHEMATIC REPRESENTATION OF NASHENDEN CROSSOVERS.

Several maintenance operations have been carried out on the track. Such maintenance affects the vehicle behaviour and, hence, the data returned by the sensors. Table 6.1 shows the reported track changes and dates on the S&C and also the repair of a wheel flat on the instrumented vehicle.

TABLE 6.1. REPORTED EVENTS OVER TIME.

Date	**Line**	**Reported Event**	**location (where applicable)**
25-Sep-2021	Up	Tamping	52.580-52.957 km
December-2021	-	Wheel flat appearing	-
February-2022	-	Wheel flat repaired	-
17-Feb-2022	Up	Reported as actionable	300 m from swing nose
27-Feb-2022	Up	Swing nose change	52.330 km
25-Mar-2022	Up	Reported as actionable	Swing nose

The equipment used is the same as for the previous chapters. In summary, a set of inertial sensors was installed in the axlebox (A), bogie (B) and cab (C) of a UK high-speed in-service passenger train. The axlebox has accelerometers measuring in the vertical direction, whilst the bogie and the cab have accelerometers and gyroscopes measuring vibrations and rotation rates in all Cartesian axes, and GNSS was used for positioning and speed data. The following section presents the analysis of data carried out from these conditions.

6.3. ANALYSIS OF DATA

This section demonstrates the data collected in three cases: comparing the signal between components, evaluating the differences between the leading and trailing coaches and up and down lines, and the evolution of data over time. In this section, the S&Cs are highlighted with vertical dashed lines.

6.3.1. Component comparison

The vertical acceleration is the only signal that allows a comparison between all components. Data derived from acceleration includes displacement, including a 35-m, 70-m, and 140-m filtering of vertical displacement, and comfort. The data used for this section are extracted from journeys on the up line, thus the vehicle is travelling in the direction in which distance according to the reference decreases. Figure 6.2 shows the vertical acceleration of the vehicle. For the figures in this section and the following, vertical dashed lines indicate the position of the S&Cs, and a black arrow indicates the direction of travel of the vehicle.

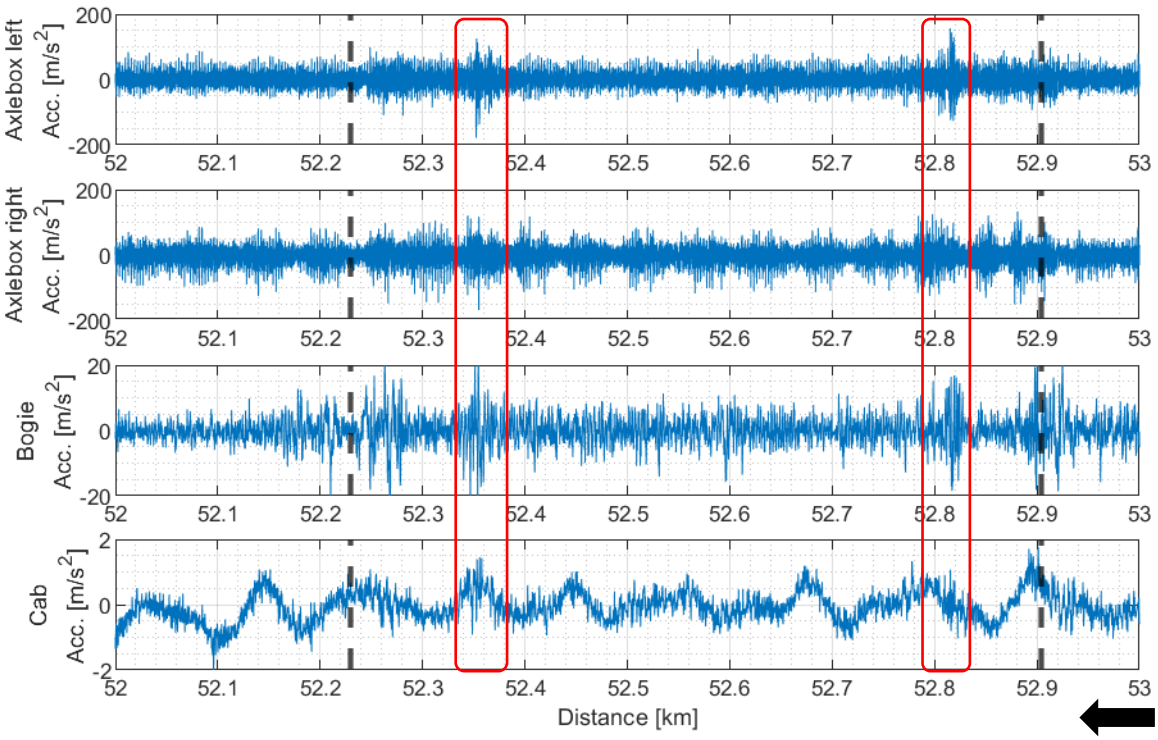


FIGURE 6.2. VERTICAL ACCELERATION COMPARISON BETWEEN COMPONENTS.

The axlebox left and bogie subfigures show small peaks corresponding to the toes in the line, with the crossing noses at km 52.32 and 52.78 appearing both in the axlebox and bogie and highlighted as red rectangles. The difference between the axlebox left and right is due to the crossing nose. The cab shows a low-frequency component similar to the one observed in the previous chapter, which is linked to a resonance mode. To extract more information from the signal, the spectrogram for each sensor is obtained, as well as the vertical displacement and passenger comfort. The effects of the vehicle passing over the S&C are observed in the spectrograms in Figure 6.3.

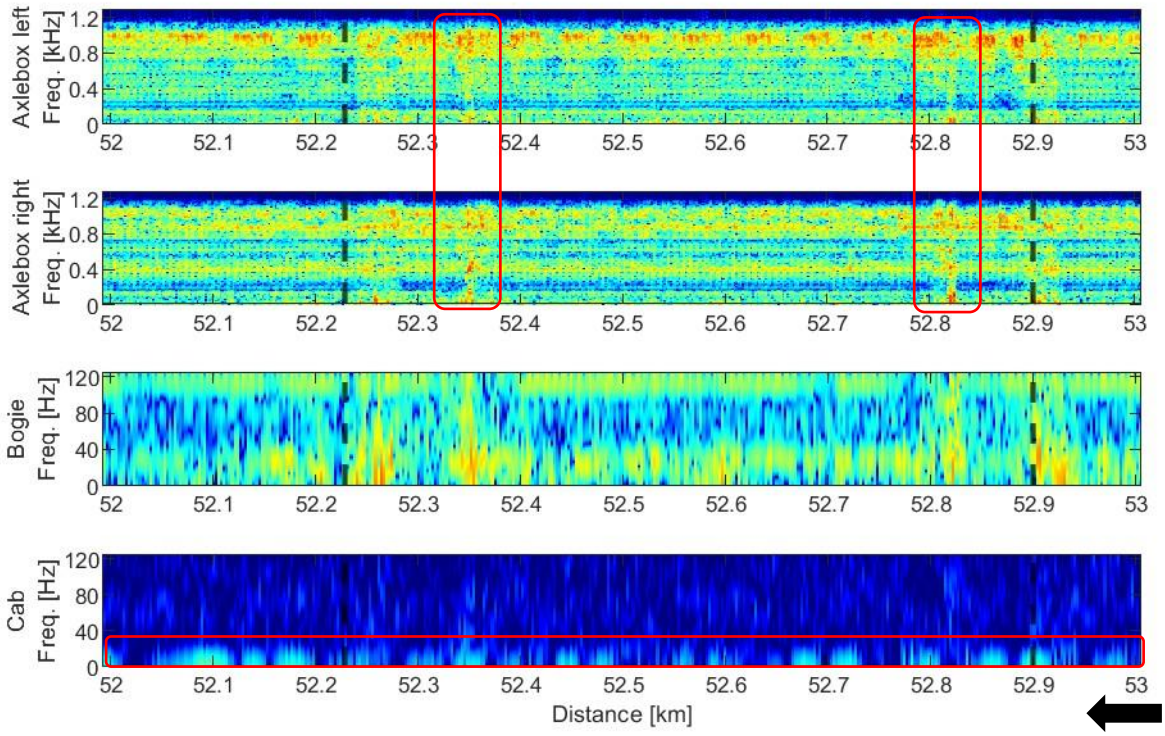


FIGURE 6.3. VERTICAL ACCELERATION SPECTROGRAMS COMPARISON BETWEEN COMPONENTS.

The crossing noses and toes are more visible in the axlebox spectrograms than in the acceleration graph, in km 52.35 and 52.9, and a high-frequency component of the signal can be observed in the axlebox at frequencies such as 400 and 1000 Hz, due to the wheel flat mentioned in Table 6.1. The bogie spectrogram shows the position of the switch noses and toes more clearly than the rest of the sensors. Sensors on the bogie may be the best choice to monitor S&Cs, although observing the rest of the signals, the differences between configurations, and the evolution of data will confirm whether this statement is valid or not. Regarding the cab, only small magnitude increases are observed in the crossing, below 20 Hz.

Displacement for each component shows a similar behaviour. It is presented in Figure 6.4. Dashed vertical lines indicate the position of the S&Cs, and a black arrow indicates the direction of travel.

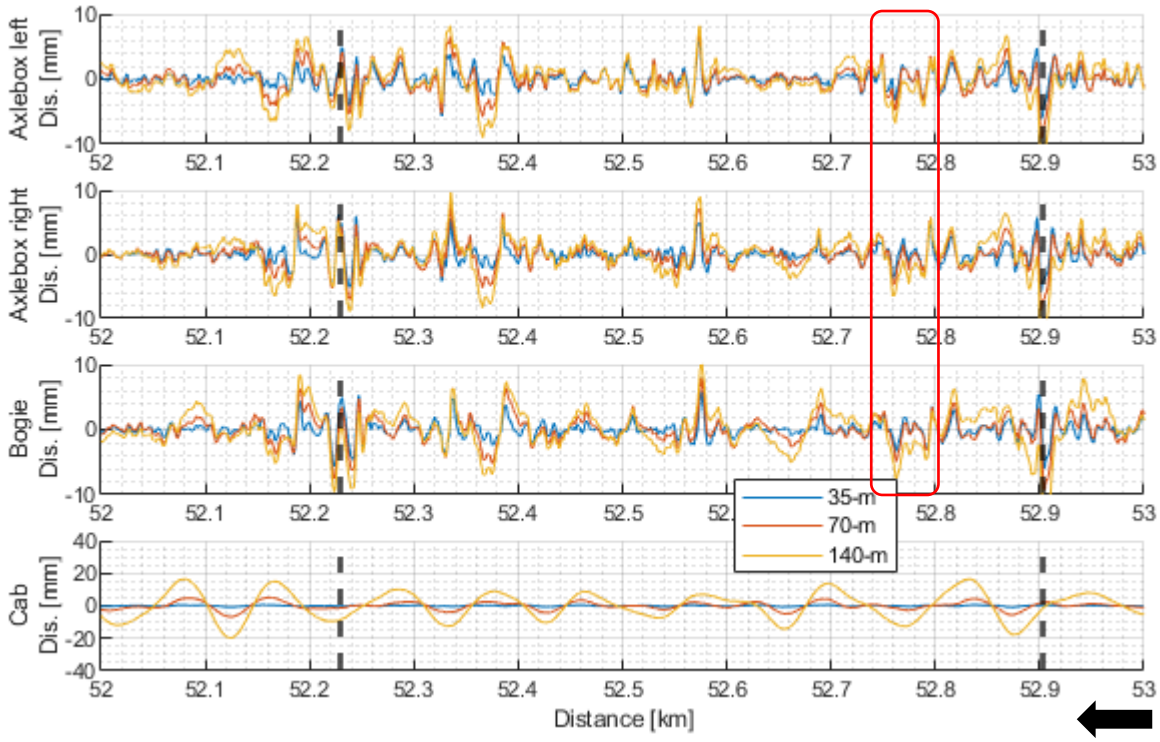


FIGURE 6.4 VERTICAL DISPLACEMENT COMPARISON BETWEEN COMPONENTS.

The crossing is observed in both axlebox and bogie signals for the three wavelength filters. There are differences in the longer wavelength-filtered signals for these components, more prevalent between km. 52.75 (highlighted as a red rectangle) and 52.9, due to the location of the crossing nose. The magnitude of the displacement is higher in the crossing at km. 52.9, suggesting a worse condition. The cab only shows displacement on the 70 and 140-m wavelength-filtered signals and is largely affected by the presence of the S&C, as there is a repetitive movement after the vehicle passes through it, from right to left in the figure. This causes a "measurement blind spot", a section of track in which no information can be extracted from this component of the vehicle. This effect should be considered for monitoring and inspection, as there are sections of track whose condition may remain unknown after travelling through them.

Continuous comfort according to the standard EN 12299 is presented in Figure 6.5.

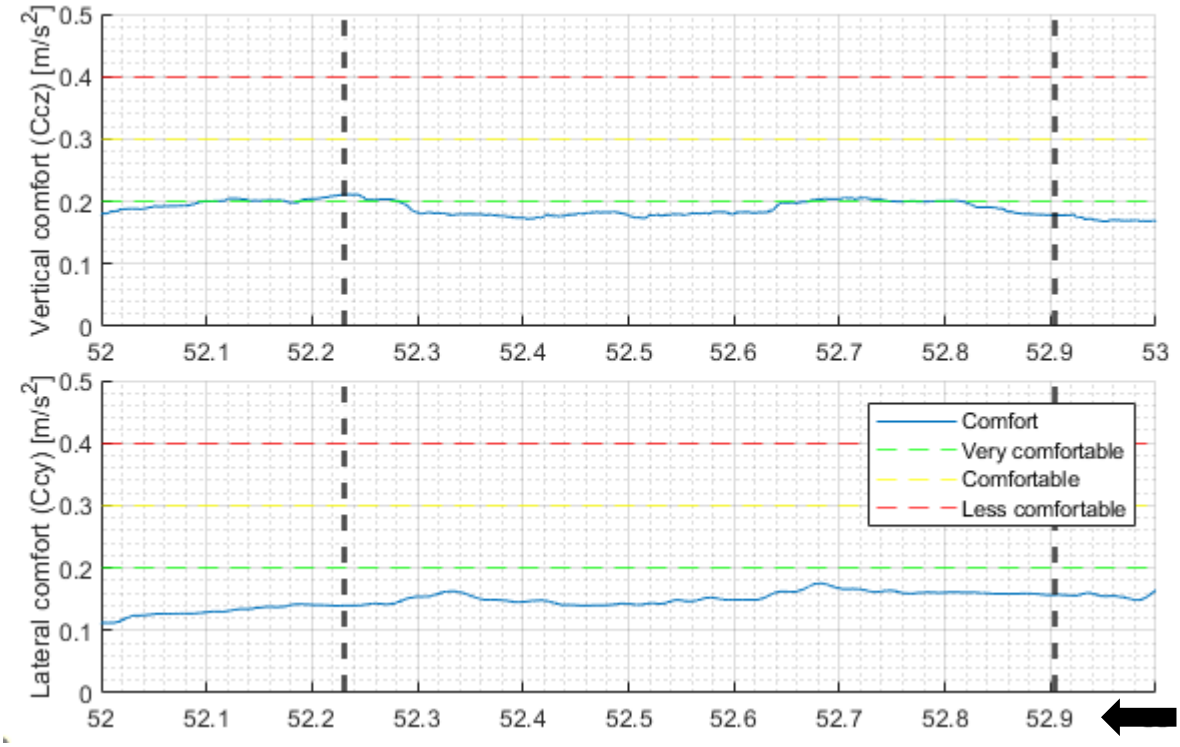


FIGURE 6.5. VEHICLE PASSENGER COMFORT.

Regarding comfort, the most notable observations extracted are the large magnitude of vertical and lateral comfort for the whole segment, above the "comfortable" threshold level for vertical comfort in some segments past km 52.7, which means a worse passenger experience. This shows that close and sudden geometry changes caused by S&Cs do not have a significantly diminishing effect on continuous comfort, neither in the vertical nor lateral direction. There are slight magnitude increases in km 52.35 and 52.7 in lateral comfort, which can be attributed to the switch noses, although the time window applied for computing the comfort indices (5 s) is too large to evaluate these effects properly. Continuous comfort indices are deemed as not useful to assess the state of the track for sudden changes. Other parameters, such as vehicle displacement, should then be considered to assess the state of the track.

In summary, this section presented the effects of a high-speed vehicle passing over an S&C on different components. All the components of the S&C are visible on both the bogie and the

axlebox, and the bogie is the most adequate component to do so as the signal-to-noise ratio is the best of all signals. The cab shows a large vertical movement associated with the S&C, but not a decrease in passenger comfort. It is concluded that the cab signal is not adequate for detecting and monitoring S&Cs.

6.3.2. Differences between configurations

As explained in the previous chapter, the four different configurations may show different responses to track condition changes. This section shows the similarities and differences between these configurations. Prior to the comparison, signals are aligned using the same method as explained in Chapter 3. The runs in the up line have been reversed and aligned using the reference provided for that line and aligned to the runs in the down line using cross-correlation in the selected segment. For this chapter, there are 46 runs available, distributed as presented in Table 6.2.

TABLE 6.2. AVAILABLE RUNS FOR EACH ORIENTATION AND CONFIGURATION.

Direction	Orientation	Available runs
Up	Leading	8
Up	Trailing	9
Down	Leading	10
Down	Trailing	19

Before comparing datasets, showing vehicle speed is necessary to consider if vehicles are in similar conditions. This appears in Figure 6.6. In this section, the crossings are marked as black dashed lines. These are in km 52.23 and 52.9 in the up line, and in km 52.5 and 52.6 in the down line.

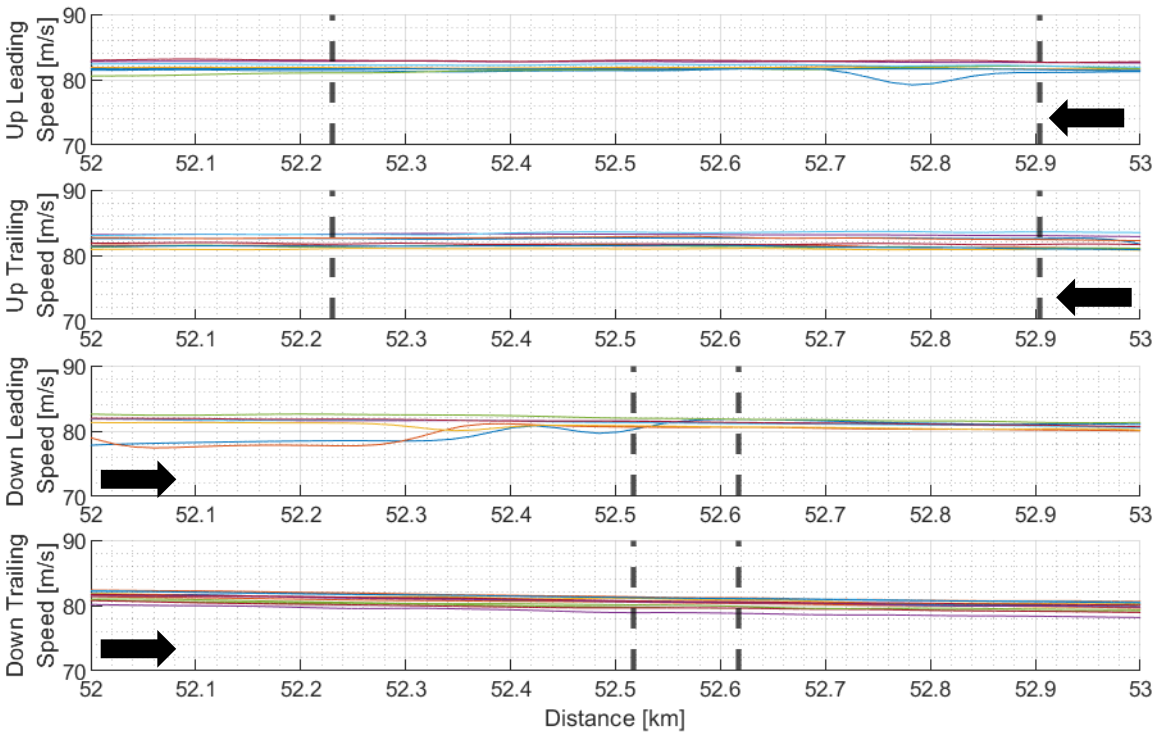


FIGURE 6.6. VEHICLE SPEED COMPARISON BETWEEN CONFIGURATIONS.

There are no significant speed differences between configurations, so the differences appearing are caused by other effects, and thus the different configurations can be compared without further processing. As explained in the previous chapter, raw acceleration does not provide much information about the state of the S&Cs nor the track, hence it is not presented in this chapter, although a discussion on the observed similarities and differences between acceleration signals is presented in the following paragraph. All axlebox signals show small changes due to the crossing noses, in km 52.3 and 52.8 in the up line, and 52.4 and 52.7 for the down line, associated with the crossing noses. As found in the previous section, the bogie signal has the largest reaction to the effects of the S&C. Both configurations in the up line present visible changes due to the switch toes and crossing noses, showing that these elements can be detected and monitored using onboard inertial sensors. Finally, the cab signal shows the same low-

frequency periodic movement in both lines, and no differences in the signal due to the S&Cs, caused by the suspension damping, and track geometry.

The same features observed for the acceleration can also be observed in the spectrograms for all signals, in Figure 6.7 to Figure 6.10. From the spectrograms, it is possible to extract information on the intensity and the frequency distribution of the signals, hence their use.

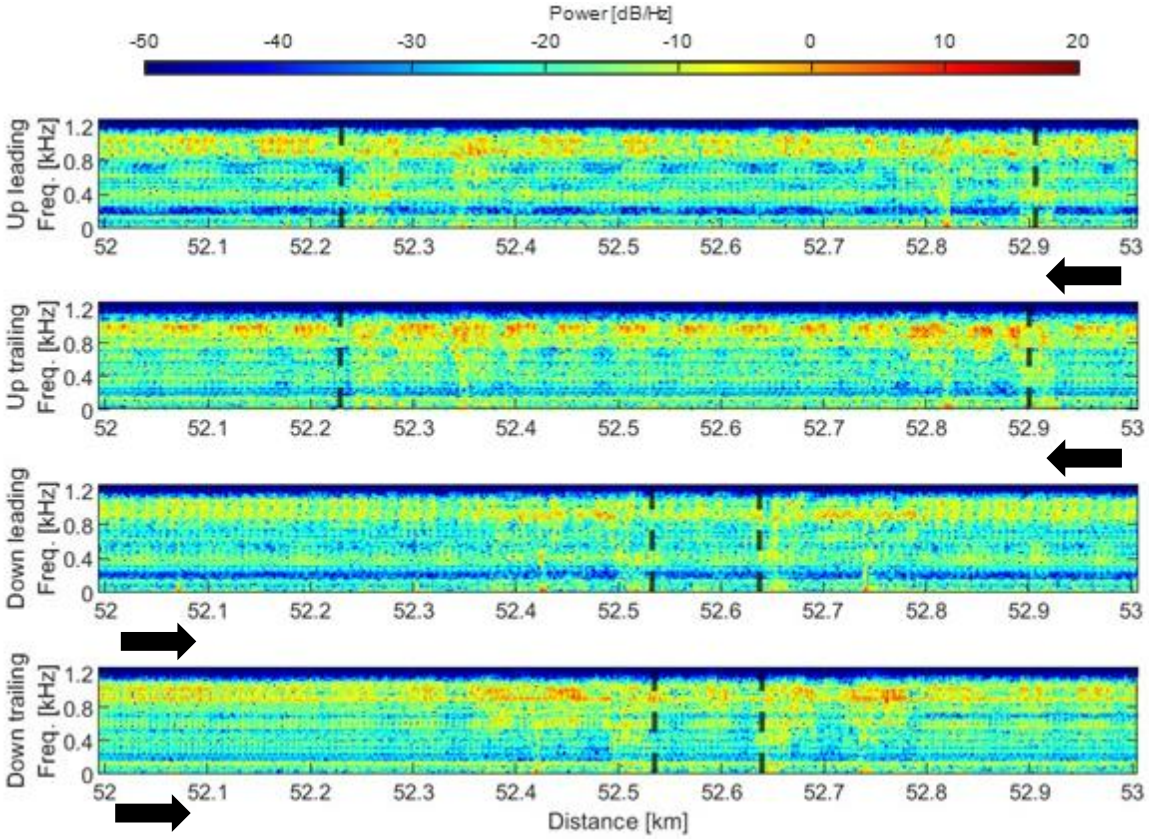


FIGURE 6.7. ACCELERATION SPECTROGRAM FOR THE AXLEBOX LEFT SENSORS.

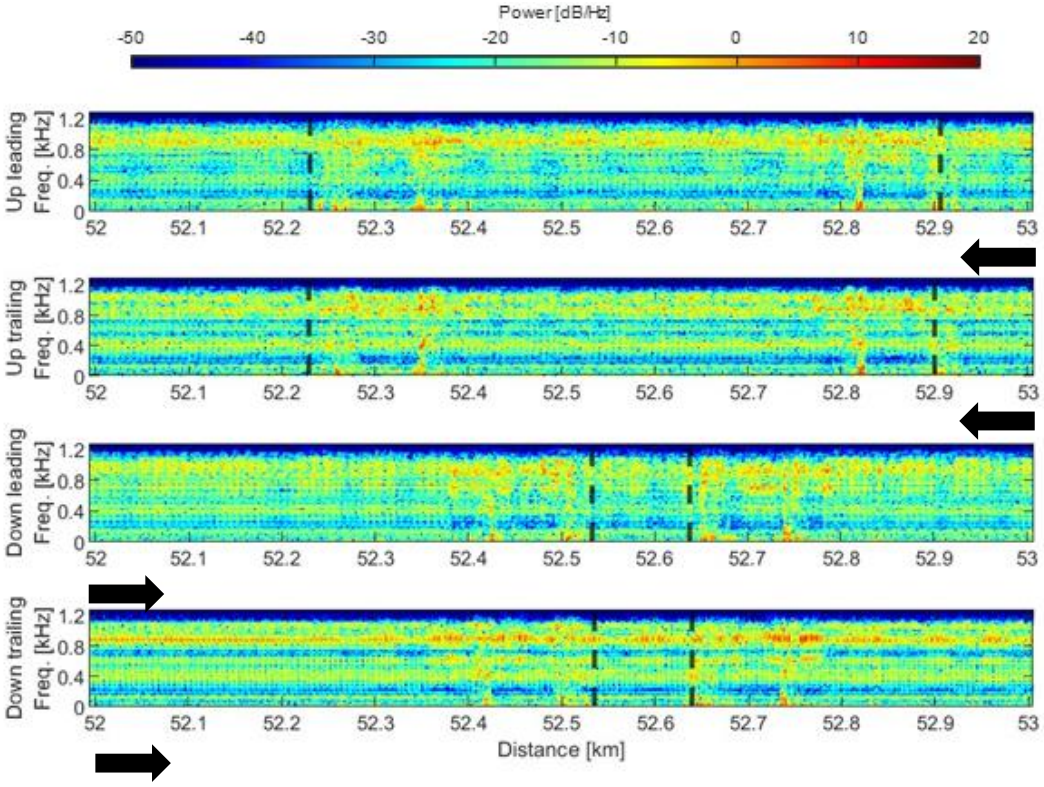


FIGURE 6.8. ACCELERATION SPECTROGRAM FOR THE AXLEBOX RIGHT SENSORS.

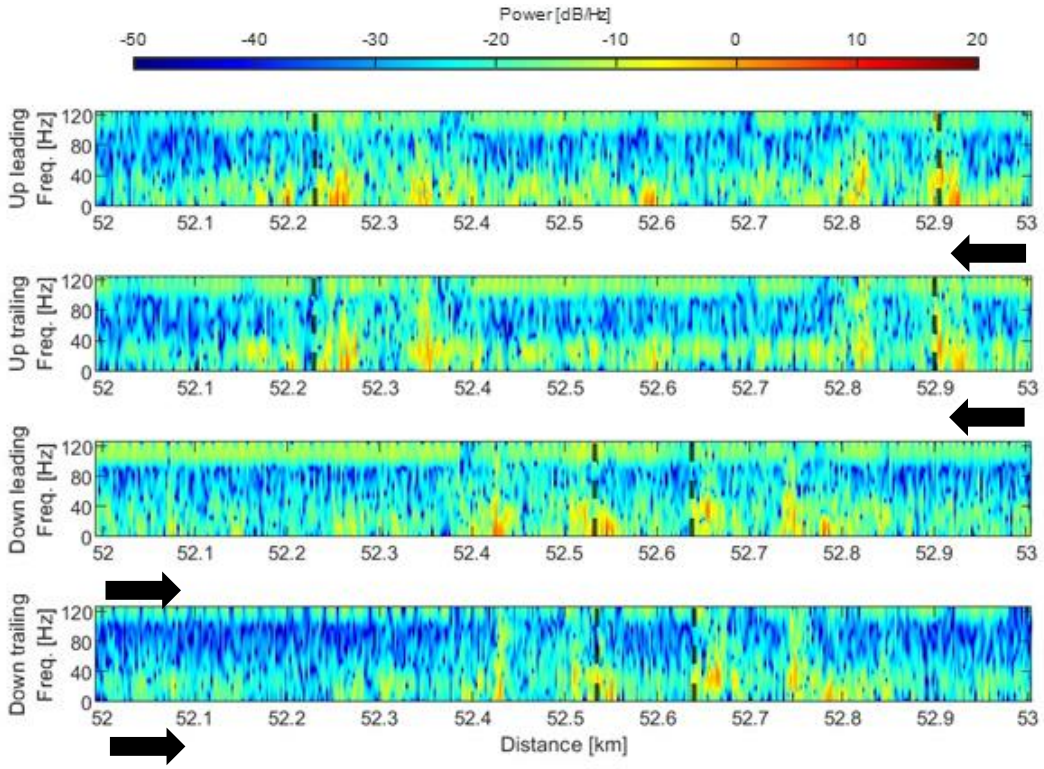


FIGURE 6.9. ACCELERATION SPECTROGRAM FOR THE BOGIE SENSORS.

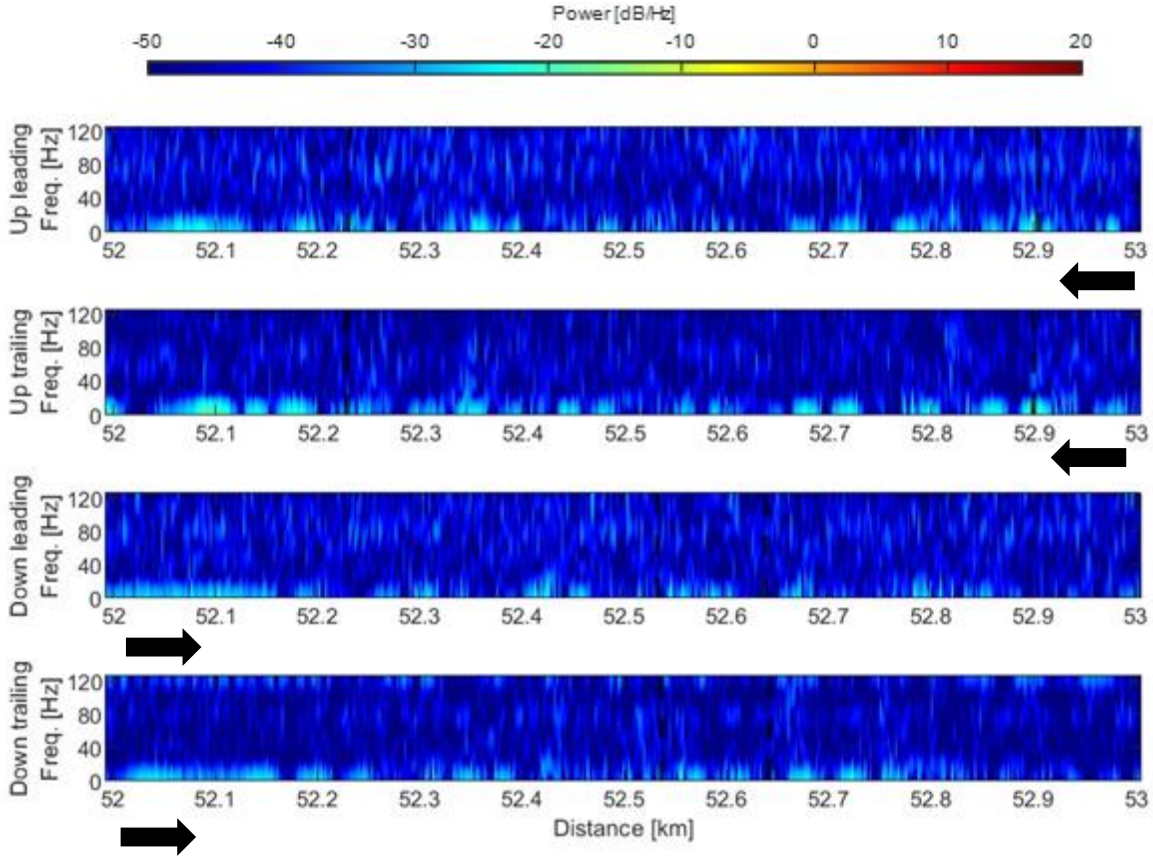


FIGURE 6.10. ACCELERATION SPECTROGRAM FOR THE CAB SENSORS.

The trailing coaches show similar resonances for the left axlebox that do not appear in the leading axlebox at 800 Hz. The effects of the vehicle passing over the S&C are visible in all signals, mostly below 200 Hz. Although the magnitude of the signal is lower in the low frequency range, the increase in magnitude is relatively larger. Bogie and cab sensors in the leading coaches have a higher signal magnitude than those trailing, mainly in the range below 20 Hz.

Differences between configurations are appreciated by observing vertical displacement processed with different wavelength filters. The following figures show the vertical displacement of the axlebox. Vehicle displacement is obtained locally in the track segment, by double-integrating the acceleration, and applying a wavelength filter to the result. For clarity, only the 140-m wavelength-filtered displacement is presented. The figures corresponding to the 70 and 35-m wavelength filters are presented in Appendix D. The switch toes are displayed with vertical dashed lines, and the direction of travel is indicated with a black arrow for each subfigure.

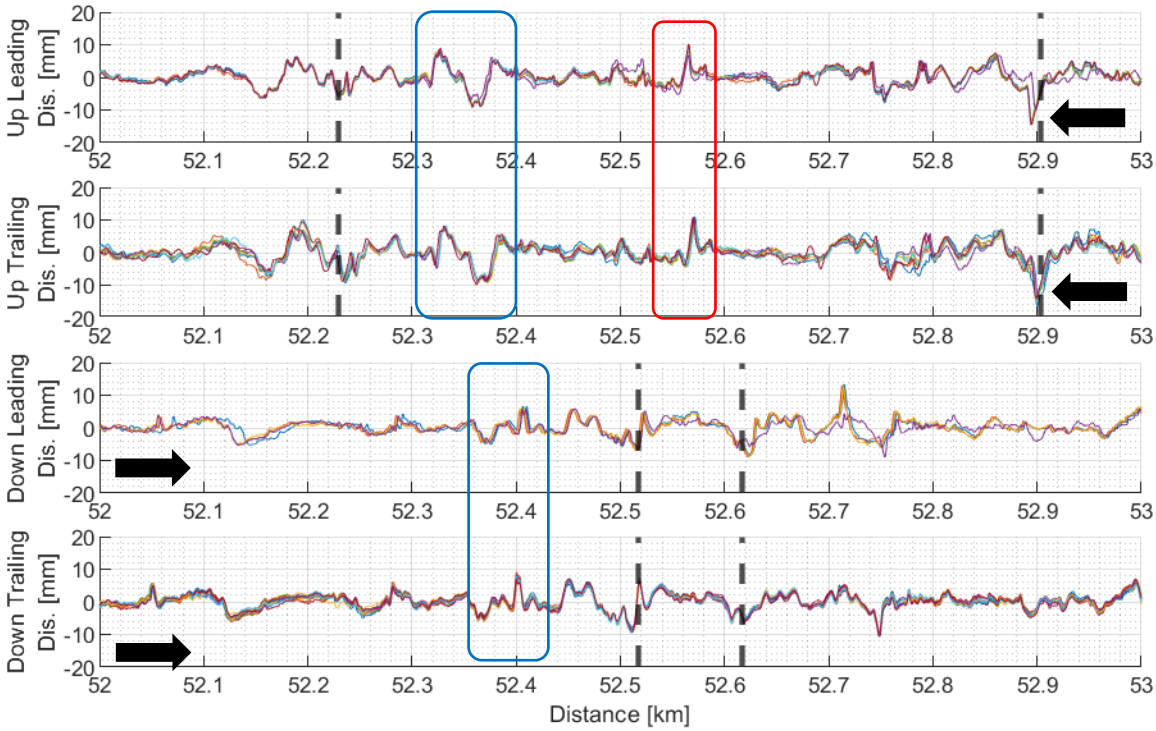


FIGURE 6.11. AXLEBOX LEFT VERTICAL DISPLACEMENT COMPARISON BETWEEN COMPONENTS.

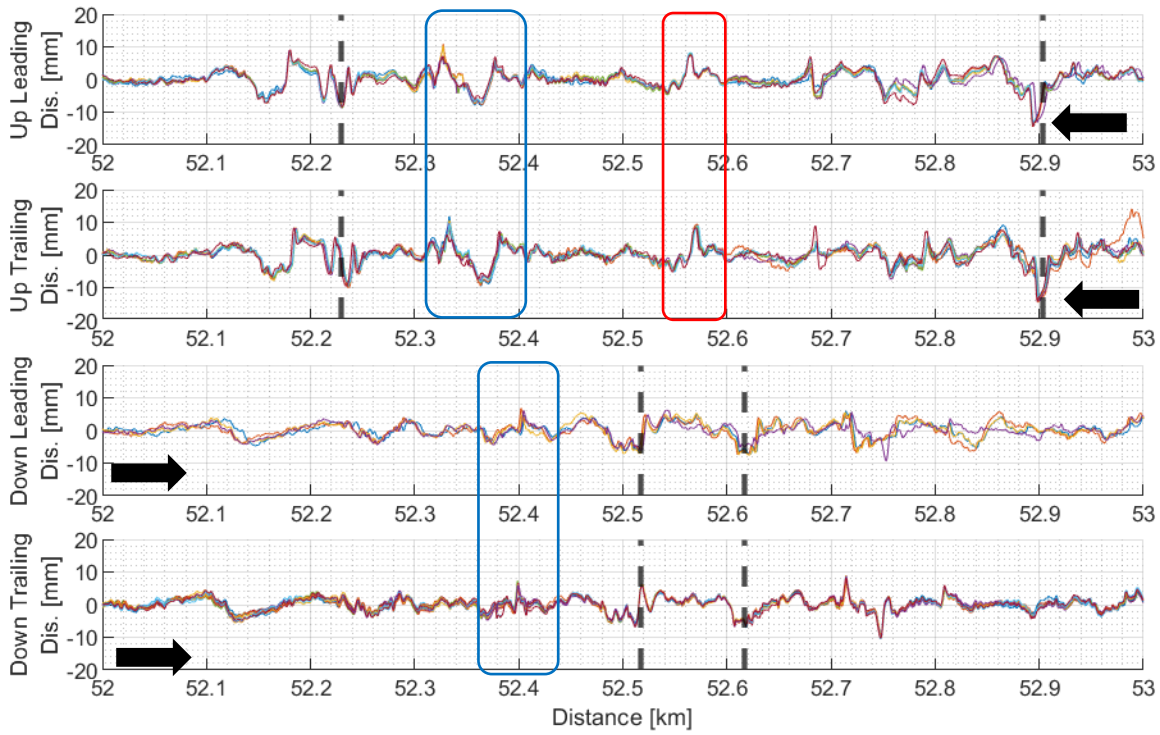


FIGURE 6.12. AXLEBOX RIGHT VERTICAL DISPLACEMENT COMPARISON BETWEEN CONFIGURATIONS.

The 35-m wavelength-filtered displacement shows similar results for both configurations and lines, although as discussed in the previous chapter, its magnitude is larger for the trailing coaches than for the leading ones, as observed in the crossing toes in both lines, and the high displacement value at km 52.55, with a difference in magnitude of 2 mm (highlighted as a red rectangle). The differences observed between signals from the same configuration are attributed to the changes and repairing of the switch components reported in Table 6.1. Additionally, the differences between left and right sensors are attributed to the differences between rails, as these are not equal over the S&C.

Regarding the 70-m wavelength filter, similar results are obtained, although the magnitude of displacement is larger due to the filter. Compared to the 35-m filtered displacement, the magnitude of some peaks in the signals, such as in km 52.32 in the up line, km 52.4 in the down line (highlighted as blue rectangles), and the km corresponding to the switch toes, is similar,

and indicates that the features associated with that peak correspond to short-wavelength features. This is expected as the S&C components are associated with short-wavelength features. However, some longer-wavelength features appear only in the 70-m wavelength filter, such as in km 52.2 and 52.35 in the up line.

Regarding the 140-m wavelength filter, the magnitude of the long-wavelength features observed for the previous filter is increased. As with the 35-m filter, there are differences observed between signals on the same configuration, such as between km 52.7 and 52.85 in the up line, and km 52.5 and 52.75 of the down line, that can be attributed to tamping and repairing operations carried out in the period when these data were recorded. Comparing signals from leading and trailing coaches, the magnitude of displacement in the latter ones is larger, both along the track and over the switch toes. This reinforces the statement that the position of the sensors along the vehicle influences the signal acquired.

The bogie vertical displacement is presented in Figure 6.13, with the switch toes marked as dashed lines and the direction of travel with a black arrow.

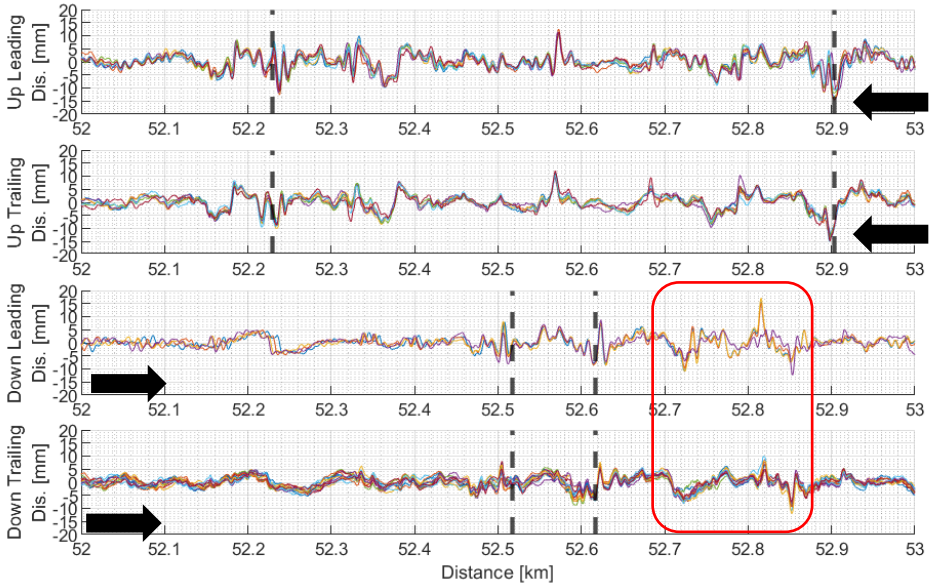


FIGURE 6.13. BOGIE VERTICAL DISPLACEMENT COMPARISON BETWEEN CONFIGURATIONS.

Regarding the 35-m wavelength-filtered displacement, the magnitude of displacement is generally larger for the leading coaches than for the trailing ones, as opposed to observed for the axlebox and cab data. This indicates that the bogie moves more freely in the leading coaches, with differences in magnitude up to 25% in the switch toes in the up line, and doubling the magnitude in the switch toes in the down line. This must be considered when acquiring data from the bogies, given that the results differ that much.

Regarding the 70-m, the aforementioned differences in magnitude are observed, although not as significant. Still, the leading coaches show a larger magnitude in the switch toes. The differences between signals observed for the axlebox data are also observed in the bogie, more notably between km 52.7 and 52.85 in the down line (highlighted as a red rectangle). This reinforces the statement that the bogie can be used to monitor and assess track state.

Finally, the data from the 140-m wavelength-filtered displacement also shows larger magnitude for the leading coaches in the toes, as well as differences in the down line due to the reported track changes. The latter ones are notably larger in the leading coaches and show that the short-wavelength features of the track can also be observed and evaluated using this filter, although it may not be ideal for this purpose.

The cab vertical displacement is presented in Figure 6.14, where the switch toes are marked as black dashed lines, and the direction of travel is indicated with a black arrow. The 70 and 35-m wavelength-filtered displacement signals are presented in Appendix D.

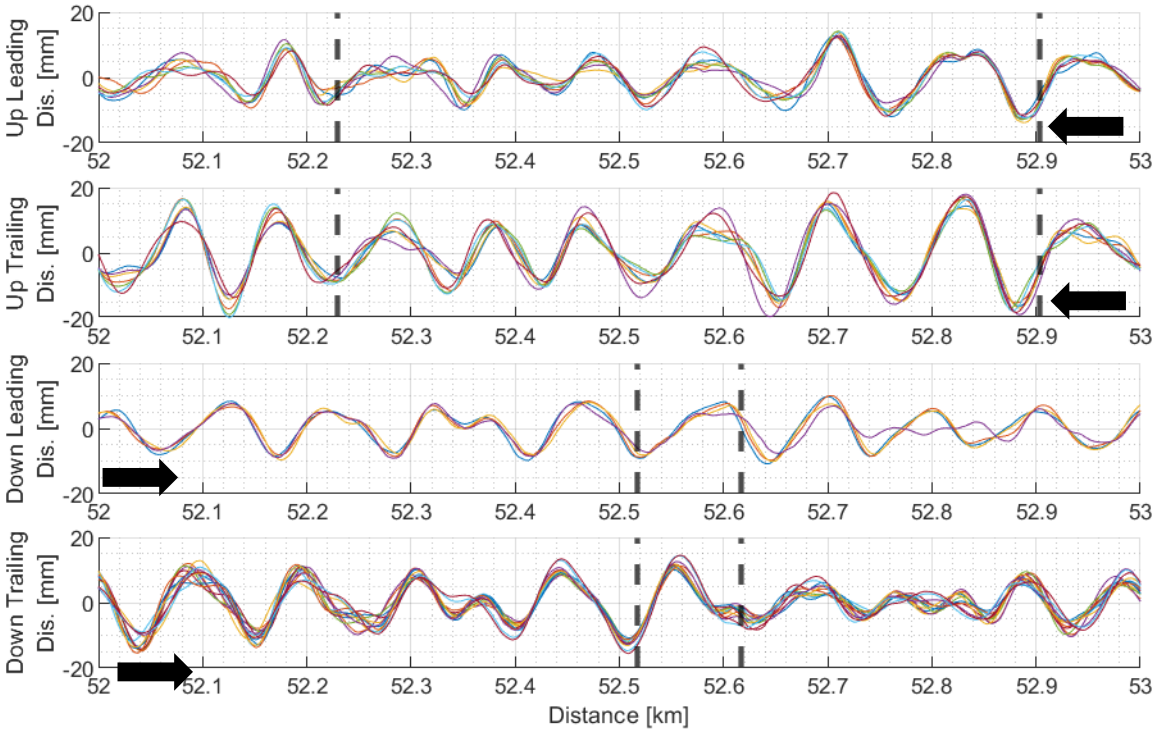


FIGURE 6.14. CAB VERTICAL DISPLACEMENT COMPARISON BETWEEN CONFIGURATIONS.

The 35-m wavelength-filtered displacement shows little influence of the switch toes, only visible as dips with a peak-to-peak amplitude below 2 mm in the up line. In the down line, there is no appreciable difference between the switch toes and the track. This shows that the signal from the cab cannot be used to monitor nor detect S&Cs. No significative differences between configurations are appreciated either.

The 70-m wavelength-filtered displacement allows the detection of the switch toes in the up line, although the signals do not allow to identify any notable features, as opposed to those observed in the axlebox and bogie sensors. As observed in the previous chapter, the magnitude of displacement is larger for the trailing coaches, mainly visible at km 52.12 and km 52.9 in the up line. Signals in the down line show the presence of the switches, although no characteristics are extracted from them.

Signals from the 140-m wavelength filter show the S&C as large dips in the up line, with a larger magnitude in the trailing coach. The cab movement is observed over both crossings, which hinders the extraction of any information on the track in this segment, and thus creates a "measurement blind zone" that must be considered when acquiring data.

Vertical comfort is presented in Figure 6.15, and lateral comfort is presented in Figure 6.16. The switch toes are marked with dashed lines, and the direction of travel is marked with a black arrow.

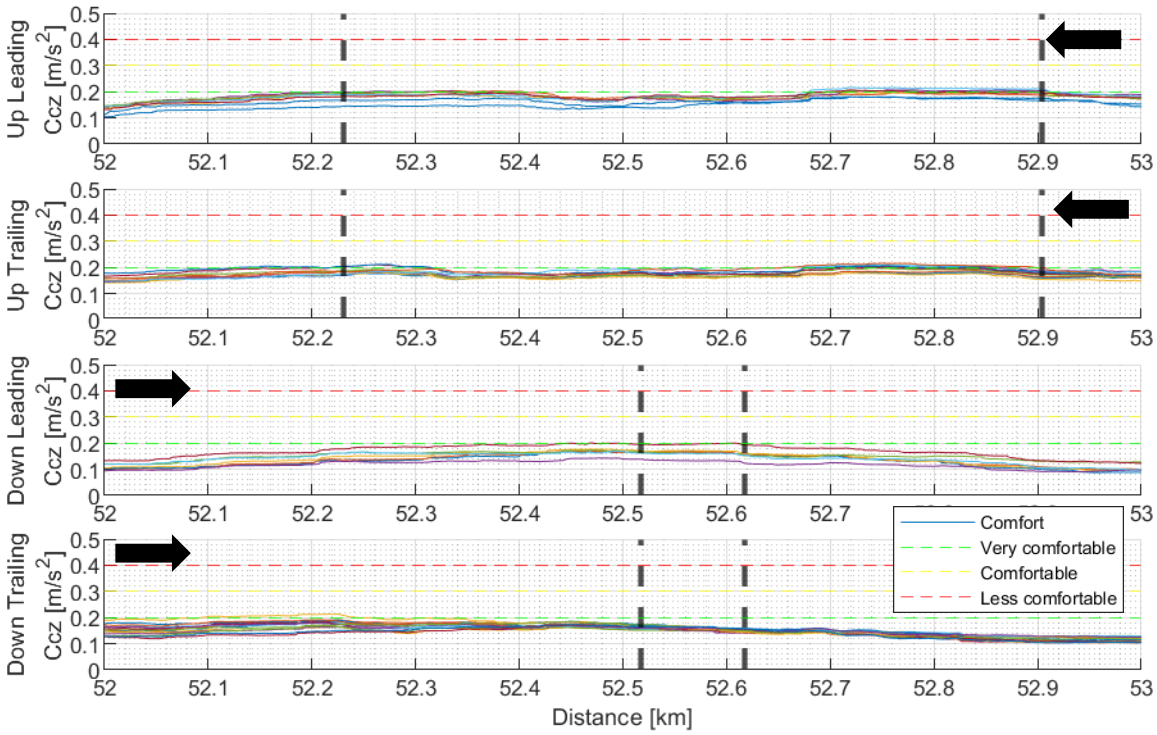


FIGURE 6.15. VERTICAL COMFORT COMPARISON BETWEEN CONFIGURATIONS.

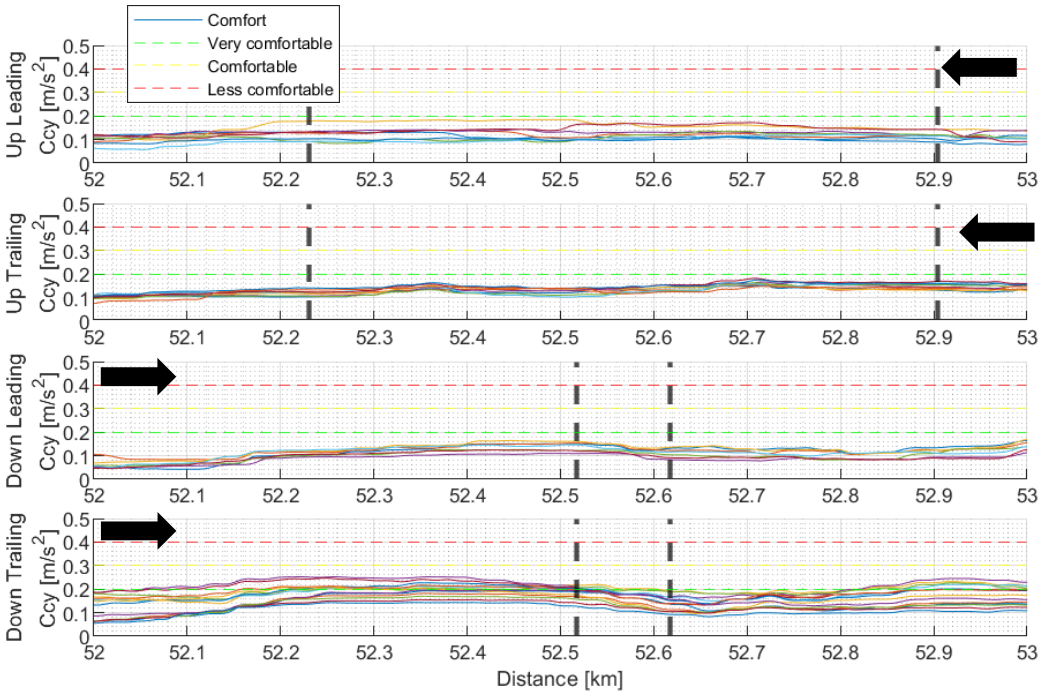


FIGURE 6.16. LATERAL COMFORT COMPARISON BETWEEN CONFIGURATIONS.

There are changes in vertical comfort over the S&Cs in both lines. In general, the variation between vertical comfort is low, which indicates a low sensitivity of this output to short-wavelength features such as the S&C. The lateral comfort shows high variability, especially in the down line with trailing sensors. The trailing coaches have a higher value of the indices C_{Cz} and C_{Cy} for both lines, which indicates a poorer passenger experience.

In summary, this section presented the main similarities and differences between configurations as the vehicle passes over an S&C. As with the previous section, the results confirm that the bogie is the preferred component for monitoring track components, as it is not as dependent on the state of the rails, and that the position of the sensors relative to the direction of travel affects the measurements received, especially in the vehicle cab. All configurations show differences between themselves, often with notable variations in magnitude. This must be considered when installing sensors for measurement and data acquisition, as many thresholds for maintenance are based on track geometry dimensions such as vertical alignment passing a value. This may

mean the difference between more frequent and costly maintenance, or more infrequent and maybe inefficient maintenance.

6.3.3. Track evolution

This section shows the evolution of the track components over time. The up line is used for the data analysis, as most of the changes were reported in this line. Since there are few runs available, runs with sensors on the leading and trailing coaches are used for this section. The position of the sensors for each run is indicated next to the date, labelled as Leading or L for the sensors on the leading coaches, and Trailing or T for the sensors on the trailing coaches. Same as with the different configurations, a comparison of speed between datasets is necessary to compare the differences between datasets. This is displayed in Figure 6.17.

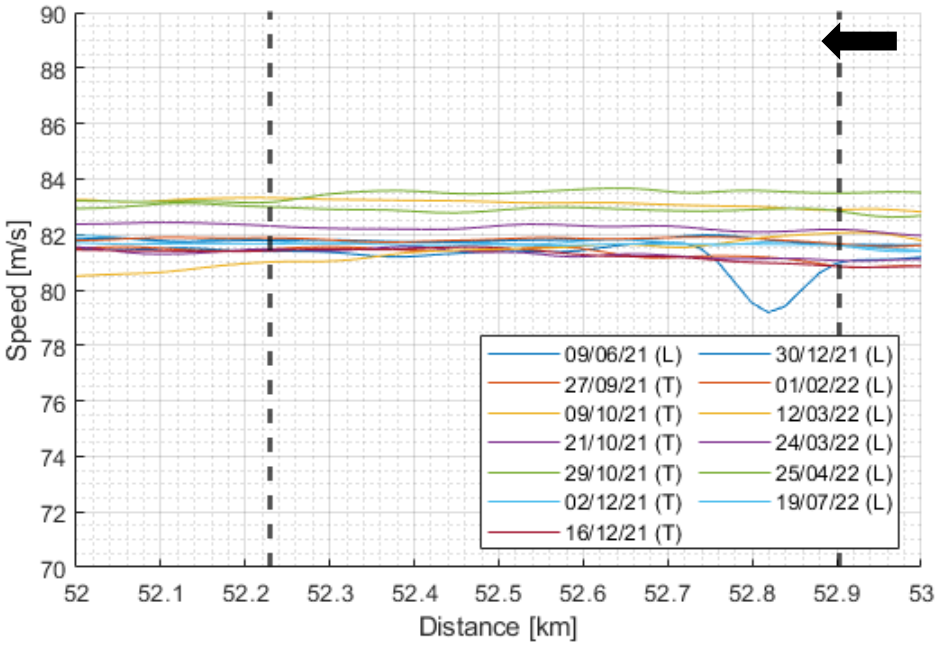


FIGURE 6.17. VEHICLE SPEED COMPARISON OVER TIME.

As the speed of all the runs is similar, the comparison can be considered fair. The spectrograms are presented in in Figure 6.18 for the left axlebox, and Figure 6.19 for the right axlebox.

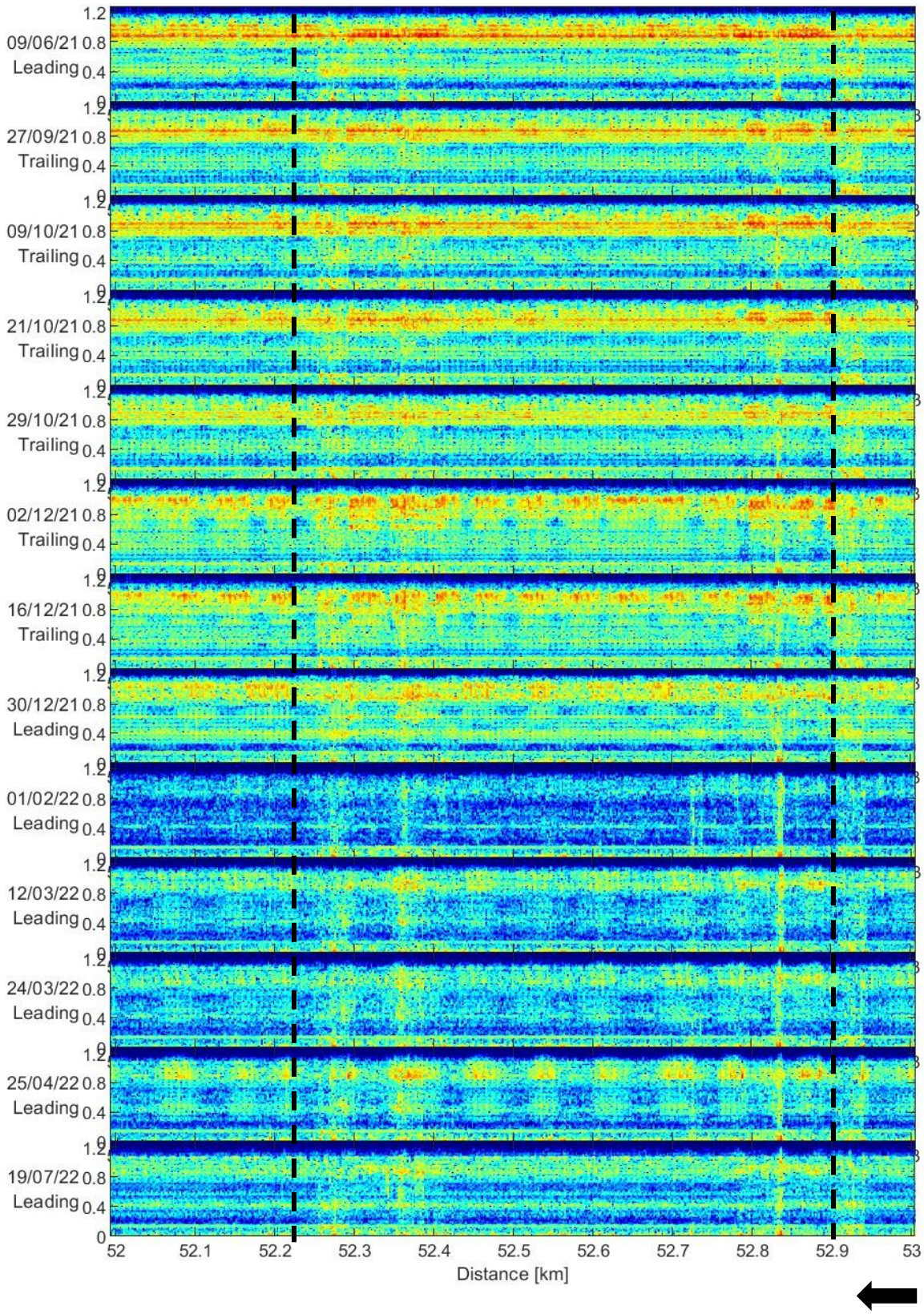


FIGURE 6.18. LEFT AXLEBOX VERTICAL ACCELERATION SPECTROGRAM EVOLUTION.

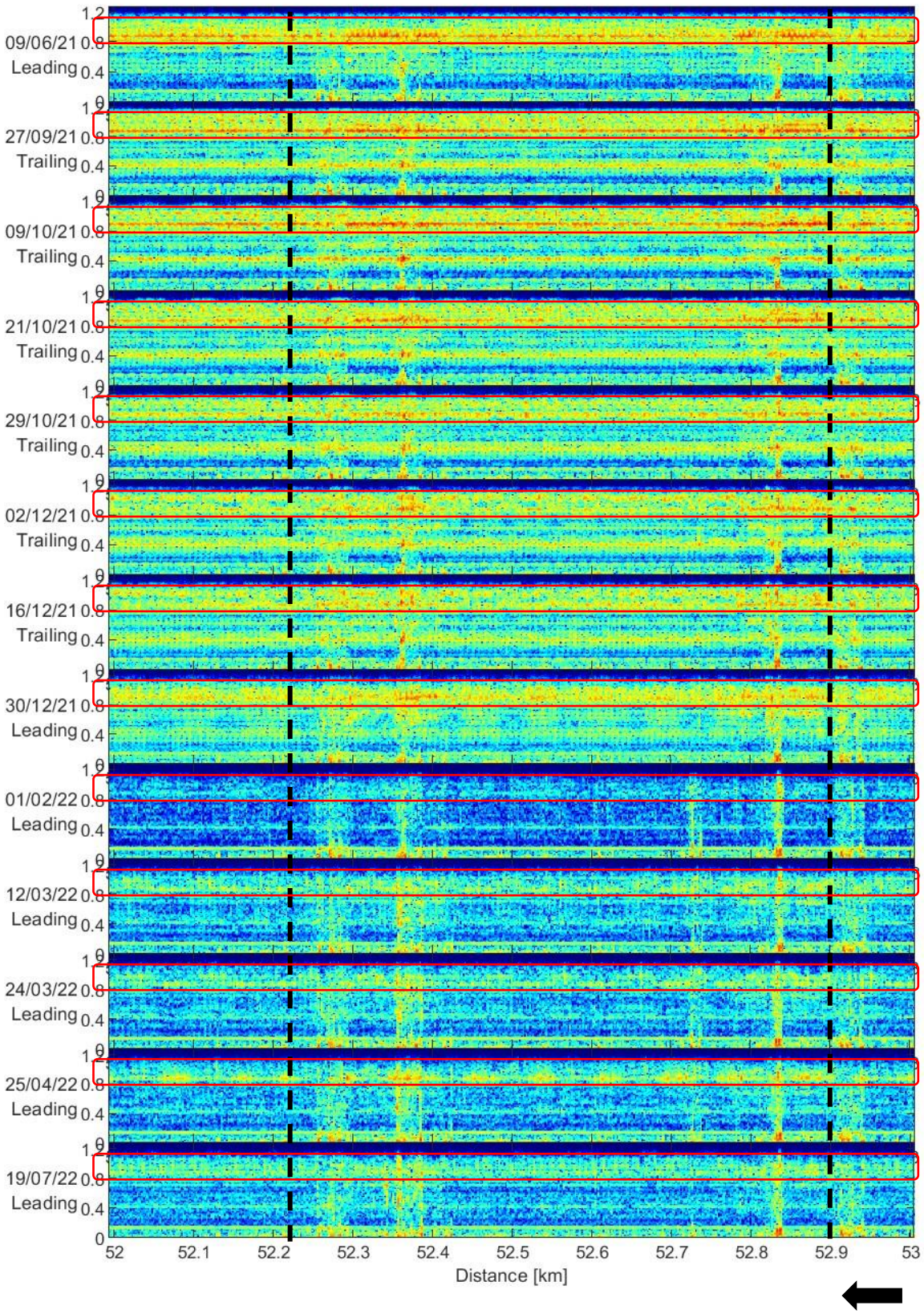


FIGURE 6.19. RIGHT AXLEBOX VERTICAL ACCELERATION SPECTROGRAM EVOLUTION.

Several changes can be attributed to the operations described in Table 6.1 (tamping in September, a wheel flat appearing in December, and the repairing of this wheel flat in February). The wheel damage is visible at the start of December, as observed in the left axlebox, which shows an increase in the signal magnitude in the datasets for that period at 1 kHz associated with the poorer state of the wheel, and its effects can also be observed in the right axlebox at the end of December. The effect of the repair (wheel profiling) is clear in the February data, which seems to quickly degrade until reaching a stage with slower growth, highlighted with red rectangles in Figure 6.19. Finally, the effects of repairing the crossing nose at km 52.3 at the end of February are not apparent in the data using the spectrograms. The most notable change in the spectrograms is the increase in the magnitude of the higher frequency harmonics of the right axlebox in December, and the decrease in signal in both wheels after the wheel repair in February. An increase in the signal magnitude is also visible in March after the wheel is repaired, in the frequencies above 200 Hz. These differences in magnitude in different frequency ranges can be used to assess both the state of the track and the wheels using axlebox data, as there is a strong correlation between their condition and the signal magnitude.

The evolution of vehicle vertical displacement is presented in the following figures. Same as for the previous section, only the 140-m filtered displacement is presented in Figure 6.20 for the left axlebox and Figure 6.21 for the right axlebox in this chapter. The 35 and 70-m wavelength filters are presented in Appendix D. The location of the sensors is indicated next to the date, where the letter L indicates that sensors were in the leading coach, and the letter T indicates that sensors were in the trailing coach.

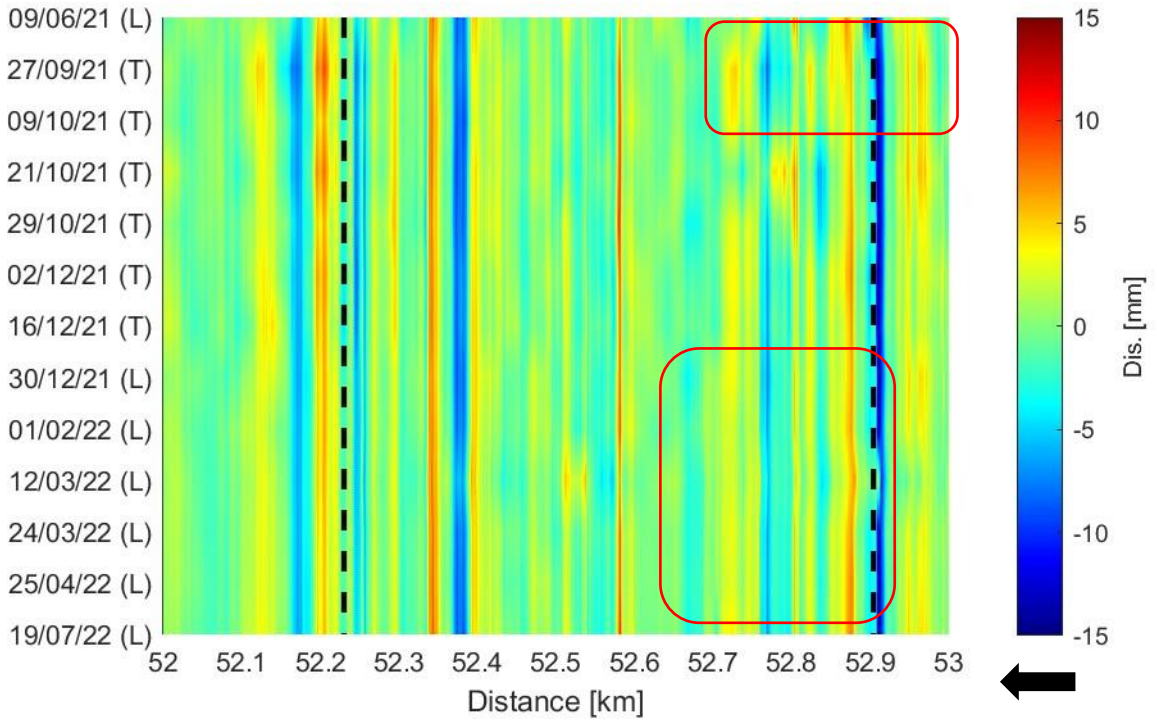


FIGURE 6.20. EVOLUTION OF LEFT AXLEBOX VERTICAL DISPLACEMENT.

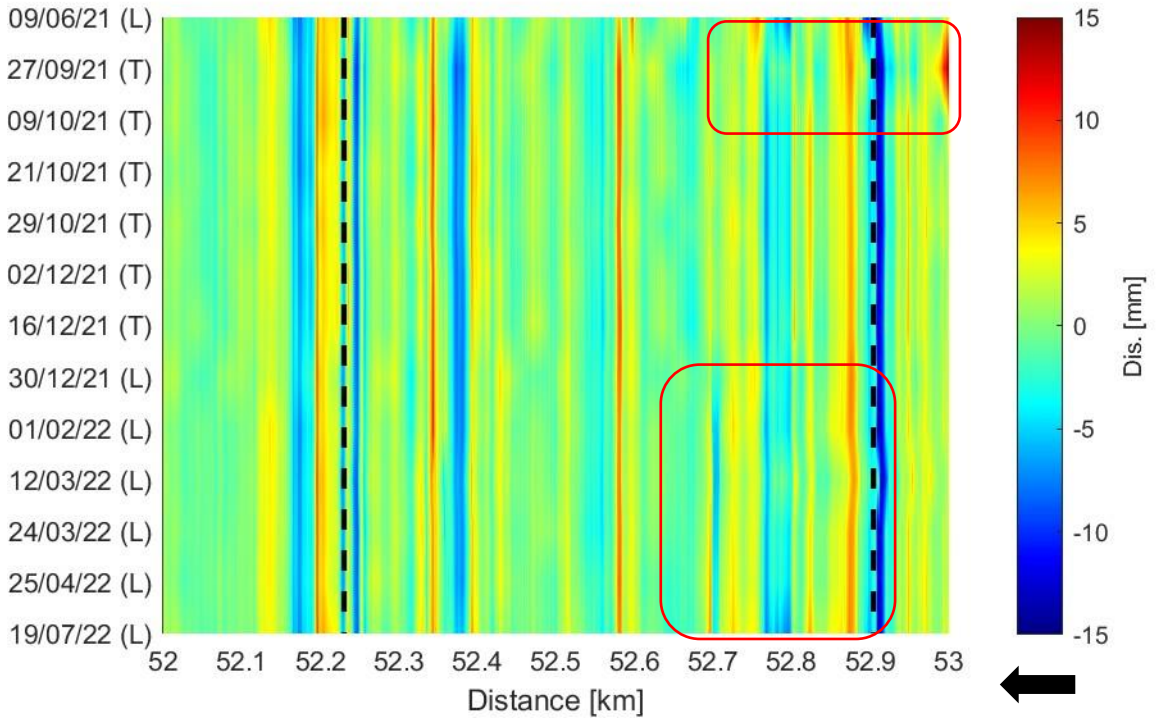


FIGURE 6.21. EVOLUTION OF RIGHT AXLEBOX VERTICAL DISPLACEMENT.

The tamping operation in September caused a decrease in the magnitude of displacement, most notably between km 52.7 and 53, observed as a shift to the green colour in that segment (top red rectangle). There are visible changes in the data after the wheel flat repair in February most visible between km 52.7 and 53 (darker blue and orange in the bottom red rectangle in Figure 6.21). The S&C components are visible in all the filters, showing the short-wavelength effects caused by the vehicle passing over these components. The sensors in the trailing coaches show a slightly larger magnitude of displacement, most visible in the 35 and 70-m filters over the switches. In general, the changes in the vertical displacement are visible throughout all the runs, showing the usefulness of axlebox data for monitoring short-wavelength track features such as the S&C presented in this chapter.

The changes in the bogie data are observed in the following figure. The spectrograms of the signals are presented in Figure 6.22.

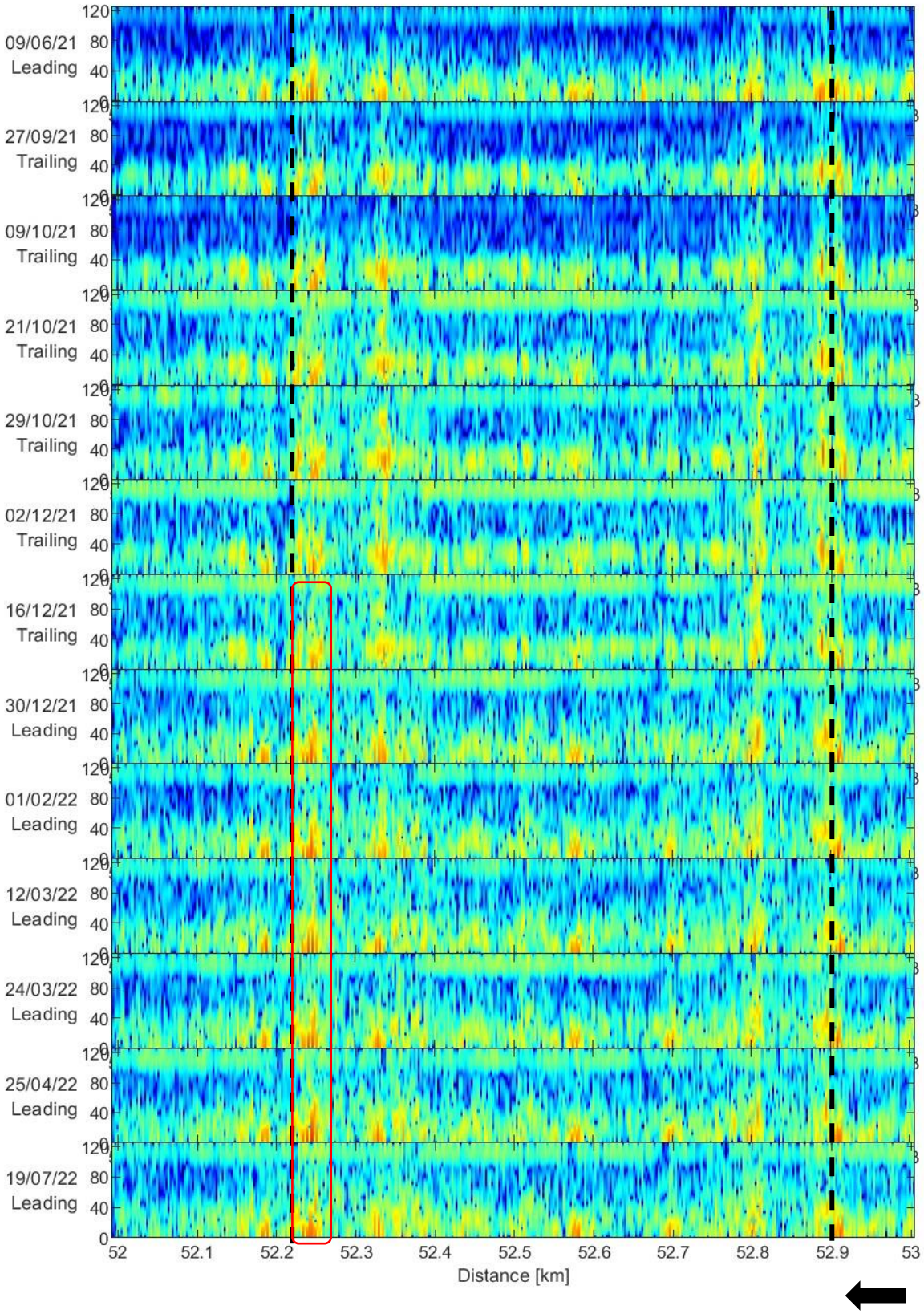


FIGURE 6.22. BOGIE VERTICAL ACCELERATION SPECTROGRAM EVOLUTION.

The figure shows an increase of the signal magnitude in frequencies over 40 Hz, more present from October, and not influenced by the tamping operations carried out in September nor the wheel flat in December. The magnitude of the sensors in trailing coaches is higher, most visible in the harmonic at 120 Hz. This agrees with previous results that showed a lower influence of the wheel condition in the data from the sensors installed on the bogie as less influenced by wheel condition, and more usefulness for track condition monitoring than the axlebox sensors. Notable changes in the crossing are observed between km 52.2 and 52.25, with an increase in magnitude since late December, and a decrease in magnitude since March, after the repairing of the nose. It is then possible to observe the evolution of the nose using the bogie spectrogram.

The evolution of bogie displacement is presented in Figure 6.23, which shows displacement after applying a 140-m wavelength filter. The location of the sensors is indicated next to the date, where the letter L indicates that sensors were in the leading coach, and the letter T indicates that sensors were in the trailing coach.

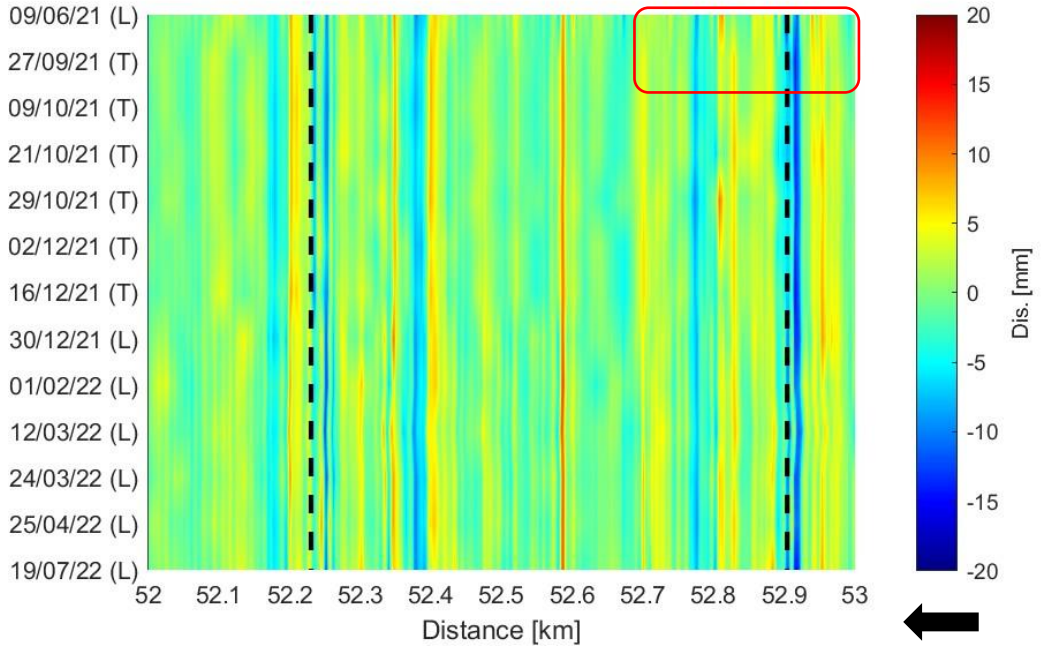


FIGURE 6.23. EVOLUTION OF BOGIE VERTICAL DISPLACEMENT

There is a slight decrease in vertical displacement between June and September 2021 in km 52.7 to 53 due to the tamping operations, although the lack of previous data hinders the extraction of more information concerning the previous state of the track. The most notable difference in both 35 and 70-m wavelength filters is an increased displacement for the leading coaches, independent of the state of the track. No changes in the bogie vertical displacement can be attributed to the wheel flat appearance and repair.

The results from the sensors installed on the cab from the cab shows differences to the bogie and the axlebox sensors. The spectrogram in Figure 6.24.

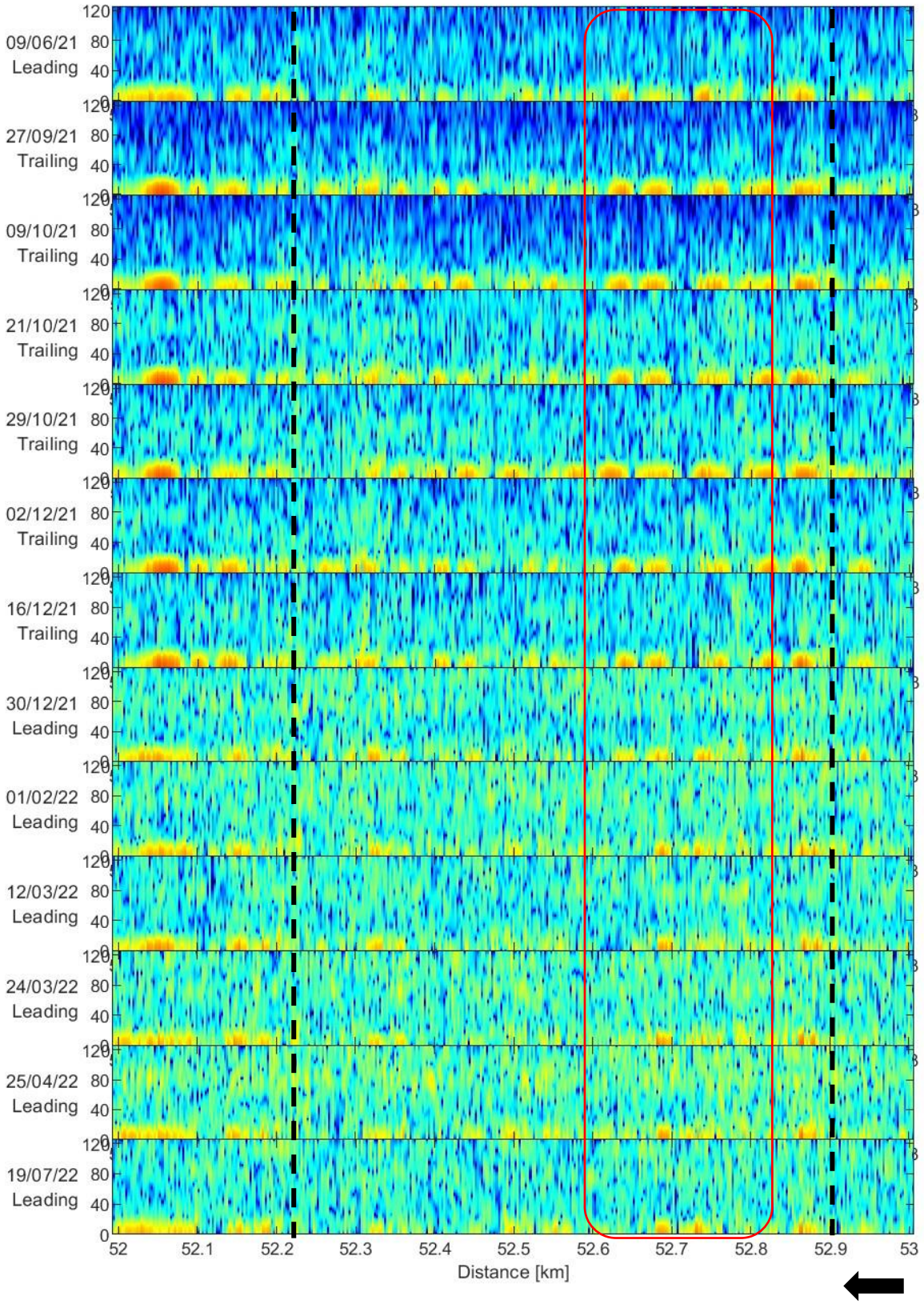


FIGURE 6.24. CAB VERTICAL ACCELERATION SPECTROGRAM.

As discussed previously, the results obtained from the cab sensors do not show large variations due to the S&C, so their evolution over time is not observed either. Similar to the bogie data, the most remarkable change is an increase of the signal magnitude over time, due to the track degradation. The spectrograms show differences between the leading and trailing coaches in the low-frequency range, in agreement with previously presented data. The trailing coaches show a larger magnitude of signal between km 52.6 and 52.8.

The evolution of cab vertical displacement is presented in Figure 6.25, which shows displacement over a 140-m wavelength filter. The location of the sensors is indicated next to the date, where the letter L indicates that sensors were in the leading coach, and the letter T indicates that sensors were in the trailing coach.

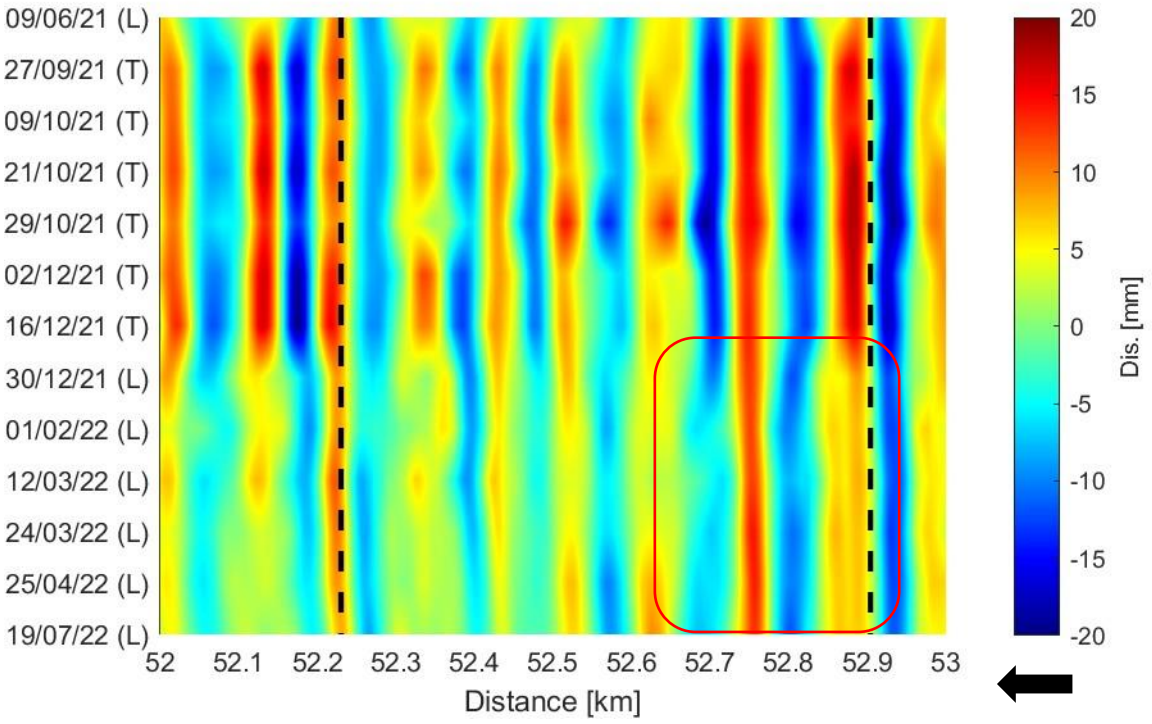


FIGURE 6.25. EVOLUTION OF CAB VERTICAL DISPLACEMENT.

There are differences not only in the magnitude of displacement (the trailing coaches show a larger magnitude), but also in the position of the movement. The 35-m wavelength filter shows a higher magnitude between km 52 and 52.2 after the train has passed over the S&C. A similar behaviour is observed in the other filters, most notably in the 140-m filtered displacement, which also shows an increased displacement between km 52.65 and 52.9 (red rectangle), most notable in the trailing coaches, confirming that the coach movement depends on its position relative to the travel, thus affecting the data acquired. There are no differences in the signal due to the tamping operation nor the wheel flat appearance and repair, which confirm that the cab is not the best-suited location for track inspection and monitoring.

The evolution of vertical comfort is presented in Figure 6.26 and lateral comfort is presented in Figure 6.27. The location of the sensors is indicated next to the date, where the letter L indicates that sensors were in the leading coach, and the letter T indicates that sensors were in the trailing coach.

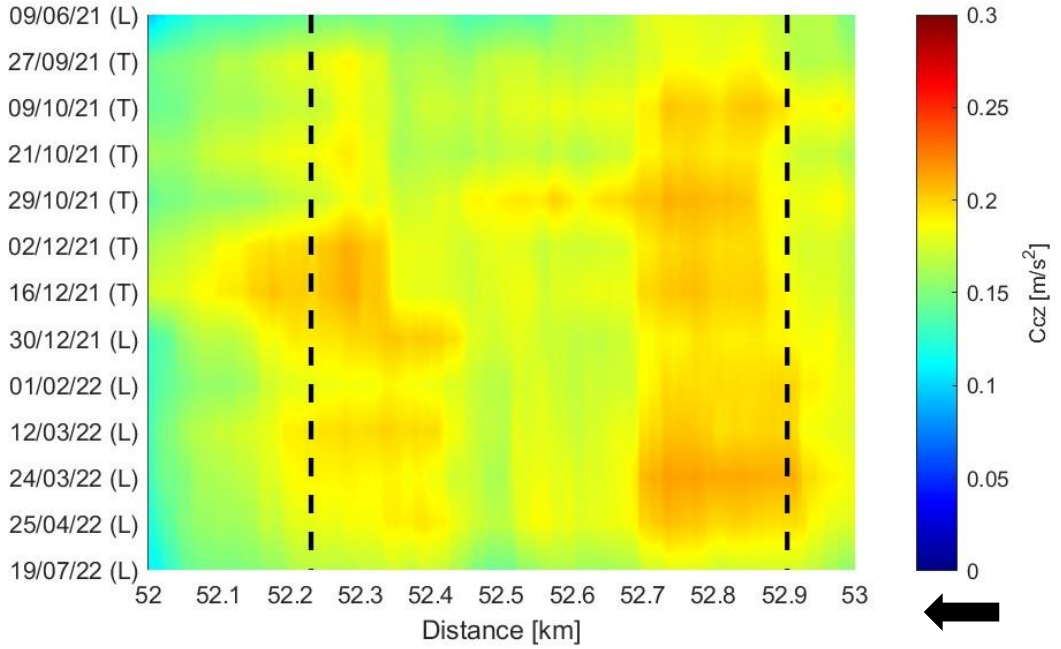


FIGURE 6.26. EVOLUTION OF VERTICAL COMFORT.

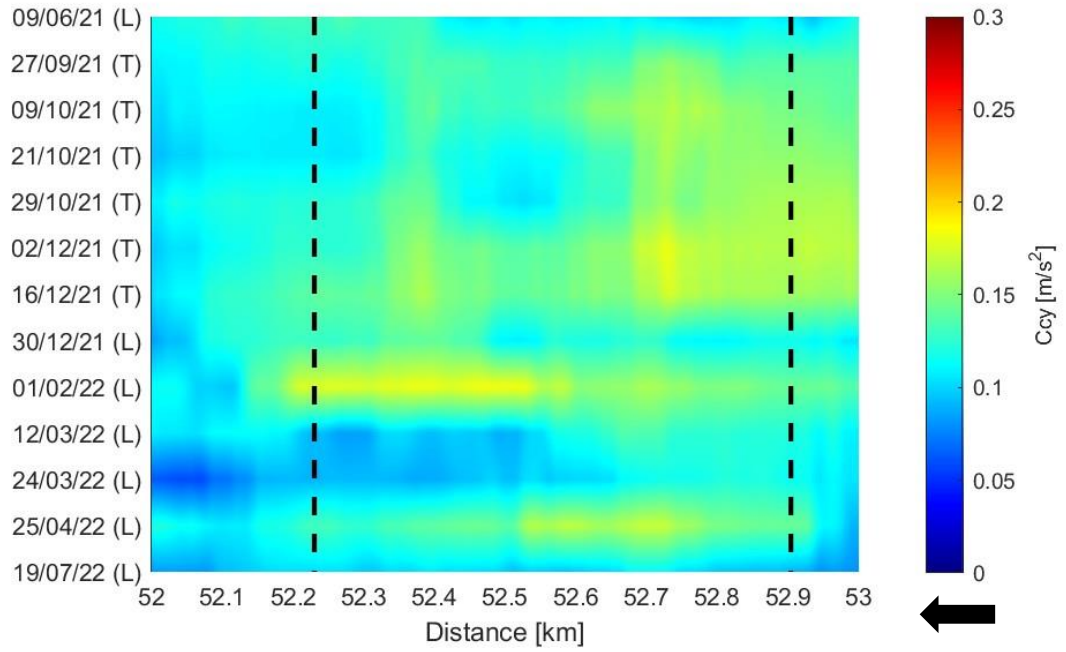


FIGURE 6.27. EVOLUTION OF LATERAL COMFORT.

The values of the comfort indices C_{Cz} and C_{Cy} increase over time, decreasing the passenger comfort perception. As in the previous chapters, the trailing coaches have a larger magnitude of comfort, meaning a worse passenger experience. Lateral comfort shows a high variability between datasets and a generally larger magnitude of this comfort index for the trailing coaches.

In summary, the evolution of the track and the effects of different operations have been observed in this section. Tamping operations caused a slight decrease of vibrations and displacement for both the axlebox and bogie, whilst the wheel flat affected mostly the axlebox. The cab was apparently unaffected by the tamping operations. Comparing the different components allowed to confirm that the axlebox and the bogie are the best places to locate sensors to extract information, although some information on the track condition could be also extracted from the cab. The differences between leading and trailing coaches are confirmed and show the need to consider this aspect for track condition monitoring.

6.4. CONCLUSIONS

This chapter analysed a track segment consisting of an S&C on which tamping and repairing operations have been performed over several months. All components of the S&C can be detected on the vehicle data, although the bogie is shown as the best location for sensors, as the proportional reaction to the S&C is the highest, and the dependence of the signal to the wheel state is lower than compared to the axlebox data. The cab shows little variations related to the S&C, and passenger comfort is slightly affected, mostly in the vertical direction. The differences between configurations confirm that the position of sensors in the vehicle with respect to the travel direction must be considered when acquiring data onboard regardless of the component the sensors are installed in.

Changes in data over time showed the effects of the tamping operation and the wheel flat, that generated differences mostly in the axlebox and bogie signal. As expected, the axlebox is the most sensitive component to wheel changes, hence the notable variations in datasets after these phenomena happened. The bogie, though not as sensitive, also shows changes that can be appreciated with more detail than for the axlebox. Finally, the cab shows a little variation due to these changes, similar to the previous chapter, showing how the wavelength of track features affects different components.

In the following chapter, the relationship between track quality and ride comfort is presented, by comparing rough ride reports provided by drivers to data recorded in the vehicles.

Chapter 7. Relationships between track quality and ride comfort

7.1. INTRODUCTION

The previous chapters discussed the application of comfort indices to track monitoring and the differences in data received due to the position of the sensor. This chapter presents a discussion of the relationship between track quality and ride quality and comfort. Track quality is estimated using vehicle displacement applying different wavelength filters, and ride quality and comfort are calculated using the methods from the standard EN 12299.

Two vehicles of different classes (Class 170 and Class 158) equipped with sensors were used for this analysis. The two different classes have different primary suspension designs, presented in Figure 7.1. Class 170 has chevron-type primary suspensions and air springs on the secondary suspension and Class 158 has two springs on each axlebox of the primary suspension and air springs on the secondary suspension.

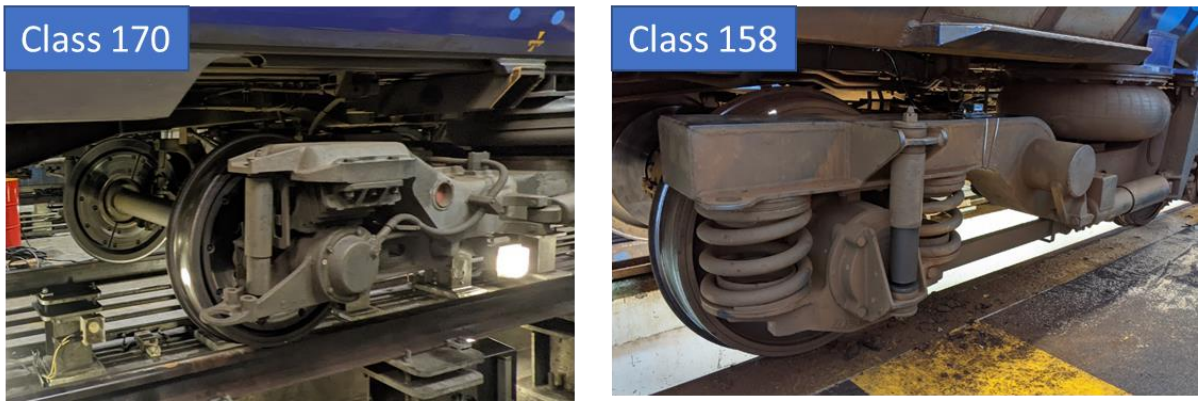


FIGURE 7.1. CLASS 170 AND CLASS 158 SUSPENSIONS.

The arrangement of sensors for both vehicle classes is as follows: a set of accelerometers and gyroscopes acquiring signal in the longitudinal (X), lateral (Y) and vertical (Z) directions at 250 Hz in both the bogie and the cab, and GNSS receivers providing data at 5 Hz.

The following sections present several applications of ride quality data for track quality monitoring. First, two cases of Driver Rough Ride Reports (DRRRs) on two separate lines (one on Stanley Icn. To Inverness Stn., and the other on Carmont). A DRRR is a report provided by a vehicle driver when they perceived an unusually bad condition of the track from the vehicle. Network Rail defines rough ride as "A term used when a member of the train crew reports a "bumpy" ride at a given location". [190].

7.2. CASE 1: STANLEY ICN. TO INVERNESS STN.

A Rough Ride Report (DRRR) was made in a regular speed line between Aviemore and Kincraig in April. The overall ride quality for this track with a Class 170 vehicle is presented in Figure 7.2, where the DRRR is highlighted with a red rectangle. Vehicle speed is presented on the top subfigure, and lateral and vertical comfort on the centre subfigures, showing the highest comfort threshold, "less comfortable", with a red dashed line. The bottom subfigures

present vehicle comfort in curve transitions (P_{CT}) and comfort in discrete events (P_{DE}). These two indices represent the percentage of passengers dissatisfied with the journey. The distance associated with DRRR is highlighted with a red rectangle.

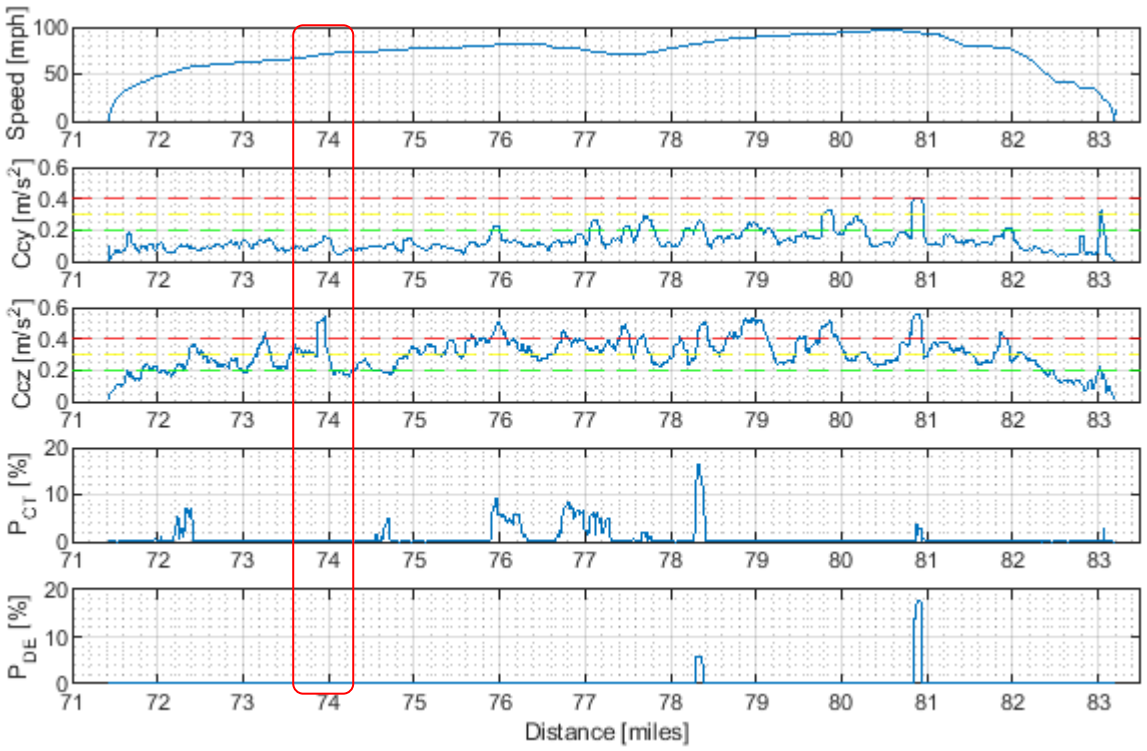


FIGURE 7.2. RIDE QUALITY RESULTS FOR THE TRACK ON A CLASS 170 VEHICLE.

Vertical comfort (C_{Cz}) according to the standard EN 12299 is presented on the map in Figure 7.3, where the location of the DRRR is highlighted with a red rectangle. This map and successive ones are done by superimposing the value of C_{Cz} to the location of the vehicle on the track.

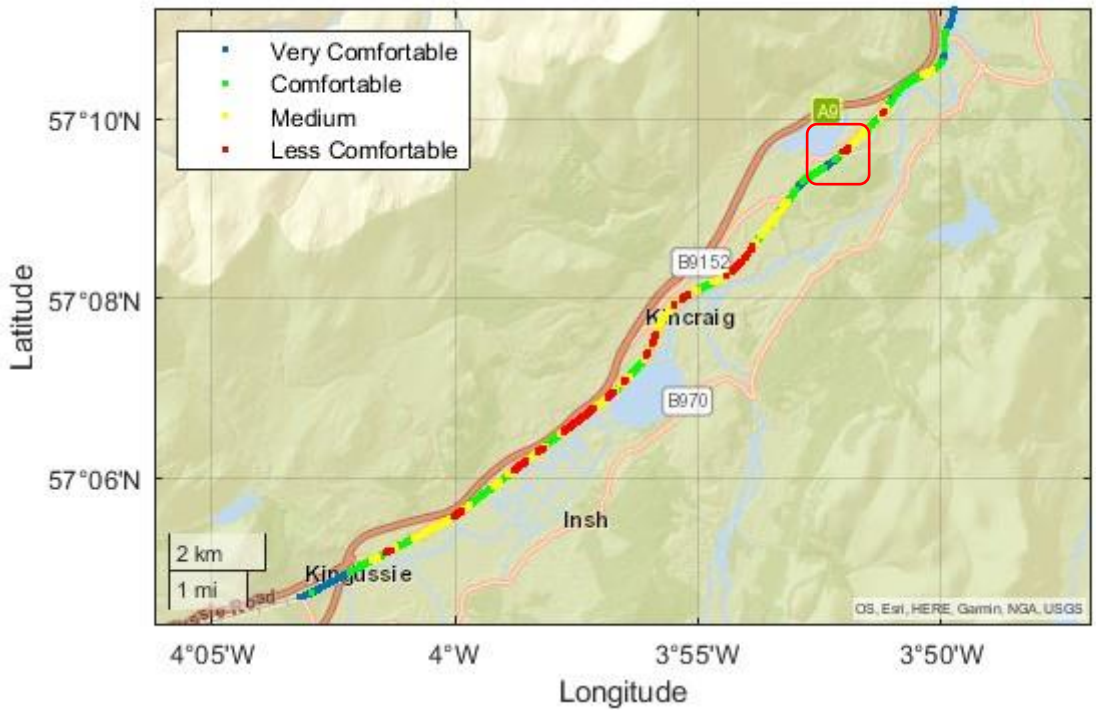


FIGURE 7.3. VERTICAL COMFORT ON THE MAP AND LOCATION OF ROUGH RIDE REPORT.

The values of C_{Cz} along this track segment exceed the "less comfortable" threshold of 0.4 throughout the whole journey. In addition to the high value of C_{Cz} reported at the marked DRRR, there are other locations with high C_{Cz}: At approximately 78.3 miles the vehicle passes through a curve, and at 80.8 miles the high C_{Cz} appears to be related to a bridge over a river. Data collected for other tests show that ride quality may decrease when a vehicle passes through a bridge, hence the reason that no DRRRs were reported at these locations may be because it is in an area of generally poor ride quality, whereas the actual DRRR report is a more isolated location of rough ride. DRRRs depend on the criteria of the vehicle driver, so they must be considered as subjective. Also, a lack of precision in the location of the DRRR must be considered, as the driver takes time to note the rough ride and to report the location of the issue. This shows how some sections with poor ride may not be reported as the driver already expects it, and thus the need for a more objective method to evaluate poor ride conditions.

The vertical ride on this section has more events (over 10 different locations) exceeding the 0.4 threshold but only one point has a high lateral comfort index value above the "less comfortable" threshold. The high C_{Cy} area also has high C_{Cz}which also leads to an increased value in the discrete event index, as observed in Figure 7.2 in mile 80.8. A detail of the vertical track geometry and comfort is presented in Figure 7.4 . Track geometry is represented by vehicle displacement estimated by double-integrating the vertical acceleration, and then applying a wavelength filter to the result. In this case, the filters applied are 35 m and 70 m, referred to as Top 35 and Top 70 in the figure, respectively.

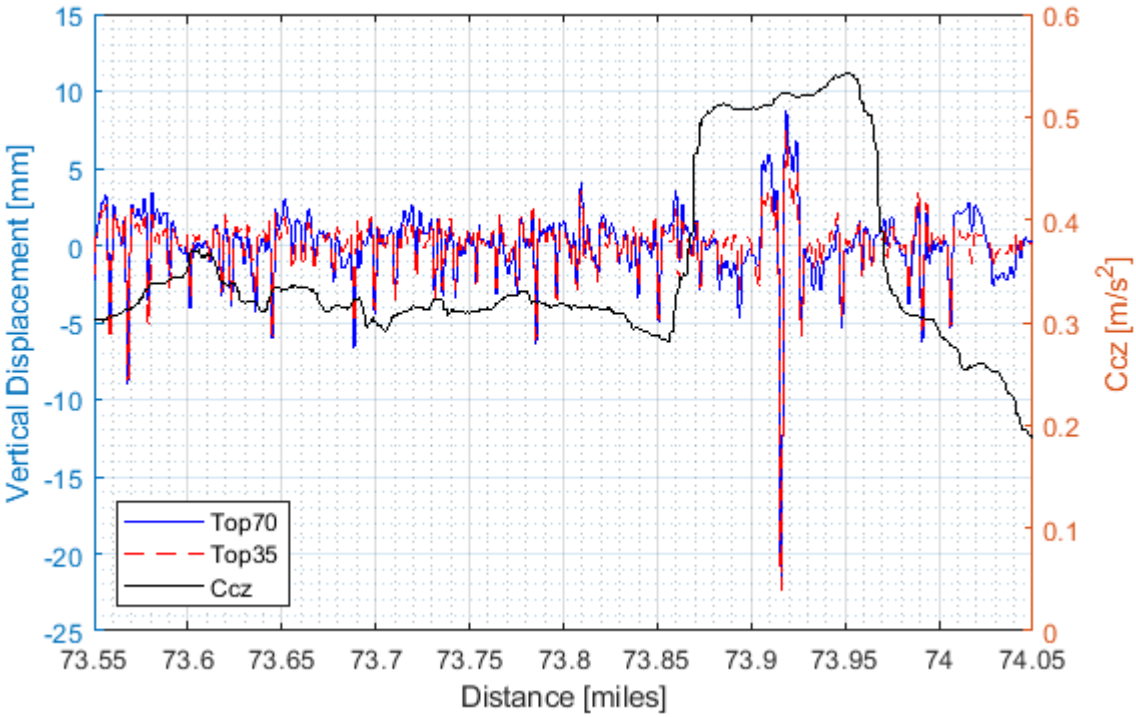


FIGURE 7.4. VERTICAL DISPLACEMENT AND COMFORT FOR A CLASS 170 VEHICLE.

The 35 and 70-m wavelength-filtered displacement (Top35 and Top70 displacement, respectively in the figure) values in this section show several large dips, including at the DRRR location, one of which corresponds to a DRRR. There are also a couple of segments with large positive vertical displacements between 73.92 and 73.93 miles, where the vertical ride quality is poor.

The figures presented previously belong to data from a Class 170 vehicle. Compared to this vehicle, it was found that the ride quality issue does not appear on Class 158 vehicles. The map of the vertical ride quality for Class 158 is shown in Figure 7.5.

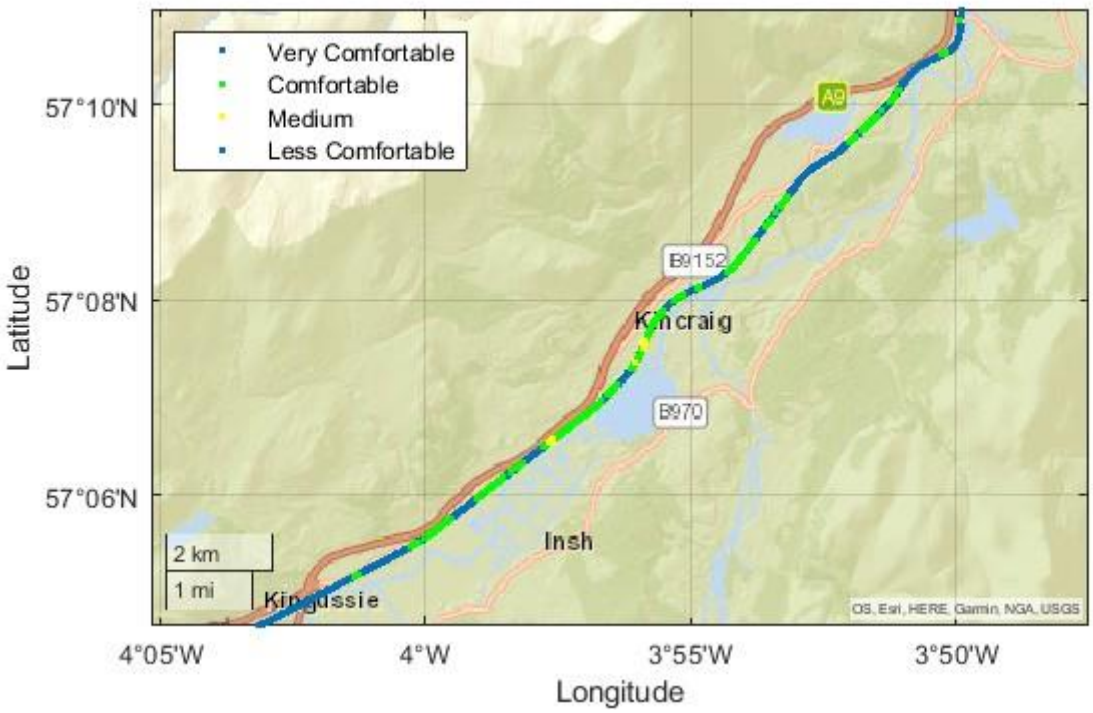


FIGURE 7.5. VERTICAL RIDE COMFORT FOR A CLASS 158 VEHICLE.

The ride comfort parameters from the Class 158 comfort are plotted alongside the Class 170 ride comfort over the same route in Figure 7.6. Speed is presented in the top subfigure, continuous comfort indices are presented in the central subfigures, and event-based comfort indices are presented in the bottom subfigures.

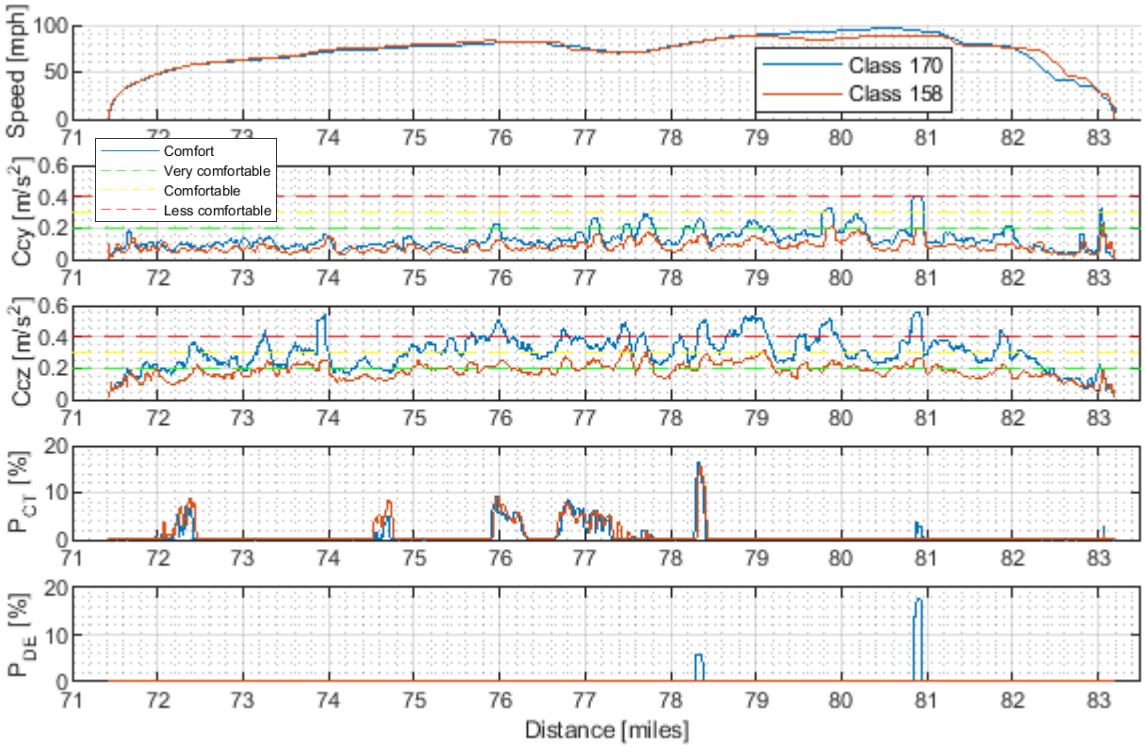


FIGURE 7.6. RIDE QUALITY COMPARISON BETWEEN CLASS 170 AND CLASS 158 VEHICLES.

The trains are travelling at similar speeds, but the vehicle body responses are different: the Class 170 has poorer ride comfort. This indicates differences in the performance of their suspensions, as there are no reported differences in vehicle speed, track condition, or weather conditions. As mentioned in the introduction, each class has a different type of suspension, which may influence the ride quality perceived by the driver and passengers.

7.3. CASE 2: CARMONT

Similar to the previous section, this section presents the comparison of travel conditions between two vehicles passing through a line after rough ride was reported. Between 19th April and 20th June 2022, a series of DRRRs were made around Carmont. The differences between both Class 158 and Class 170 vehicles are evaluated in this section. Figure 7.7 shows the ride comfort map for the up line on a Class 170 vehicle, and Figure 7.8 shows the ride comfort map

for the up line on a Class 158 vehicle. The track section where DRRRs were reported is highlighted with a red rectangle in Figure 7.7.

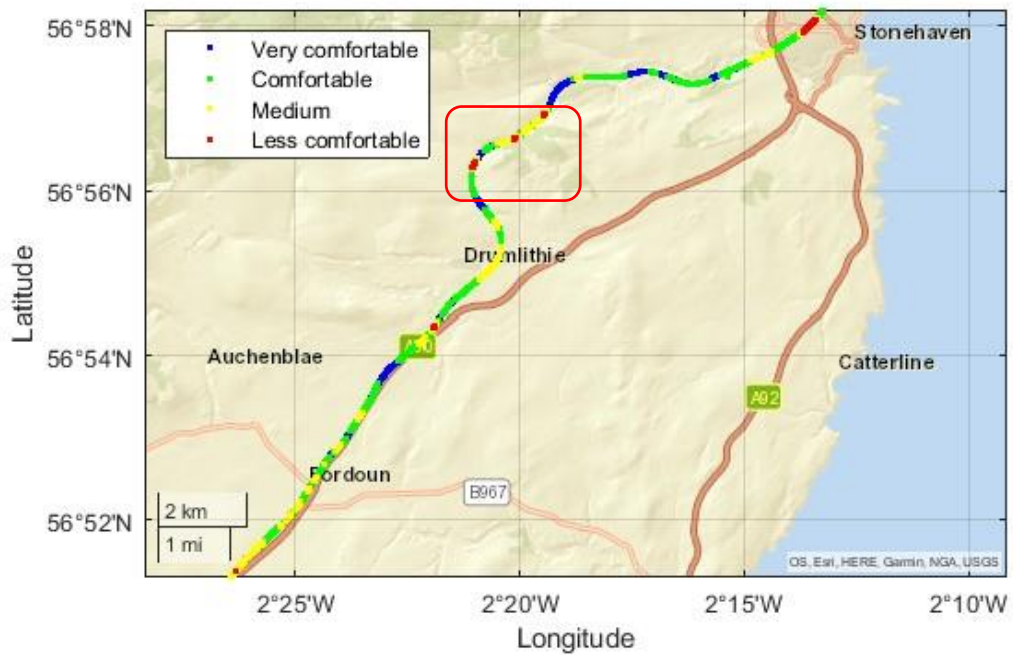


FIGURE 7.7. RIDE COMFORT MAP FOR CLASS 170 ON THE UP LINE.



FIGURE 7.8. RIDE COMFORT MAP FOR CLASS 158 ON THE UP LINE.

It is deduced from Figure 7.7 and Figure 7.8 that the two vehicle classes present different responses on the Up line, with the Class 158 appearing to experience a much better quality ride according to the EN 12299 standard than the Class 170 vehicle, despite the small differences in speed. No location on this route exceeds the 0.4 threshold on the Class 158, whilst there are several locations exceeding this value for the Class 170 vehicle.

The vehicle response of the Class 158 vehicle is significantly better than that of the Class 170. The values of C_{Cz} are generally between 30 and 50% lower for the Class 158 vehicle, indicating better ride quality. At around 220 miles the value of C_{Cz} is doubled on both vehicles compared to close segments. At this location, the value of C_{Cz} for the Class 158 vehicle is 35% smaller than for the Class 170 vehicle.

From the rough ride report, there are two different issues close to each other on that line, one related to the crossing, and one was assumed to be associated with a track fault. The issue from the crossing affects the ride on Class 158 but not enough to exceed the maximum threshold. The track was examined by the infrastructure operator, but no track fault was detected.

Data on the down line shows similar results. The Class 170 vehicle shows poorer ride quality than the Class 158 vehicle along this line. Figure 7.9 shows the map of vertical comfort for the Class 170, and Figure 7.10 shows the map of vertical comfort for the Class 158.

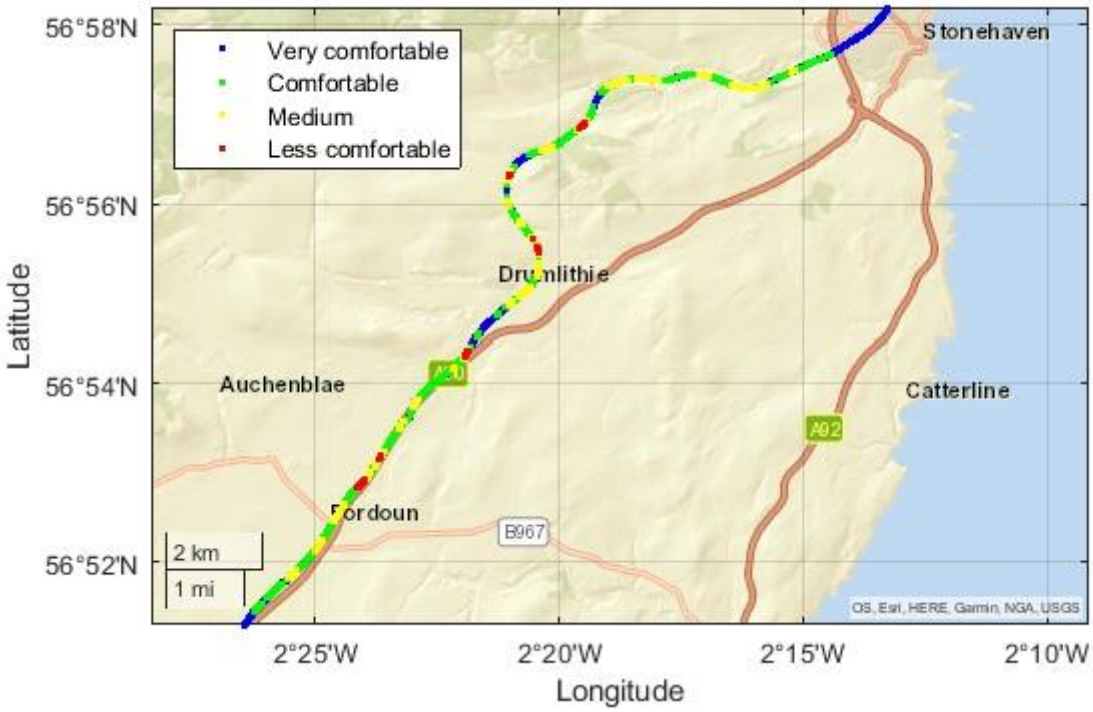


FIGURE 7.9. RIDE COMFORT MAP FOR CLASS 170 ON THE DOWN LINE.



FIGURE 7.10. RIDE COMFORT MAP FOR CLASS 158 ON THE DOWN LINE.

From these plots, it is deduced that the vehicle response in both directions is of a similar magnitude. This is expected, as both lines run parallel, and their track geometry is expected to be highly similar.

7.4. CORRELATION BETWEEN DRRR AND COMFORT

This section presents DRRR reports that were investigated to assess whether there is a correlation between the Driver Reported Rough Rides (DRRRs) and the EN 12299 "less comfortable" threshold for vertical or lateral ride quality. There were 19 DRRRs available for the Class 158 vehicle, and 21 DRRRs available for the Class 170, with suitable equipment on the vehicle. Data from classes 158 and 170 were analysed.

To enable a fair comparison, the journey closest in date to that of each DRRR was selected for analysis. The data including lateral and vertical ride comfort (C_{Cy} and C_{Cz}) were extracted from the reported DRRR location within 500 m of the journey on either side of the primary location.

The vertical and lateral displacement of the vehicle cab using 70-m wavelength filters were calculated to determine the excessive displacement that the train driver could potentially feel. A threshold of 10 mm was then selected to examine the correlation for both directions. It is not normal to use 70-m filtered vertical displacement from cab-mounted sensors, because this result is not the same as the 70-m vertical alignment. Generally, the cab 70-m filtered displacement is smaller than the 70-m track geometry variation. In this section, journeys from Class 158 and Class 170 trains are selected using the closest date to the DRRR and analysed separately.

7.4.1. Rough rides and Class 158

A summary of the relationship between DRRR and track quality is presented in Table 7.1. Each row shows the journey ID, and whether each track quality parameter was above the defined threshold in the DRRR: C_{Cy} and C_{Cz} above 0.4, vertical and lateral 70-m bogie displacement over 10 mm, and cab vertical displacement over 10 mm.

TABLE 7.1. IDENTIFICATION OF CLASS 158 DRRR STATISTICS.

Journey	$C_{Cy} > 0.4$	$C_{Cz} > 0.4$	Vertical 70-m > 10 mm	Lateral 70-m > 10 mm	Cab displacement > 10 mm
1	FALSE	FALSE	TRUE	TRUE	TRUE
2	FALSE	FALSE	TRUE	FALSE	TRUE
3	FALSE	FALSE	TRUE	TRUE	TRUE
4	FALSE	FALSE	TRUE	FALSE	TRUE
5	FALSE	FALSE	FALSE	FALSE	FALSE
6	FALSE	FALSE	TRUE	FALSE	TRUE
7	FALSE	FALSE	TRUE	FALSE	TRUE
8	FALSE	FALSE	TRUE	TRUE	TRUE
9	FALSE	FALSE	TRUE	TRUE	TRUE
10	FALSE	FALSE	TRUE	FALSE	TRUE
11	FALSE	FALSE	TRUE	TRUE	TRUE
12	FALSE	FALSE	TRUE	TRUE	TRUE
13	FALSE	FALSE	TRUE	TRUE	TRUE
14	FALSE	FALSE	TRUE	TRUE	TRUE
15	FALSE	FALSE	TRUE	TRUE	TRUE
16	FALSE	FALSE	TRUE	TRUE	TRUE
17	FALSE	FALSE	TRUE	FALSE	TRUE
18	FALSE	FALSE	TRUE	TRUE	TRUE
19	FALSE	TRUE	TRUE	TRUE	TRUE
Detected (%)	0.0	5.3	94.7	63.2	94.7

The analysis of the results in Table 7.1 shows that the relation between EN12299 and possibly reported rough ride is only about 5.3%. However, large body movements using the body vertical and/or lateral movement results matched up to 94% of the DRRR, which shows the relationship between large body movements and rough ride. This indicates that the overall suspension

performance of this type of train does not make the passenger or the driver experience rough ride from the irregularity in the track.

7.4.2. Rough rides and Class 170

A summary of the relationship between DRRR and track quality is presented in Table 7.2. Each row shows the journey ID, and whether each track quality parameter was above the defined threshold in the DRRR: C_{Cy} and C_{Cz} above 0.4, vertical and lateral 70-m displacement over 10 mm, and cab vertical displacement over 10 mm.

TABLE 7.2. IDENTIFICATION OF CLASS 170 DRRR STATISTICS.

Journey	$C_{Cy} > 0.4$	$C_{Cz} > 0.4$	Vertical 70-m > 10mm	Lateral 70-m > 10 mm	Cab displacement > 10 mm
1	FALSE	TRUE	TRUE	TRUE	TRUE
2	FALSE	TRUE	TRUE	FALSE	TRUE
3	FALSE	FALSE	TRUE	TRUE	TRUE
4	FALSE	TRUE	TRUE	FALSE	TRUE
5	FALSE	FALSE	FALSE	FALSE	FALSE
6	FALSE	FALSE	TRUE	FALSE	TRUE
7	FALSE	TRUE	TRUE	FALSE	TRUE
8	FALSE	TRUE	TRUE	TRUE	TRUE
9	FALSE	TRUE	TRUE	TRUE	TRUE
10	FALSE	FALSE	FALSE	FALSE	FALSE
11	FALSE	FALSE	TRUE	TRUE	TRUE
12	TRUE	TRUE	TRUE	TRUE	TRUE
13	FALSE	FALSE	TRUE	TRUE	TRUE
14	FALSE	FALSE	TRUE	TRUE	TRUE
15	TRUE	TRUE	TRUE	TRUE	TRUE
16	FALSE	TRUE	FALSE	FALSE	FALSE
17	FALSE	TRUE	TRUE	TRUE	TRUE
18	TRUE	TRUE	TRUE	TRUE	TRUE
19	FALSE	FALSE	TRUE	TRUE	TRUE
20	FALSE	FALSE	TRUE	TRUE	TRUE
21	FALSE	FALSE	TRUE	TRUE	TRUE
Detection (%)	14.3	52.4	76.2	57.1	76.2

The analysis of the results for the Class 170 vehicles shows that 52% of the DRRRs are associated to a C_{Cz} over 0.4, which indicates poor ride quality This is significantly larger than for the Class 158 trains, with only 5.3% of the DRRRs related to high C_{Cz}. However, identified excessive body movements (over 10 mm) using the body vertical and lateral movement results can be found for 76% of the reported events in the Class 170 vehicles. This suggests that the ride quality of the Class 170 vehicles is generally poorer, resulting in fewer instances of crossing the 0.4 threshold for C_{Cz} to correspond to DRRRs.

The comparison of DRRRs between two types of trains demonstrates that, on tracks with a similar condition, the type of vehicle secondary suspension affects the travel experience notably, as there are notable differences in the movement of the vehicle cab.

In this case, the larger values of C_{Cz} for the Class 170 in comparison to the values for the Class 158 are likely due to short-wavelength defects that may be filtered out using the processing from the comfort indices. This processing is based on applying a moving RMS to the acceleration data with a window of 5 s, which causes the high frequency components of the acceleration signal to be filtered out. To complement the information extracted from the comfort indices, other processing methods are required, such as displacement estimation using wavelength filters, as applied in Chapters 5 and 6 of this thesis.

7.5. CONCLUSIONS

In this chapter, the relationship between rough ride and track quality was presented. Two cases of rough ride were presented, and a correlation between DRRR and ride comfort was attempted. From the data provided it is concluded that inertial sensors onboard passenger trains can potentially be used to directly link DRRRs to either track or vehicle faults. By combining the

regular track geometry data collected by the system these can detect a range of track faults that can be associated with DRRRs. Uncertainty in the location and certainty of the issue must be considered due to the response time and criteria of the driver reporting it.

Differences between the two vehicle classes were identified, with Class 170 vehicles showing a poorer ride quality than Class 158 vehicles. These showed the effects of suspension on ride quality under similar speed and track conditions.

The analysis of the EN 12299 standard between the two classes shows a significant difference attributed to the different suspensions. It is shown that there are several areas related to assets, such as bridges or crossings, that exceed the thresholds but are not reported by the drivers. This may be due to the drivers assuming that rough ride and large movement are expected and thus not reporting it. As opposed to DRRRs, which are qualitative and subjective, using the EN 12299 standard provides quantitative and objective indices, which can be associated more consistently with the track quality. The use of passenger comfort to assess track condition over time has already been discussed in Chapter 6, showing both the possibility to detect changes in the track condition and the limitations of this signal processing technique for short-wavelength features.

In the following chapter, a summary of the research carried out during the PhD is presented. The main advances are summarized, the relationship between them and the hypothesis is discussed, and the publications and collaborations related to this research are listed.

Chapter 8. Conclusions

8.1. INTRODUCTION

This chapter presents the conclusions of the thesis. The key achievements of the work are summarised; and the links established between the main hypothesis and the chapters are reviewed. Finally, the publications and collaborations extracted from this work are presented.

8.2. KEY ACHIEVEMENTS

The main achievements of this work are summarised in the following items:

- A state of the art of current methods for monitoring vehicles and tracks was presented, with the focus on the use of non-intrusive inertial sensors onboard passenger vehicles.
- A novel method to estimate vehicle speed and position using inertial sensors has been developed, thus reducing the dependency on tachometers and GNSS, especially in tunnels. Furthermore, the method has been complemented with a dynamic alignment technique to align data using crosslevel as a reference and fine-tuned using cross-correlation.
- A comparison between the standards used for comfort assessment in railways has been carried out for a ballasted and a slab track.
- Two case studies were conducted to assess the impact of sensor positioning on measurements. These case studies demonstrated that the installation of sensors on either the leading or trailing coaches heavily influences the results obtained.

- The relationship between track quality and perceived ride comfort has been discussed. This relationship was examined by using reports of poor ride conditions and associating ride quality indices, such as the ones provided by the standard EN 12299, with known track issues.

8.3. HYPOTHESIS AND OBJECTIVES DISCUSSION

The main hypothesis of this work was tested through four objectives to be proven. The discussion on answering these objectives is the following:

1. Localisation of track irregularities using in-service vehicles:

This objective was achieved in Chapter 3, and was necessary to locate track issues. The use of an in-service vehicle instrumented with an IMU showed that it is possible to estimate the speed and position of a vehicle in areas with poor or none GNSS signal. The accurate localisation of the vehicle allowed the use of the signals derived from the IMU to detect and locate elements of the track, such as S&Cs (discussed in Chapter 6), and issues within these elements.

2. Assessment of Ride Quality and Passenger Comfort using in-service data:

This objective was discussed in Chapters 4 to 7. The differences in the comfort estimation methods were discussed in Chapter 4, using data from a high-speed track, where the standard EN 12299 was considered the most useful for comfort assessment. The effects in ride quality of track features were discussed in Chapters 5 and 6, considering both comfort and vehicle displacement on high-speed tracks according to the standards. The relationship between track quality and passenger comfort were discussed in Chapter 7 considering different types of vehicles.

3. Evaluation of Sensor Placement:

This objective was discussed in Chapters 5 and 6. These chapters presented case studies that showed how the position of the sensors relative to the direction of travel of the vehicle influences the signals received, where sensors on the trailing coaches generally show higher displacement and a poorer ride quality.

4. Effects of Track Quality on Vehicle Movement and Perception:

This objective was discussed in Chapter 7. This chapter showed how track quality perceived by the passengers is subjective, as well as the limitations of DRRRs due to their subjectiveness compared to ride comfort standards to assess track quality and to relate it to passenger comfort.

In summary, the main hypothesis of this work, "sensors onboard in-service vehicles can provide useful information about the state of the track through its effect on ride quality, that could be used to substitute driver rough ride reports", was proved correct through the achievement of the four objectives above discussed. Having sensors installed on in-service vehicles can provide comfort, replace DRRRs, and acquire data with enough frequency as to find developing poor track geometry earlier than using dedicated vehicles.

8.4. PUBLICATIONS AND COLLABORATIONS

Research during this period produced several publications, including journal and conference articles, and posters. These are listed as follows:

1. Poster presented at the University of Birmingham Research Poster Conference in June 2019, explaining the speed estimation and crosslevel adaptation. This poster is in Appendix E. Research Poster Conference 2019.

2. Conference paper presented at the World Congress on Railway Research (WCRR) in 2019 in Japan. The main contribution of the author to this paper was related to comfort estimation. This article is in Appendix F. WCRR 2019.
3. Poster presented at the University of Birmingham Research Poster Conference in July 2021, showing the first analysis of data related to Chapter 4. This poster is in Appendix G. Research Poster Conference 2021.
4. Journal article published on Vehicle System Dynamics in August 2021. This article explains the process to estimate speed and position, and correct the estimation using crosslevel, as presented in Chapter 3. This article can be found at https://doi.org/10.1080/00423114.2021.1968443. This article is in Appendix H. Journal article 1.
5. Conference article presented at the CONTROL 2022 conference in April 2022, explaining the evolution of data over time. This article can be found at https://doi.org/10.1109/Control55989.2022.9781456 This article is in Appendix I. CONTROL 2022.
6. Poster presented at Rail Live congress in November 2022 in Málaga, Spain, showing the applications of onboard sensors for railway track condition monitoring. This poster is in Appendix J. Rail Live 2022.
7. Journal article published in IEEE Transactions on Intelligent Transportation Systems in December 2022. This article is a review of the factors affecting track geometry, and the data analysis techniques currently employed for the processing of the signals provided. The main contribution of the author is the review of data analytic techniques. This article can be found at https://doi.org/10.1109/TITS.2022.3214121. This article is in Appendix K. Journal article 2.

8. A 2022 “On The Move” grant was awarded to the researcher for collaboration in Spain in Ingenium Research Group, in Universidad de Castilla-la Mancha. The focus of the research for this grant was the exchange of knowledge between both groups.

References

1. Office of Rail and Road. *How many people use the railway*. 2022 [cited 2022 December]; Available from: https://dataportal.orr.gov.uk/popular-statistics/how-many-people-use-the-railway.
2. Liu, X., M.R. Saat, and C.P. Barkan, *Analysis of causes of major train derailment and their effect on accident rates.* Transportation Research Record Journal, 2012. **2289**(1): p. 154-163.
3. Sperry Rail Service. *Rail health services*. 2021 [cited 2021 February]; Available from: https://www.sperryrail.com/rail-health-services.php.
4. ENSCO. *Rail Track Inspection Vehicles | Self-propelled Rail Cars | Hi-rail Vehicles | ENSCO*. 2021 [cited 2021 February]; Available from: https://www.ensco.com/rail/track-inspection-vehicles.
5. Network Rail. *New Measurement Train (NMT) - Network Rail*. 2022 [cited 2022 August]; Available from: https://www.networkrail.co.uk/running-the-railway/looking-after-the-railway/our-fleet-machines-and-vehicles/new-measurement-train-nmt/.
6. RailAdvent. *Network Rail awards £8m contract for New Measurement Train*. 2022 [cited 2022 August]; Available from: https://www.railadvent.co.uk/2020/01/network-rail-awards-8m-contract-for-new-measurement-train.html.
7. Board, T.R., E. National Academies of Sciences, and Medicine, *Track Design Handbook for Light Rail Transit, Second Edition*, ed. I.P. Brinckerhoff, et al. 2012, Washington, DC: The National Academies Press. 647.
8. British Standards Institution, *GC/RT 5017: Track Standards Manual. Section 8: Track Geometry*. 1998, United Kingdom.
9. British Standards Institution, *BS EN 13848-1:2019: Railway Applications: Track. Track geometry quality*. 2019, United Kingdom.
10. British Standards Institution, *BS EN 13803:2017: Railway applications: Track. Track alignment design parameters. Track gauges 1435 mm and wider*. 2017, United Kingdom.
11. British Standards Institution, *BS EN 12299:2009: Railway Applications: Ride comfort for passengers. Measurement and evaluation*. 2009, United Kingdom.
12. Connolly, D.P., et al., *Benchmarking railway vibrations – Track, vehicle, ground and building effects.* Construction and Building Materials, 2015. **92**: p. 64-81.
13. Zhou, L., X.-Z. Liu, and Y.-Q. Ni, *Contemporary inspection and monitoring for high-speed rail system*, in *High-speed rail*. 2018, IntechOpen.
14. British Standards Institution, *TMC 226: Rail defects handbook*. 2012, Transport Rail Corp: United Kingdom.
15. Wei, X., et al., *Railway track fastener defect detection based on image processing and deep learning techniques: A comparative study.* Engineering Applications of Artificial Intelligence, 2019. **80**: p. 66-81.
16. British Standards Institution, *BS EN 13145:2001+A1:2011: Railway applications: Track. Wood sleepers and bearers*. 2011, British Standards Institution: United Kingdom.

17. British Standards Institution, *BS EN 13230-1:2016: Railway applications: Track: Concrete sleepers and bearers. Part 1. General requirements*. 2016, BSI Standards: United Kingdom.
18. British Standards Institution, *BS 500:2000: Steel sleepers*. 2000, British Standards Institution: United Kingdom.
19. Ferdous, W. and A. Manalo, *Failures of mainline railway sleepers and suggested remedies–review of current practice.* Engineering Failure Analysis, 2014. **44**: p. 17-35.
20. Zeman, J.C., et al. *Failure mode and effect analysis of concrete ties in North America*. in *Proc. of the 9th International Heavy Haul Conference*. 2009.
21. Sabato, A. and C. Niezrecki, *Feasibility of digital image correlation for railroad tie inspection and ballast support assessment.* Measurement, 2017. **103**: p. 93-105.
22. Hassankiadeh, S.J., *Failure analysis of railway switches and crossings for the purpose of preventive maintenance*, in *Department of Transport Science*. 2011, School of Architecture and the Built Environment: Transport Science.
23. Lim, W.L., *Mechanics of railway ballast behaviour*. 2004, University of Nottingham Nottingham, UK.
24. Franklin, A. *Current practice in ballast maintenance & renewal*. in *Improving the Performance of Ballasted Rail Track: from research to practice*. 2006. Nottingham.
25. Milne, D., et al., *Monitoring and repair of isolated trackbed defects on a ballasted railway.* Transportation Geotechnics, 2018. **17**: p. 61-68.
26. Indraratna, B., L.-j. Su, and C. Rujikiatkamjorn, *A new parameter for classification and evaluation of railway ballast fouling.* Canadian Geotechnical Journal, 2011. **48**(2): p. 322-326.
27. Silvast, M., et al., *An inspection of railway ballast quality using ground penetrating radar in Finland.* Proceedings of the Institution of Mechanical Engineers, Part F: Journal of Rail and Rapid Transit, 2010. **224**(5): p. 345-351.
28. Prescott, D. and J. Andrews, *A track ballast maintenance and inspection model for a rail network.* Proceedings of the Institution of Mechanical Engineers, Part O: Journal of risk and reliability, 2013. **227**(3): p. 251-266.
29. Soleimanmeigouni, I., A. Ahmadi, and U. Kumar, *Track geometry degradation and maintenance modelling: A review.* Proceedings of the Institution of Mechanical Engineers, Part F: Journal of Rail and Rapid Transit, 2018. **232**(1): p. 73-102.
30. Guler, H., *Decision support system for railway track maintenance and renewal management.* Journal of Computing in Civil Engineering, 2013. **27**(3): p. 292-306.
31. Chen, R., et al., *Degradation mechanism of CA mortar in CRTS I slab ballastless railway track in the Southwest acid rain region of China – Materials analysis.* Construction and Building Materials, 2017. **149**: p. 921-933.
32. Zhu, S., et al., *Damage evolution and dynamic response of cement asphalt mortar layer of slab track under vehicle dynamic load.* Science China Technological Sciences, 2014. **57**(10): p. 1883-1894.
33. Usman, K., M. Burrow, and G. Ghataora, *Railway track subgrade failure mechanisms using a fault chart approach.* Procedia Engineering, 2015. **125**: p. 547-555.
34. Xiao, J. and L. Liu. *Multi-frequency GPR signal fusion using forward and inverse S-transform for detecting railway subgrade defects*. in *2015 8th International Workshop on Advanced Ground Penetrating Radar (IWAGPR)*. 2015. IEEE.
35. Hugenschmidt, J., *Railway track inspection using GPR.* Journal of Applied Geophysics, 2000. **43**(2-4): p. 147-155.

36. Xu, X., Y. Lei, and F. Yang, *Railway subgrade defect automatic recognition method based on improved Faster R-CNN.* Scientific Programming, 2018. **2018**.
37. Kassa, E. *Analysis of failures within switches and crossings using failure modes and effects analysis methodology*. in *Proceedings of Intelliswitch Symposium*. 2017.
38. Sysyn, M., et al., *Common crossing condition monitoring with on-board inertial measurements.* 2019.
39. Le Pen, L., et al., *Behaviour of under sleeper pads at switches and crossings–Field measurements.* Proceedings of the Institution of Mechanical Engineers, Part F: Journal of rail and rapid transit, 2018. **232**(4): p. 1049-1063.
40. Márquez, F.P.G. and D.J. Pedregal, *Applied RCM2 algorithms based on statistical methods.* International Journal of Automation Computing, 2007. **4**(2): p. 109-116.
41. Le Pen, L., et al., *The behaviour of railway level crossings: insights through field monitoring.* Transportation Geotechnics, 2014. **1**(4): p. 201-213.
42. Varandas, J.N., P. Hölscher, and M.A. Silva, *Dynamic behaviour of railway tracks on transitions zones.* Computers structures, 2011. **89**(13-14): p. 1468-1479.
43. Priest, J., et al., *Measurements of transient ground movements below a ballasted railway line.* Géotechnique, 2010. **60**(9): p. 667-677.
44. Yeo, G., P. Weston, and C. Roberts. *Assessing rail deflection data from inertial measurements collected from on board a railway vehicle*. in *11th World Congress on Railway Research*. 2016. Milan, Italy.
45. Kim, H., et al. *Measuring the deflection of a sequence of sleepers at a transition zone*. in *6th IET Conference on Railway Condition Monitoring (RCM 2014)*. 2014. IET.
46. Yeo, G., P. Weston, and C. Roberts, *The utility of continual monitoring of track geometry from an in-service vehicle.* 2014.
47. Nielsen, J.C. and A. Johansson, *Out-of-round railway wheels-a literature survey.* Proceedings of the Institution of Mechanical Engineers, Part F: Journal of Rail and Rapid Transit, 2000. **214**(2): p. 79-91.
48. Nielsen, J., *Out-of-round railway wheels*, in *Wheel–Rail Interface Handbook*. 2009, Elsevier. p. 245-279.
49. Amini, A., *Online condition monitoring of railway wheelsets*. 2016, University of Birmingham.
50. British Standards Institution, *ESR 0330: Wheel defect manual*. 2013, Transport RailCorp.
51. Cho, J. and P. Eng, *Development of an Accelerometer Based Wheel-Flat Detection System for a Subway Transit System in Toronto.* 2013.
52. Belotti, V., et al., *Wheel-flat diagnostic tool via wavelet transform.* Mechanical Systems and Signal Processing, 2006. **20**(8): p. 1953-1966.
53. Radu, C., *The most common causes of bearing failure and the importance of bearing lubrication*. 2010, RKB: RKB Technical Review-February. p. 1-7.
54. Alemi, A., F. Corman, and G. Lodewijks, *Condition monitoring approaches for the detection of railway wheel defects.* Proceedings of the Institution of Mechanical Engineers, Part F: Journal of Rail and Rapid Transit, 2017. **231**(8): p. 961-981.
55. Connor, P. *The Railway Technical Website*. [cited 2020 December]; Available from: http://www.railway-technical.com/.
56. Iwnicki, S.D., et al., *Dynamics of railway freight vehicles.* Vehicle System Dynamics, 2015. **53**(7): p. 995-1033.
57. Fu, Y., et al. *High-speed railway bogie fault diagnosis using LSTM neural network*. in *2018 37th Chinese Control Conference (CCC)*. 2018. IEEE.

58. Lu, Y., et al., *Analysis of the effects of vibration modes on fatigue damage in high-speed train bogie frames.* Engineering Failure Analysis, 2018. **89**: p. 222-241.
59. Trilla, A. and P. Gratacòs, *Maintenance of bogie components through vibration inspection with intelligent wireless sensors: A case study on axle-boxes and wheel-sets using the empirical mode decomposition technique.* Proceedings of the Institution of Mechanical Engineers, Part F: Journal of Rail and Rapid Transit, 2016. **230**(5): p. 1408-1414.
60. Topp, D. and M. Smith, *Application of the ACFM inspection method to rail and rail vehicles.* Insight-Non-Destructive Testing and Condition Monitoring, 2005. **47**(6): p. 354-357.
61. Bernal, E., M. Spiryagin, and C. Cole, *Onboard condition monitoring sensors, systems and techniques for freight railway vehicles: a review.* IEEE Sensors Journal, 2018. **19**(1): p. 4-24.
62. Sharma, S.K., et al., *Challenges in rail vehicle-track modeling and simulation.* International Journal of Vehicle Structures Systems, 2015. **7**(1): p. 1.
63. Zhai, W., K. Wang, and C. Cai, *Fundamentals of vehicle–track coupled dynamics.* Vehicle System Dynamics, 2009. **47**(11): p. 1349-1376.
64. Wei, X., L. Jia, and H. Liu, *A comparative study on fault detection methods of rail vehicle suspension systems based on acceleration measurements.* Vehicle System Dynamics, 2013. **51**(5): p. 700-720.
65. Mei, T. and X. Ding, *A model-less technique for the fault detection of rail vehicle suspensions.* Vehicle System Dynamics, 2008. **46**(S1): p. 277-287.
66. Wei, X., H. Lui, and Y. Qin. *Fault isolation of rail vehicle suspension systems by using similarity measure*. in *Proceedings of 2011 IEEE International Conference on Service Operations, Logistics and Informatics*. 2011.
67. Li, P., et al., *Estimation of railway vehicle suspension parameters for condition monitoring.* Control engineering practice, 2007. **15**(1): p. 43-55.
68. Milne, D., et al., *The influence of variation in track level and support system stiffness over longer lengths of track for track performance and vehicle track interaction.* Vehicle System Dynamics, 2019: p. 1-24.
69. Cheli, F. and R. Corradi, *On rail vehicle vibrations induced by track unevenness: Analysis of the excitation mechanism.* Journal of Sound and Vibration, 2011. **330**(15): p. 3744-3765.
70. British Standards Institution, *BS ISO 2631-1:1997: Mechanical vibration and shock: Evaluation of human exposure to whole-body vibration. Part 1: General Requirements*. 1997, BSI Standards: United Kingdom.
71. British Standards Institution, *BS ISO 2631-4:2001+A1:2010: Mechanical vibration and shock: Evaluation of human exposure to whole-body vibration. Part 4: Guidelines for the evaluation of the effects of vibration and rotational motion on passenger and crew comfort in fixed-guideway transport systems*. 2010: United Kingdom.
72. Peng, Y., et al., *A review of passenger ride comfort in railway: assessment and improvement method.* Transportation Safety and Environment, 2022. **4**(2).
73. Schwanitz, S., et al., *Pressure variations on a train – Where is the threshold to railway passenger discomfort?* Applied Ergonomics, 2013. **44**(2): p. 200-209.
74. Rail Tec Arsenal. *Thermal Comfort in Rail vehicles*. 2023 [cited 2023 June]; Available from: https://www.rta.eu/en/.

75. Jiang, Y., B.K. Chen, and C. Thompson, *A comparison study of ride comfort indices between Sperling's method and EN 12299.* International Journal of Rail Transportation, 2019. **7**(4): p. 279-296.
76. Zhou, J., et al., *Influences of car body vertical flexibility on ride quality of passenger railway vehicles.* Proceedings of the Institution of Mechanical Engineers, Part F: Journal of Rail and Rapid Transit, 2009. **223**(5): p. 461-471.
77. Dumitriu, M., *Influence of the suspension damping on ride comfort of passenger railway vehicles.* UPB Scientific Bulletin, Series D: Mechanical Engineering, 2012. **74**(4): p. 75-90.
78. Dumitriu, M. and M.C. Leu. *Correlation between Ride Comfort Index and Sperling's Index for Evaluation Ride Comfort in Railway Vehicles*. in *Applied Mechanics and Materials*. 2018. Trans Tech Publ.
79. Kim, Y., et al., *Correlation of ride comfort evaluation methods for railway vehicles.* Proceedings of the Institution of Mechanical Engineers, Part F: Journal of Rail and Rapid Transit, 2003. **217**(2): p. 73-88.
80. Sun, J., et al., *An investigation into evaluation methods for ride comfort of railway vehicles in the case of carbody hunting instability.* Proceedings of the Institution of Mechanical Engineers, Part F: Journal of Rail and Rapid Transit, 2020: p. 0954409720949116.
81. Liu, C., et al., *Effect of train speed and track geometry on the ride comfort in high-speed railways based on ISO 2631-1.* Proceedings of the Institution of Mechanical Engineers, Part F: Journal of Rail and Rapid Transit, 2020. **234**(7): p. 765-778.
82. Wu, J. and Y. Qiu. *Analysis of Ride Comfort of a High-Speed Train Based on a Coupled Track-Train-Seat-Human Model with Lateral, Vertical and Roll Vibrations*. in *Advances in Dynamics of Vehicles on Roads and Tracks*. 2020. Cham: Springer International Publishing.
83. Pradhan, S., A.K. Samantaray, and R. Bhattarcharyya. *Evaluation of Ride Comfort in a Railway Passenger Vehicle With Integrated Vehicle and Human Body Bond Graph Model*. in *ASME 2017 International Mechanical Engineering Congress and Exposition*. 2017.
84. Zhou, J., et al., *Evaluation and prediction method of railway passenger long-term vibration comfort under complex operating conditions.* Ergonomics, 2023: p. 1-13.
85. Kouroussis, G., et al., *Review of trackside monitoring solutions: from strain gages to optical fibre sensors.* Sensors, 2015. **15**(8): p. 20115-20139.
86. Otegui, J., et al., *A survey of train positioning solutions.* IEEE Sensors Journal, 2017. **17**(20): p. 6788-6797.
87. Rosenberger, M., *Future Challenges to Axle Counting Systems.* Institution of Railway Signal Engineers, 2012.
88. Lai, C., et al., *Development of a fiber-optic sensing system for train vibration and train weight measurements in Hong Kong.* Journal of Sensors, 2012. **2012**.
89. Entezami, M., et al., *Lineside and on-board monitoring techniques for infrastructure and rolling stock on high-speed lines.* The International Journal of Railway Technology, 2017. **6**.
90. Marais, J., J. Beugin, and M. Berbineau, *A Survey of GNSS-Based Research and Developments for the European Railway Signaling.* IEEE Transactions on Intelligent Transportation Systems, 2017. **18**(10): p. 2602-2618.

91. Liu, J., et al. *A GPS/compass based train integrated positioning method for high-speed railways*. in *2012 IEEE-APS Topical Conference on Antennas and Propagation in Wireless Communications (APWC)*. 2012. IEEE.
92. British Standards Institution, *BS 3403:1972: Indicating tachometer and speedometer systems for industrial, railway and marine use*. 1972, United Kingdom.
93. Malvezzi, M., et al. *Train position and speed estimation by integration of odometers and IMUs*. in *9th World Congress on Railway Research, Lille, France*. 2011.
94. Jiang, Q., et al., *A new filtering and smoothing algorithm for railway track surveying based on landmark and IMU/odometer.* Sensors, 2017. **17**(6): p. 1438.
95. Falamarzi, A., S. Moridpour, and M. Nazem, *A review on existing sensors and devices for inspecting railway infrastructure.* Jurnal Kejuruteraan, 2019. **31**(1): p. 1-10.
96. Papaelias, M., C. Roberts, and C.L. Davis, *A review on non-destructive evaluation of rails: state-of-the-art and future development.* Proceedings of the Institution of Mechanical Engineers, Part F: Journal of Rail and Rapid transit, 2008. **222**(4): p. 367-384.
97. Xiao, J. and L. Liu. *Multi-frequency GPR signal fusion using forward and inverse S-transform for detecting railway subgrade defects*. in *2015 8th International Workshop on Advanced Ground Penetrating Radar (IWAGPR)*. 2015 1(1): p. 1-4. IEEE.
98. Weston, P., et al., *Perspectives on railway track geometry condition monitoring from in-service railway vehicles.* Vehicle System Dynamics, 2015. **53**(7): p. 1063-1091.
99. Farkas, A., *Measurement of Railway Track Geometry: A State-of-the-Art Review*. Periodica Polytechnica Transportation Engineering, 2020. **48**(1): p. 76-88.
100. Bolshakova, A., et al. *The Possibility of Using Inertial Sensor Data for Detection of Long Wavelength Rail Irregularities*. in *2022 29th Saint Petersburg International Conference on Integrated Navigation Systems (ICINS)*. 2022.
101. Le Pen, L., et al., *Evaluating railway track support stiffness from trackside measurements in the absence of wheel load data*. Canadian Geotechnical Journal, 2016. **53**(7): p. 1156-1166.
102. Bowness, D., et al., *Monitoring the dynamic displacements of railway track.* Proceedings of the Institution of Mechanical Engineers, Part F: Journal of Rail and Rapid Transit, 2007. **221**(1): p. 13-22.
103. Milne, D., et al., *Proving MEMS technologies for smarter railway infrastructure.* Procedia engineering, 2016. **143**: p. 1077-1084.
104. Priest, J. and W. Powrie, *Determination of dynamic track modulus from measurement of track velocity during train passage.* Journal of geotechnical geoenvironmental engineering, 2009. **135**(11): p. 1732-1740.
105. Cho, J. and P. Eng, *Development of an Accelerometer Based Wheel-Flat Detection System for a Subway Transit System in Toronto*, in *AREMA Annual Conference 2013*. 2013: Indianapolis, IN, USA.
106. Entezami, M., et al., *Perspectives on railway axle bearing condition monitoring.* Proceedings of the Institution of Mechanical Engineers, Part F: Journal of Rail and Rapid Transit, 2020. **234**(1): p. 17-31.
107. Wei, C., et al., *Real-time train wheel condition monitoring by fiber Bragg grating sensors.* International Journal of Distributed Sensor Networks, 2011. **8**(1): p. 409048.
108. Ni, Y.-Q. and Q.-H. Zhang. *A Bayesian Machine Learning Approach for Online Wheel Condition Detection Using Track-side Monitoring*. in *2018 International Conference on Intelligent Rail Transportation (ICIRT)*. 2018. IEEE.

109. Amini, A., et al., *Wayside detection of faults in railway axle bearings using time spectral kurtosis analysis on high-frequency acoustic emission signals.* Advances in Mechanical Engineering, 2016. **8**(11): p. 1687814016676000.
110. Mosleh, A., et al., *10 - Approaches for weigh-in-motion and wheel defect detection of railway vehicles*, in *Rail Infrastructure Resilience*, R. Calçada and S. Kaewunruen, Editors. 2022, Woodhead Publishing. p. 183-207.
111. Mosleh, A., et al., *An approach for wheel flat detection of railway train wheels using envelope spectrum analysis.* Structure and Infrastructure Engineering, 2021. **17**(12): p. 1710-1729.
112. Soleimanmeigouni, I., et al., *Investigation of the effect of the inspection intervals on the track geometry condition.* Structure and Infrastructure Engineering, 2020. **16**(8): p. 1138-1146.
113. Solomon, B., *Railway Maintenance Equipment: The Men and Machines That Keep the Railroads Running*. 2001: MBI Publishing Company.
114. Hronik, R.H., B.D. Smith, and J. Wallen Jr, *Apparatus for high-speed measurement of track geometry*. 1970, Google Patents.
115. Network Rail. *New Measurement Train (NMT) - Network Rail*. 2020 [cited 2021 February]; Available from: https://www.networkrail.co.uk/running-the-railway/looking-after-the-railway/our-fleet-machines-and-vehicles/new-measurement-train-nmt/.
116. Bokhman, E., et al. *Optical-inertial system for railway track diagnostics*. in *2014 DGON Inertial Sensors and Systems (ISS)*. 2014. IEEE.
117. Puckette IV, C.M., et al., *Apparatus and method for rail track inspection*. 2003, Google Patents.
118. Trosino, M., J.J. Cunningham, and A.E. Shaw III, *Automated track inspection vehicle and method*. 2000, Google Patents.
119. British Standards Institution, *BS EN 61373:2010: Railway applications. Rolling stock equipment. Shock and vibration tests*. 2010, British Standards Institution.
120. Kabir, S., *Assessment and monitoring for railway tracks reliability and safety using nondestructive testing measurement systems.* International Journal of Railway Research, 2015. **2**(1): p. 24-32.
121. Muñoz, J.C., F.G. Márquez, and M. Papaelias, *Railroad inspection based on ACFM employing a non-uniform B-spline approach.* Mechanical Systems Signal Processing, 2013. **40**(2): p. 605-617.
122. Weston, P., et al., *Monitoring lateral track irregularity from in-service railway vehicles.* Proceedings of the Institution of Mechanical Engineers, Part F: Journal of Rail and Rapid Transit, 2007. **221**(1): p. 89-100.
123. Weston, P., et al., *Monitoring vertical track irregularity from in-service railway vehicles.* Proceedings of the institution of mechanical engineers, Part F: Journal of Rail and Rapid Transit, 2007. **221**(1): p. 75-88.
124. Abuhamdia, T., et al. *Rail defect detection using data from tri-axial accelerometers*. in *ASME/IEEE Joint Rail Conference*. 2014. American Society of Mechanical Engineers.
125. Barbosa, R.S., *New method for railway track quality identification through the safety dynamic performance of instrumented railway vehicle.* Journal of the Brazilian Society of Mechanical Sciences Engineering Applications of Artificial Intelligence, 2016. **38**(8): p. 2265-2275.
126. Entezami, M., et al. *Continuous railway track monitoring using passenger trains*. in *World Congress on Railway Research*. 2019. Tokyo, Japan.

127. Yeo, G., P. Weston, and C. Roberts, *Detection of vertical track faults using an instrumented in-service vehicle: Considering efficient real-time fault detection*, in *IMechE Stephenson conference*. 2015. p. 1-9.
128. Heirich, O., et al. *Measurement and analysis of train motion and railway track characteristics with inertial sensors*. in *2011 14th international IEEE conference on intelligent transportation systems (ITSC)*. 2011. IEEE.
129. Cantero, D. and B. Basu, *Railway infrastructure damage detection using wavelet transformed acceleration response of traversing vehicle.* Structural Control and Health Monitoring, 2015. **22**(1): p. 62-70.
130. Balouchi, F., A. Bevan, and R. Formston. *Detecting railway under-track voids using multi-train in-service vehicle accelerometer*. in *7th IET Conference on Railway Condition Monitoring 2016 (RCM 2016)*. 2016. IET.
131. Bocciolone, M., et al., *A measurement system for quick rail inspection and effective track maintenance strategy.* Mechanical Systems and Signal Processing, 2007. **21**(3): p. 1242-1254.
132. Bezin, Y., et al., *An investigation of sleeper voids using a flexible track model integrated with railway multi-body dynamics.* Proceedings of the Institution of Mechanical Engineers, Part F: Journal of Rail and Rapid Transit, 2009. **223**(6): p. 597-607.
133. De Rosa, A., S. Alfi, and S. Bruni, *Estimation of lateral and cross alignment in a railway track based on vehicle dynamics measurements.* Mechanical Systems and Signal Processing, 2019. **116**: p. 606-623.
134. Sysyn, M., et al., *Common crossing condition monitoring with on-board inertial measurements.* 2019. **59**(4): p. 423-434.
135. Yeo, G.J., *Monitoring railway track condition using inertial sensors on an in-service vehicle*. 2017, University of Birmingham.
136. Xiao, X., W. Shen, and X.J.J.o.E.M. He, *Track irregularity monitoring on high-speed railway viaducts: A novel algorithm with unknown input condensation.* 2021. **147**(6): p. 04021029.
137. Malekjafarian, A., P.J. McGetrick, and E.J. Obrien, *A Review of Indirect Bridge Monitoring Using Passing Vehicles.* Shock and Vibration, 2015. **2015**: p. 286139.
138. Micu, E.A., et al., *Bridge damage and repair detection using an instrumented train.* Journal of Bridge Engineering, 2022. **27**(3): p. 05021018.
139. Tsunashima, H., et al., *Condition monitoring of railway track using in-service vehicle.* Reliability safety in railway, 2012. **12**: p. 334-356.
140. Chudzikiewicz, A., et al., *Condition monitoring of railway track systems by using acceleration signals on wheelset axle-boxes.* 2018. **33**(2): p. 555–566-555–566.
141. Paixão, A., E. Fortunato, and R. Calçada, *Smartphone's Sensing Capabilities for On-Board Railway Track Monitoring: Structural Performance and Geometrical Degradation Assessment.* Advances in Civil Engineering, 2019. **2019**: p. 1729153.
142. Amini, A., *Online condition monitoring of railway wheelsets*. 2016, University of Birmingham.
143. Amini, A., et al., *Evaluation of the effect of speed and defect size on high-frequency acoustic emission and vibration condition monitoring of railway axle bearings.* Insight-Non-Destructive Testing Condition Monitoring, 2017. **59**(4): p. 184-188.
144. Amini, A., M. Entezami, and M. Papaelias, *Onboard detection of railway axle bearing defects using envelope analysis of high frequency acoustic emission signals.* Case Studies in Nondestructive Testing Evaluation, 2016. **6**: p. 8-16.

145. Bernal, E., M. Spiryagin, and C. Cole, *Onboard Condition Monitoring Sensors, Systems and Techniques for Freight Railway Vehicles: A Review.* IEEE Sensors Journal, 2019. **19**(1): p. 4-24.
146. Ji, H. and D. Zhou, *Incipient fault detection of the high-speed train air brake system with a combined index.* Control Engineering Practice, 2020. **100**: p. 104425.
147. Zhou, D., et al., *Fault Detection and Isolation of the Brake Cylinder System for Electric Multiple Units.* IEEE Transactions on Control Systems Technology, 2018. **26**(5): p. 1744-1757.
148. Feng, D., et al., *Reliability Evaluation for Traction Power Supply System of High-Speed Railway Considering Relay Protection.* IEEE Transactions on Transportation Electrification, 2019. **5**(1): p. 285-298.
149. Garramiola, F., et al., *A Review in Fault Diagnosis and Health Assessment for Railway Traction Drives.* Applied Sciences, 2018. **8**(12).
150. Strano, S. and M. Terzo, *Review on model-based methods for on-board condition monitoring in railway vehicle dynamics.* Advances in Mechanical Engineering, 2019. **11**(2): p. 1687814019826795.
151. Bruni, S., et al., *Control and monitoring for railway vehicle dynamics.* Vehicle System Dynamics, 2007. **45**(7-8): p. 743-779.
152. Shafiullah, G.M., et al., *Predicting Vertical Acceleration of Railway Wagons Using Regression Algorithms.* IEEE Transactions on Intelligent Transportation Systems, 2010. **11**(2): p. 290-299.
153. Kalman, R.E., *A new approach to linear filtering and prediction problems.* Journal of basic Engineering, 1960. **82**(1): p. 35-45.
154. Saab, S.S., *A map matching approach for train positioning. I. Development and analysis.* IEEE Transactions on Vehicular Technology, 2000. **49**(2): p. 467-475.
155. Saab, S.S., *A map matching approach for train positioning. II. Application and experimentation.* IEEE Transactions on Vehicular Technology, 2000. **49**(2): p. 476-484.
156. Malvezzi, M., et al., *A localization algorithm for railway vehicles based on sensor fusion between tachometers and inertial measurement units.* Proceedings of the Institution of Mechanical Engineers, Part F: Journal of Rail Rapid Transit, 2014. **228**(4): p. 431-448.
157. Allotta, B., et al. *A localization algorithm for railway vehicles*. in *2015 IEEE International Instrumentation and Measurement Technology Conference (I2MTC) Proceedings*. 2015. IEEE.
158. Malvezzi, M., B. Allotta, and M. Rinchi, *Odometric estimation for automatic train protection and control systems.* Vehicle system dynamics, 2011. **49**(5): p. 723-739.
159. Mirabadi, A., N. Mort, and F. Schmid. *Application of sensor fusion to railway systems*. in *1996 IEEE/SICE/RSJ International Conference on Multisensor Fusion and Integration for Intelligent Systems (Cat. No. 96TH8242)*. 1996. IEEE.
160. Jiao, Y., et al. *Research on Maglev Train Positioning System Based on Multi-Information Fusion*. in *2018 2nd IEEE Advanced Information Management, Communicates, Electronic and Automation Control Conference (IMCEC)*. 2018. IEEE.
161. Crespillo, O.G., O. Heirich, and A. Lehner. *Bayesian GNSS/IMU tight integration for precise railway navigation on track map*. in *2014 IEEE/ION Position, Location and Navigation Symposium-PLANS 2014*. 2014. IEEE.
162. Li, D., X. Jia, and J. Zhao, *A Novel Hybrid Fusion Algorithm for Low-Cost GPS/INS Integrated Navigation System During GPS Outages.* IEEE Access, 2020. **8**: p. 53984-53996.

163. Cai, B. and X. Wang, *Train positioning via integration and fusion of GPS and inertial sensors*. WIT Transactions on the Built Environment, 2000. **50**.
164. Jiang, W., et al., *A Multi-Sensor Positioning Method-Based Train Localization System for Low Density Line*. IEEE Transactions on Vehicular Technology, 2018. **67**(11): p. 10425-10437.
165. Goya, J., et al., *Advanced Train Location Simulator (ATLAS) for developing, testing and validating on-board railway location systems.* European Transport Research Review, 2015. **7**(3): p. 24.
166. Heirich, O., P. Robertson, and T. Strang. *RailSLAM-Localization of rail vehicles and mapping of geometric railway tracks*. in *2013 IEEE International Conference on Robotics and Automation*. 2013. IEEE.
167. Mei, T. and H. Li, *Measurement of vehicle ground speed using bogie-based inertial sensors*. Proceedings of the Institution of Mechanical Engineers, Part F: Journal of Rail and Rapid Transit, 2008. **222**(2): p. 107-116.
168. Carnevale, M., I. La Paglia, and P. Pennacchi, *An algorithm for precise localization of measurements in rolling stock-based diagnostic systems.* Proceedings of the Institution of Mechanical Engineers, Part F: Journal of Rail and Rapid Transit, 2021. **235**(7): p. 827-839.
169. Zhou, Y., et al., *Onboard Train Localization Based on Railway Track Irregularity Matching.* IEEE Transactions on Instrumentation and Measurement, 2022. **71**: p. 1-13.
170. Marinoni, M., et al., *A Novel Approach for Reducing Train Localization Errors by Inertial Measurements.* IEEE Access, 2023. **11**: p. 5281-5295.
171. Li, C.-T. and W.-C. Siu. *Fast Monocular Vision-based Railway Localization for Situations with Varying Speeds*. in *2018 Asia-Pacific Signal and Information Processing Association Annual Summit and Conference (APSIPA ASC)*. 2018. IEEE.
172. Mockel, S., F. Scherer, and P.F. Schuster. *Multi-sensor obstacle detection on railway tracks*. in *IEEE IV2003 Intelligent Vehicles Symposium. Proceedings (Cat. No. 03TH8683)*. 2003. IEEE.
173. Stein, D., et al., *Rail detection using LIDAR sensors.* International Journal of Sustainable Development Planning, 2016. **11**(1): p. 65-78.
174. Yufeng, L., C. Tefang, and C. Shu. *Processing and Fusion of Velocity and Position Signal of Medium and High Speed Maglev Train*. in *2018 13th World Congress on Intelligent Control and Automation (WCICA)*. 2018. IEEE.
175. Li, C., et al., *An overview: modern techniques for railway vehicle on-board health monitoring systems.* Vehicle System Dynamics, 2017. **55**(7): p. 1045-1070.
176. Tsunashima, H. and H. Mori. *Condition monitoring of railway vehicle suspension using adaptive multiple model approach*. in *ICCAS 2010*. 2010. IEEE.
177. Palese, J.W., A.M. Zarembski, and N.O. Attoh-Okine, *Methods for aligning near-continuous railway track inspection data.* Proceedings of the Institution of Mechanical Engineers, Part F: Journal of Rail and Rapid Transit, 2020. **234**(7): p. 709-721.
178. Khosravi, M., et al., *Reducing the positional errors of railway track geometry measurements using alignment methods: A comparative case study.* Measurement, 2021. **178**: p. 109383.
179. Khosravi, M., et al., *Modification of correlation optimized warping method for position alignment of condition measurements of linear assets.* Measurement, 2022. **201**: p. 111707.

180. Eklöf, K., A. Nwichi-Holdsworth, and J. Eklöf, *Novel algorithm for mutual alignment of railway track geometry measurements.* Transportation Research Record, 2021. **2675**(12): p. 995-1004.
181. Peinado Gonzalo, A., et al., *Railway track location estimation using onboard inertial sensors.* Vehicle System Dynamics, 2021: p. 1-19.
182. Network Rail, *Channel Tunnel Rail Link - Schematic layout alignment*. 2018. p. 1.
183. British Standards Institution, *BS EN 14363:2016: Railway Applications: - Testing and Simulation for the acceptance of running characteristics of railway vehicles — Running Behaviour and stationary tests*. 2016, United Kingdom.
184. Vilhelmsson, R., *Vibration analysis for speed estimation of wheeled indoor vehicles*, in *Department of Electrical Engineering, Automatic Control*. 2017, Linköping University.
185. Wang, Z., et al., *Effect of vehicle vibration environment of high-speed train on dynamic performance of axle box bearing.* Vehicle System Dynamics, 2019. **57**(4): p. 543-563.
186. Sañudo, R., et al. *Sleepers Spacing Analysis in Railway Track Infrastructure*. Infrastructures, 2022. **7**, DOI: 10.3390/infrastructures7060083.
187. Faragher, R., *Understanding the Basis of the Kalman Filter Via a Simple and Intuitive Derivation [Lecture Notes]*. IEEE Signal Processing Magazine, 2012. **29**(5): p. 128-132.
188. Blanco-Lorenzo, J., et al., *Dynamic comparison of different types of slab track and ballasted track using a flexible track model.* Proceedings of the Institution of Mechanical Engineers, Part F: Journal of Rail and Rapid Transit, 2011. **225**(6): p. 574-592.
189. Grossoni, I., et al., *The role of track stiffness and its spatial variability on long-term track quality deterioration.* Proceedings of the Institution of Mechanical Engineers, Part F: Journal of Rail and Rapid Transit, 2019. **233**(1): p. 16-32.
190. Network Rail. *Rough Ride | Safety Central* 2023 [cited 2023 January]; Available from: https://safety.networkrail.co.uk/jargon-buster/rough-ride/.

Appendix A. Comfort indices

This annex explains the basis of comfort according to the standards ISO 2631 [70, 71] and EN 12299 [11]. According to ISO 2631 [70, 71], "In railways, comfort is understood as a compound of sensations (noise, vibrations, temperature, humidity, seating quality) perceived by passengers that affect the experience of travel". This standard is the basis for EN 12299 [11], and both are applied to evaluate the effects of comfort based on vibrations on railway passengers. Both methods propose thresholding levels to evaluate ride comfort but, as this is heavily influenced by the passenger perception and expectations, these values are only indicative and serve more as a qualitative than a quantitative indication of comfort. This appendix explains the ISO 2631 and EN 12299 standards, as they are the most extended in research.

Both ISO 2631 and EN 12299 use cab acceleration to extract information, applying different frequency weighting functions depending on the application. The frequency weighting functions applied are named W_d for the horizontal vibration along the x and y-axis on the floor, and W_b for the vertical vibrations along the z-axis, whose parameters are defined in the standards. These functions are based on the resonances of the human body while standing or seated on a passenger train. Both are presented in Figure A.1. There are other weighting functions defined for other applications and positions, such as health, perception and motion sickness, applied on the seat or when the passenger is not standing. These are not presented here as the cab sensors are only installed on the floor. It is necessary to mention that the standard EN 12299 only defines the weighting functions between 0.1 to 100 Hz, whilst ISO 2631

comprises 0.01 to 400 Hz. As discussed in the following chapters, this is because most of the cab vibrations are in the low-frequency range.

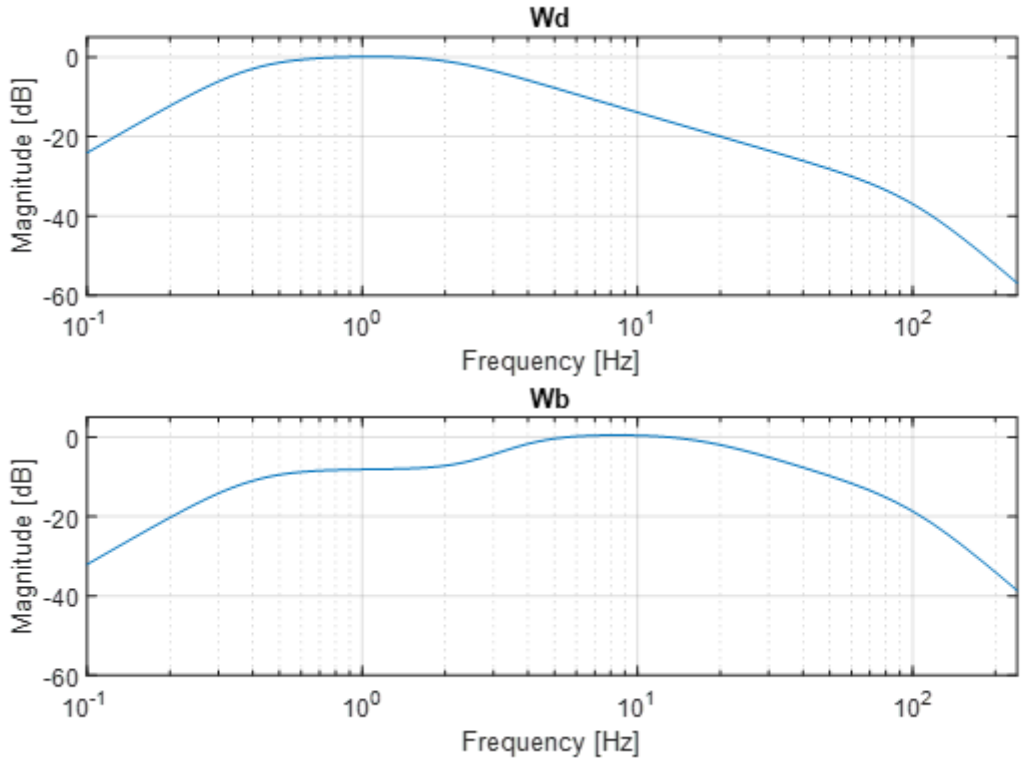


FIGURE A.1. FREQUENCY WEIGHTING CURVES FOR VEHICLE VIBRATIONS [11].

Both ISO 2631 and EN 12299 apply frequency weighting functions to acceleration and the Root Mean Square (RMS) to the result, as expressed in Equation (A.1).

$$a_W(t) = \left[\frac{1}{T}\int_{t-T}^{t} a_W^2(\tau)d\tau\right]^{\frac{1}{2}} \ [m/s^2] \tag{A.1}$$

Where $a_W(t)$ is the RMS of the frequency-weighted acceleration, T and t are time magnitudes being respectively 5 s and a multiple of 5 s for comfort, and $a_W(\tau)$ is the frequency-weighted acceleration. ISO 2631 directly uses weighted acceleration as a guide for comfort, providing Table A.1. as a reference.

TABLE A.1. COMFORT PERCEPTION REFERENCE FOR ISO 2631-1 [70].

$a_W(t) \leq 0.315\ m/s^2$	Not uncomfortable
$0.315\ m/s^2 \leq a_W(t) \leq 0.63\ m/s^2$	A little uncomfortable
$0.5\ m/s^2 \leq a_W(t) \leq 1\ m/s^2$	Fairly uncomfortable
$0.8\ m/s^2 \leq a_W(t) \leq 1.6\ m/s^2$	Uncomfortable
$1.25\ m/s^2 \leq a_W(t) \leq 2.5\ m/s^2$	Very uncomfortable
$2\ m/s^2 \leq a_W(t)$	Extremely uncomfortable

BS 12299 uses RMS acceleration extending it to all three Cartesian axes and renaming them as continuous comfort indices. Comfort evaluation is separated into three types: continuous, mean and event-based; the latter one is subdivided into comfort in discrete events and comfort in curve transitions. Continuous comfort is evaluated as a continuous measurement of acceleration in all cartesian axes averaged using a 5-second RMS filter. This acceleration is measured on the cab floor or the seat depending on the mean comfort method to be applied afterwards (standard or complete). The indices applied for continuous comfort are C_{Cx} for the longitudinal axis, C_{Cy} for the lateral axis, and C_{Cz} for the vertical axis, and are expressed in equations (A.2), (A.3), and (A.4) respectively.

$$C_{Cx} = a_W^X = \left[\frac{1}{T} \cdot \int_{t-T}^{t} a_X^2(\tau) d\tau\right]^{1/2} \quad [m/s^2] \tag{A.2}$$

$$C_{Cy} = a_W^Y = \left[\frac{1}{T} \cdot \int_{t-T}^{t} a_Y^2(\tau) d\tau\right]^{1/2} \quad [m/s^2] \tag{A.3}$$

$$C_{Cz} = a_W^Z = \left[\frac{1}{T} \cdot \int_{t-T}^{t} a_Z^2(\tau) d\tau\right]^{1/2} \quad [m/s^2] \tag{A.4}$$

The nomenclature is the same as for Equation 1 The reference for comfort according to EN 12299 is presented in Table A.2, defined only for C_{Cy} and C_{Cz}.

TABLE A.2. COMFORT PERCEPTION REFERENCE FOR EN 12299 [11].

$C_{Cy}(t)\ ,\ C_{Cz}(t) < 0.20\ m/s^2$	Very comfortable
$0.20\ m/s^2 \leq C_{Cy}(t)\ ,\ C_{Cz}(t) < 0.30\ m/s^2$	Comfortable
$0.30\ m/s^2 \leq C_{Cy}(t)\ ,\ C_{Cz}(t) < 0.40\ m/s^2$	Medium
$0.40\ m/s^2 \leq C_{Cy}(t)\ ,\ C_{Cz}(t)$	Uncomfortable

EN 12299 also provides two methods to evaluate comfort over longer periods, multiples of 5 minutes, by averaging the continuous comfort indices. The standard proposes two methods to evaluate it, defined as standard and complete. The standard method considers only acceleration measured on the vehicle floor (defined in Equation (A.5)), whilst the complete method considers both measurements on the vehicle seat (Equation (A.6)) and on the floor (Equation (A.7)). The measuring method considers the 95th or 50th percentile of RMS acceleration data and then averages them to obtain a mean estimation of comfort for each 5-minute period. The equations used for the methods are:

$$N_{MV} = 6 \cdot \sqrt{(a_{X95}^F)^2 + (a_{Y95}^F)^2 + (a_{Z95}^F)^2} \tag{A.5}$$

$$N_{VA} = 4 \cdot (a_{Z95}^F) + 2 \cdot \sqrt{(a_{Y95}^S)^2 + (a_{Z95}^S)^2} + 4 \cdot (a_{Y95}^S) \tag{A.6}$$

$$N_{VD} = 3 \cdot \sqrt{16 \cdot (a_{X50}^F)^2 + 4 \cdot (a_{Y50}^F)^2 + (a_{Z50}^F)^2} + 5 \cdot (a_{Y95}^F) \tag{A.7}$$

Where N_{MV} is the standard method, N_{VA} is the complete method for seated passengers, and N_{VD} is the complete method for standing passengers. The superscript corresponds to data measured on the seat (S) or the floor (F) and the subscript corresponds to the axis direction in which data has been measured (X, Y or Z) and the percentile considered (95 or 50). The reference scale for mean comfort is presented in Table A.3.

TABLE A.3. REFERENCE FOR THE MEAN COMFORT INDICES [11].

$N_{MV} < 1.5$	Very comfortable
$1.5 \leq N_{MV} < 2.5$	Comfortable
$2.5 \leq N_{MV} < 3.5$	Medium
$3.5 \leq N_{MV} < 4.5$	Uncomfortable
$4.5 \leq N_{MV}$	Very uncomfortable

As stated previously, event-based comfort is divided into discrete events and curve transitions. The standard understands comfort on discrete events (P_{DE}, as defined in Equation (A.8)) as the sudden change of the feeling of ride comfort due to local track irregularities, and comfort on curve transitions (P_{CT}, as defined in Equation (A.9)) as the sudden change of the feeling of ride comfort due to vehicle behaviour on interactions with compound curves. In this case, the indices are defined as the percentage of passengers dissatisfied with comfort on the discrete event or curve transition. The formulas to define them are the following:

$$P_{CT} = 100 \cdot \max[(A \cdot |\ddot{y}_{1s}|_{\max} + B \cdot |\ddot{y}_{1s}|_{\max} - C); 0] + 100 \cdot (D \cdot |\dot{\varphi}_{1s}|_{\max})^{E} \quad \text{(A.8)}$$

$$P_{DE}(t) = 100 \cdot \max\left[a \cdot \ddot{y}_{pp}(t) + b \cdot \ddot{y}_{2s}(t) - c; 0\right] \quad \text{(A.9)}$$

Where A, B, C, D, E, a, b and c are constants defined in the norm, y is the displacement measured in the lateral direction on the vehicle floor, φ is the body yaw rate measured on the vehicle floor, and the subscripts $1\ s, 2\ s$ and pp correspond to the 1 and 2-second average and peak to peak measurement in one second, respectively. There is no scale to use as a reference for these two indices. It is also worth mentioning that the formulas to obtain comfort for seated and standing passengers are the same, changing only the values of the constants.

The standard ISO 2631 also covers passenger perception, health and motion sickness derived from vibration. Passenger vibration perception is considered as a threshold value of 0.015 m/s^2, whilst both health and vibration indices are determined through a dose value.

Passenger health is determined by the weighted acceleration over time and limited as in Figure A.2, where the regular and dashed lines represent different criteria for health risk based on vibration.

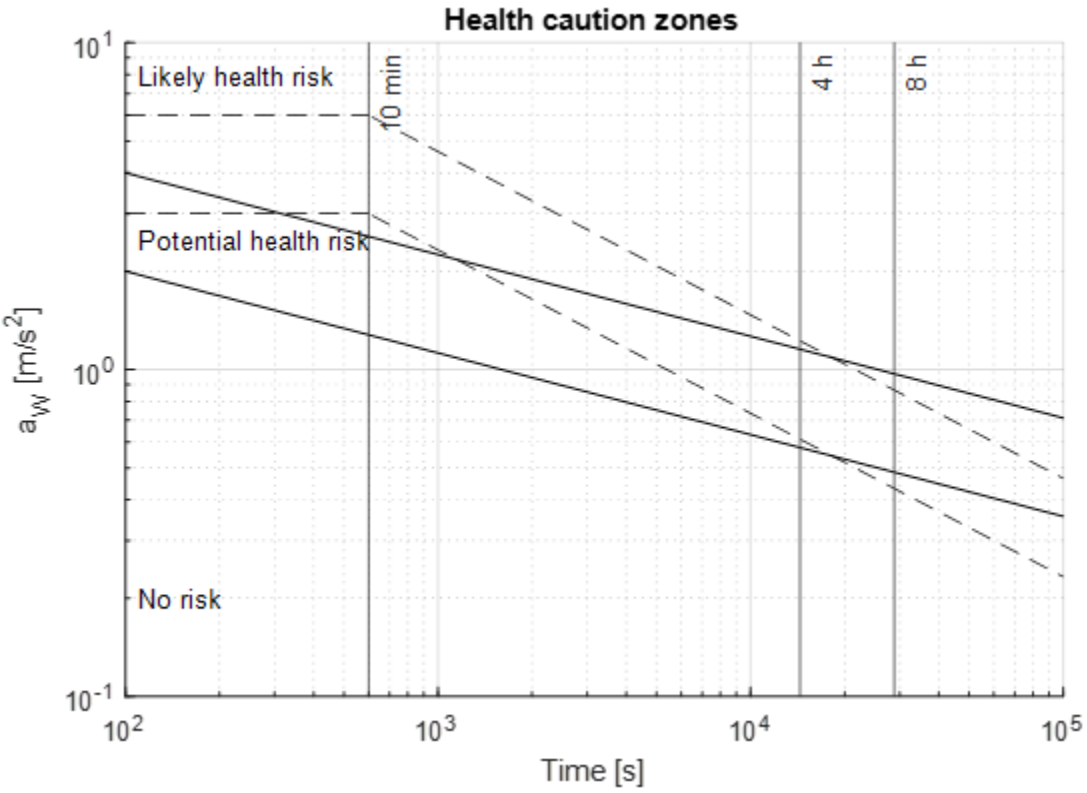


FIGURE A.2. HEALTH GUIDANCE CAUTION ZONES [70].

Motion sickness is also defined based on the dose value over the whole journey, with the index representing the total amount of people who may vomit. The ISO 2631 standard explains that this index is primarily applied for ships and that the prevalence of symptoms is likely to vary between individuals and due to adaptation.

Appendix B. Kalman filter

This annex explains the basis of the Kalman filter [153, 187]. The Kalman filter is a data fusion algorithm based on the application of mean and covariance of statistical distributions. The assumed linear system is given by equations (B.1) and (B.2):

$$x_{k+1} = Ax_k + Bu_k + w_k \tag{B.1}$$

$$z_k = Hx_k + v_k \tag{B.2}$$

where x_k is the true state at time instant k, z_k is the observation at time instant k. The process noise w_k accounts for differences between the model and the true behaviour and v_k accounts for noise in the observations. There is an assumption that state transition matrix A, input gain matrix B and observation matrix H are all time-invariant (constant) in this thesis but this is not necessary. The process noise w_k and observation noise v_k are assumed to be independent (in time) and to have expected values 0 and covariances Q and R, respectively.

The state predictions are made by recursively applying matrix operations to the state vector (vector used for defining the state). The prediction step moves the state estimate to the next time instant without the new observation, then the latest observations are used to update the state estimate and corresponding error covariance.

The Kalman filter is separated into two phases: the *a priori* prediction step and the *a posteriori* observation update step. In the *a priori* prediction, the state of the system is predicted considering its previous value and the known inputs. In the *a posteriori* step, the system observations are used to update the state estimate and its error covariance.

The *a priori* prediction consists of the elements in Equation (B.3):

$$\begin{cases} x_{k+1}^{*} = A \cdot x_k + B \cdot u_k \\ P_{k+1}^{*} = A \cdot P_k \cdot A^T + Q \end{cases} \quad \text{(B.3)}$$

Where:

- x_{k+1}^{*} is the state estimate at time $k+1$, based on the prediction step, but not yet using the latest observations.
- P_{k+1}^{*} is a covariance of the state estimate errors before measurements are used, i.e. *a priori*. P changes because of the state transition matrix A and increases because of uncertainty in the process noise.
- A is the matrix defining the time evolution of the state.
- $B \cdot u_k$ are the control matrix and control (input) vector, respectively, that define the influence of control variables on the system.
- Q is the process noise covariance matrix.

This prediction is corrected by using the system measurements, formulated in Equation (B.4):

$$\begin{cases} \eta_{k+1} = z_{k+1} - H \cdot x_{k+1}^{*} \\ S_{k+1} = H \cdot P_{k+1}^{*} \cdot H^T + R \\ K_{k+1} = P_{k+1}^{*} \cdot H^T \cdot S_{k+1}^{-1} \end{cases} \quad \text{(B.4)}$$

Where:

- η_{k+1} is a vector relating measurements and prediction, named ‘innovation’.
- z_k is the measurement vector. This vector contains the measurements acquired in the system.
- H is a matrix relating state prediction and its units to the innovation factor, named measurement matrix.

- R is the matrix defining the variance of the measurement noise, or measurement noise covariance matrix.
- K is the Kalman gain, which says how much of the innovation to add to the current state estimate.

Once the measurements have been made, the final prediction is corrected by combining them with the prediction before observations are taken into account, as presented in Equation (B.5):

$$\begin{cases} x_{k+1} = x_{k+1}^{*} - K_{k+1} \cdot \eta_{k+1} \\ P_{k+1} = P_{k+1}^{*} - K_{k+1} \cdot H \cdot P_{k+1}^{*} \end{cases} \tag{B.5}$$

The value of $\hat{x}_{k+1}$ is the *a posteriori* estimate of the system state, i.e., after measurements are taken into account. $P_k = E\{(x_k - \hat{x}_k)(x_k - \hat{x}_k)^T\}$ is the covariance of the error between the state estimate and the true state (if the assumptions hold).

Variations of the filter are applied for more complex, non-linear systems, such as the Extended Kalman Filter, which considers nonlinearities in the state evolution equation and the measurements vector.

Appendix C. Results obtained for long-wavelength track feature

This appendix shows the data obtained and not displayed in Chapter 5. The black arrow in the figures indicates the direction of travel, and the grey shading indicates the location of the change in vertical alignment.

C.1. DATA DISPLAYED PER SENSOR

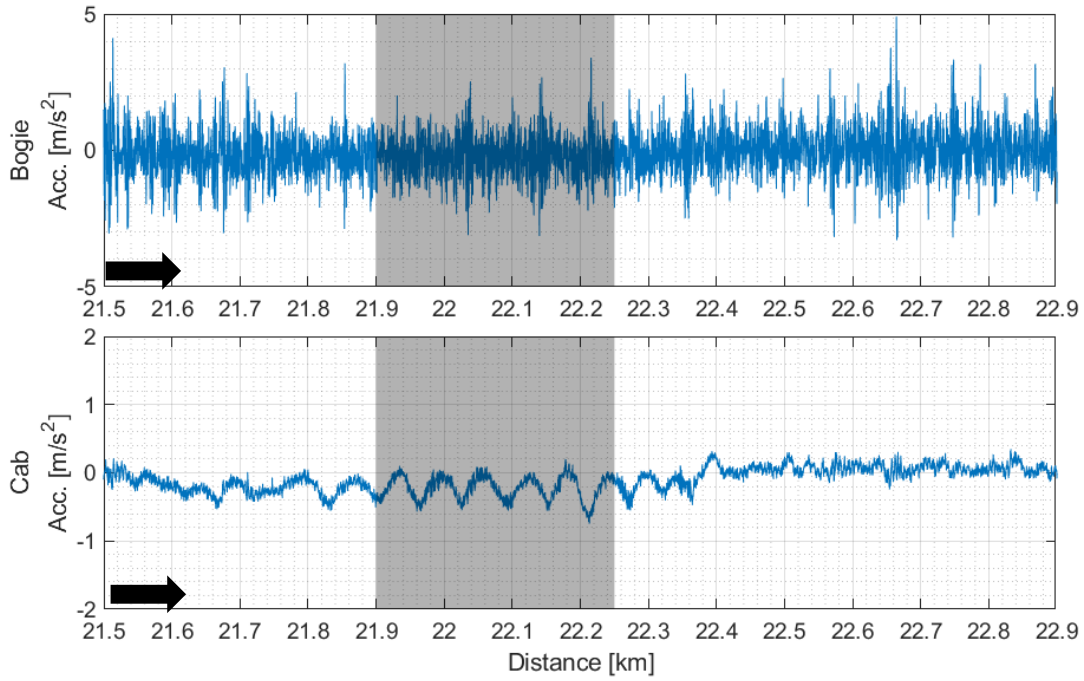


FIGURE C.1. BOGIE AND CAB LATERAL ACCELERATION.

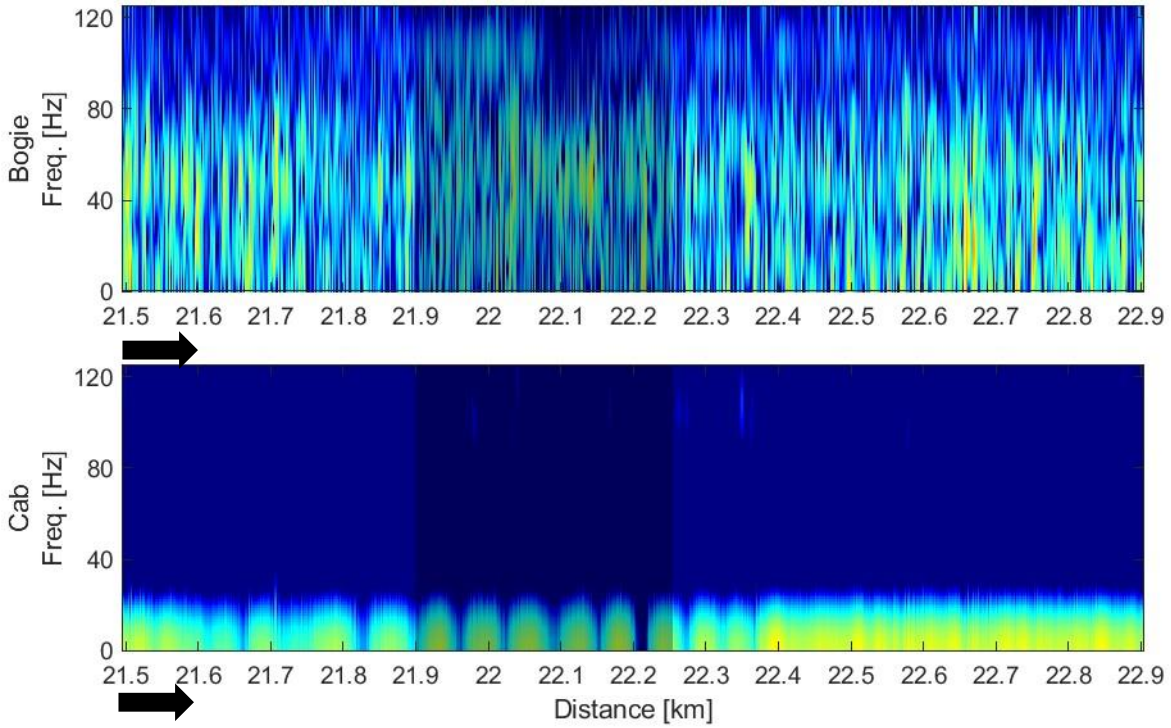


FIGURE C.2. BOGIE AND CAB LATERAL ACCELERATION SPECTROGRAM.

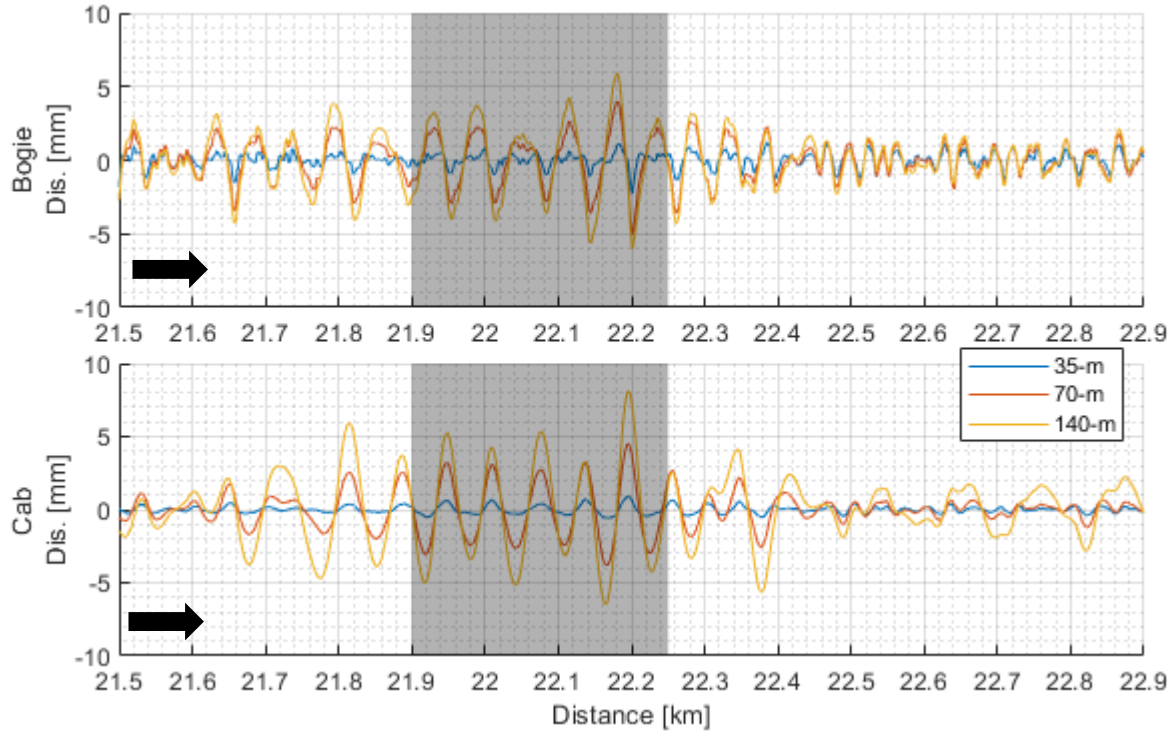


FIGURE C.3. BOGIE AND CAB LATERAL DISPLACEMENT.

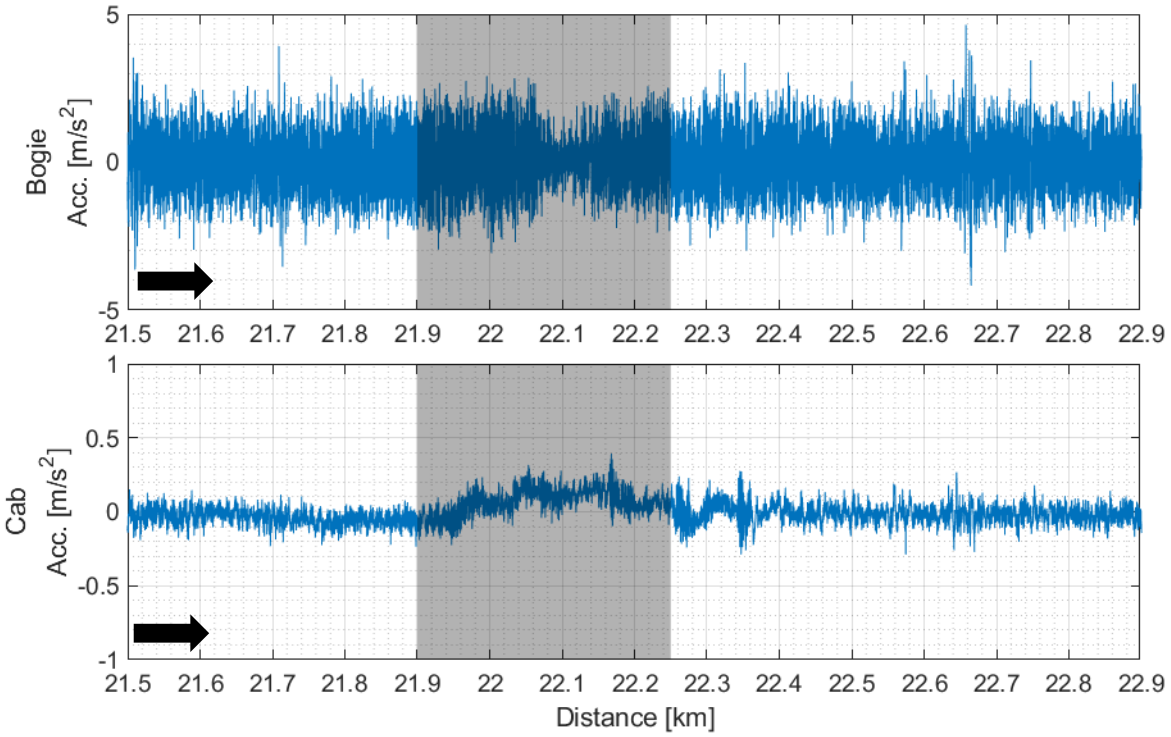


FIGURE C.4. BOGIE AND CAB LONGITUDINAL ACCELERATION.

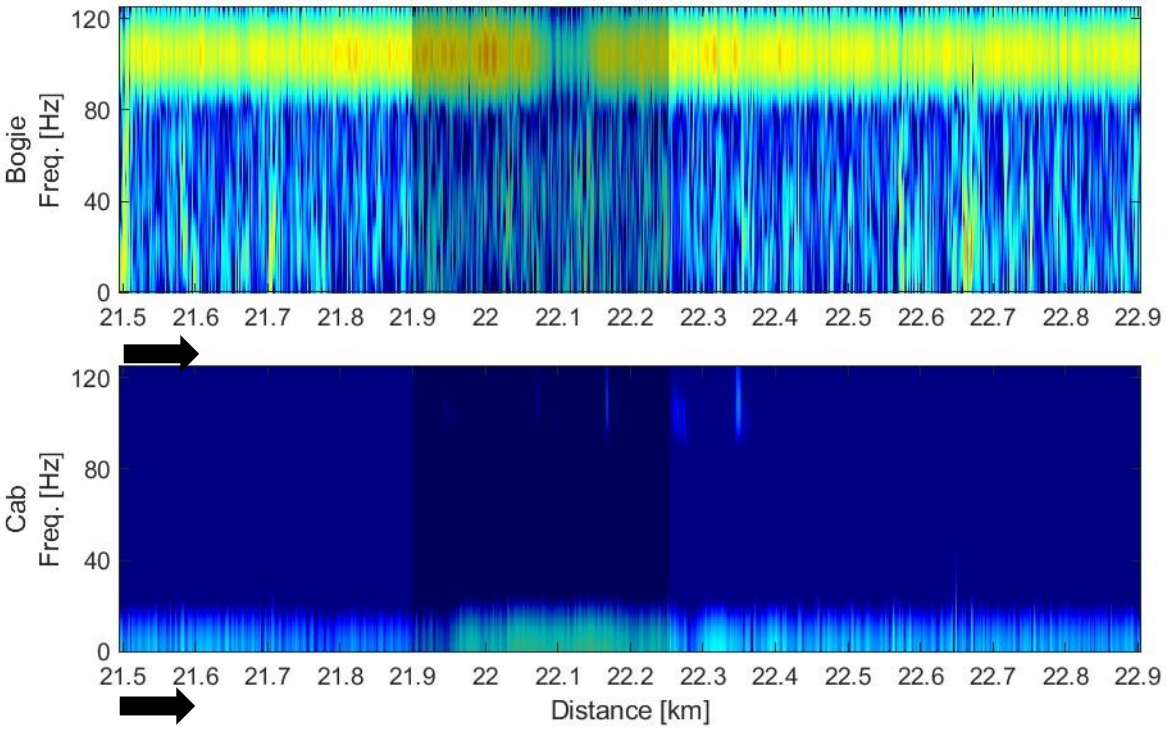


FIGURE C.5. BOGIE AND CAB LONGITUDINAL ACCELERATION SPECTROGRAM.

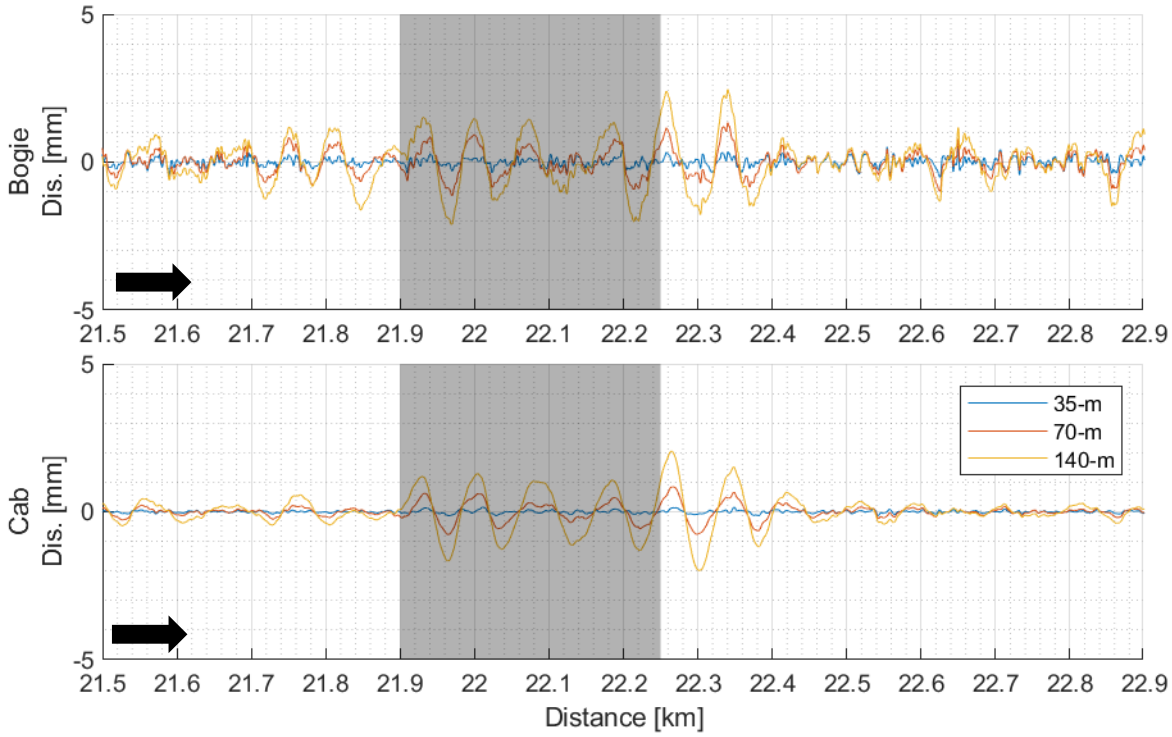


FIGURE C.6. BOGIE AND CAB LONGITUDINAL DISPLACEMENT.

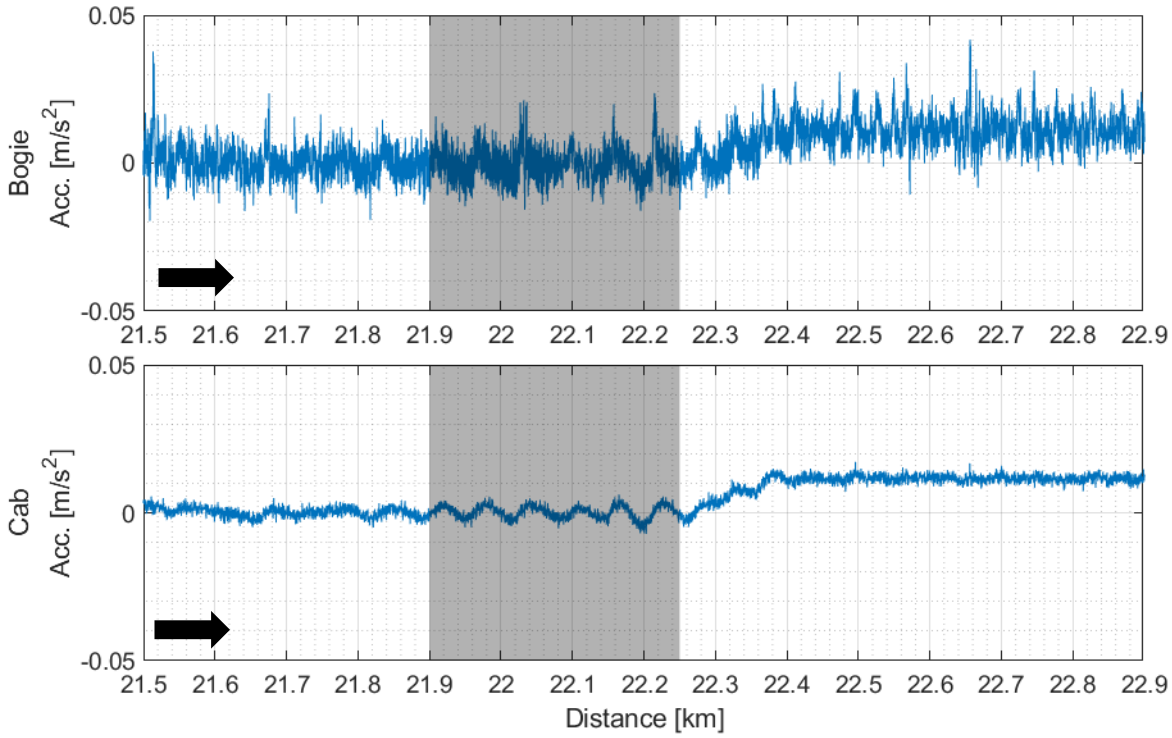


FIGURE C.7. BOGIE AND CAB YAW RATE.

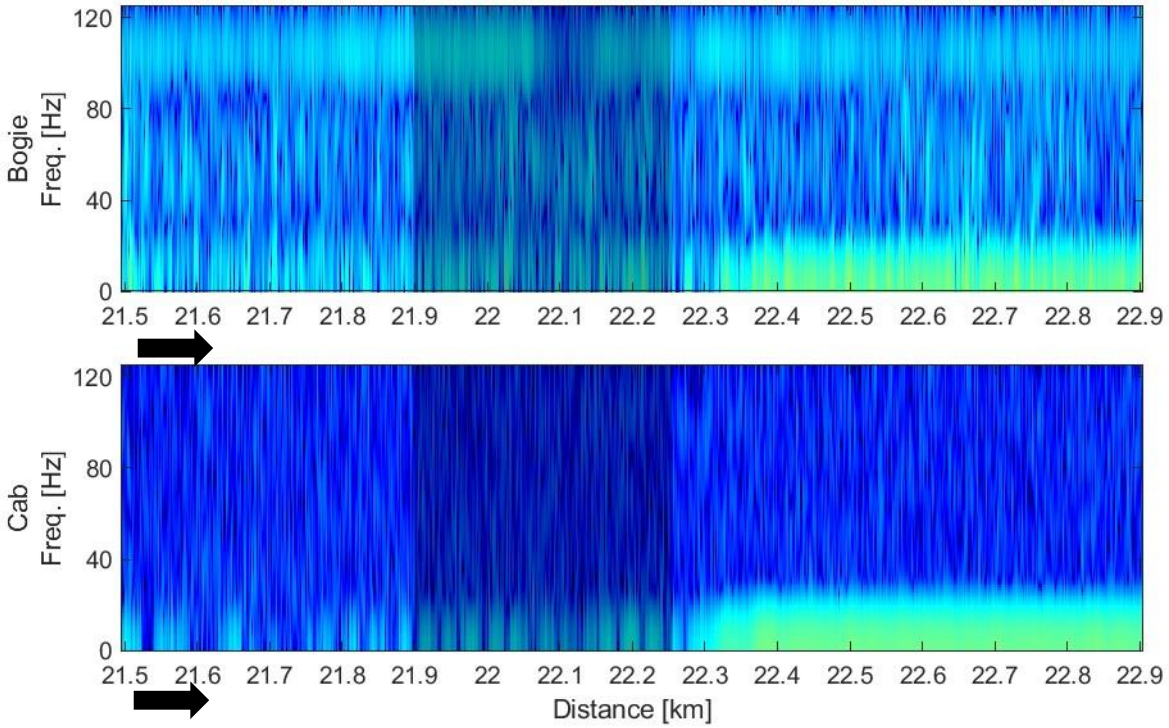


FIGURE C.8. BOGIE AND CAB YAW RATE SPECTROGRAMS.

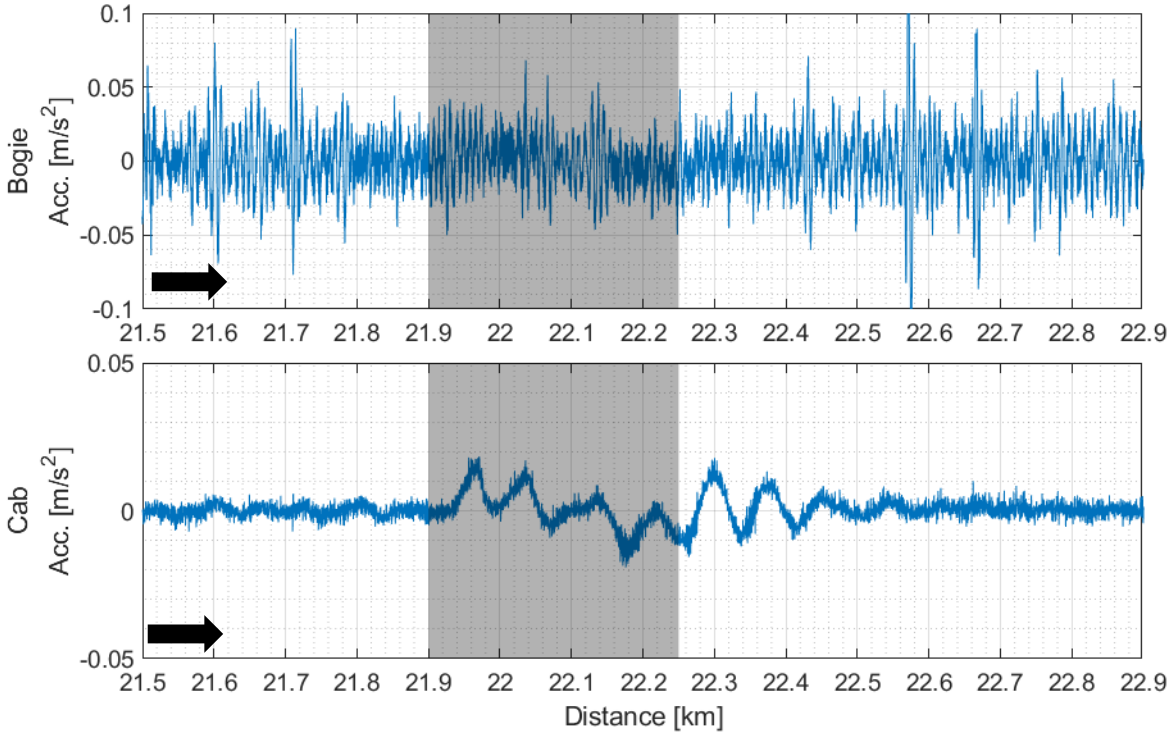


FIGURE C.9. BOGIE AND CAB PITCH RATE.

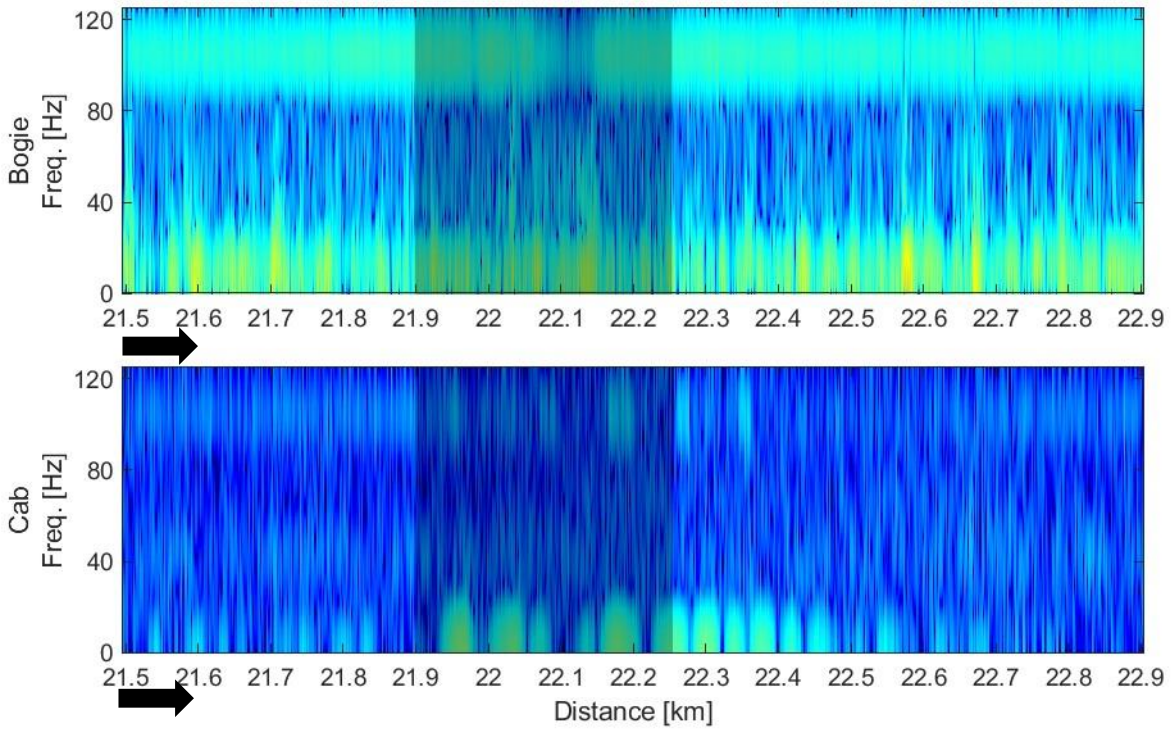


FIGURE C.10. BOGIE AND CAB PITCH RATE SPECTROGRAMS.

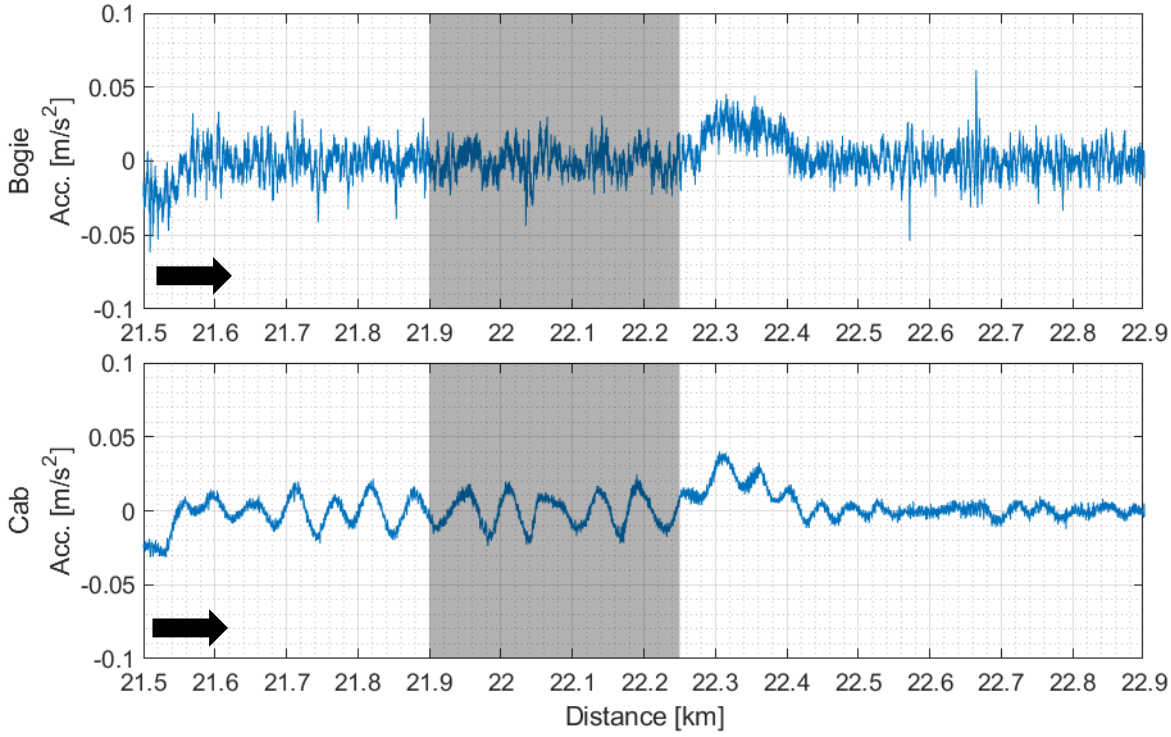


FIGURE C.11. BOGIE AND CAB ROLL RATE.

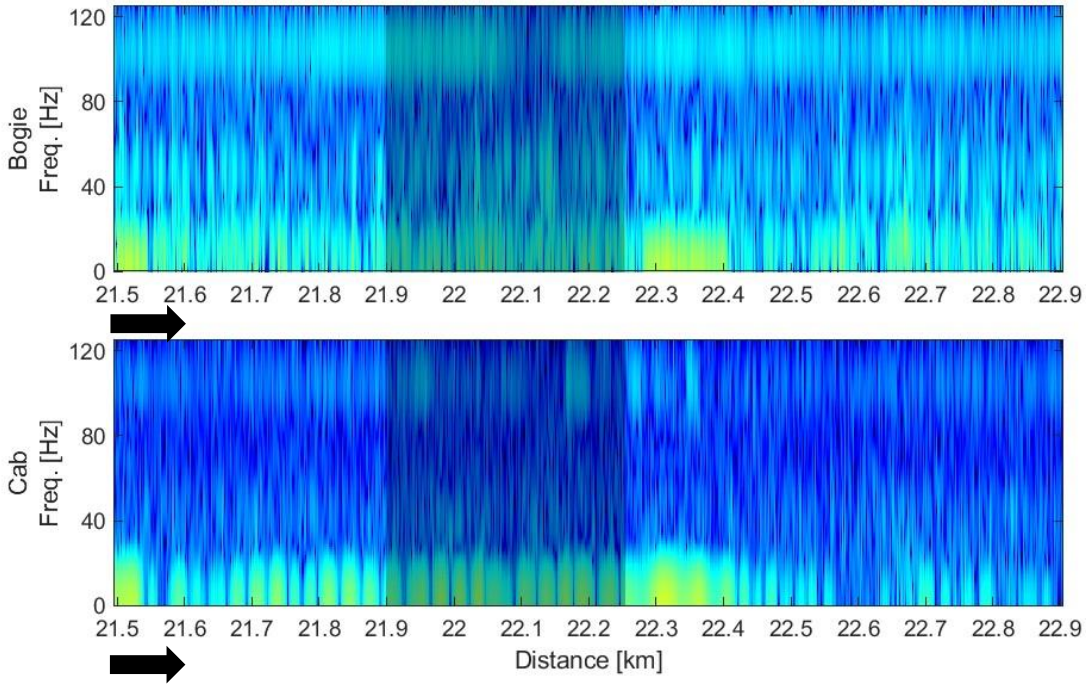


FIGURE C.12. BOGIE AND CAB ROLL RATE SPECTROGRAMS.

C.2. DATA DISPLAYED PER CONFIGURATION

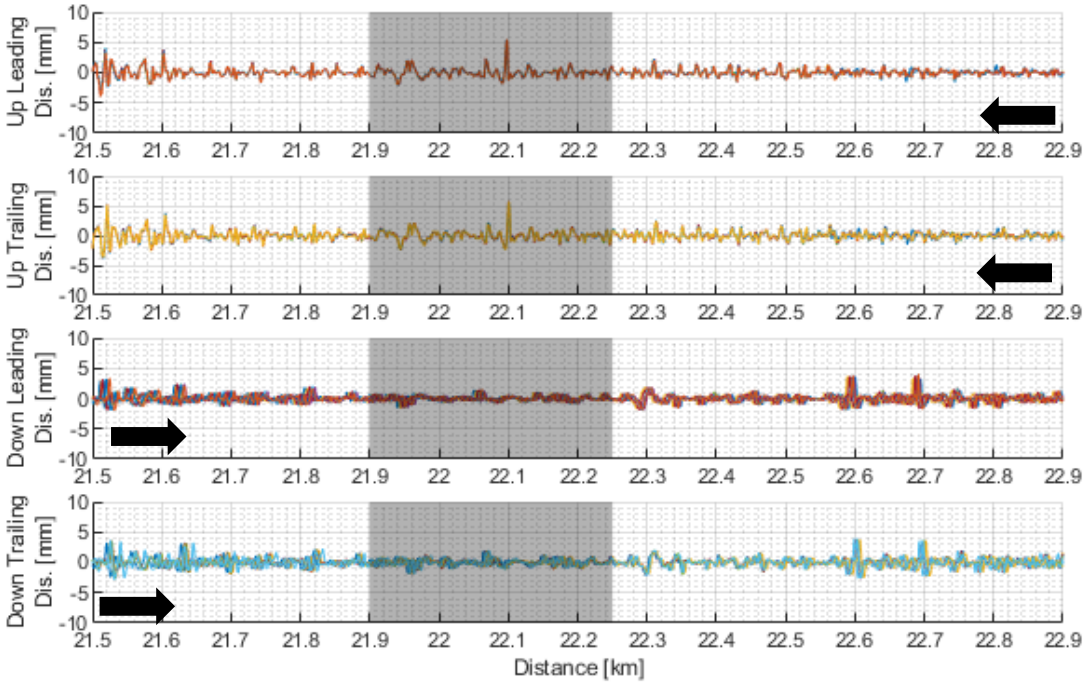


FIGURE C.13. AXLEBOX LEFT VERTICAL DISPLACEMENT (35-M WAVELENGTH FILTER).

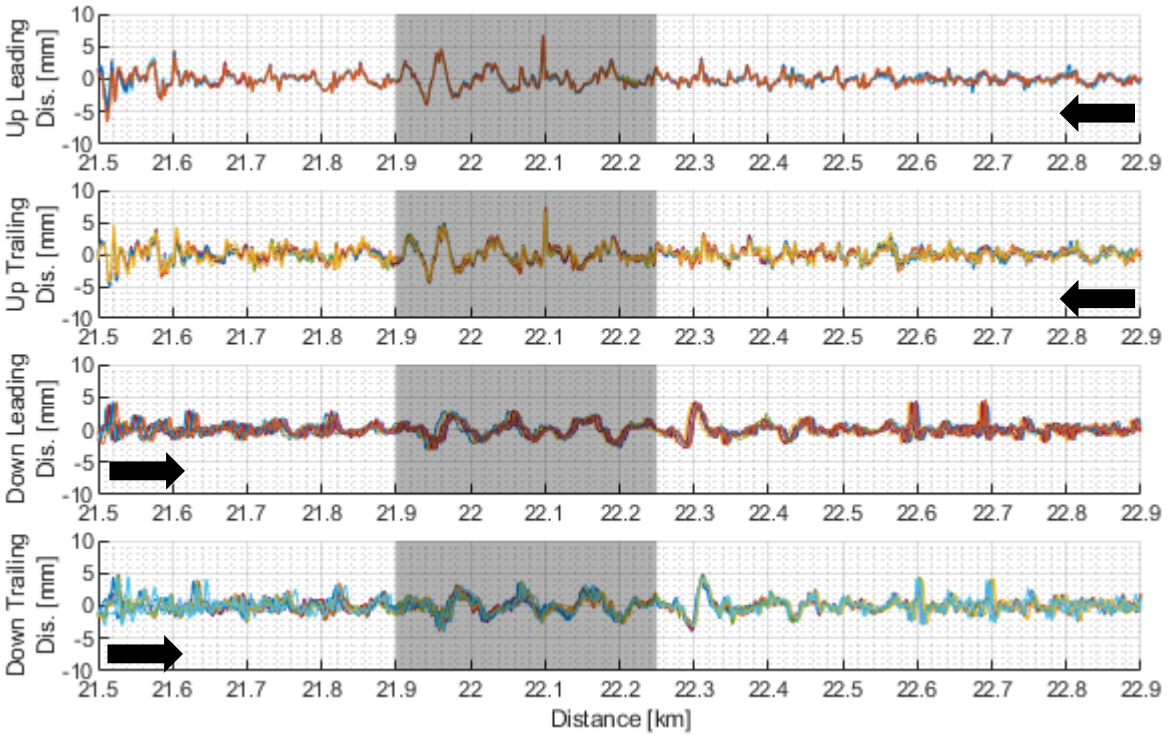


FIGURE C.14. AXLEBOX LEFT VERTICAL DISPLACEMENT (70-M WAVELENGTH FILTER).

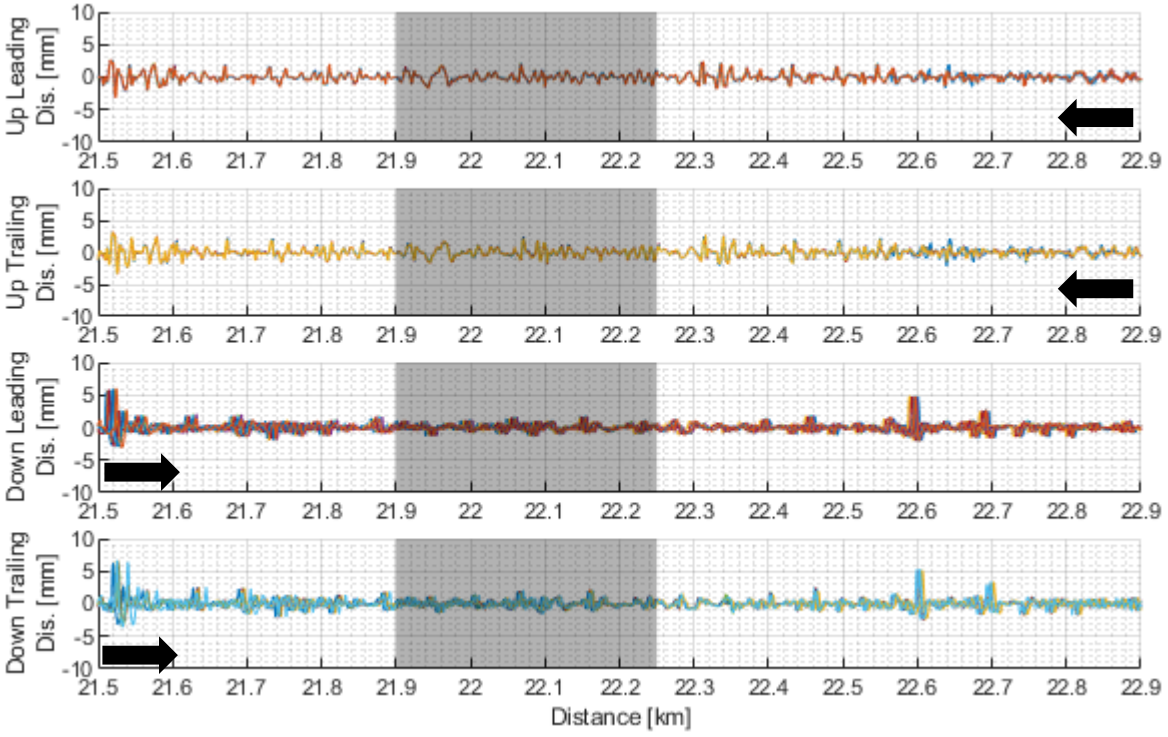


FIGURE C.15. AXLEBOX RIGHT VERTICAL DISPLACEMENT (35-M WAVELENGTH FILTER).

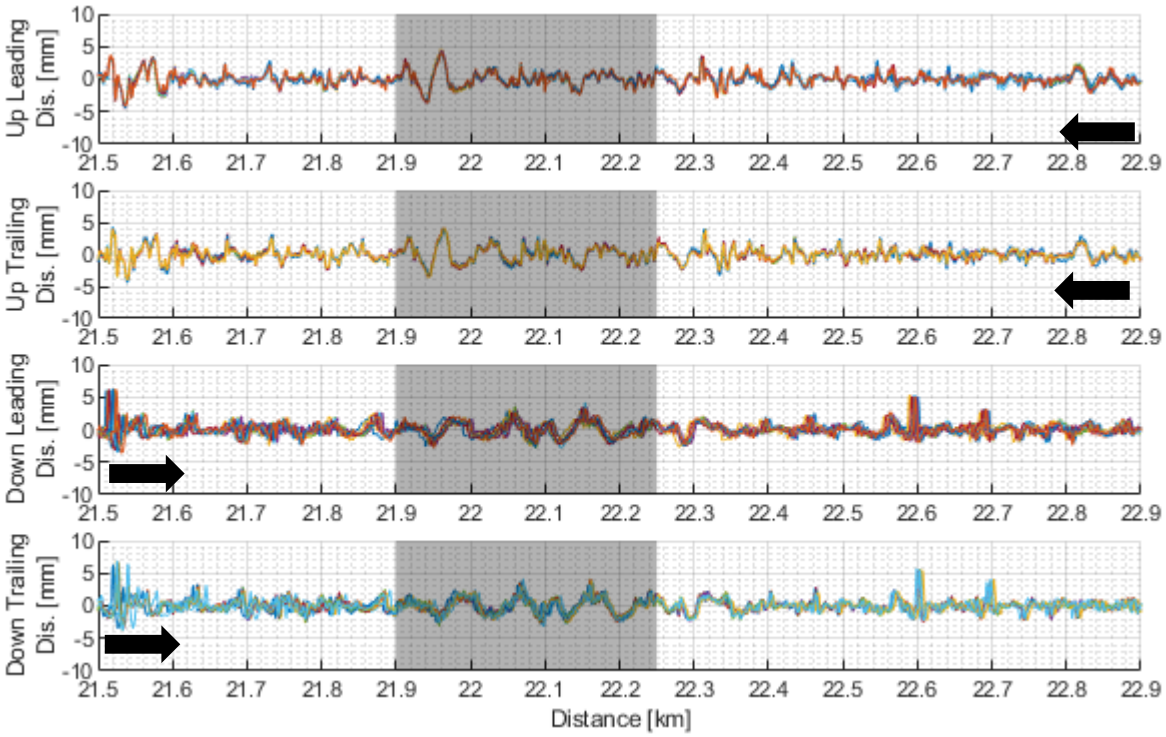


FIGURE C.16. AXLEBOX RIGHT VERTICAL DISPLACEMENT (70-M WAVELENGTH FILTER).

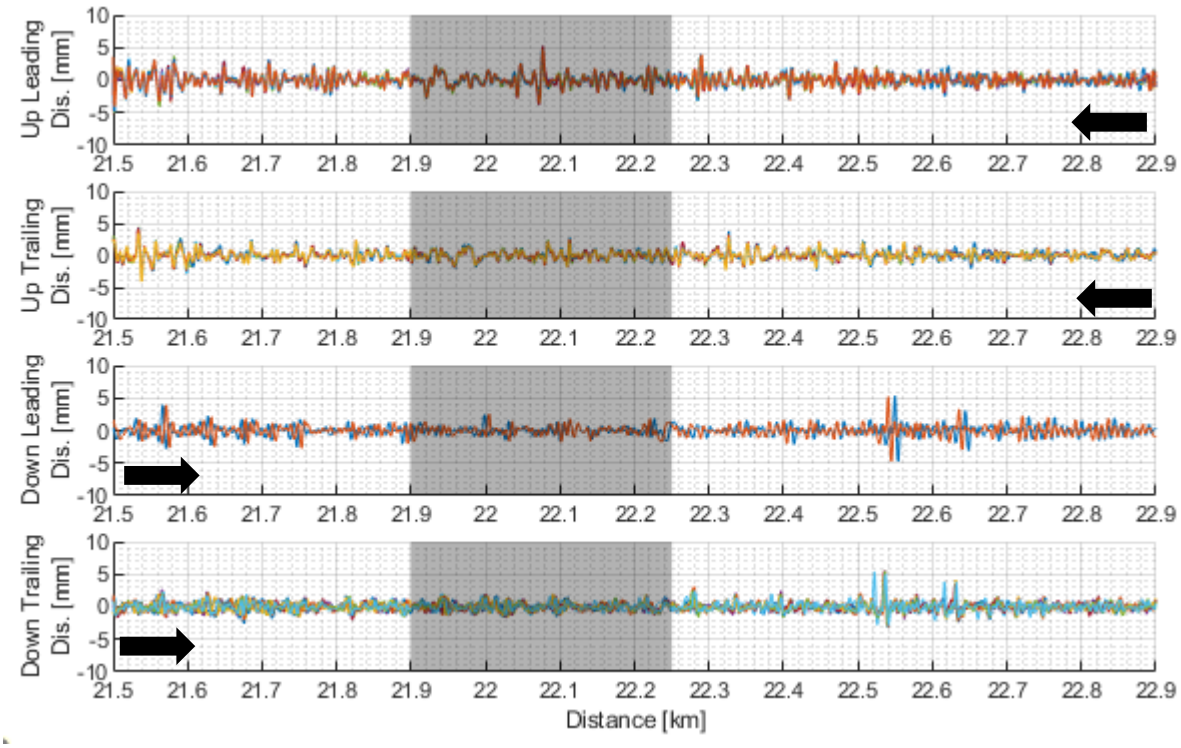


FIGURE C.17. BOGIE VERTICAL DISPLACEMENT (35-M WAVELENGTH FILTER).

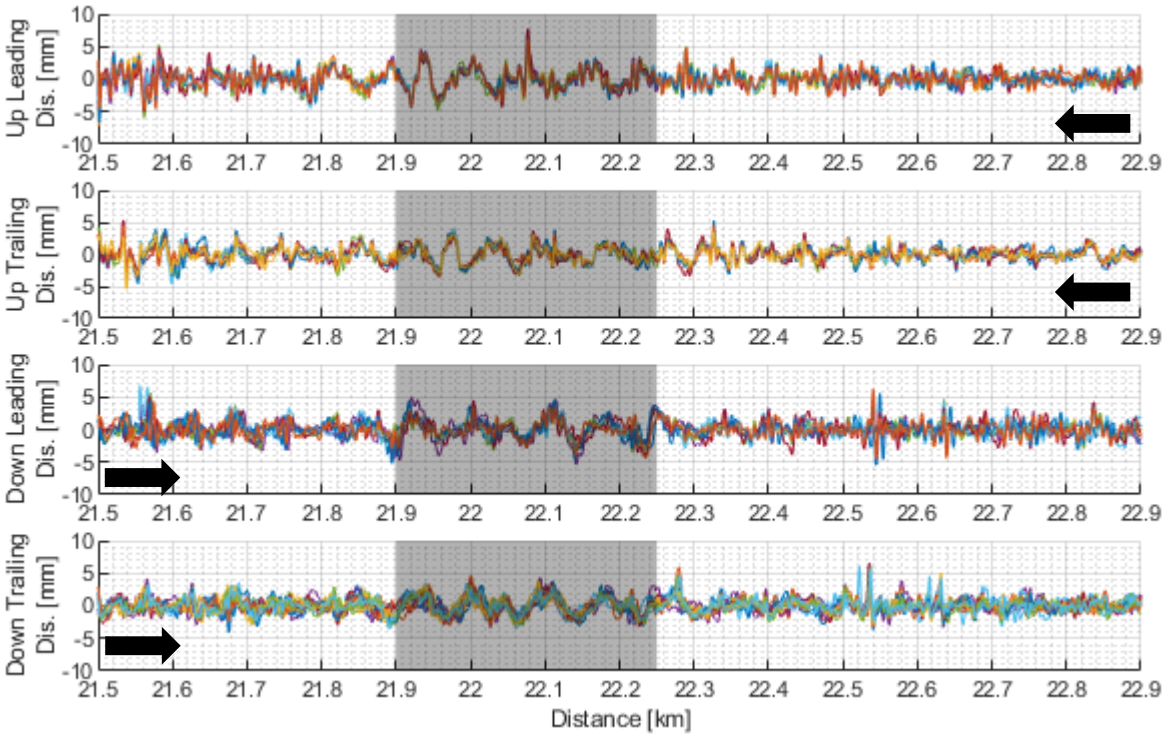


FIGURE C.18. BOGIE VERTICAL DISPLACEMENT (70-M WAVELENGTH FILTER).

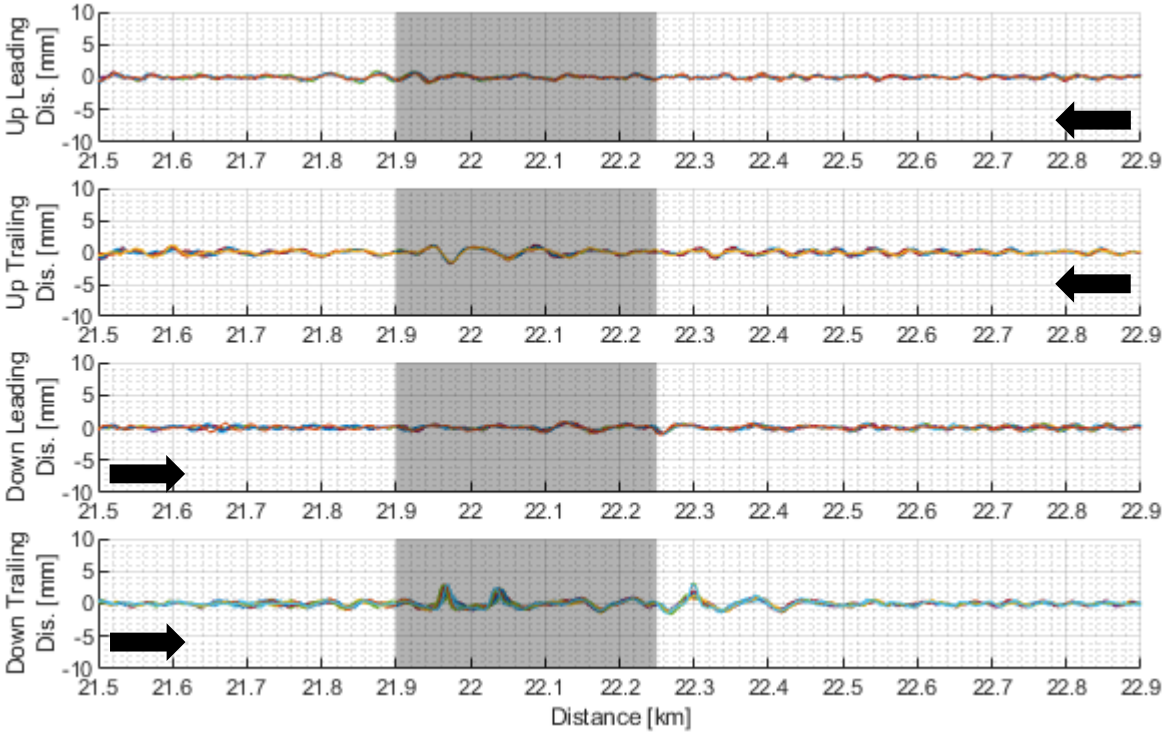


FIGURE C.19. CAB VERTICAL DISPLACEMENT (35-M WAVELENGTH FILTER).

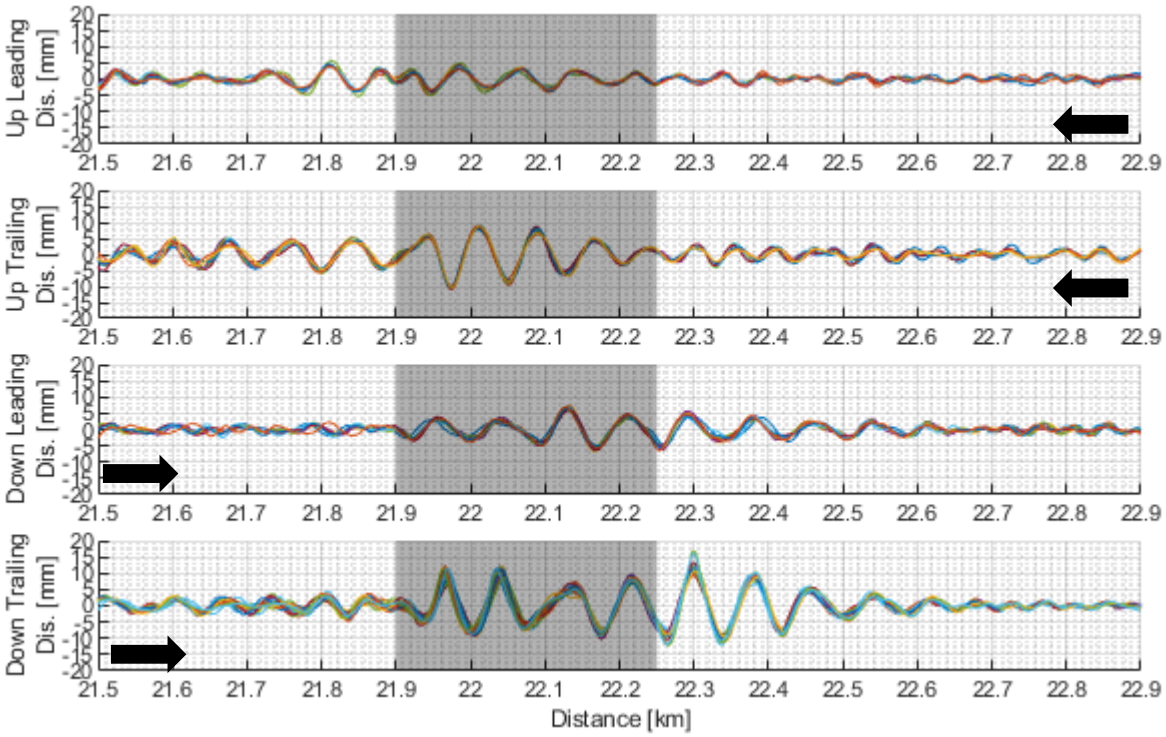


FIGURE C.20. CAB VERTICAL DISPLACEMENT (70-M WAVELENGTH FILTER).

Appendix D. Results obtained for switch and cross

This appendix shows the data obtained and not displayed in Chapter 6. The black arrow in the figures indicates the direction of travel, and the dashed lines indicate the position of the S&Cs.

D.1. DATA DISPLAYED PER SENSOR

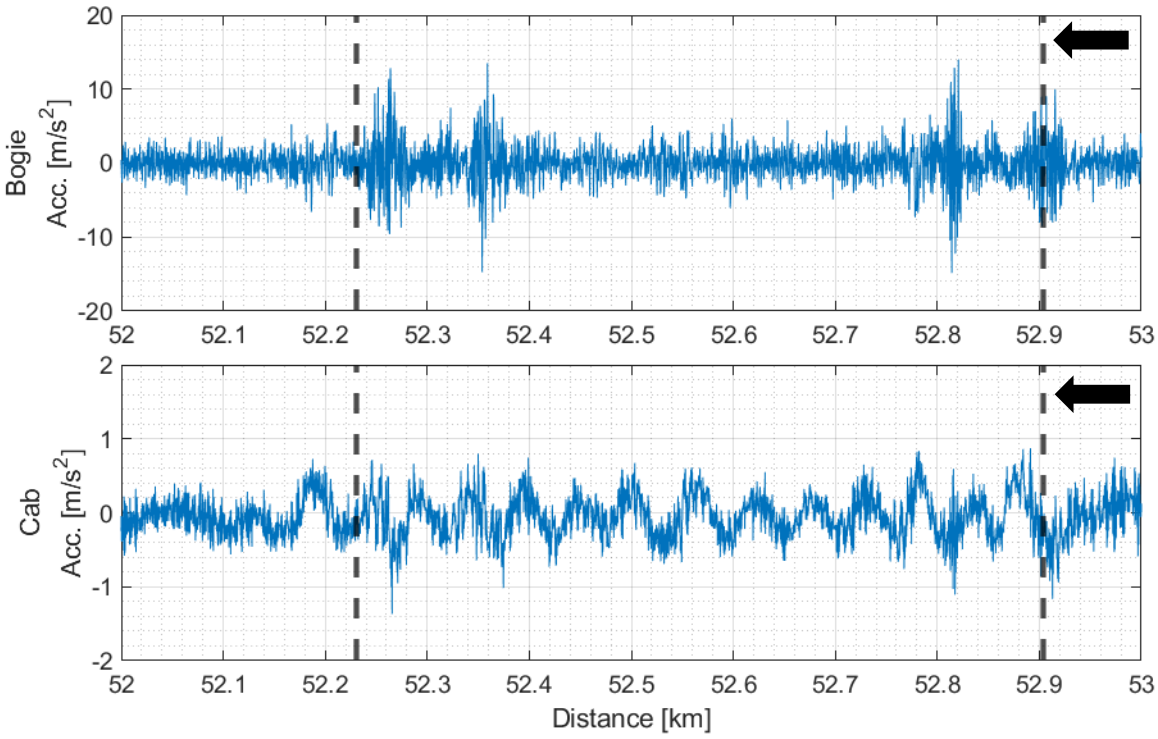


FIGURE D.1. BOGIE AND CAB LATERAL DISPLACEMENT.

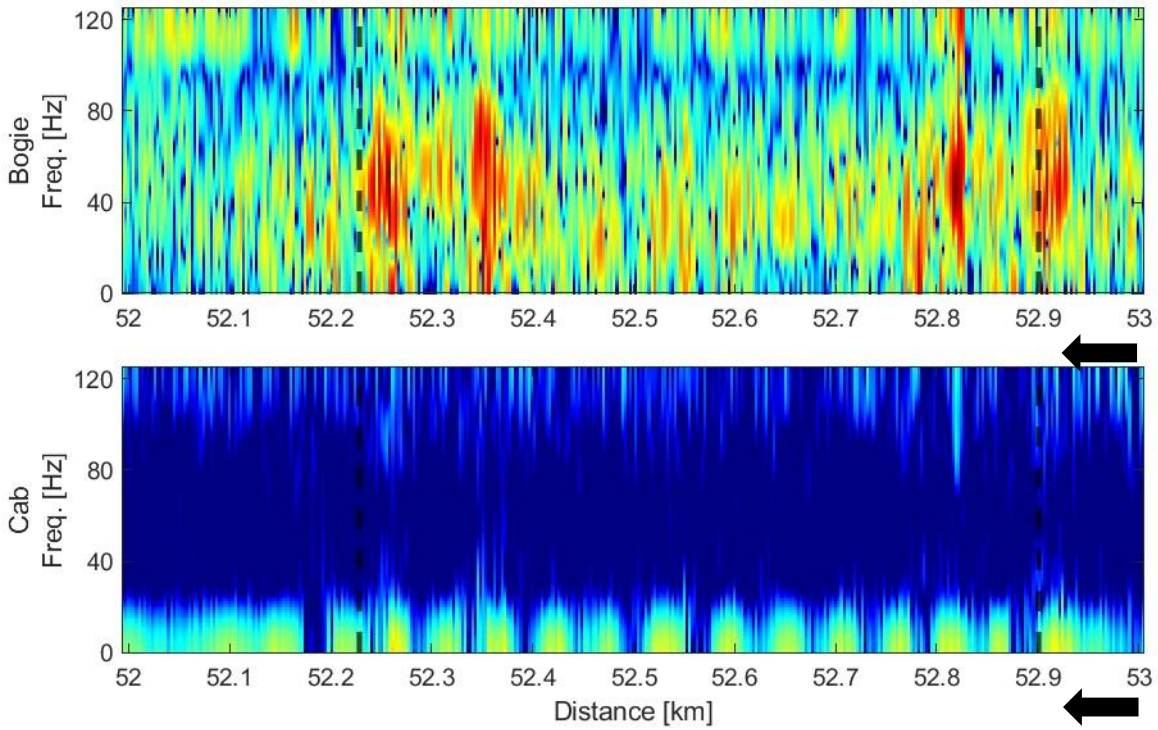


FIGURE D.2. BOGIE AND CAB LATERAL DISPLACEMENT SPECTROGRAMS.

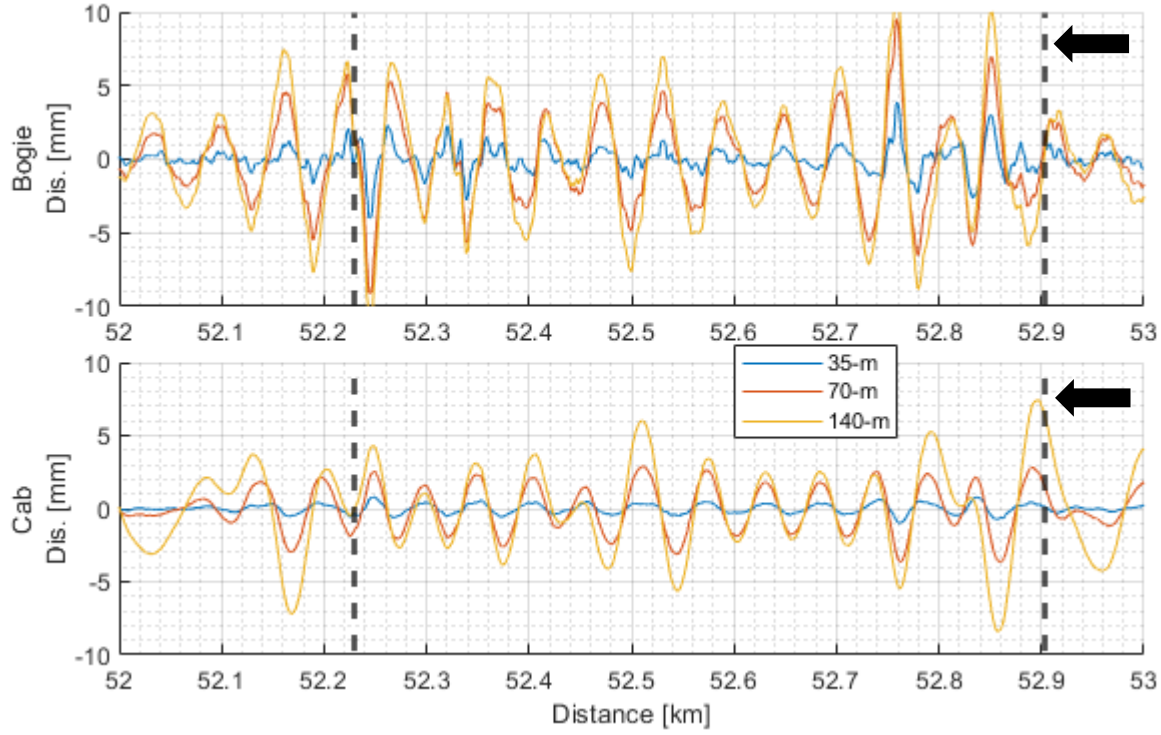


FIGURE D.3. BOGIE AND CAB LATERAL DISPLACEMENT.

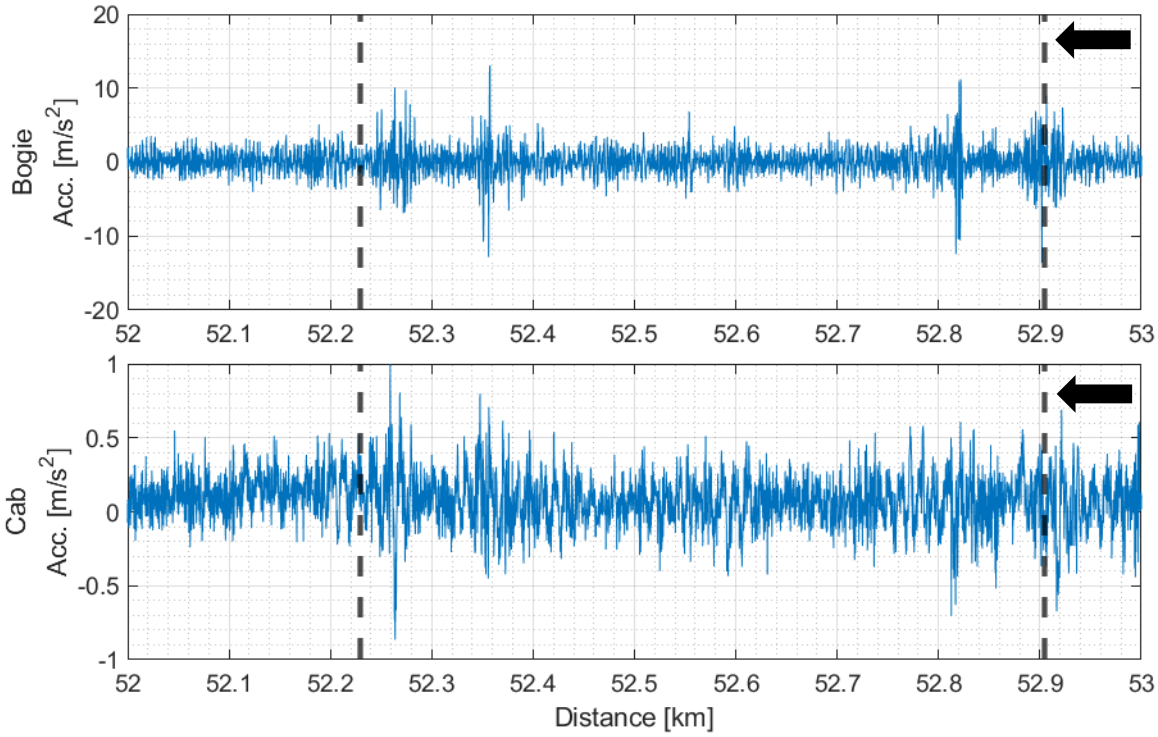


FIGURE D.4. BOGIE AND CAB LONGITUDINAL ACCELERATION.

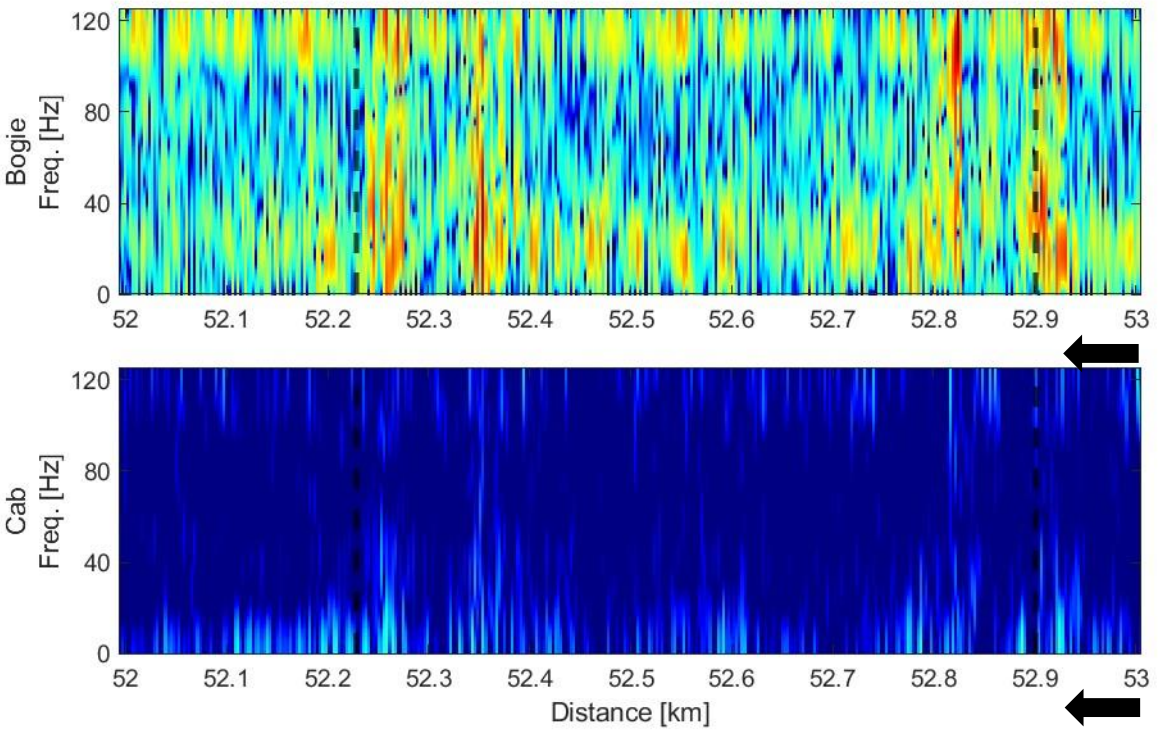


FIGURE D.5. BOGIE AND CAB LONGITUDINAL ACCELERATION SPECTROGRAMS.

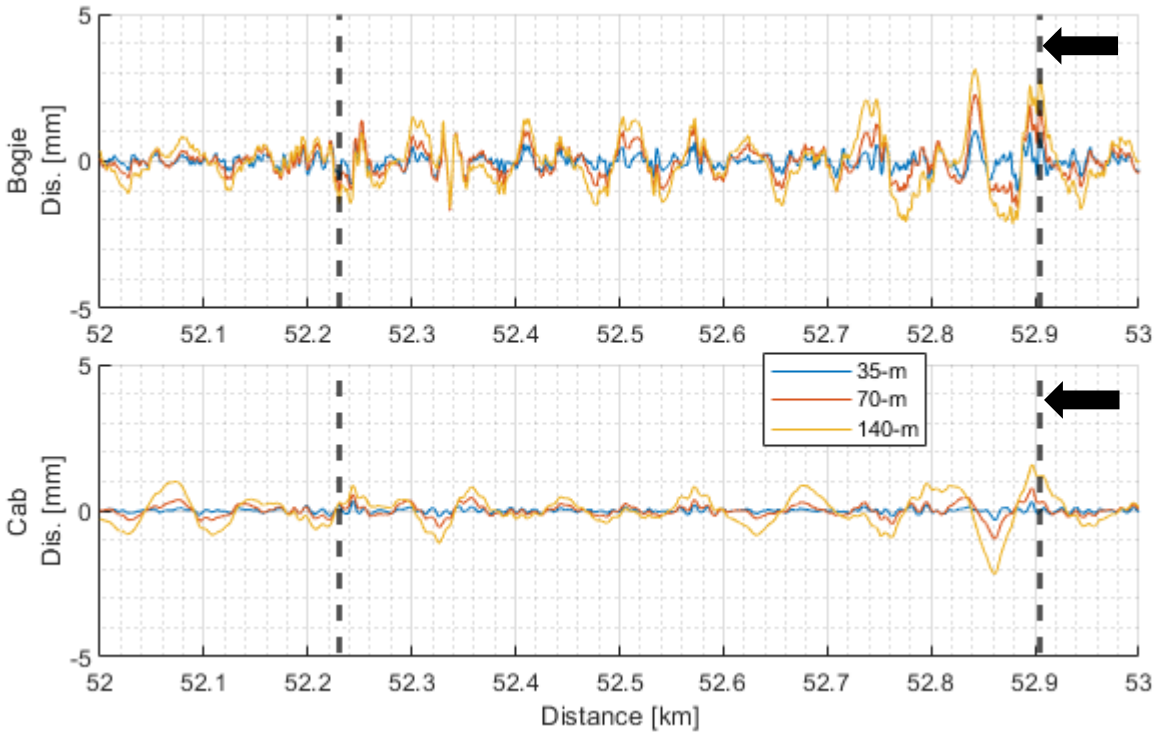


FIGURE D.6. BOGIE AND CAB LONGITUDINAL DISPLACEMENT.

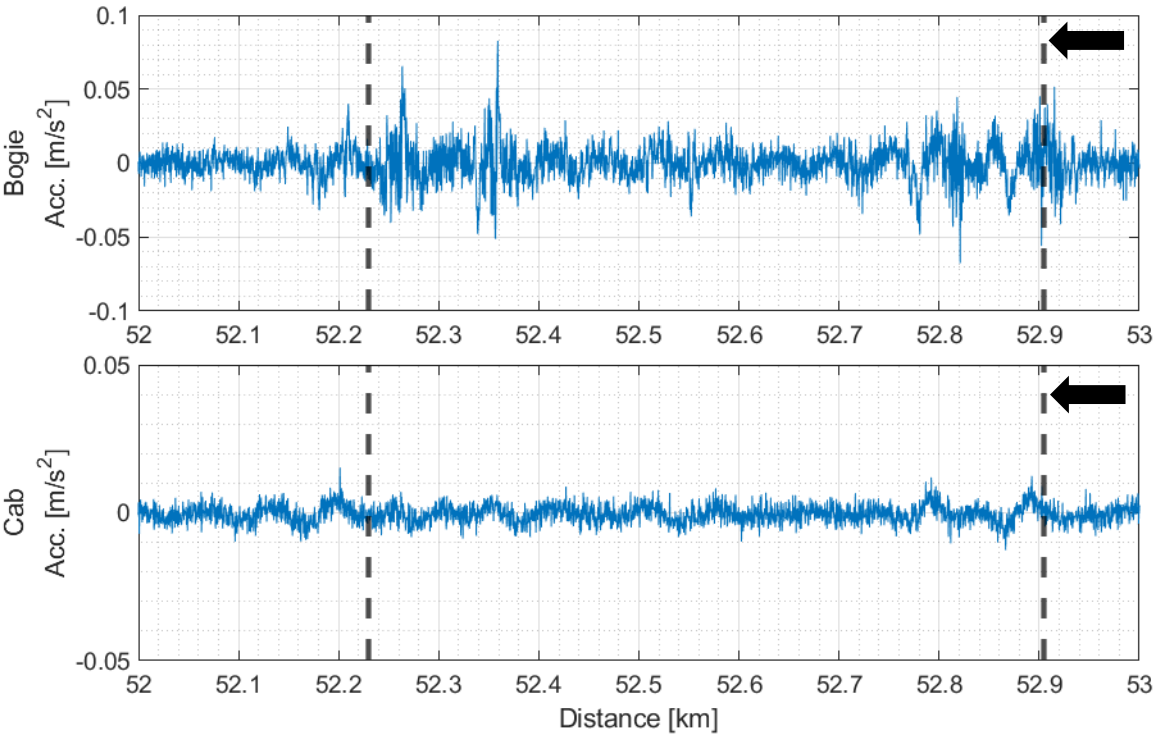


FIGURE D.7. BOGIE AND CAB YAW RATE.

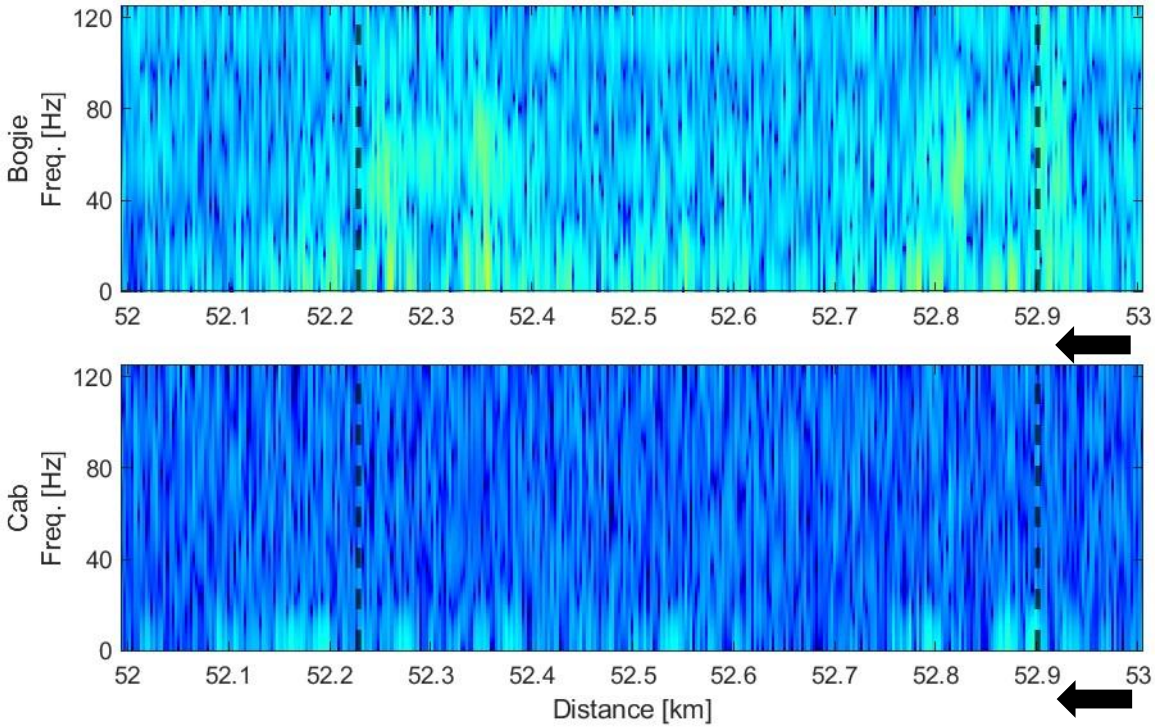


FIGURE D.8. BOGIE AND CAB YAW RATE SPECTROGRAMS.

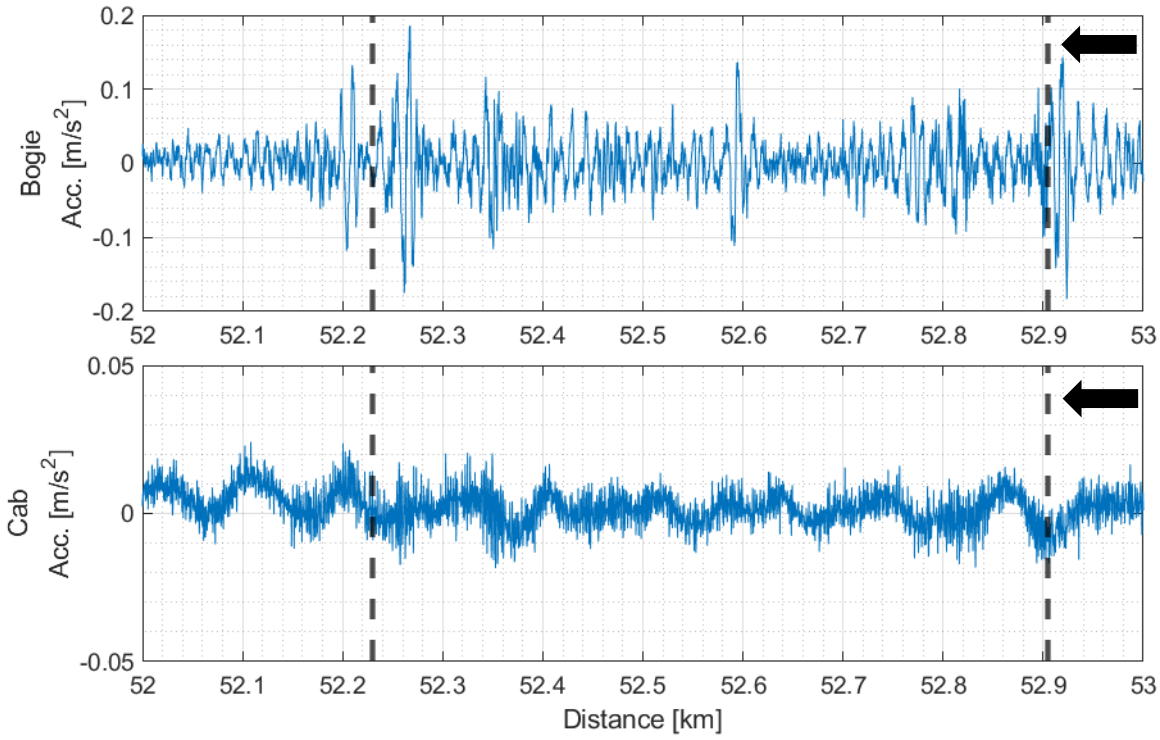


FIGURE D.9. BOGIE AND CAB PITCH RATE.

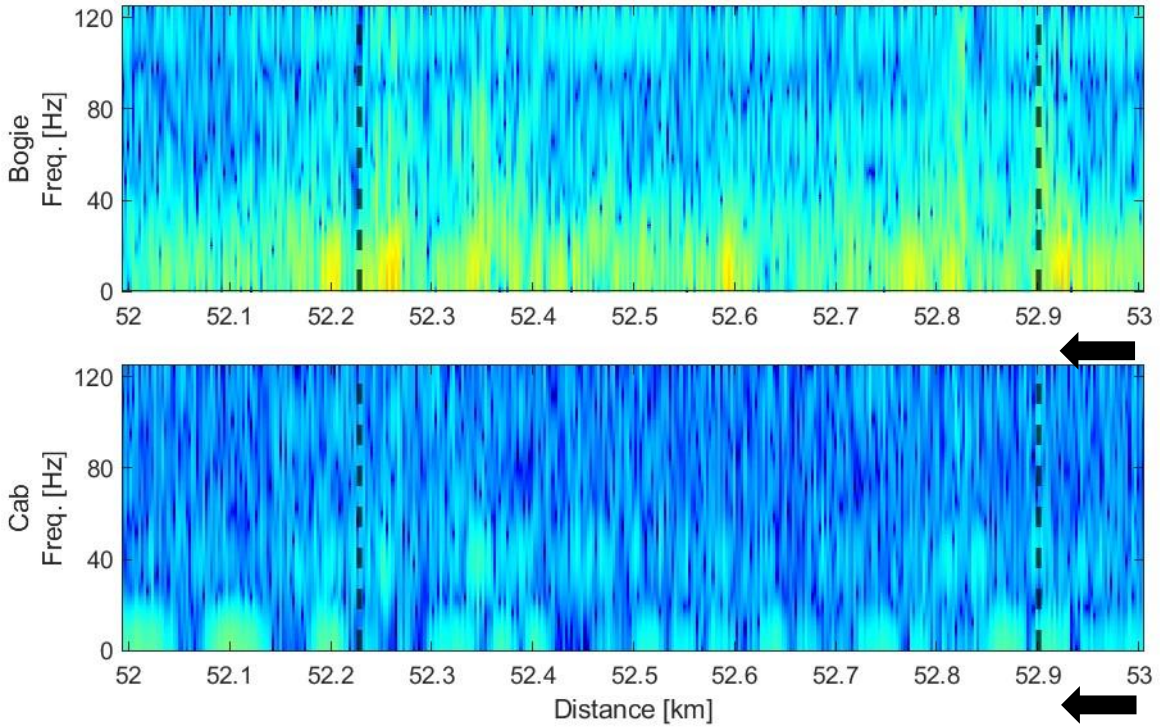


FIGURE D.10. BOGIE AND CAB PITCH RATE SPECTROGRAMS.

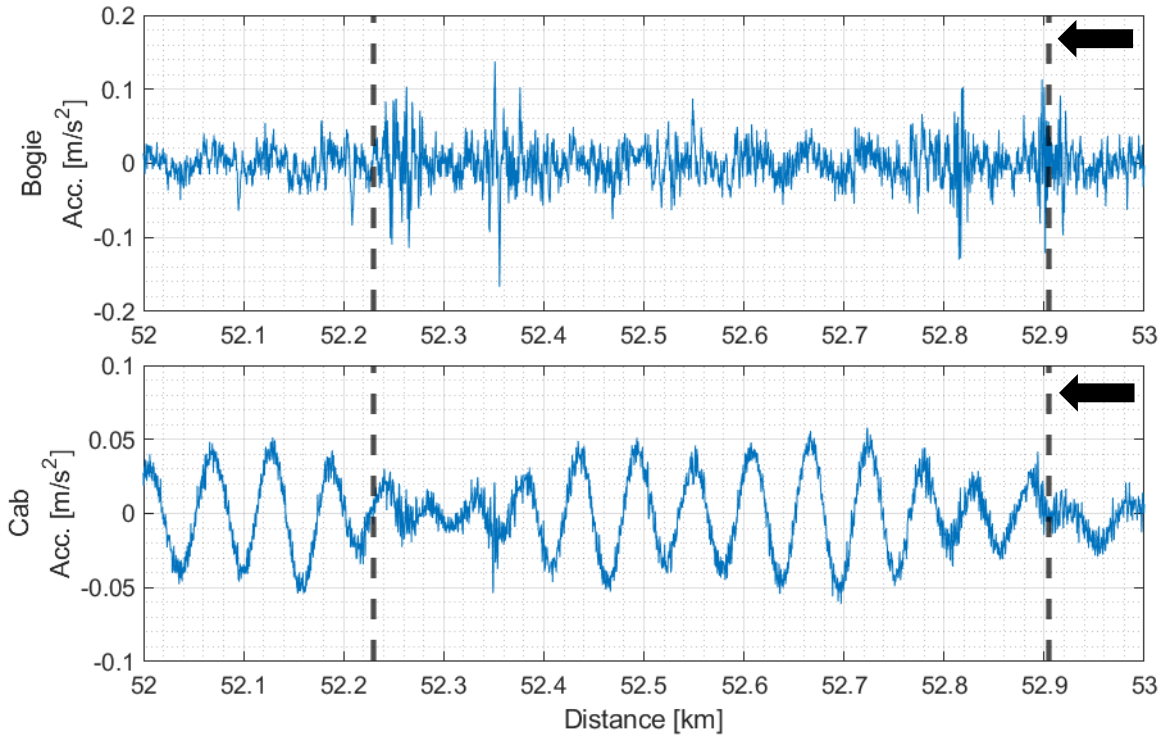


FIGURE D.11. BOGIE AND CAB ROLL RATE.

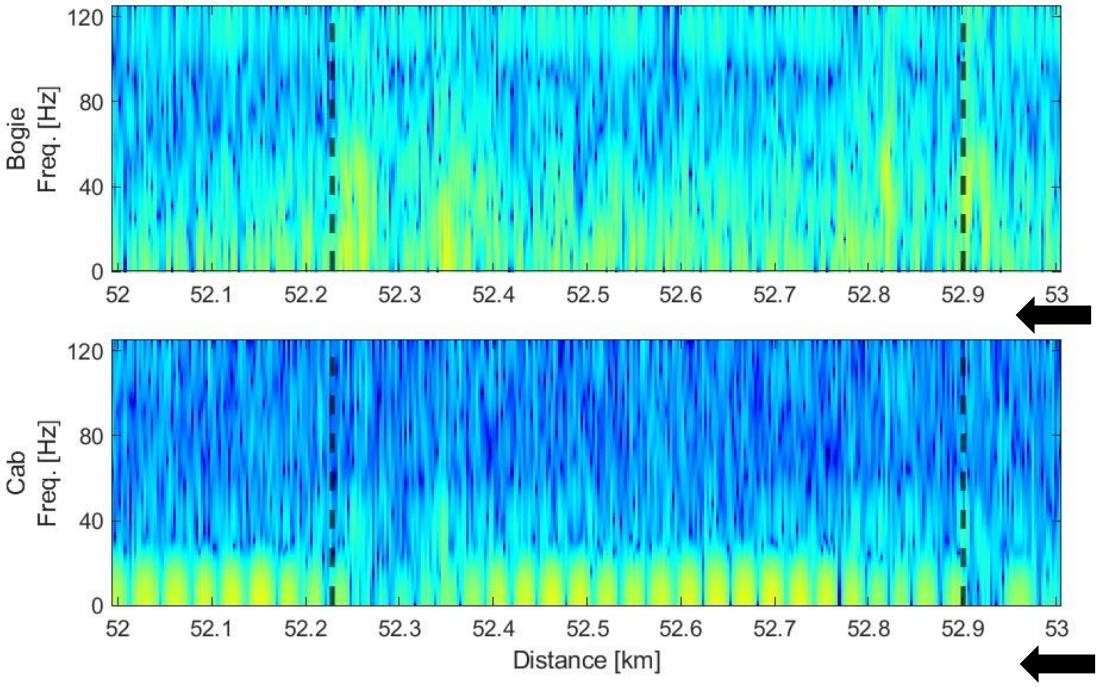


FIGURE D.12. BOGIE AND CAB ROLL RATE SPECTROGRAMS.

D.2. DATA DISPLAYED PER CONFIGURATION

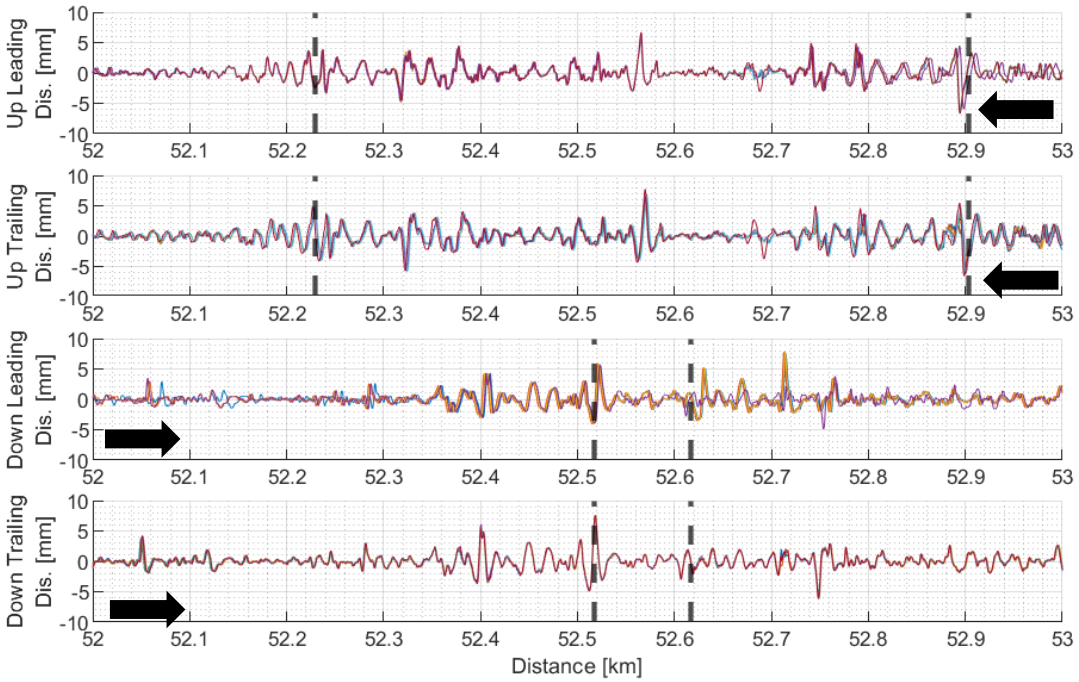


FIGURE D.13. AXLEBOX LEFT VERTICAL DISPLACEMENT (35-M WAVELENGTH FILTER).

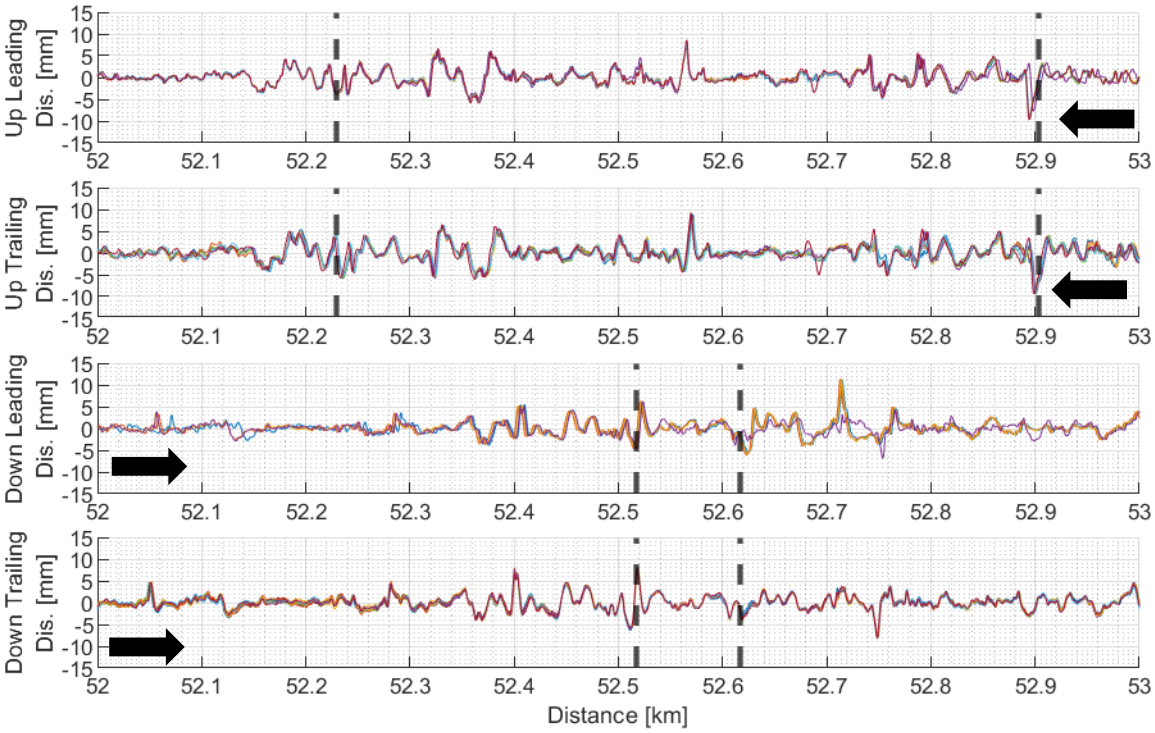


FIGURE D.14. AXLEBOX LEFT VERTICAL ACCELERATION (70-M WAVELENGTH FILTER).

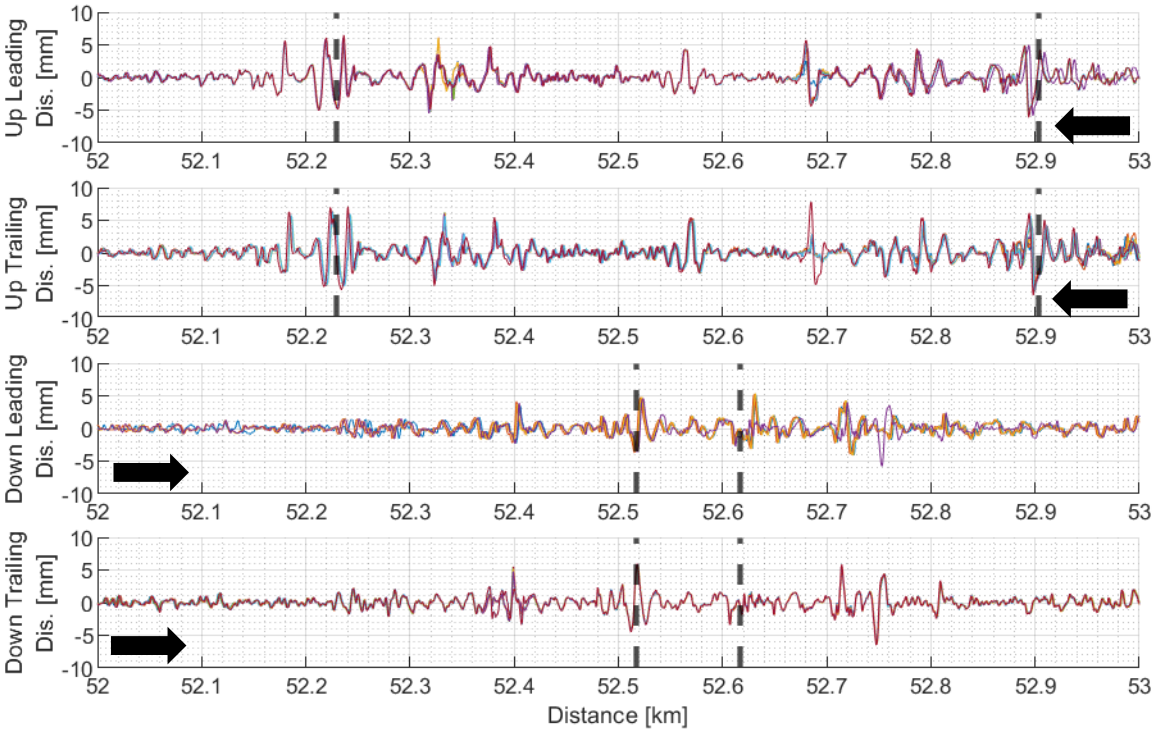


FIGURE D.15. AXLEBOX RIGHT VERTICAL DISPLACEMENT (35-M WAVELENGTH FILTER).

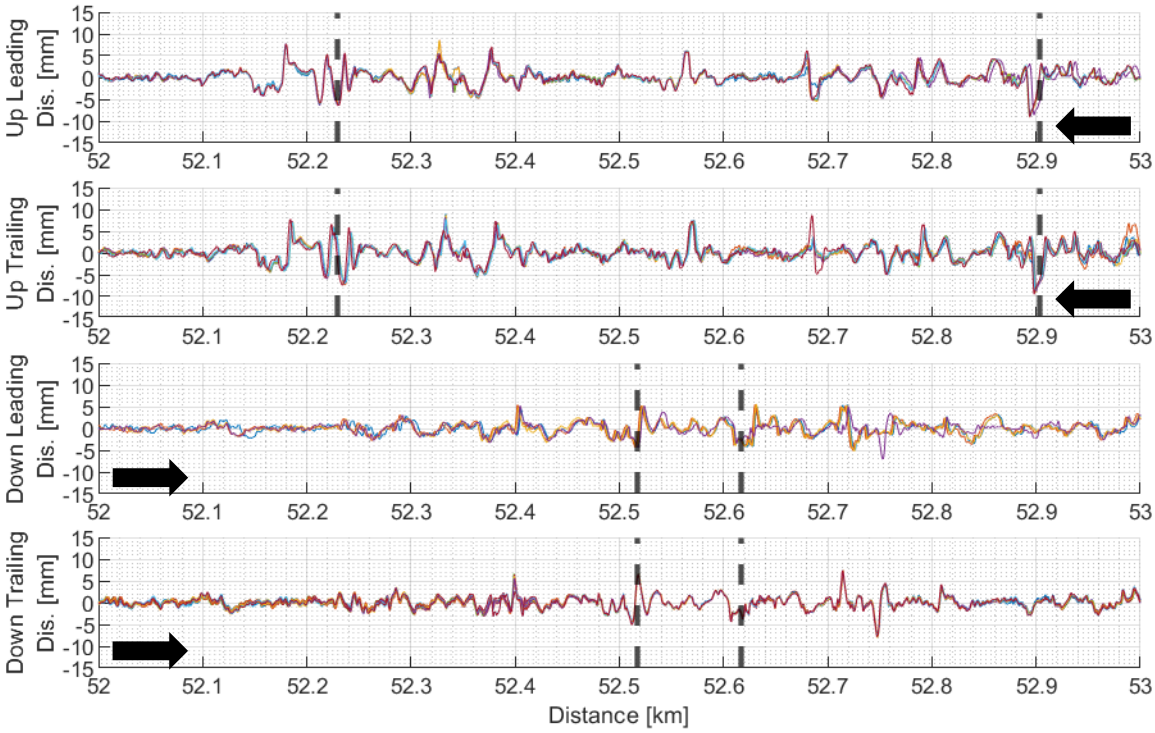


FIGURE D.16. AXLEBOX RIGHT VERTICAL DISPLACEMENT (70-M WAVELENGTH FILTER).

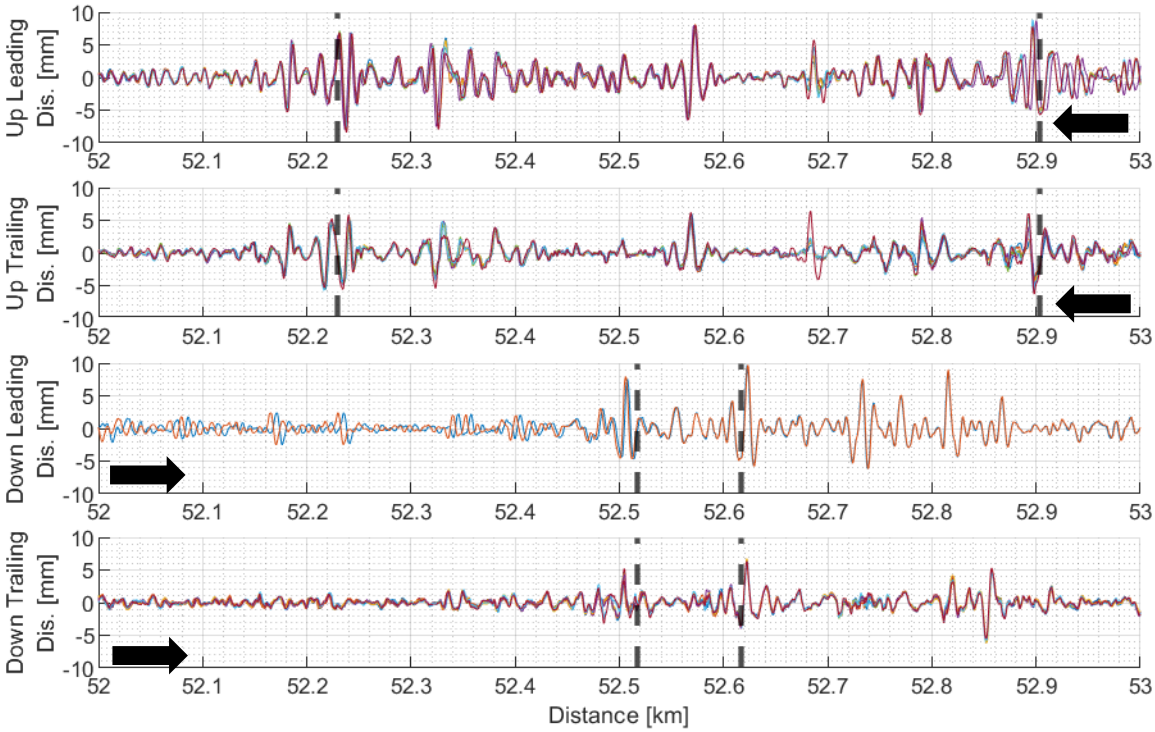


FIGURE D.17. BOGIE VERTICAL DISPLACEMENT (35-M WAVELENGTH FILTER).

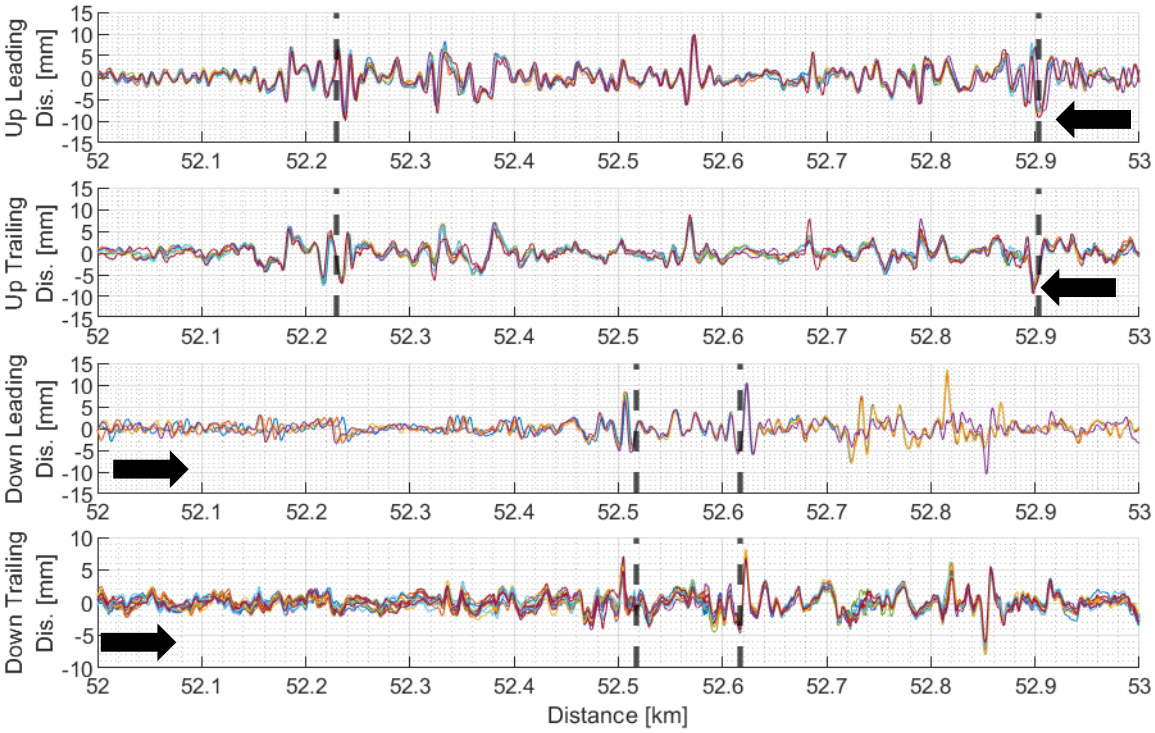


FIGURE D.18. BOGIE VERTICAL DISPLACEMENT (70-M WAVELENGTH FILTER).

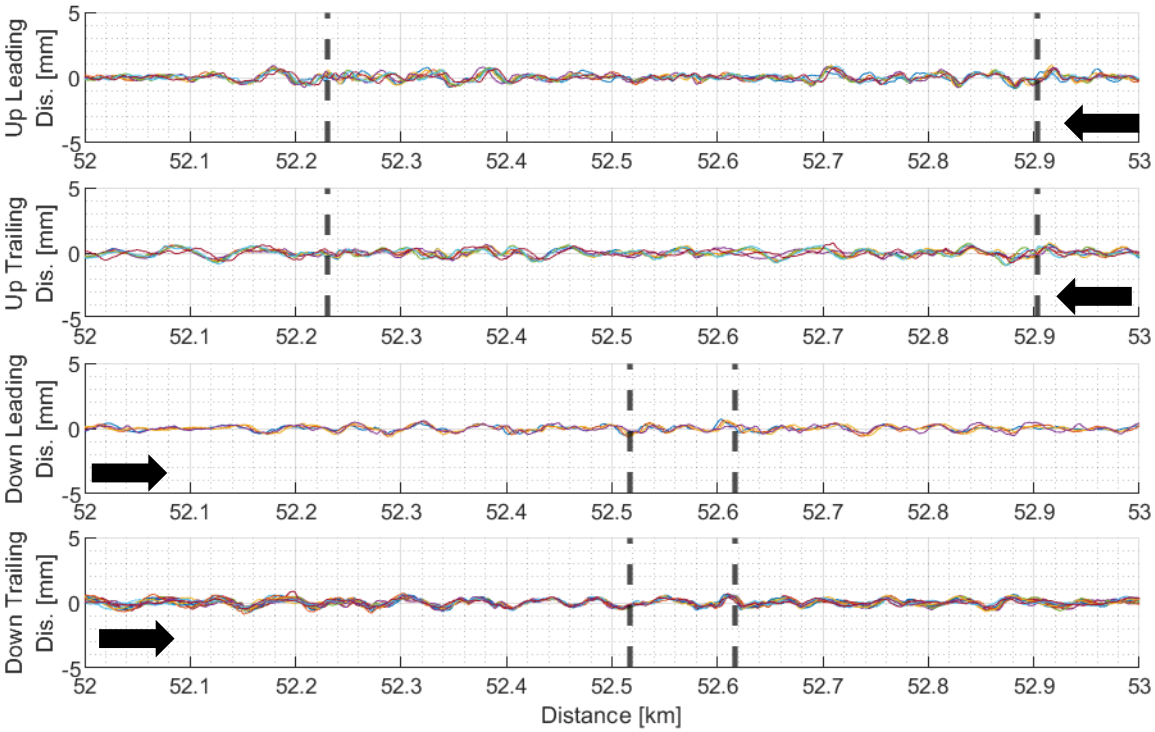


FIGURE D.19. CAB VERTICAL DISPLACEMENT (35-M WAVELENGTH FILTER).

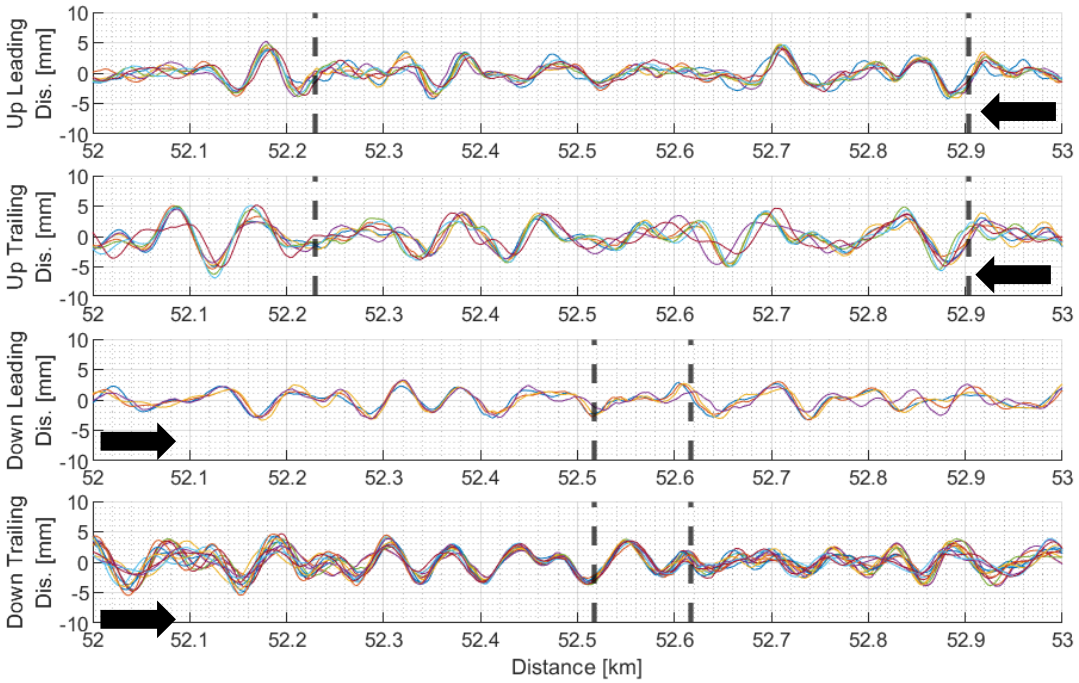


FIGURE D.20. CAB VERTICAL DISPLACEMENT (70-M WAVELENGTH FILTER).

D.3. EVOLUTION OF DATA

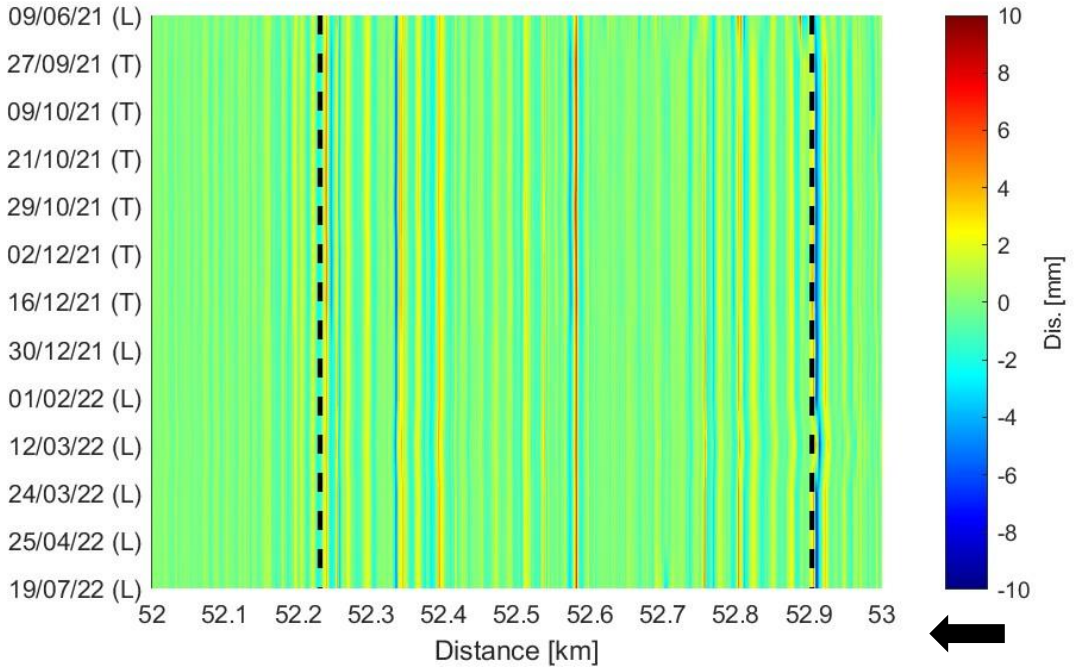


FIGURE D.21. EVOLUTION OF LEFT AXLEBOX VERTICAL DISPLACEMENT (35-M WAVELENGTH FILTER).

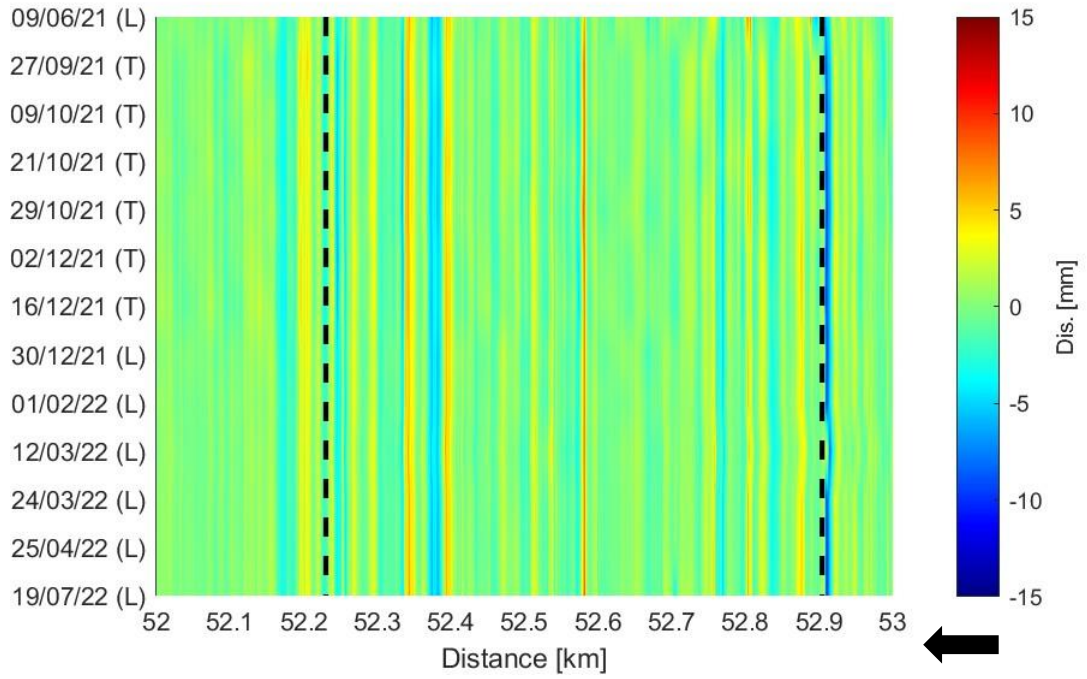


FIGURE D.22. EVOLUTION OF LEFT AXLEBOX VERTICAL DISPLACEMENT (70-M WAVELENGTH FILTER).

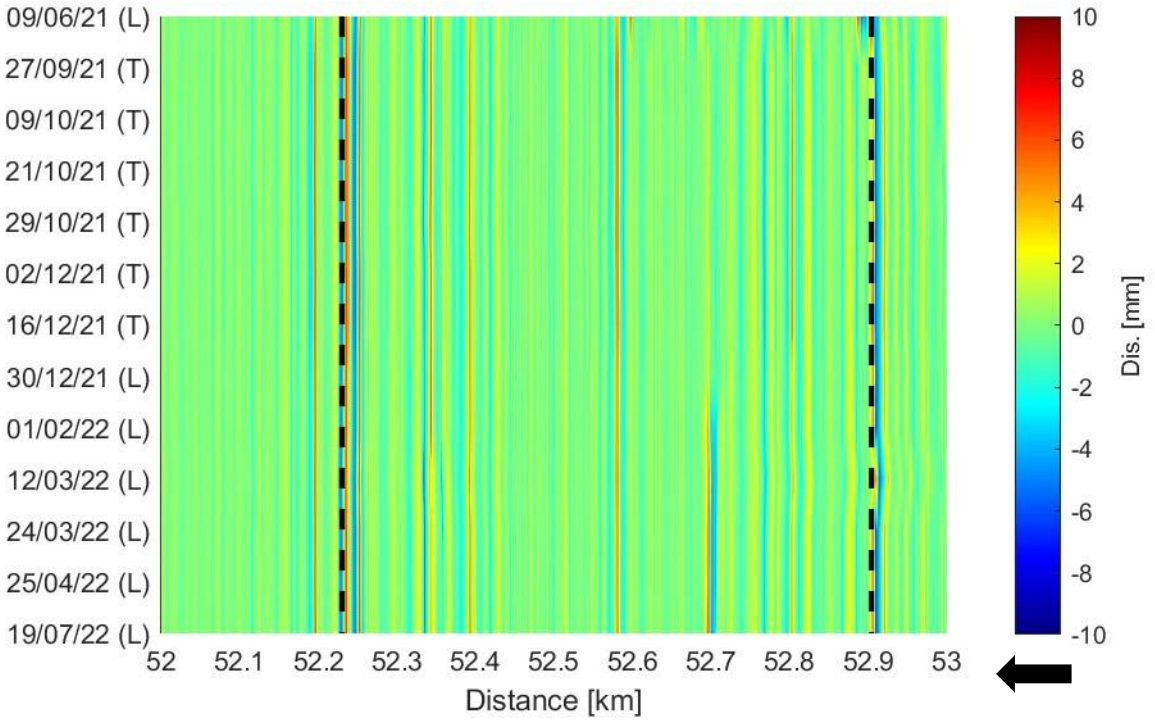


FIGURE D.23. EVOLUTION OF RIGHT AXLEBOX VERTICAL DISPLACEMENT (35-M WAVELENGTH FILTER).

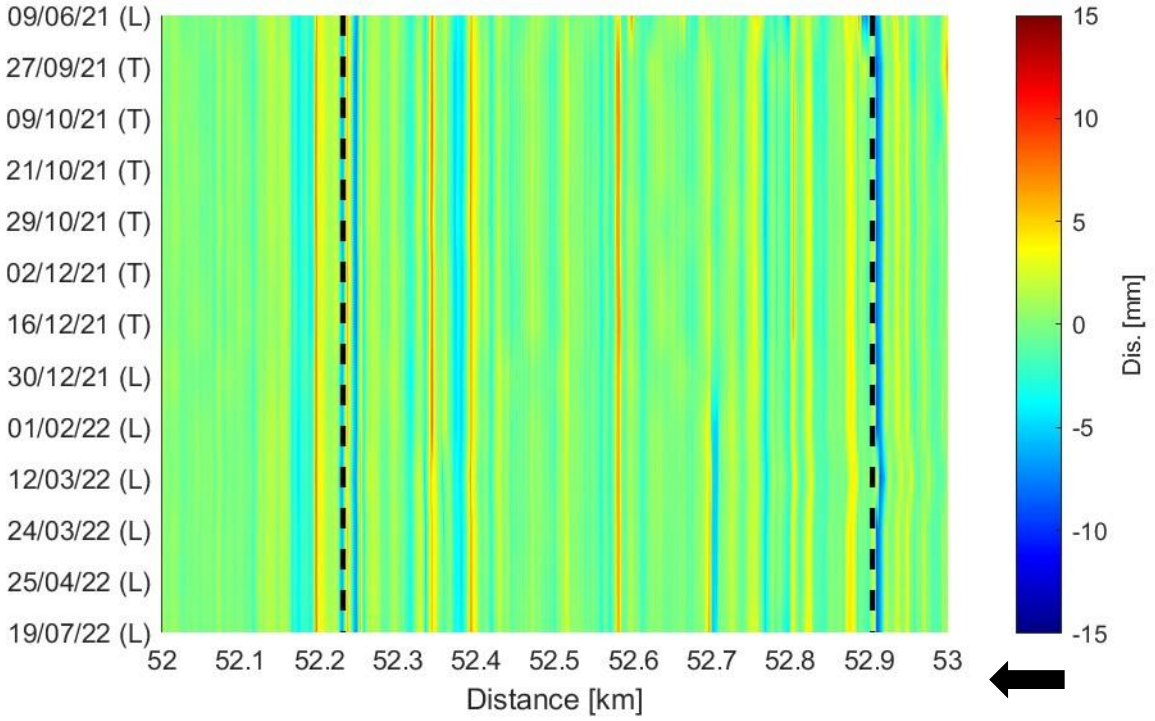


FIGURE D.24. EVOLUTION OF RIGHT AXLEBOX VERTICAL DISPLACEMENT (70-M WAVELENGTH FILTER).

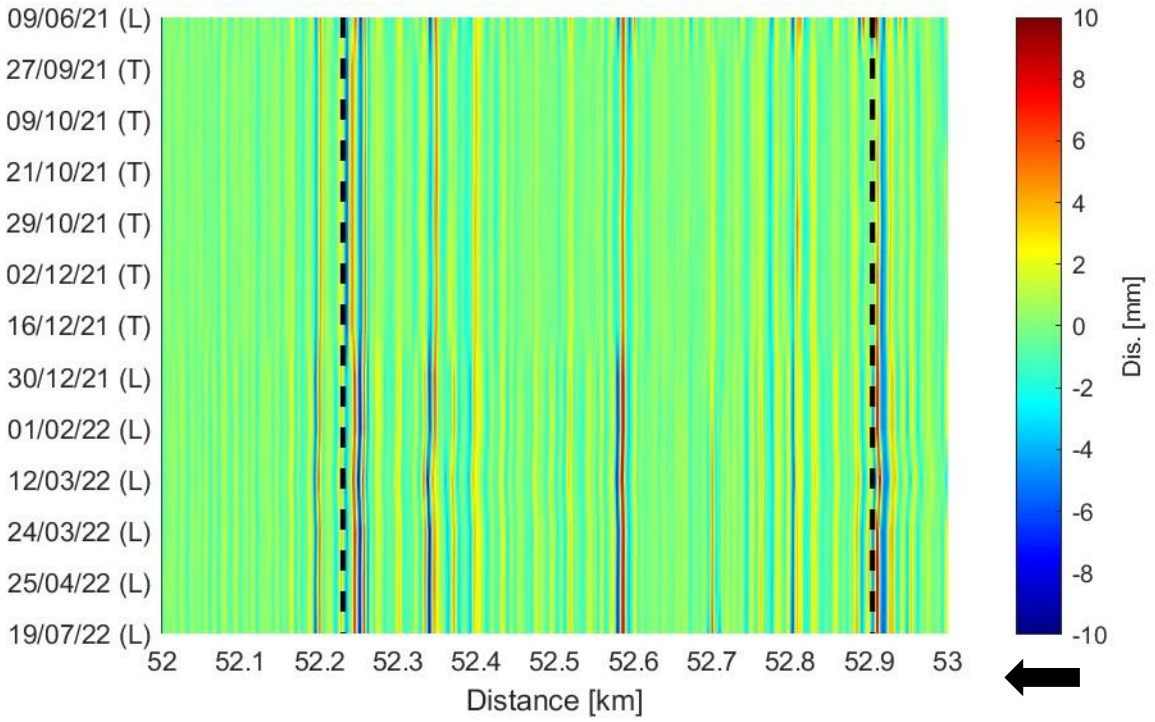


FIGURE D.25. EVOLUTION OF BOGIE VERTICAL DISPLACEMENT (35-M WAVELENGTH FILTER).

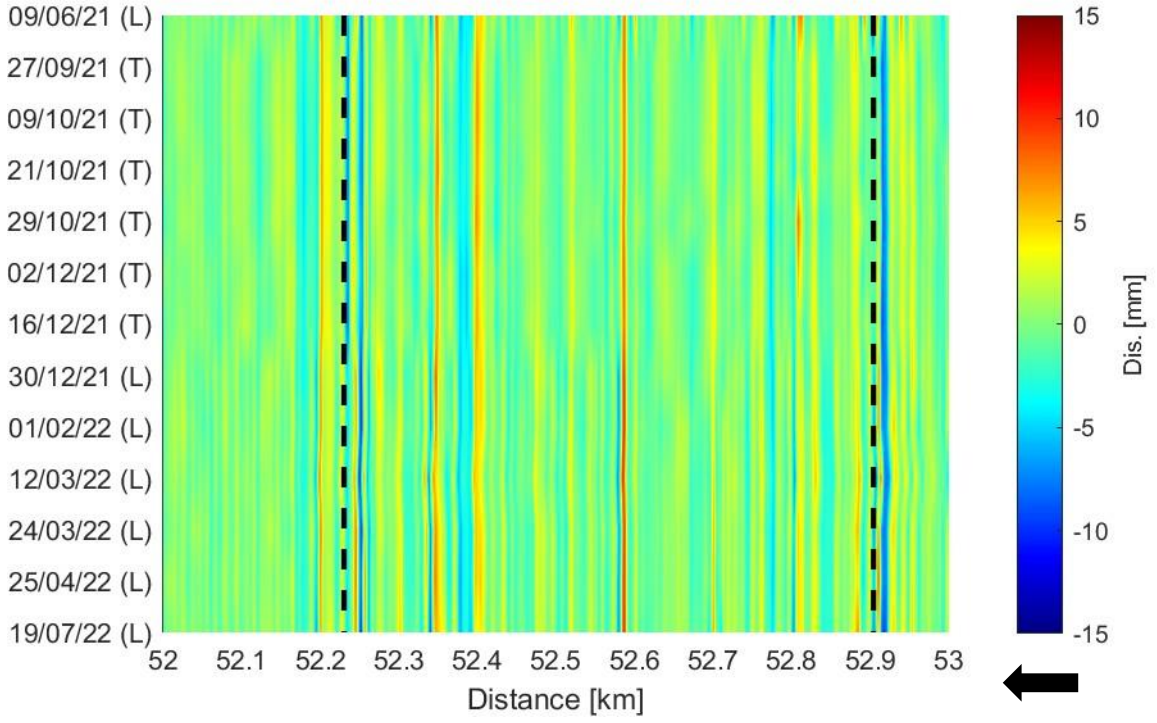


FIGURE D.26. EVOLUTION OF BOGIE VERTICAL DISPLACEMENT (70-M WAVELENGTH FILTER).

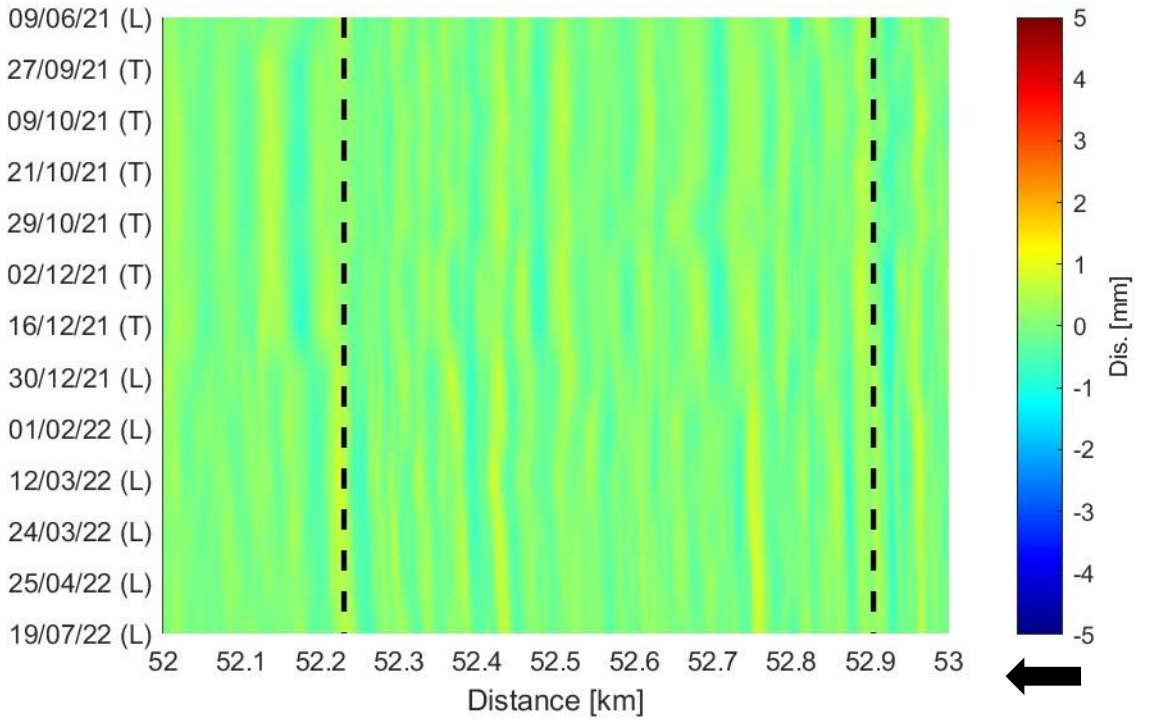


FIGURE D.27. EVOLUTION OF CAB VERTICAL DISPLACEMENT (35-M WAVELENGTH FILTER).

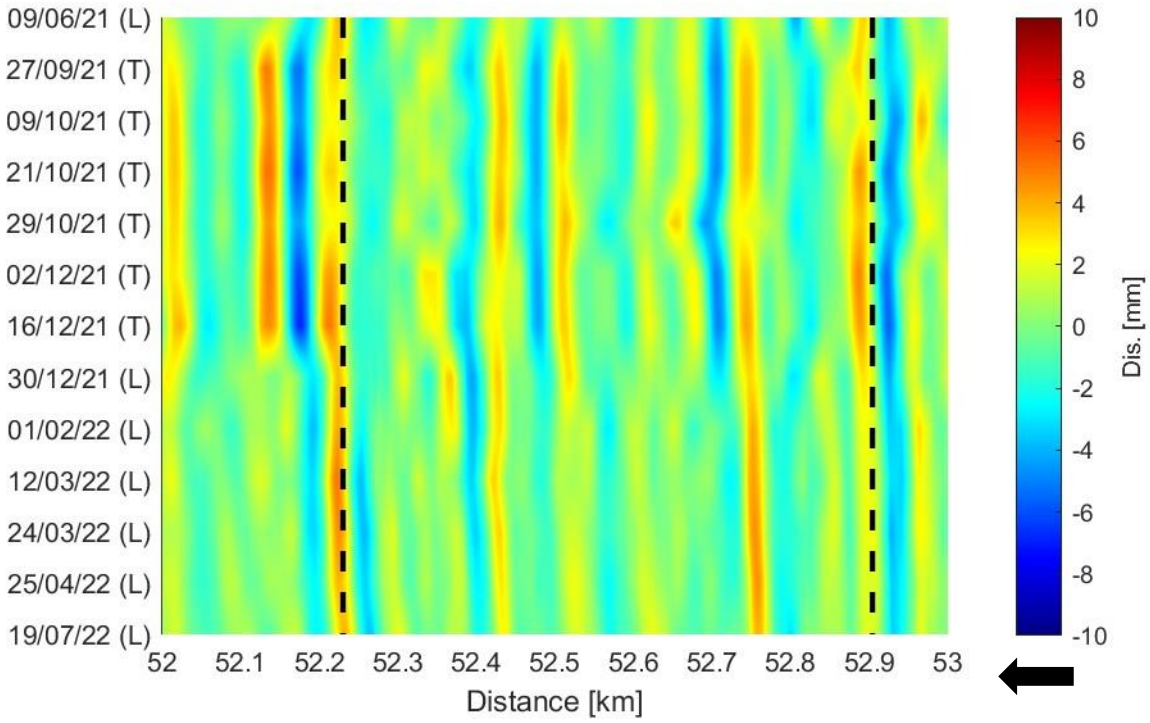
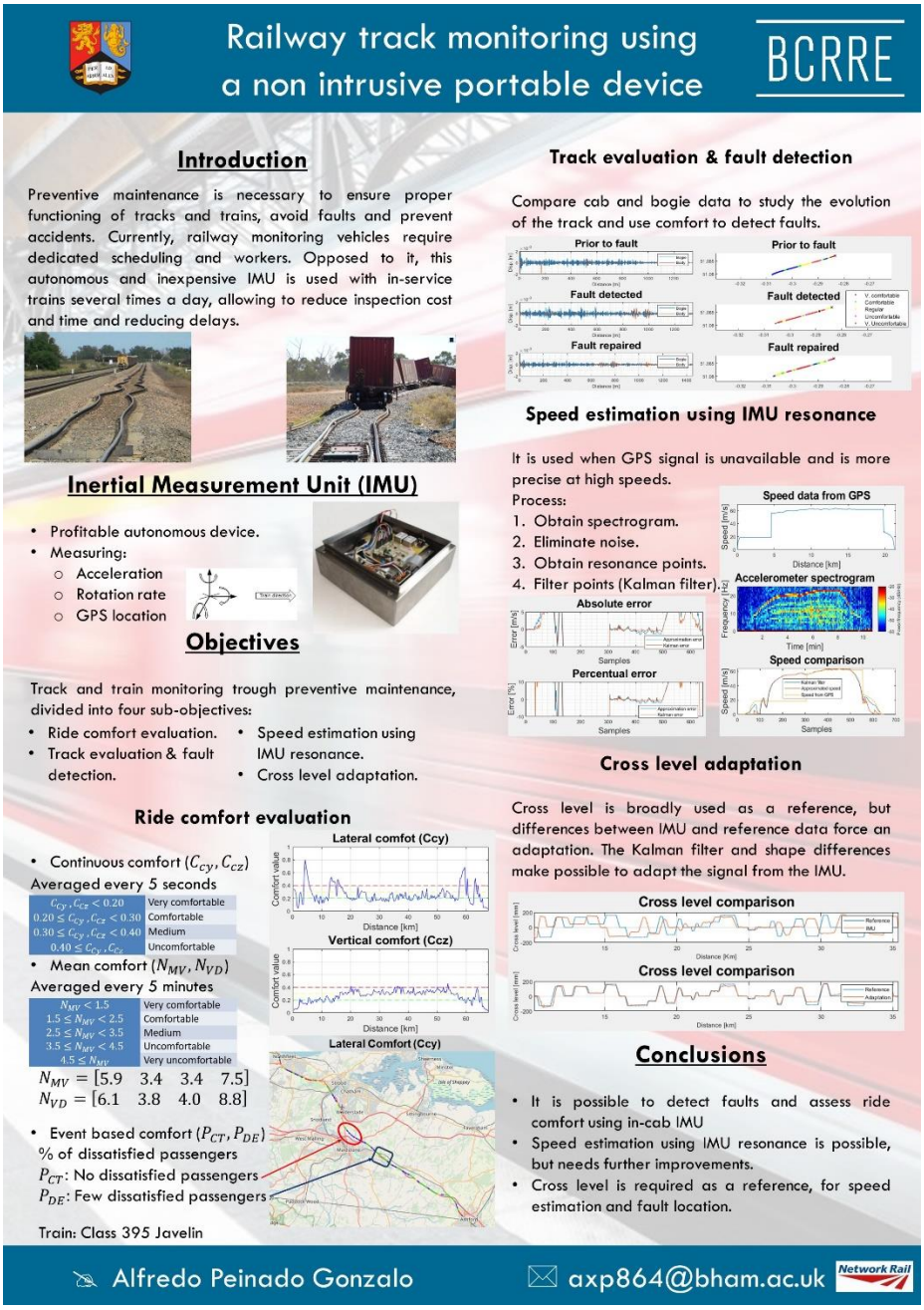


FIGURE D.28. EVOLUTION OF CAB VERTICAL DISPLACEMENT (70-M WAVELENGTH FILTER).

Appendix E. Research Poster

Conference 2019



Appendix F. WCRR 2019



Continuous Railway Track Monitoring Using Passenger Trains

Clive ROBERTS[1], Mani ENTEZAMI[2], Edward STEWART[1], Graeme YEO[1],
Alfredo Peinado GONZALO[1], Mick HAYWARD[3], Peter AINSWORTH[2]

[1]Birmingham Centre for Railway Research and Education, University of Birmingham, Birmingham, UK
[2]MoniRail Ltd., Birmingham, UK
[3]Network Rail High Speed UK, Kent, UK
Corresponding Author: Edward STEWART (e.j.c.stewart@bham.ac.uk)

Abstract

Efficacy in railway track maintenance is not only critical for safe operation, but by reducing delays and increasing capacity, can result in economic benefits for rail operators.

Currently, rail infrastructure managers have dedicated vehicles to carry out track measurement. These vehicles are, however, expensive to procure and run as they need specially trained crews to operate them. Furthermore, they require uninterrupted access to the track, and so are difficult to schedule around other services. Consequently, the UK only has 6 such measurement vehicles and the mainline network is only inspected on a 4-6 weekly cycle (less regularly for other services).

This work demonstrates the application of an inexpensive inertial measurement unit (IMU), installed on an in-service passenger train, and using novel algorithms, to provide continuous monitoring of the track and its degradation. Two IMUs were fitted, one on the bogie and one in the cab.

Inertial data from the bogie mounted IMU was collected and processed to provide vertical and lateral displacement profiles of sections of track from multiple passes of a rail vehicle. A modified Kalman filter was used to produce the associated dataset profiles to within 0.2 mm location accuracy. Profiles calculated from multiple passes of the same area of track were compared to monitor track degradation.

Inertial data from the IMU mounted in a driver's cab was also collected and used to calculate the ride comfort using BS EN 12299. The ride comfort indices were compared to recommended limits on acceleration and change of acceleration (jerk).

Analysis of the results were used to determine whether trains on the measured routes meet current standards for ride comfort.

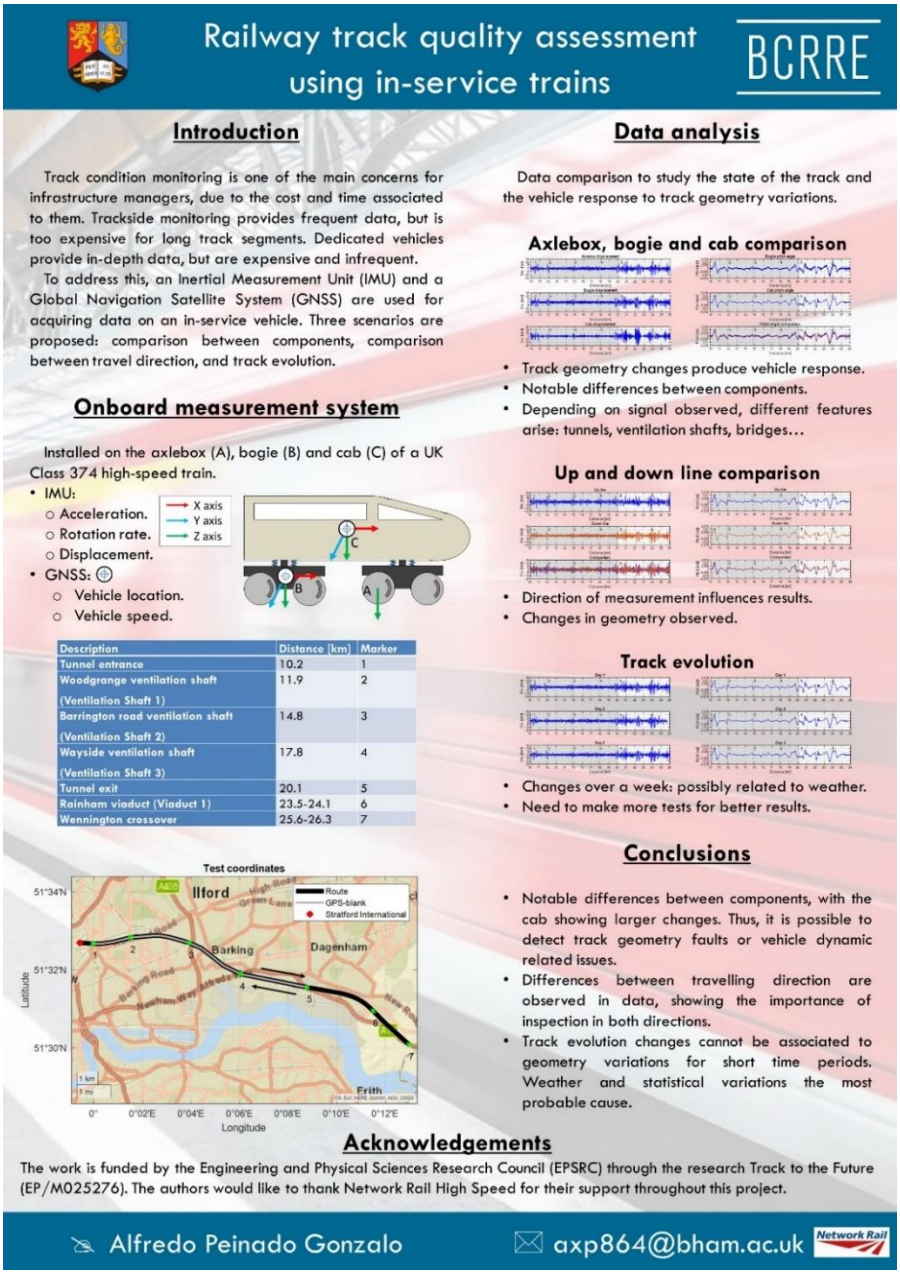
Reported issues on the measured routes from the Network Rail Fault Management System (FMS) and data from New Measurement Train (NMT) were used to evaluate the performance of the IMU based system against current UK industry track monitoring practices and results were comparable. The findings from this project show that an IMU mounted on the bogie of an in-service railway vehicle allows track geometry data to be measured at more frequent intervals than with a dedicated track measurement vehicle and at a fraction of the cost.

Keywords: in-service monitoring, track alignment, ride quality, inertial measurement

1. Introduction

With an increasing emphasis on rail digitisation and the use of Internet of Things (IoT) type approaches to collect data about rail systems in order to support decision making, there is increased focus on the practicalities and quality of the data generated by such approaches. This is particularly true for rail vehicle and infrastructure maintenance. Traditionally, safety related decisions within this realm have

Appendix G. Research Poster Conference 2021



Appendix H. Journal article 1

VEHICLE SYSTEM DYNAMICS
https://doi.org/10.1080/00423114.2021.1968443





Taylor & Francis
Taylor & Francis Group



Railway track location estimation using onboard inertial sensors

Alfredo Peinado Gonzalo [a], Mani Entezami[a], Clive Roberts[a], Paul Weston[a], Edward Stewart[a], Mick Hayward[b] and Sin Sin Hsu[b]

[a]Birmingham Centre for Railway Research and Education, University of Birmingham, Birmingham, UK; [b]Network Rail High Speed, Kent, UK

ABSTRACT

In railways, using a track- and ride-quality monitoring system on in-service train has become desirable for coordination and security. Identification of the track- or train-related rough rides via train crew can be estimated to the nearest kilometre. However, if the train is equipped with a monitoring system a better location and track quality evaluation can be provided. These systems commonly use information such as GNSS and/or an odometer to provide location information. This work proposes a practical method for track alignment estimation using real data from an in-cab inertial measurement system and using also a novel method based on crosslevel variations. The speed estimation is done through speed-related harmonics detected on inertial sensors, which depend on speed and track characteristics; and distance correction is provided by comparing crosslevel derived from inertial sensors and a reference track geometry. The effectiveness and accuracy of the method is demonstrated with data collected between London and Ashford.

ARTICLE HISTORY
Received 5 March 2021
Revised 21 June 2021
Accepted 10 August 2021

KEYWORDS
Railway; speed estimation; inertial sensors; track monitoring; crosslevel

1. Introduction

Positioning systems are generally divided into trackside and on-board equipment, aiming to obtain different results [1,2]. Trackside equipment is usually aimed at train integrity, wheelset monitoring and evaluating vehicles as they pass by the inspection points [3–5]. On-board equipment, such as Global Navigation Satellite Systems (GNSS) and tachometers, is used to identify the location and speed of the vehicle. On-board equipment can be mounted at various locations, such as on the bogie or on the cab floor. Most common sensors are inertial sensors, eddy current sensors, odometers and tachometers [1]. Sensor fusion is commonly used to improve the measurements provided by different sensors, as explained in the paragraphs below.

Tachometers and odometers are commonly installed on trains for speed and distance estimation, respectively, by measuring wheel rotations. Tachometers obtain speed by measuring the rotation rate of the wheel and then multiplying this by the wheel circumference, whilst odometers use the circumference and rotation count to measure distance [6]. Both

CONTACT Alfredo Peinado Gonzalo railcm@contacts.bham.ac.uk

© 2021 Informa UK Limited, trading as Taylor & Francis Group

Appendix I. CONTROL 2022

Observations on track evolution from onboard inertial measurements

Alfredo Peinado Gonzalo
Birmingham Centre for Railway Research and Education
University of Birmingham
Birmingham, United Kingdom
axp864@student.bham.ac.uk

Mani Entezami
Birmingham Centre for Railway Research and Education
University of Birmingham
Birmingham, United Kingdom
M.Entezami@bham.ac.uk

Clive Roberts
Birmingham Centre for Railway Research and Education
University of Birmingham
Birmingham, United Kingdom
C.ROBERTS.20@bham.ac.uk

Paul Weston
Birmingham Centre for Railway Research and Education
University of Birmingham
Birmingham, United Kingdom
P.WESTON@bham.ac.uk

Graeme Yeo
Birmingham Centre for Railway Research and Education
University of Birmingham
Birmingham, United Kingdom
G.J.Yeo@bham.ac.uk

Richard Horridge
Birmingham Centre for Railway Research and Education
University of Birmingham
Birmingham, United Kingdom
RXH437@student.bham.ac.uk

Edward Stewart
Birmingham Centre for Railway Research and Education
University of Birmingham
Birmingham, United Kingdom
E.J.C.Stewart@bham.ac.uk

Mick Hayward
Network Rail High Speed
Kent, United Kingdom
mick.hayward@networkrail.co.uk

Matthew Rippin
Network Rail High Speed
Kent, United Kingdom
Matthew.Rippin@networkrail.co.uk

***Abstract*— Distance estimation is necessary in railway track condition monitoring to evaluate the state of the track and locate faults. To do that, this paper proposes a novel method that combines an Inertial Measurement Unit (IMU) and Global Navigation Satellite System (GNSS) to estimate distance and then correct it using track geometry features such as crosslevel as a reference. This correction is used to align the track data accurately, which helps to observe the evolution of the track over a year and to evaluate the effects of track features such as tunnels, bridges, or switches and crosses, demonstrating that the distance estimation method is reliable and allows supervision of the track.**

Keywords—Inertial sensors, railway, track monitoring, crosslevel, condition monitoring, in-service vehicle

I. Introduction

The use of instrumented in-service vehicles for track monitoring and ride quality is increasing due to their regularity of use and availability, although placement of the sensors introduces technical challenges that must be overcome to ensure proper functioning of both the vehicle and the sensor without interference. Inertial, acoustic, optical and eddy current sensors are the most common ones for monitoring track condition while withstanding the harsh environments in which they are located [1, 2].

Among them, inertial sensors are largely used. These are often combined with other sensors to avoid drift and to enhance system capabilities [3]. Examples of their application for speed and distance estimation can be found in Ernest et al. [4], who combined an odometer and inertial sensors to estimate speed and distance in the absence of a GNSS signal; and Malvezzi et al. [5, 6], who combined a tachometer and inertial sensors using Kalman filtering and developed a suspension model in MATLAB/Simulink. This model was used by Allota et al. [7] under laboratory conditions at speeds up to 50 m/s obtaining errors below 0.5 m/s. Similar approaches can be found in the automotive sector, such as in [8, 9], who measured wheel angle and slip combining GNSS and inertial sensors, reducing inaccuracies and improving their precision.

The Birmingham Centre for Railway Research and Education (BCRRE), based at the University of Birmingham, has several publications focused on use of an IMU for railway track condition monitoring. Research done by Weston et al. [10, 11] focused on monitoring track irregularities with an IMU installed on the axlebox and the bogie of several vehicles. In publications by Yeo et al. [12, 13, 14] the IMU was installed on the bogie to observe the evolution and degradation of a track over nine months, study track deflection and stiffness and detect vertical track faults.

This paper focuses on the use of the IMU designed by the University of Birmingham [15, 16] to observe the degradation of track and its effects on ride quality over a period of one year, developing a novel method to adapt all datasets for a better comparison of information and the possible detection of degradation and failures in the track. This method is explained on Section III and uses crosslevel as a reference for adapting the distance estimated by the IMU, where crosslevel or cant is defined as the difference in height between two rails on the same track.

Ride quality is evaluated using passenger comfort based on the standard EN 12299 [17]. According to the standard,

Appendix J. Rail Live 2022

Remote Condition Monitoring of Track Geometry and Ride Comfort from In-service Trains

BCRRE

Introduction

Rail infrastructure managers have dedicated vehicles to carry out track measurement. These vehicles are, however, expensive to procure and run as they need specially trained crews to operate them.

This work demonstrates the application of an inexpensive inertial measurement unit (IMU), installed on an in-service passenger train, and using novel algorithms, to provide continuous monitoring of the track and its degradation. IMU sensors along with Global Navigation Satellite System (GNSS) are used in this work to estimate distance, assess passenger comfort, examine the effects of sensors positions, calculate track geometry parameters. The track geometry results are also compared to track recording vehicles, e.g. Network Rail New Measurement Train.

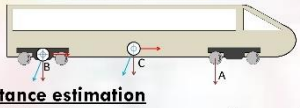
Onboard measurement system

Installed on the Axlebox, Bogie and Cab of a UK Class 374 high-speed train.

- IMU:
  - Acceleration.
  - Rotation rate.
  - Displacement.
- GNSS:
  - Vehicle location.
  - Vehicle speed.

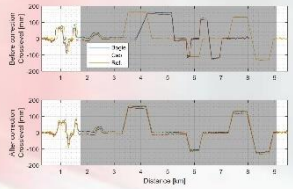






Distance estimation

Due to complexity in installation and approval process, acquiring speed data from train system was not possible, and the GNSS has limitations such as unavailability in tunnels. The solution proposed is based on using harmonics caused by vehicle vibrations to estimate speed, and combining the estimation with the GNSS via a Kalman filter. The distance is estimated by integrating the speed over time. The estimation is inaccurate at low speeds, and corrected using track crosslevel as a reference.

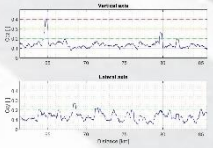


Distance estimation correction using crosslevel

Passenger comfort

Comfort evaluation based on ISO 2631 and EN 12299. Can be used for detecting track irregularities, such as switches and crosses or bridges.

Value	Passenger experience
$C_{Cp}(t)$, $C_{Cv}(t) < 0.20\ m/s^2$	Very comfortable
$0.20\ m/s^2 \leq C_{Cp}(t)$, $C_{Cv}(t) < 0.30\ m/s^2$	Comfortable
$0.30\ m/s^2 \leq C_{Cp}(t)$, $C_{Cv}(t) < 0.40\ m/s^2$	Medium
$0.40\ m/s^2 < C_{Cp}(t)$, $C_{Cv}(t)$	Uncomfortable



Passenger comfort along the line



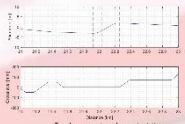
Vertical passenger comfort

Effects of sensor location and vehicle direction

Measurements depend on the location of the sensor in the coach (axlebox, bogie or cab), the position of the coach respect to the vehicle (leading or trailing), and the direction of travel (up or down line).

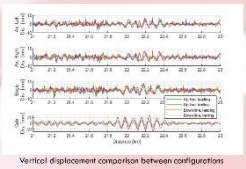
There are four sensor configurations:

- Up line with sensors in leading coach.
- Up line with sensors in trailing coach.
- Down line with sensors in leading coach
- Down line with sensors in trailing coach.

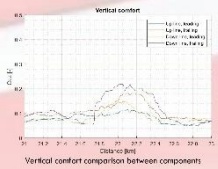


Track geometry characteristics

Comparison between configurations



Vertical displacement comparison between configurations

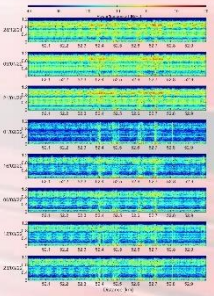


Vertical comfort comparison between components

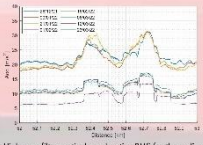
Evolution of track geometry

There are several phenomena that may affect the signals measured on the vehicle: Track degradation, that generates irregularities in the track geometry, track maintenance activities aiming at restoring the original geometry, or vehicle faults, such as wheel flats.

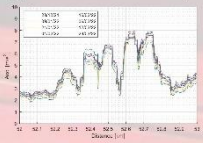
Date	Effect reported	Km
December	Wheel Flat	-
February	Wheel Flat repaired	-
17-Feb-2022	Reported as actionable	300 m from swing nose
27-Feb-2022	Swing nose change	52.330
25-Mar-2022	Reported as actionable	Swing nose



Vertical acceleration spectrogram evolution for the up line

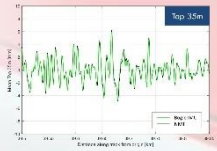


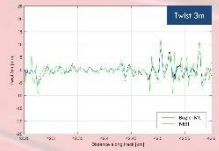
High-pass filter vertical acceleration RMS for the up line



Low filter vertical acceleration RMS for the up line

Comparison to Network Rail NMT





Conclusions

Track geometry can be monitored and evaluated using inertial sensors onboard passenger trains, as its effects can be observed in the axlebox, bogie and cab of the vehicle. The position of the sensors in the vehicle is relevant, as there is a correlation between measurements and their location.

Acknowledgements

The work is partly funded by the Innovate UK Smart Grant 103294: Track and ride condition correlation for optimised rail maintenance, and by the SRUK On the Move funded mobility fellowship, in collaboration with INGENIUM research group in UCLM. The authors would like to thank Network Rail High Speed and Eurostar Ltd for their support throughout this project.

MoniRail

Alfredo Peinado Gonzalo

M. Entezami, G. Yeo, E. Stewart, P. Ainsworth, C. Roberts

axp864@bham.ac.uk

alfredo@monirail.co.uk

Appendix K. Journal article 2

This article has been accepted for inclusion in a future issue of this journal. Content is final as presented, with the exception of pagination.

Review of Data Analytics for Condition Monitoring of Railway Track Geometry

Alfredo Peinado Gonzalo, Richard Horridge, Heather Steele, Edward Stewart, and Mani Entezami

***Abstract*— Railway track geometry varies along routes depending on topographical, operational and safety constraints. Tracks are prone to degrade over time due to various factors, with deviations from the original geometry design having potential implications for comfort and safety. Regular inspections are carried out to evaluate track condition and determine whether maintenance interventions should be undertaken to correct track geometry. The dynamic measurement of track geometry parameters generates large volumes of data that must be analysed to evaluate track degradation. This work comprehensively explains how track quality is evaluated, introducing four main categories of factors affecting it. These are track design, loading, environment and maintenance. The most common techniques applied to evaluate track condition and predict degradation and faults, categorised into statistical, Machine Learning, Big Data and other, are also introduced. Specifically, the influence of each factor on track geometry is stated and the common techniques applied to each factor determined from this review. The utility of loading and maintenance data for fault prediction depend on the availability of records, whilst the impact of environmental conditions is expected to become increasingly important due to climate change. Artificial Neural Networks, Bayesian models and regression are the most applied techniques for determining track degradation behaviour and fault prediction, considering several different factors in their models. Increasingly sophisticated algorithms can consider multiple factors in tandem to predict faults based on the unique conditions of specified tracks.**

***Index Terms*— Artificial intelligence, machine learning, rail transportation, track geometry.**

I. Introduction

RAILWAY tracks are designed and built with specific geometry, which varies along a route due to topography constraints. Once operational, the track can degrade due to several factors, causing deviations from the designed geometry that must be corrected to ensure passenger comfort and safety. Regular inspection is undertaken to assess track degradation and faults (where degradation refers to the general state of the track and its geometry, whilst a track fault refers to a discrete element of the track) and track condition, using a combination of manual inspection and Track Recording Vehicles (TRVs). Typically, thresholds are set for specific faults and statistical measures of track quality, which if exceeded instigate maintenance activities.

Both track geometry and track structure may be considered when determining track quality [1]. Track geometry comprises the following primary parameters: longitudinal level (vertical profile, top or surface), lateral alignment (horizontal profile or line), gauge, cross-level and horizontal curvature, from which secondary measures such as twist, cyclic top, corrugation and cant deficiency can be derived [2]. Measures of track geometry are predominantly used to assess track quality, by setting parameter thresholds and statistical Track Quality Indices (TQIs). TQIs provide information about the track state using some quantified parameters and typically differ both between infrastructure managers and researchers [3]. These indices may not only use track geometry parameters but also parameters related to passenger safety [4], [5], [6]. In Europe, standard TQIs include the standard deviation of the mean longitudinal level and lateral alignment over track sections of specified length e.g. 200m [7]. Longitudinal level and lateral alignment are high pass filtered so that height is measured with respect to a short (e.g. 35 m) or long (e.g. 70 m) length of track rather than absolute height, to negate the need for reference data. Track Structure Indices (TSIs) relate to the condition of the track (rail, sleeper, fastening systems, subgrade, and drainage systems), and typically rely upon visual evaluation [8], [9]. Both ballasted and newer ballastless track structures can be considered.

TRVs that include visual, radar, ultrasounds and induction sensors are in use around the globe to dynamically measure track geometry. In the United Kingdom, Network Rail's 'New Measurement Train' takes measurements with the aim of preventing three main track defects: twist, cyclic top and gauge problems [8], using lasers and cameras to detect faulty or missing track components as the train passes [10]. Japanese 'Dr Yellow' inspection vehicles evaluate gauge, crosslevel, alignment, longitudinal level and twist at more than 250 km/h on the Shinkansen network [11] using inertial and optical sensors [12], [13]. TRV's belonging to ENSCO in the USA [14] offer services related to track inspection and maintenance. China's Comprehensive Inspection Trains are high speed inspection trains employed for dynamic and static track geometry status analysis, among other tasks [15].

TRVs provide accurate data, but fleet size is usually limited. Inspections can take place infrequently depending on the track

Manuscript received 24 August 2021; revised 12 April 2022 and 27 July 2022; accepted 13 September 2022. This work was supported in part by the Shift2Rail Innovation Program Project IN2TRACK2 (work package 3) and in part by the Innovate U.K. Smart through Track and Ride Condition Correlation for Optimized Rail Maintenance under Grant 103294. The Associate Editor for this article was M. Gao. *(Corresponding author: Alfredo Peinado Gonzalo.)*

The authors are with the Birmingham Centre for Railway Research and Education, B15 2TT Birmingham, U.K. (e-mail: railcm@contacts.bham.ac.uk; rxh437@student.bham.ac.uk; h.j.j.steele@bham.ac.uk; e.j.c.stewart@bham.ac.uk; m.entezami@bham.ac.uk).

Digital Object Identifier 10.1109/TITS.2022.3214121

1558-0016 © 2022 IEEE. Personal use is permitted, but republication/redistribution requires IEEE permission.
See https://www.ieee.org/publications/rights/index.html for more information.

Authorized licensed use limited to: UNIVERSITY OF BIRMINGHAM. Downloaded on November 07,2022 at 15:56:27 UTC from IEEE Xplore. Restrictions apply.